Outdoor Laboratory and Testbed for Bridge Health

FINAL REPORT

Richard L. Wood (PI); Mitra Nasimi, Bowen Yang, Christine E. Wittich (co-PI); Joshua S. Steelman (co-PI); Jay A, Puckett (co-PI); Daniel G. Linzell (co-PI); Jinying Zhu (co-PI), Mohammad Ebrahim Mohammadi

University of Nebraska-Lincoln

Department of Civil and Environmental Engineering

900 N 16th St, Lincoln, NE 68588

Sponsored By

Nebraska Department of Transportation and U.S. Department of Transportation Federal Highway Administration

June 2022

NEBRASKA
Good Life. Great Journey.
DEPARTMENT OF TRANSPORTATION

UNIVERSITY OF Nebraska® Lincoln

1. Report No. M107	2. Government Accession No.	3. Recipient's Catalog No.
4. Title and Subtitle M107: Outdoor Laboratory and Testbed for Bridge Health		**5. Report Date** June 2022 **6. Performing Organization Code**
7. Author(s) Richard L. Wood, Mitra Nasimi, Bowen Yang, Christine E. Wittich, Joshua S. Steelman, Jay A. Puckett, Daniel G. Linzell, Jinying Zhu, Mohammad Ebrahim Mohammadi		**8. Performing Organization Report No.** SPR-P1(20) M107
9. Performing Organization Name and Address University of Nebraska-Lincoln 1400 R St, Lincoln, NE 68588		**10. Work Unit No.** **11. Contract** 26-1121-4048
12. Sponsoring Agency Name and Address Nebraska Department of Transportation Research Section 1500 Hwy 2 Lincoln, NE 68502		**13. Type of Report and Period Covered** Final Report July 2019 – June 2022 **14. Sponsoring Agency Code**
15. Supplementary Notes		

16. Abstract

Due to the aging problem of bridges and the limited financial resources in the United States, it is necessary to form a deeper understanding of existing, aging bridges in an effort to extend their in-service life. To address this problem, researchers from the University of Nebraska-Lincoln (UNL) and engineers from the Nebraska Department of Transportation (NDOT) identified three, out-of-service bridges (two steel and one concrete) to establish the Nebraska Outdoor Bridge Lab (NOBL). As the first step in NOBL's development, geometric surveys of the current condition of each bridge were produced using lidar and Structure-from-Motion (SfM). This data contributed to the generation of finite element analysis models for each bridge, which were used to anticipate bridge response under various loading patterns, and were validated using measured ambient vibration tests. Live load demonstrations were further performed for each bridge under various traffic loads. Geometric data, finite element models, and the results of the live load demonstrations are detailed in this report and are available for use by researchers and practitioners utilizing the NOBL facility moving forward. Additional potential uses of the NOBL facility are included along with areas for further research as concluding remarks in this report.

17. Key Words	18. Distribution Statement
bridge lab, damaged bridge, steel bridge, concrete bridge, live-load testing	No restrictions

19. Security Classification (of this report)	20. Security Classification (of this page)	21. No. of Pages	22. Price
Unclassified	Unclassified	66	

Form DOT F 1700.7 (8-72) Reproduction of completed page authorized

Table of Contents

List of Figures

List of Tables

DISCLAIMER

The contents of this report reflect the views of the authors, who are responsible for the facts and the accuracy of the information presented herein. The contents do not necessarily reflect the official views or policies neither of the Nebraska Department of Transportations nor the University of Nebraska-Lincoln. This report does not constitute a standard, specification, or regulation. Trade or manufacturers' names, which may appear in this report, are cited only because they are considered essential to the objectives of the report.

The United States (U.S.) government and the State of Nebraska do not endorse products or manufacturers. This material is based upon work supported by the Federal Highway Administration under SPR-P1(20) M107. Any opinions, findings and conclusions, or recommendations expressed in this publication are those of the author(s) and do not necessarily reflect the views of the Federal Highway Administration."

ACKNOWLEDGEMENTS

This project was funded by the Nebraska Department of Transportation (NDOT) under project number M104 – Outdoor Laboratory and testbed for Bridge Health. The authors would like to express their gratitude to the following collaborators: researchers from SC Solutions, the University of Nevada at Reno (UNR), and the University of California, Los Angeles (UCLA) .The external research collaborators were under the direction and supervision by Matt Bowers of SC Solutions.

Additionally, field support was generously provided by NDOT District 2 under the supervision of Dave Casper. Without the field support of District 2, the work performed and future activities could not occur at the NOBL facilities. Field support at the NOBL North Facility was also supported by the NDOT Snooper team with Seth Brashears, Mike Mosiman, and Dallas Pears. Moreover, the research team would also like to appreciate the support and assistance of the Technical Advisory Committee (TAC) throughout this project. This includes the following member (in alphabetical order): Mark Ahlman, Mark Fischer, Lieska Halsey, David Hansen, Kirk Harvey, Fouad Jaber, Kent Miller, Babrak Niazi, Tom Renninger, Mark Traynowicz, Tim Weander, Brandon Varilek, and Mike Vigil.

ABSTRACT

Due to the aging problem of bridges and the limited financial resources in the United States, it is necessary to form a deeper understanding of existing, aging bridges in an effort to extend their in-service life. To address this problem, researchers from the University of Nebraska-Lincoln (UNL) and engineers from the Nebraska Department of Transportation (NDOT) identified three, out-of-service bridges (two steel and one concrete) to establish the Nebraska Outdoor Bridge Lab (NOBL). As the first step in NOBL's development, geometric surveys of the current condition of each bridge were produced using lidar and Structure-from-Motion (SfM). This data contributed to the generation of finite element analysis models for each bridge, which were used to anticipate bridge response under various loading patterns, and were validated using measured ambient vibration tests. Live load demonstrations were further performed for each bridge under various traffic loads. Geometric data, finite element models, and the results of the live load demonstrations are detailed in this report and are available for use by researchers and practitioners utilizing the NOBL facility moving forward. Additional potential uses of the NOBL facility are included along with areas for further research as concluding remarks in this report.

1 Introduction

1.1 Project overview

The purpose of this project is to establish the Nebraska Outdoor Bridge Lab (NOBL). To accomplish this project, two steel bridges near Yutan and one concrete bridge near Omaha were selected. This project was performed in four main phases or tasks and is described herein. Before starting any site characterization or fieldwork and to increase safety, an operational and safety document was developed, and then site access was limited with additional fencing (at Yutan). Then, site characterization was done by remote sensing using point clouds generated by lidar scanning and supplemental Structure-from-Motion data using an uncrewed (or unmanned) aerial system (UAS). This site characterization provides current geometric information at each bridge site at the centimeter level, which is needed to construct the finite element analysis (FEA) models. In addition to geometric information, system identification provided a quantification of the vibrational response of the bridges under ambient vibrations to verify and calibrate the FEA models. These calibrated or refined models are updated to reflect field measurements and bridge response. These models aim to include realistic conditions of each bridge site, which may include: deterioration, boundary conditions, unintended composite action, and construction tolerances. Lastly, demonstrative live load testing was done at each bridge site to quantify and measure the bridge response under a series of live load patterns. The live load consisted of two 50-kip triaxial trucks operated at various speeds, spacings, and configurations.

1.2 Benefits and tasks

The project aims to establish a research and educational facility related to bridge health and the training of students/future engineers, bridge engineers, and bridge inspectors. Due to the closed-traffic conditions of these bridges, this laboratory facility enables a test bridge to explore analytical modeling (with calibration), remote sensing, diagnostic techniques, and structural health monitoring. This project will provide a detailed

characterization of realistically aged bridges (two steel bridges at Yutan and one concrete bridge at Omaha). In the long term, this project aims to study key questions on bridge health to address statewide and national needs.

This project has four identified research tasks to achieve and meet the project objectives. An overview flowchart is shown in Figure *1.1* which outlines the interconnectedness and flow of the project. The four tasks include (1) Site Staging, (2) Site Characterization, (3) Facility Demonstration, and (4) Reporting. Each of these four tasks contributes to the overarching objective: *to transform three bridges into a national research and educational facility for bridge health and testing*.

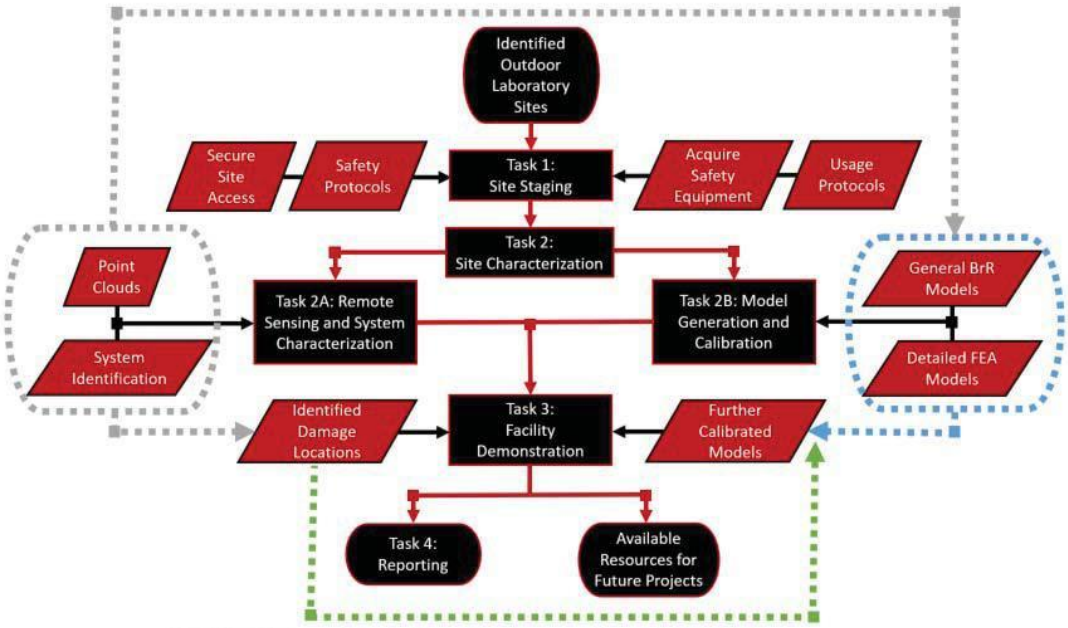

Figure 1.1. Flow chart of the research tasks.

1.3 Outline of report

This report consists of six chapters. Chapter 1 outlines the motivation for the work, defines the project, and summarizes the scope. Chapter 2 outlines the safety and operational document as well as site staging (Task 1). Chapter 3 briefly describes the three-dimensional geometric data collection for site characterization as well as the ground-penetrating radar (GPR) for assessment of the bridge deck (Task 2A). Chapter 3 also

summarizes the finite element analysis (FEA) models of the bridge site (Task 2B). Chapter 4 summarizes the demonstration with the live loads (Task 3), which includes an overview of the experiment, sensors used, processing, and quantification of the data. Chapter 5 focuses on a strain gauge assessment of the concrete bridge at Omaha (Task 3). Chapter 5 provides conclusions of this project and recommends future research topics (Task 4). Appendix A presents the Safety Protocol and Information document, as specified developed and related to the NOBL facility. Appendix B outlines and summarizes the site demonstration data (Task 3).

2 Site setup and facility establishment

2.1 Site selection

The Nebraska Outdoor Bridge Lab (NOBL) is comprised of three bridges at two sites. Currently, the bridge sites are minimally not in regular service or completely out of service. This chapter aims to describe and outline the bridge details by each site as well as the safety and operational procedures and securement of the site. This chapter closely relates to Task 1 of the project.

2.1.1 NOBL (Steel Bridges at Yutan)

The (primary) NOBL site is located on Nebraska State Route 92 over the Platte River just east of Yutan, as shown in Figure *2.1*. Herein, this is known as the "Yutan (steel) bridge site". At this site, two steel girder bridges cross the river in two separate crossings (with an island). These bridges were decommissioned in 2005 when replacement bridges were constructed just to the north of the bridge lab.

These bridges have nominal lengths of 400-feet (east bridge) and 1000-feet (west bridge). Overview photos of the bridges are illustrated in Figure *2.2*. As illustrated in Figure 2.3, these steel bridges exhibit various damage mechanisms due to environmental and mechanical loads. This includes steel girder corrosion, abutment cracking, anticipated concrete delamination, and cracking in the asphalt overlay. The east bridge consists of (4) 100-feet spans comprised of approximately 54-inch welded plate girders with pin and hanger connections. The west bridge consists of eight 112-feet spans comprised of approximately 54-inch welded plate girders with pin and hanger connections. Both bridges at this site were designed in 1960. Information, structure numbers, and properties for both steel bridges at Yutan are summarized in Table 2.1.

(a) Detailed view of NOBL lab at Yutan

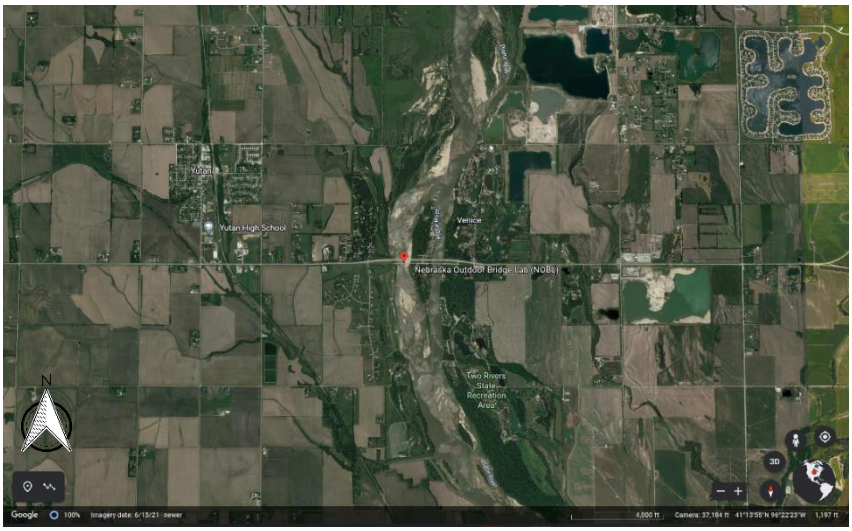

(b) Satellite view of NOBL lab at Yutan

Figure 2.1. Site view of NOBL lab at Yutan.

(a) NOBL East bridge at Yutan overview (NOBL East)

(b)Yutan west steel bridge overview (NOBL West)

Figure 2.2. Yutan Steel bridge.


(a) Example corrosion and delamination


(b) Abutment damage


(c) Pin lost at pin-hanger connection (d) bridge deck with cracking

Figure 2.3. Example images of the steel girder bridge damages at Yutan bridge site.

Table 2.1. Tabular summary of the NOBL bridges.

Description	Yutan Steel Bridge Site (East)	Yutan Steel Bridge Site (West)	Omaha Concrete Bridge
Structure Number	S092 46282R	S092 46256R	S036 02040L
Year Built	1960	1960	1979
Year Decommissioned	2005	2005	--
Bridge Length (ft [m])	600 [182.9]	1000 [304.8]	156 [47.55]
Bridge Width (ft [m])	32 [9.8]	32 [9.8]	39.5 [12]
Number of Spans	4	8	3
Span Length (ft [m])	100 [30.5]	112 [34.1]	60 [18.29]
End Span Length (ft [m]), if different	--	--	48 [14.63]
Number of Girders	4	4	5
Girder Type	Welded plate with pin and hanger connection	Welded plate with pin and hanger connection	AASHTO type 3A
Bridge Location (latitude, longitude)	State Route 92, East of Yutan, NE	State Route 92, East of Yutan, NE	State Route 36, North of Omaha, NE
Deck Surface Type	Concrete	Concrete	Concrete
Membrane	No	No	Yes
Overlay	Latex modified structural concrete	Latex modified structural concrete	Asphalt concrete (A.C)
Deck Protection	Asphalt	Asphalt	Asphalt
Deck Thickness (in [cm])	7 [17.78]	7 [17.78]	7.5 [19.05]

2.1.2 NOBL North (Concrete Bridge at Omaha)

The (other) bridge site is located on State Route 36 over the Glenn Cunningham Reservoir just north of Omaha, as shown in Figure *2.4*. Herein this is known as the “Omaha (concrete) bridge site” or “NOBL

North". This concrete bridge was originally designed for a potential four-lane divided highway expansion in 1979, but has seen only minimal traffic loads. This bridge site does experience occasional traffic associated with recreational users (e.g., horseback vehicles), training exercises (e.g., NDOT, Omaha Police Department, etc.), and construction traffic (as in 2022). The concrete bridge at Omaha consists of three spans (as shown in Figure *2.5*) of 48, 60, and 48-feet, respectively; and is comprised of AASHTO girder type 3A (Shown in Figure *2.6*). This bridge was designed in 1979 as a pair, at the time of construction, this bridge was one of the twenty bridges that received an asphalt with waterproofing membrane on the original construction and before opening to service. Now the north pair of the bridge is unused while the south pair of the bridge has supported regular traffic of Nebraska State Highway 36 since construction. As illustrated in Figure *2.7*, various damage modes can be observed in this structure despite its minimal use of mechanical loads (vehicles) as well as environmental loads. This includes localized scour at the abutment, abutment cracking, suspected delamination near the bridge deck weep holes, and cracks in the asphalt deck overlay. Information, structure number, and properties for this bridge are summarized in Table 2.1

.

(a) Detailed view of NOBL North bridge in Omaha

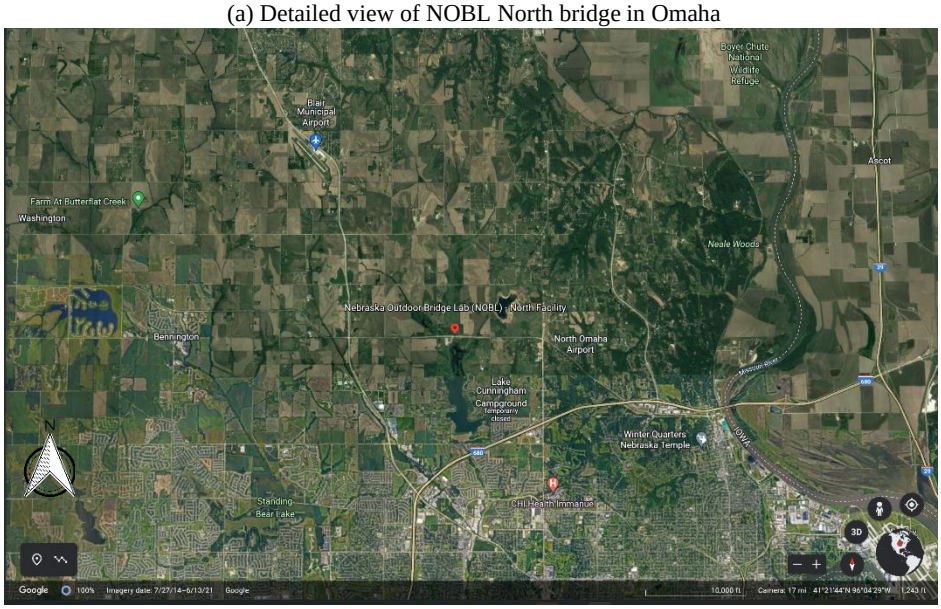

(b) Satellite view of NOBL lab located in North Omaha

Figure 2.4. Site view of NOBL North bridge in Omaha .

Figure 2.5. Overview of the NOBL North bridge in Omaha .

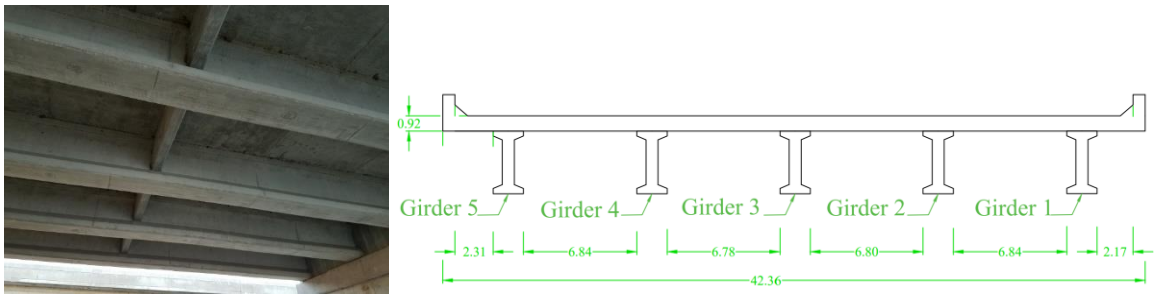

(b) View of concrete girders from below (b) cross-section of the concrete bridge

Figure 2.6. Cross-section and girder details related to NOBL North bridge in Omaha .

(a) Abutment Damage

(b) Bridge deck condition with cracks

(c) Delamination at weep hole

(d) East abutment damage and exposed pile

Figure 2.7. Damage example images of the NOBL North bridge in Omaha site.

2.2 Safety and operational document

These bridges were previously selected for educational, research, and outreach/engagement purposes by both UNL and NDOT in joint collaboration. To facilitate operation and safety at these sites, a dedicated operations document was generated and reviewed by the UNL Office of Environmental Safety. The document in its entirety is compiled in Appendix A (Safety and Operational Document) as well as hosted on the NOBL website (http://nobl.unl.edu). Note this document aims to be updated regularly, given

anticipated personnel and operational changes at UNL. The latest version of this document is compiled in this report.

2.3 Site staging and security

At Yutan, these bridges are in close proximity to routine traffic loads (Nebraska State Route 92) as well as see occasional and unapproved recreational uses, despite both of these two bridges at Yutan posted for no trespassing. Fencing gates are installed at this site for safety and limit access for personnel and equipment uses at this site, as part of this project. The purpose of these gates is to create a safe laboratory environment for both the UNL/NDOT participants, their invited guests, and the public as well as permit access by approved personnel. To accomplish this, fencing was installed to limit access to the general public and traffic. Access to open these gates is controlled by a state-owned padlock (with a key for DOT and other state agencies' access (e.g., Nebraska State Patrol)) and a numeric combination lock (for NOBL uses). Figure 2.8 shows the location and details of each of the abutments of the NOBL facility at Yutan. The official signature for the facility exists on both Yutan bridges. Moreover, no fencing or gates were placed at the NOBL North site in Omaha.

2.4 Intermediate conclusions

Task 1 of this project, as summarized in this chapter, enabled safe and controlled usage of the bridge facilities for various interested parties and project participants. This was done in close coordination with NDOT for safety and right-of-way (ROW) permits. The safety document for site access is maintained for all interested parties to review before facility usage. With the site secured, additional tasks were then able to be completed.

(a) Gate locations in NOBL lab at Yutan

(b) Gate C detailed view

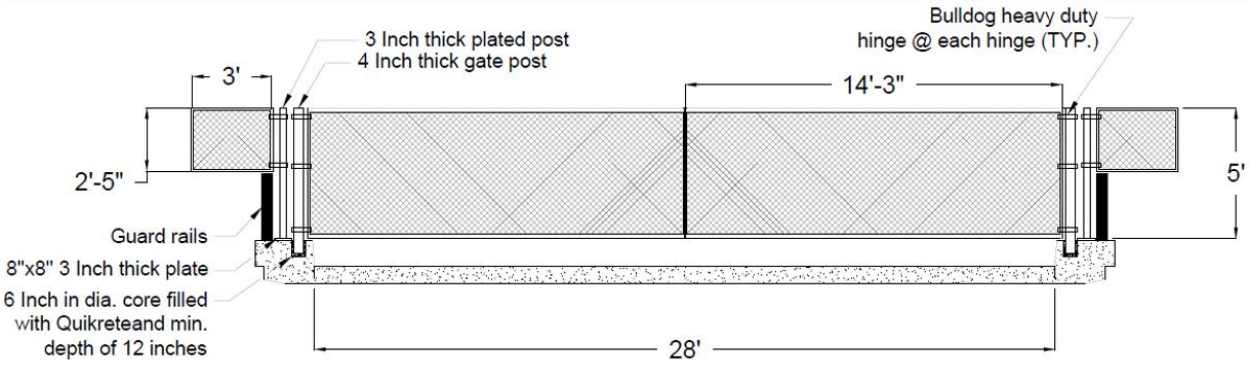

(c) Geometric information of gates

Figure 2.8. Detailed information of the gates placed in NOBL lab at Yutan.

3 Initial site characterization

3.1 Introduction

The three bridge structures at Yutan and Omaha have experienced a variety of environmental and service loads since their initial construction. Given construction tolerances and changing bridge conditions, one of the earliest tasks was to nondestructively characterize these bridges in terms of structural and geometric properties for further investigations. This was accomplished using lidar and Uncrewed (or unmanned) Aerial Systems (UAS) surveying for the geometry, initial accelerometer measurements for system identification, preliminary finite element analysis (FEA) model construction, and ground-penetrating radar scanning. Summary details are provided below. This chapter closely relates to Task 2 of the project.

3.2 Lidar and UAS

Light detection and ranging (lidar) scans were collected using two scanners, Faro Focus^{3D} X130 and S350 laser scanners, for each bridge structure. The Faro Focus^{3D} X130 lidar or laser scanner and Faro focus S350 laser scanner was utilized during the site investigations and are used to scan profiles in distance ranging up to 130 (426 [ft]) and 350 (1148 [ft]) meters, respectively. For terrestrial-based scanning, multiple scans at various locations with adequate overlap are required to create a dense point cloud, reduce areas of occlusions, and improve the alignment accuracy. These points aid in quantifying the static geometry of the bridges. One delay during the project did arise in the field deployment of the S350 lidar scanner. This sustained damage in the field at the NOBL North site given traffic-induced wind but was successfully repaired after an unfortunate and extended delay.

The lidar scan files are uploaded into various computer software platforms, such as Faro Scene, Cloudcompare, and Autodesk Recap, for point cloud processing for take-off geometry. Each individual scan file contains inherent noise, which is unavoidable. Most of these points are removed with segmentation (manually) and filtering techniques. A statistical outlier removal (SOR) filter is used to eliminate most of

the noise and erroneous points with automation, especially those caused by sharp object edges. This filter estimates the mean distance between the inputted number of random points and removes the points outside of the specified standard deviation threshold. Filtered point clouds provide accurate information about the geometric information and could use for further comparison purposes as the bridge condition changes.

Uncrewed (or Unmanned) Aerial Systems (UASs or commonly known as drones) are one of the commonly used methods for mapping. In this research, a DJI Inspire 2 UAS was used along with ground control points using a Global Navigation Satellite System (GNSS) survey technique georeference the collected data. Georeferencing was implemented through the use of ground control points (GCPs) and checkpoints (CPs). The use of GCPs significantly increases the accuracy of the obtained data in PIX4Dmapper software and this was achieved at the centimeter level horizontally 5 cm (2 in), as confirmed in the checkpoints. However, the accuracy of the collected data depends on the vegetation, overlap of the images, the precision of the real-time kinematic (RTK) survey, and light condition (on the images). The maximum error was below 8 cm (3 in) in the vertical direction. In the final step (for each bridge site), the two point clouds as generated using UAS and lidar scanner were uploaded to CloudCompare software and aligned with each other by selecting at least three common points using a technique called Single Value Decomposition (Liao et al., 2020) The point clouds can then be used to quantify areas of spalling or corrosion, measure deflection, and generate the necessary geometry for finite element analysis (FEA) modeling. In this project, the primary usage of the point clouds was for geometric input for the FEA modeling as well as general visualization of the sites. Figure 3.1 shows the final point cloud generated for the three selected bridges. Note visualizations of these sites are also available on the NOBL website (NOBL, n.d.).

(a) NOBL East steel bridge at Yutan (NOBL East)

(b) NOBL West steel bridge at Yutan (NOBL West)

(c) NOBL North concrete bridge in Omaha (NOBL North)

Figure 3.1. Point clouds for the three selected bridge sites.

3.3 Finite element analysis (FEA) models

To identify the response of the bridge under various loads, a numerical finite element analysis (FEA) model analysis was performed using the point cloud data geometry and bridge plans to obtain the modal frequencies and other response behavior. The FEA modeling of the bridge was generated using CSiBridge to study the bridge response, where these models are available for use by interested parties. These bridge models were developed based on the material properties identified in the available reference (Ocel, 2021), plan drawings, and engineering judgment. For the deck concrete compressive strength, while it is expected that an undamaged concrete deck strength would exceed the 28-day design compressive strength of 3.0 ksi, no overstrength is considered in these models. By neglecting the overstrength here, this accounts for some concrete degradation in the deck which is exhibited in the photos and field visit. This assumption results in a lower deck stiffness due to existing deck deterioration and it will be assessed in the field for its validity. Table *3.1* shows the material properties used for modeling. Figure *3.2* shows the developed finite element model of the bridges.

Table 3.1. Material properties used to model NOBL bridges.

Properties	Yutan Steel Bridge Site	Omaha Concrete Bridge
Deck concrete strength ([ksi])	3.0	3.0
Concrete elastic modulus ([ksi])	3604.9	3604.9
Reinforcement steel	Gr60	Gr60
Girder steel	A7	
Web height ([inches])	54	--
Web thickness ([inches])	1	--
Flange width ([inches])	13.8	--
Flange thickness ([inches])	1.79	--
Girder concrete strength ([ksi])	--	4
Prestress tendon	--	GR270
Girder	--	AASHTO- Type 3A

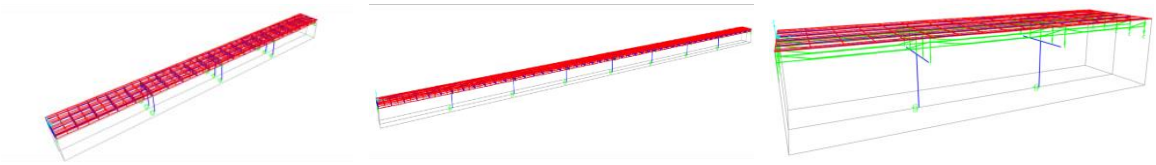

(a) NOBL East bridge at Yutan (b) NOBL West bridge at Yutan (c) NOBL North bridge in Omaha

Figure 3.2. CSiBridge finite element modeling of the three selected bridges.

An eigenvalue analysis was also conducted for each of these models. Table *3.2* summarizes the three natural frequencies obtained from the initial numerical model analysis. Based on the achieved natural frequencies NOBL concrete bridge at North Omaha (NOBL North) is more rigid than the East Yutan bridge. Moreover, the East Yutan bridge (NOBL East) is less flexible than the West bridge (NOBL West). This behavior is anticipated, as in general, when various parameters are consistent, a steel bridge is often more flexible than concrete and the flexibility of a bridge increases with length (Martindale et al., 2019; and etc.). Figure *3.3*

shows the mode shapes generated for each selected bridge in CSiBridge. System identification was done based on the first three natural frequencies using the Artemis platform (Döhler et al., 2017). As noted in a previous NDOT project on Inverted Tees Bridges, the extended unweighted principal component method provided clear results (Martindale et al., 2019). Note the dynamic properties of these initial models have been verified/confirmed in Chapter 4.

Table 3.2. Natural frequency for the three selected bridges from the FEA models.

Mode	NOBL East Frequency (Hz)	NOBL West Frequency (Hz)	NOBL North Frequency (Hz)
1	3.45	2.77	9.29
2	4.17	3.02	9.78
3	4.31	3.15	11.02

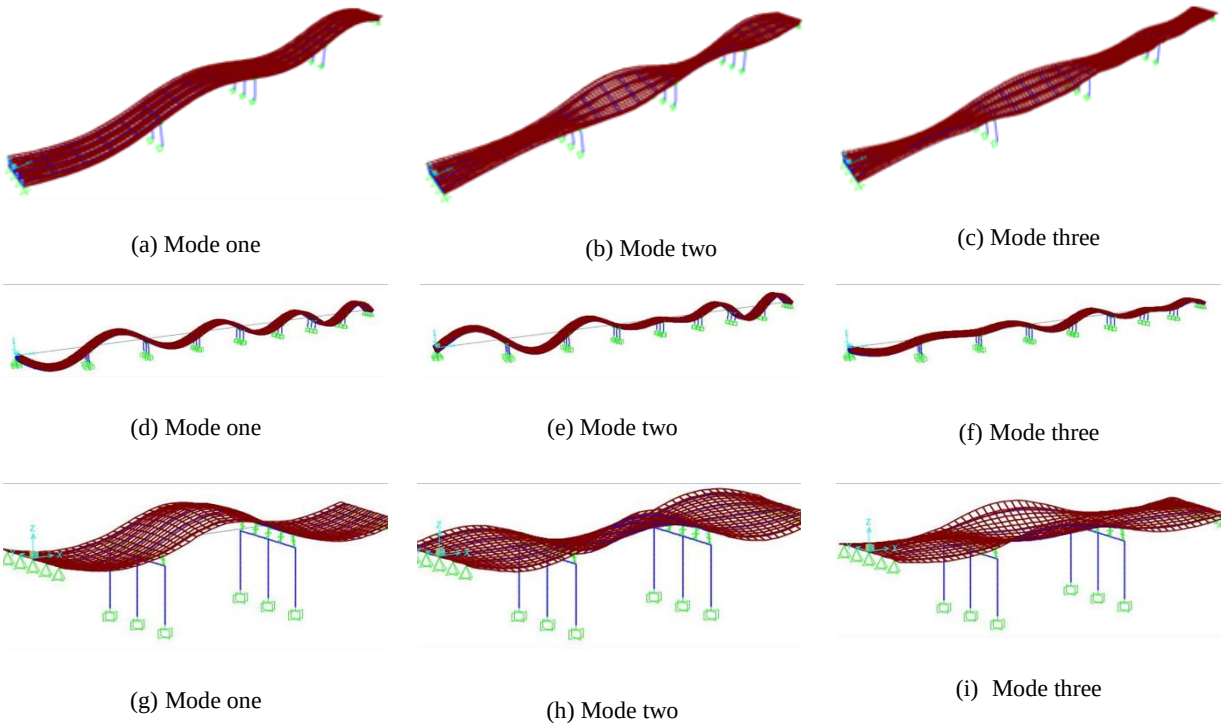

(a) Mode one (b) Mode two (c) Mode three

(d) Mode one (e) Mode two (f) Mode three

(g) Mode one (h) Mode two (i) Mode three

Figure 3.3. Mode shapes of the three selected bridges; (a), (b), (c) NOBL East steel bridge at Yutan; (d), (e), (f) NOBL West steel bridge at Yutan; (g), (h), (i) NOBL North concrete bridge in Omaha.

3.4 GPR scanning

Ground Penetrating Radar (GPR) scanning is a signal-based non-destructive technique that is widely used to detect surface objects. In this research, GPR has been used to determine rebar and the potential location of the concrete deterioration. GPR transmits radar pulses and based on the obtained reflections from rebars, and wave velocity, the depth of the rebar can be calculated. At the same time, the amplitude of the reflected waves was measured along the span of the bridge. Lower amplitude and weaker signal show the potential location of the deck cover concrete deterioration or rebar corrosion (Zhu & Pashoutani, 2020). In this project, the lower amplitude signals likely represent significant concrete degradation and/or delamination. Figure *3.4* shows GPR mapping for three selected bridges. The NOBL East bridge structure at Yutan demonstrates significantly degraded concrete at the approach spans as well as distributed throughout. To validate the results obtained from the GPR scanning, in the future work it would be desirable to do select coring in arbitrary locations of the bridge decks. However, these locations have not been finalized.

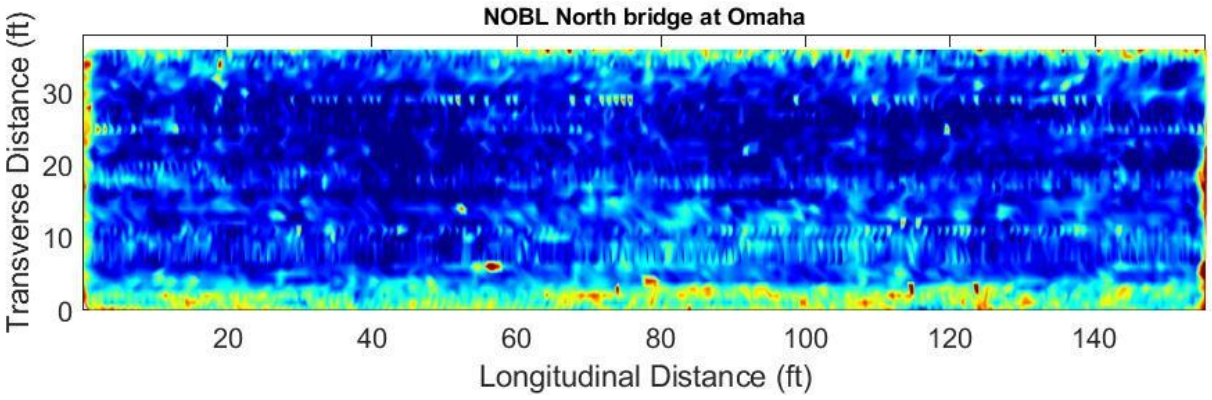

(a) NOBL North bridge at Omaha

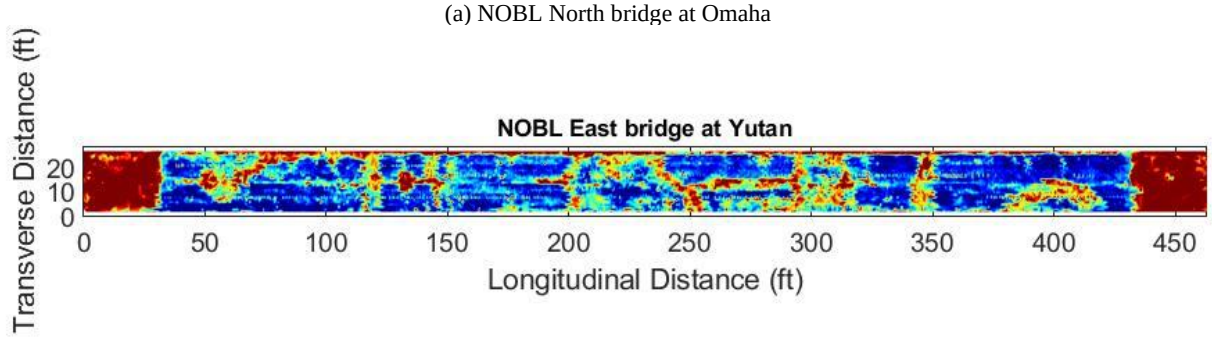

(b) NOBL East bridge at Yutan

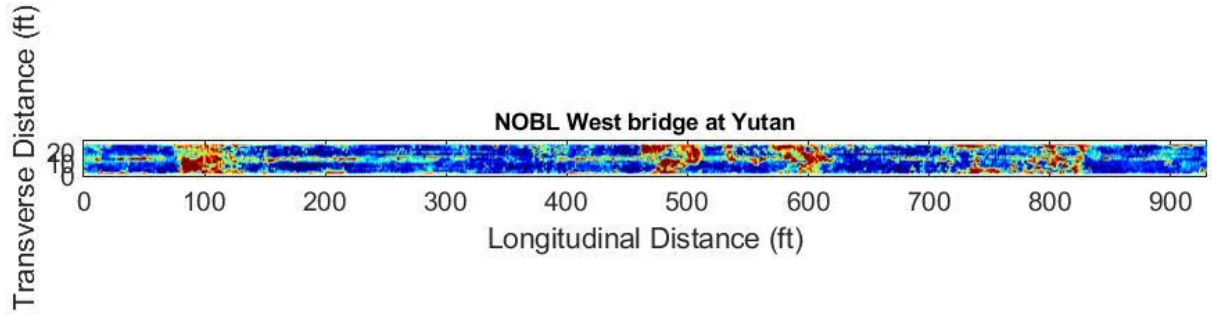

(c) NOBL West bridge at Yutan

Figure 3.4. Concrete deck GPR scan mapping results in the entire bridge width and length.

3.5 Intermediate conclusions

Task 2 of this project, as summarized in this chapter, provides the site characterization data for each of the bridge sites. This initial site characterization data consists of high-detailed, high-fidelity point clouds, finite element analysis models, and ground-penetration radar scans of each bridge site. This data is available for use by request. It is also envisioned that this data will support the project's goal of establishing a research and educational facility related to bridge health and the training of students/future engineers, bridge engineers, and bridge inspectors.

4 Site demonstration

4.1 Overview

The purpose of this chapter is to demonstrate how the NOBL facilities can be used by other researchers, engineers, students, etc. In this task, the focus was on the evaluation and assessment of bridge health (of the three bridges) using non-destructive testing techniques. To help identify dynamic responses, a series of accelerometers and strain gauges are mounted to the deck and girders of the bridges to collect vibrational response data during the live loads. These sensors were explicitly used by the UNL research team. Live loads were supplied to the bridges using a set of two triaxial trucks of 50-ton capacity (nominal weight).

Within this research, the primary measurement of the dynamic behavior was uniaxial piezoelectric accelerometers. This type of sensor has been shown viable for civil infrastructure (bridges and buildings) on various frequencies with notable results (Bose, et al., 2015) and (Martindale, et al., 2019). This sensor measures the vibrations of the bridge, which vary on truck speed, the weight of the truck, type of the bridge structure, condition of the deck, and sensor location or placement. To generalize the sensor response from the time domain, peak acceleration envelope values are summarized for each of the live loading cases (per bridge site). The objective of this task and chapter is to quantify the bridge response under various traffic loads to inform this project (in terms of modeling) as well as future research. This chapter closely relates to Task 3 of the project.

4.2 Sensor overview

Datasets from the bridge were collected using different types of sensors such as wired and wireless accelerometers, strain gauges, video monitoring, and displacement gauges. This was done for each pass of the live load (one or two triaxial trucks at various speeds, patterns, etc.). Note this chapter focuses exclusively on the uniaxial accelerometers, where Chapter 5 discusses the strain gages as deployed on NOBL North. Moreover, external researchers used wireless accelerometers, video monitoring, and

displacement gages in support of their FHWA SBIR Project (SC Solutions, n.d.). The upcoming section will provide a summary of the wired accelerometers.

4.2.1 Uniaxial accelerometers

To collect data during the field experiments a series of cabled uniaxial sensors were used to record the bridge vibration response of the bridge system under various load patterns. The uniaxial sensors are wired piezoelectric accelerometers, shown in Figure *4.1*. The PCB 393B04 accelerometers have a measurement range of ±5g and a broadband resolution of 3x10 µg root mean square (RMS). This type of sensor is a high-sensitivity seismic accelerometer that is extremely sensitive to indiscernible vibrations. It has been successfully used on bridge structures in the past, but is heavily used and validated in the NDOT Inverted Tee Project (Martindale, et al., 2019). This sensor collected data at a sampling frequency of 2096 Hz, which provided ample frequency resolution for post-processing to quantify the bridge response reliably.

Figure 4.1. Example placement of a wired uniaxial accelerometer.

4.3 Deck setup

During the field experiments, accelerometers are attached to the top portion of the deck of the bridge in each span at 1/3 points along the length. Figure *4.2* shows example instrumentation for NOBL North bridge. For this type of setup, accelerometers are typically placed in opposing pairs on the deck curb (north and south curbs on the deck). The deck setup for NOBL North is shown in Figure *4.3*. An assembly of the

NOBL East and NOBL West plots is compiled in Appendix B. Note that the sensor placements at NOBL East and NOBL West (at the Yutan site) closely mimic the placements at NOBL North. Due to the number of spans at NOBL West, only the east half of the bridge was instrumented by the UNL team. An upcoming and collaborative dataset for the entire bridge is still being processed by the external researchers (in collaboration with the UNL team) under the direction of SC Solutions.

(a) deck setup

(b)) girder setup for NOBL North bridge

Figure 4.2. Field accelerometer instrumentations as placed for NOBL North.

4.4 Girder setup

This accelerometer setup quantifies the response of each girder under the live load and is indicative of the potential independent girder response (due to insufficient transverse load distribution). This type of accelerometer placement was done on a single span on each bridge structure. The NOBL East girder setup was performed on only four girders of the first span of the bridge from the east side. In NOBL West accelerometer was mounted to the four girders from the east and middle span of the bridge. For the NOBL North accelerometers were installed only to five girders of the first span from the east. The number of girders available for sensor placements was a function of the available equipment and site conditions. The girder setup for NOBL North bridge is shown in Figure *4.3,* and Figure *4.4*. Note that the sensor placements on the bottom side of the girders at NOBL East and NOBL West (at the Yutan site) closely mimic the placements at NOBL North.

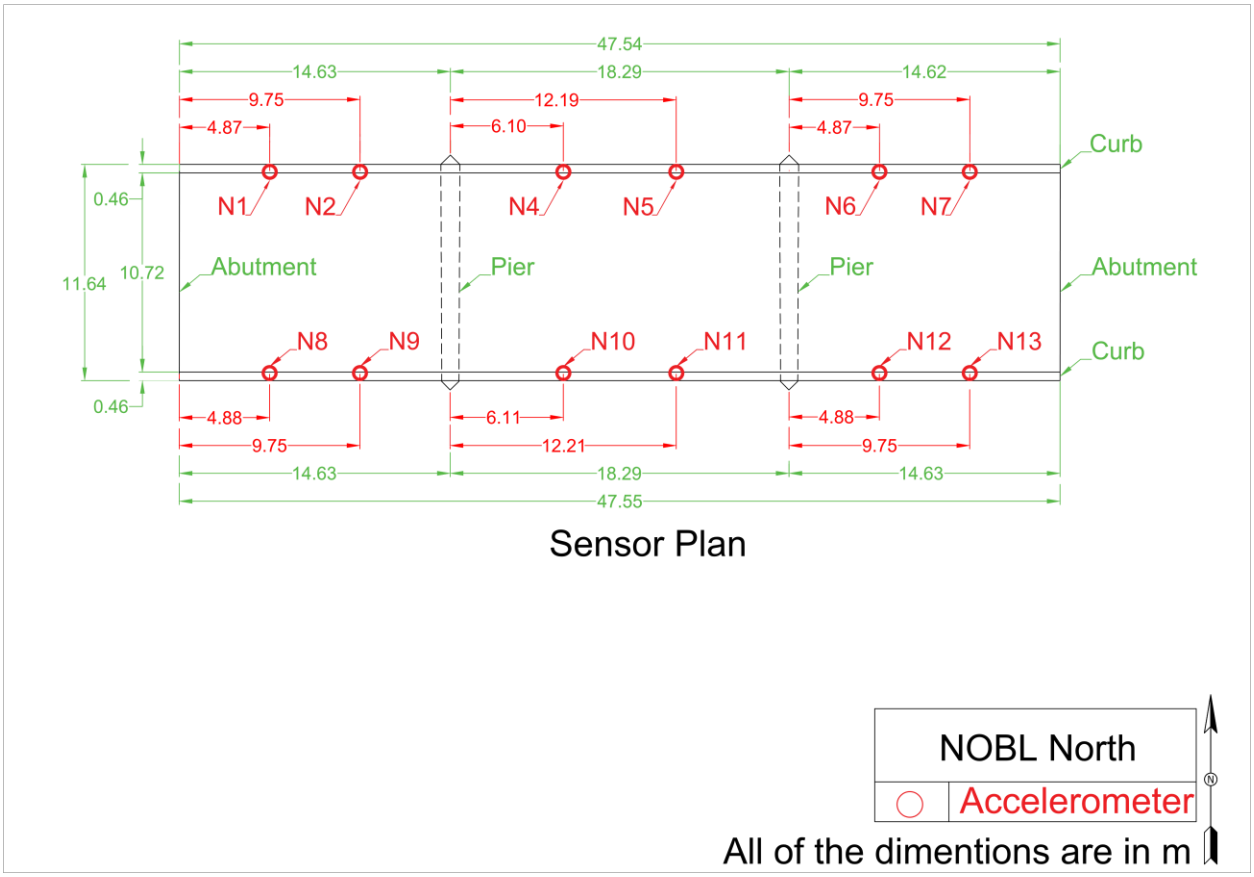

Figure 4.3. Locations of the accelerometer instrumented for NOBL North.

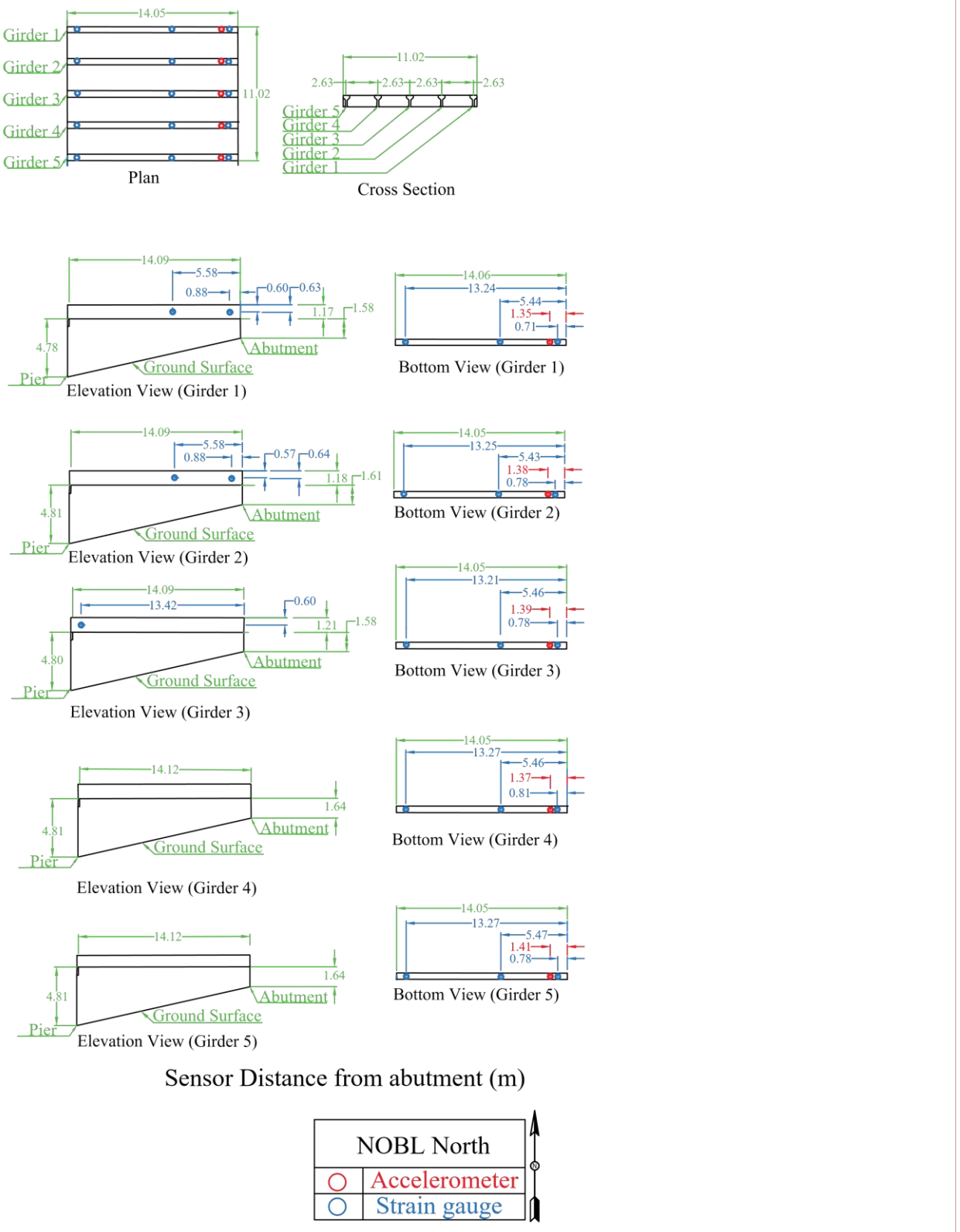

Figure 4.4. Locations of the accelerometers instrumented to girders for NOBL North.

4.5 Test procedure and truck arrangement

In this research and to quantify the bridge behavior under traffic loads, two triaxial trucks with known weights passed through the bridges many times with previously defined speed and spacings. Figure *4.5* shows the two trucks passing through the bridge. The test trucks were 3-axle vehicles with different weights, where one truck denoted as number one was 50,400 lb, and truck denoted as number two of 30,560 lb. Figure *4.6* shows the two trucks used for this bridge loading test at the NOBL West bridge at Yutan. The acceleration values were recorded for every single truck pass, as a function of time, and for both two trucks as side-by-side and back-to-back in one or two different traffic lanes. The tests were repeated for approximately sixty times for each of the bridges with various speeds ranging from 5-60 miles per hour. The load combination for NOBL North bridge is shown in Table 4.1. Load combinations related to the other two bridges can be found in appendix B, which closely mimics that of the NOBL North bridge.

(a) side-by-side truck passing

(b) Back-to-back truck passing

Figure 4.5. Example of side-by-side and back-to-back truck passing load test.

Table 4.1. Live load test for NOBL North bridge.

Run #	Dir.	Speed (mph)	Truck No.	Lane
1	W[1]	5	1	C [3]
2	E [2]	5	1	C
3	W	5	1	C
4	E	5	1	C
5	W	10	2	C
6	E	10	2	C
7	W	10	2	C
8	E	10	2	C
9	W	20	1	C
10	E	20	1	C
11	W	20	1	C
12	E	20	1	C
13	W	40	2	C
14	E	40	2	C
15	W	40	2	C
16	E	40	2	C
17	W	60	1	C
18	E	60	1	C
19	W	60	1	C
20	E	60	1	C
21	W	10	1	N [4]
22	E	10	1	N
23	W	10	1	S [5]
24	E	10	1	S
25	W	40	1	N
26	E	40	1	N
27	W	40	1	S
28	E	40	1	S
29	W	60	1	N
30	E	60	1	N
31	W	60	1	N
32	E	60	1	N
33	W	60	1	S
34	E	60	1	S
35	W-W [6]	10-10	2-1	S-N [8]
36	E-E [7]	10-10	2-1	S-N
37	W-W	10-10	2-1	S-N
38	E-E	10-10	2-1	S-N
39	W-W	40-40	2-1	S-N
40	E-E	40-40	2-1	S-N
41	W-W	60-60	2-1	S-N

42	E-E	60-60	2-1	S-N
43	W-W	60-60	2-1	S-N
44	E-E	60-60	2-1	S-N
45	W	5	1	N^{+} (9)
46	E	5	1	N^{+}
47	W	5	1	N^{+}
48	E	5	1	N^{+}
49	W/W (10)	10/10	1/2	N/N (12)
50	E/E (11)	10/10	1/2	N/N
51	W/W	10/10	1/2	S/S (13)
52	E/E	10/10	1/2	S/S
53	W/W	40/40	1/2	N/N
54	E/E	40/40	1/2	N/N
55	W/W	40/40	1/2	S/S
56	E/E	40/40	1/2	S/S
57	W/E	40/40	1/2	N/S (14)

1. Truck pass from East to West direction.
2. Truck pass from East to West direction.
3. Truck pass through the center of the bridge.
4. Truck pass through the North Lane of the bridge.
5. Truck pass through the South Lane of the bridge.
6. Trucks pass side-by-side from East to West direction.
7. Trucks pass side-by-side from West to East direction.
8. Trucks pass side-by-side in North and South Lane.
9. 2 [ft] away from the North edge of the North Lane.
10. Trucks pass back-to-back from East to West direction.
11. Trucks pass back-to-back from West to East direction.
12. Trucks pass back-to-back in the North Lane.
13. Trucks pass back-to-back in the South Lane.
14. Trucks pass back-to-back in the North and South Lane.

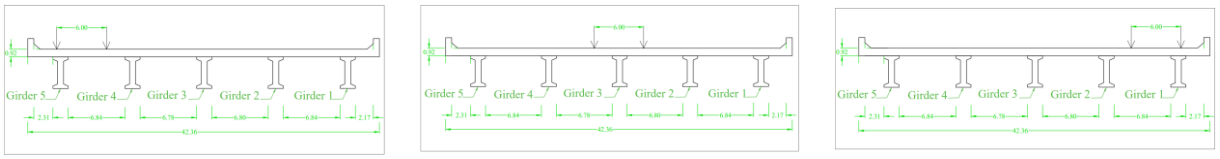

(a) North lane with 2 feet away from the curb (b) center lane (c) South lane with 2 feet away from the lane

Figure 4.6. Truck loading path at the NOBL North bridge at Omaha .

4.6 Analyzed data

The accelerometer data was processed in the time and frequency domain to apply instrument calibration factors and filtering. The data was processed using a Hampel filter for noise spikes and a finite impulse response (FIR) filter of order 4096 over two distinct ranges. The filtering range for the Yutan steel bridges was 2-25 Hz and for the Omaha concrete bridge at NOBL North from 5-25 Hz. This range varied slightly to capture only the lowest frequencies that correspond to the first mode. Using the processed data, frequencies can be determined as well as the maximum acceleration envelopes. The upcoming sections will provide a summary of each method.

4.6.1 Stochastic subspace identification

Stochastic subspace identification (SSI) is an algorithm that is commonly used to extract structural vibration characteristics from operational vibration measurements. Specifically in this project, the extended unweighted principal component method provided clear results (Martindale et al., 2019) using the Artemis platform (Döhler et al., 2017). Comparing these values for two of the bridge sites on ambient vibrations (not during the live loads), the first three modes of each bridge are experimentally (denoted as SSI) determined as summarized in Table 4.2. The results show very a good match with each other and consequently, the initial FEA models did not require an update for general usage. The first or primary mode of each structure was analytically captured within 3%, indicating an extremely good match. Note, that ambient vibrations were not collected at the NOBL East bridge at Yutan.

Table 4.2. Frequency of the bridge based on the stochastic subspace identification.

Mode	NOBL West Frequency (Hz)			NOBL North Frequency (Hz)		
	SSI	FEA	Percent difference	SSI	FEA	Percent difference
1	2.71	2.77	2.2	9.57	9.29	2.9
2	3.09	3.02	2.3	10.5	9.78	6.9

4.6.2 Maximum acceleration envelopes

The acceleration data can provide valuable information about the natural frequency, displacement, and dynamic characteristics of the bridge. Using the processed time histories, peak acceleration values can be determined for each test (or live load run) for a given location on the bridge. Figure *4.7* and Figure *4.8* shows the accelerometer peak values determined by each test (each truck run) at NOBL North. These plots indicate the peak values by each channel (each sensor) where the peak values obtained by the channel are shown in Figure *4.9*. Using these peak values, an envelope of the maximum acceleration experienced can be done for each live load run. This highlights the maximum response for a given location on the bridge and has been interpolated, not that the piers are presumed to have no acceleration. These acceleration maps identify the maximum acceleration envelopes and can be used to validate models and other future usages. Note that the figures presented here show the deck and girder time histories for NOBL North, where the complete set is in Appendix B.

4.7 Intermediate conclusions

Task 3 of this project provides an example facility demonstration. Under the guidance of the project team and the TAC panel, this resulted in an extensive live load test at each bridge. Within the live load tests, acceleration and strain datasets were captured and processed. This chapter outlined and summarized the acceleration data, including acceleration envelope data, which indicate the maximum acceleration for a given live load run. The next chapter will outline the strain data processing for NOBL North. The experimental datasets are available for use by request. It is also envisioned that this experimental data will support the project's goal of establishing a research and educational facility related to bridge health and the training of students/future engineers, bridge engineers, and bridge inspectors.

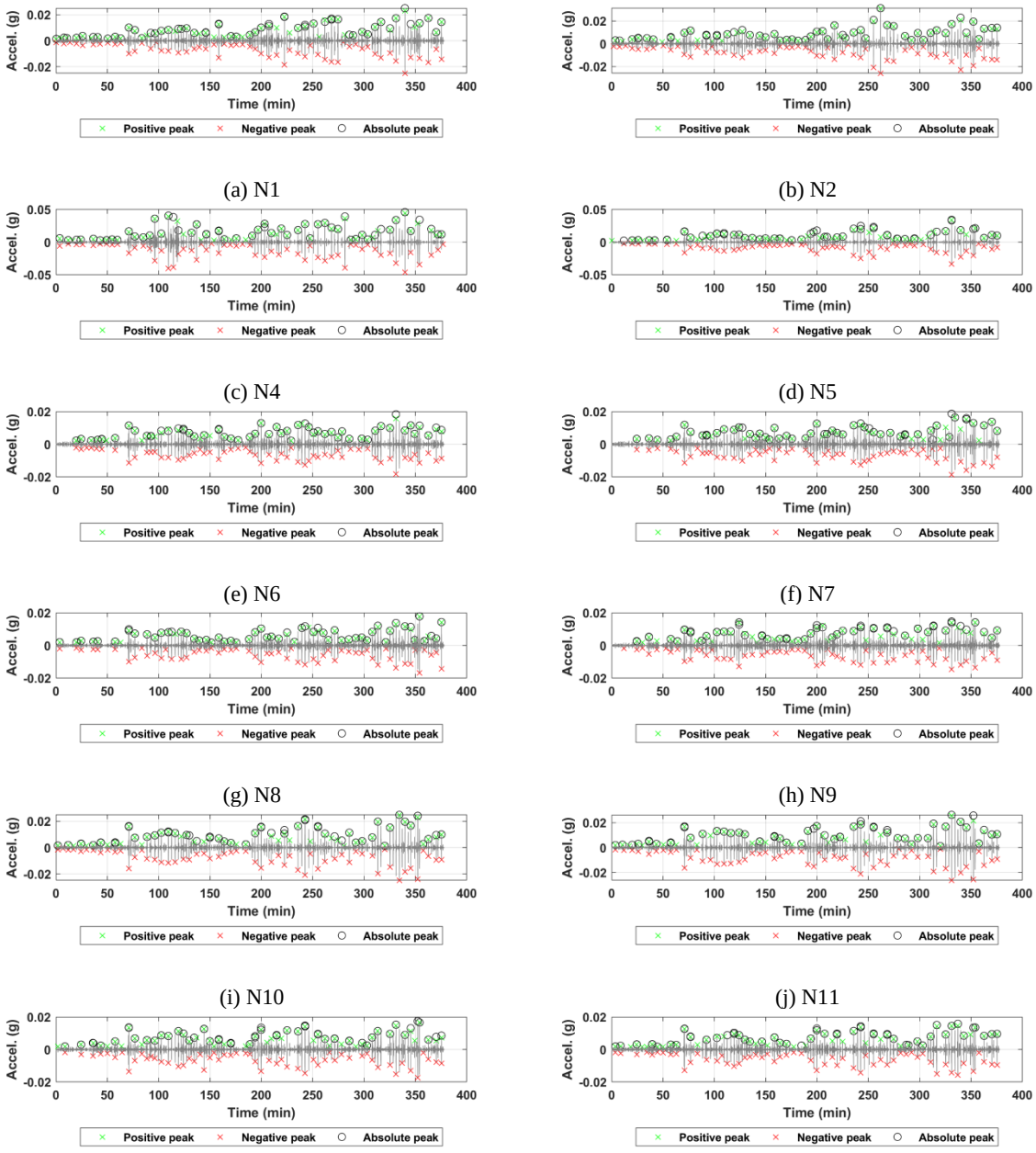

(a) N1 (b) N2

(c) N4 (d) N5

(e) N6 (f) N7

(g) N8 (h) N9

(i) N10 (j) N11

(k) N12 (l) N13

Figure 4.7. Acceleration time histories of the deck sensors for all truck passes at NOBL North.

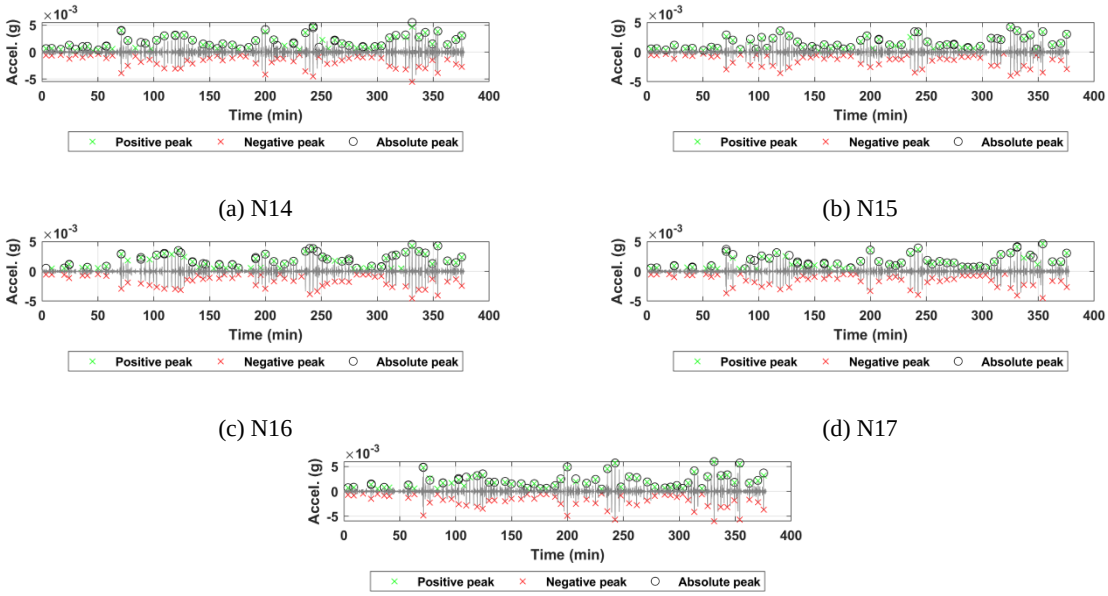

(a) N14

(b) N15

(c) N16

(d) N17

(e) N18

Figure 4.8. Acceleration time histories of the girder sensors for all truck passes at NOBL North.

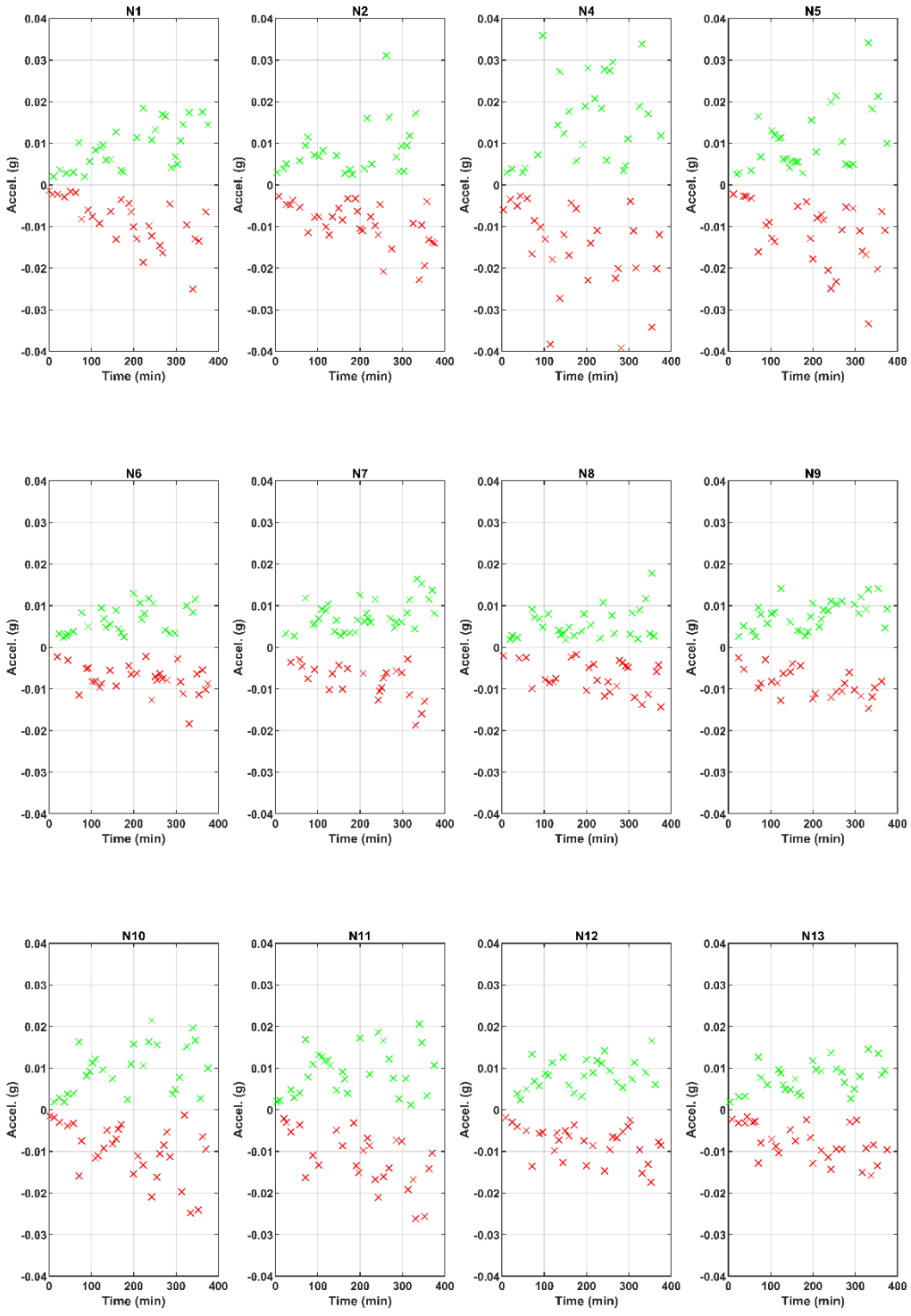

Figure 4.9. Maximum acceleration values for each truck pass at the NOBL North.

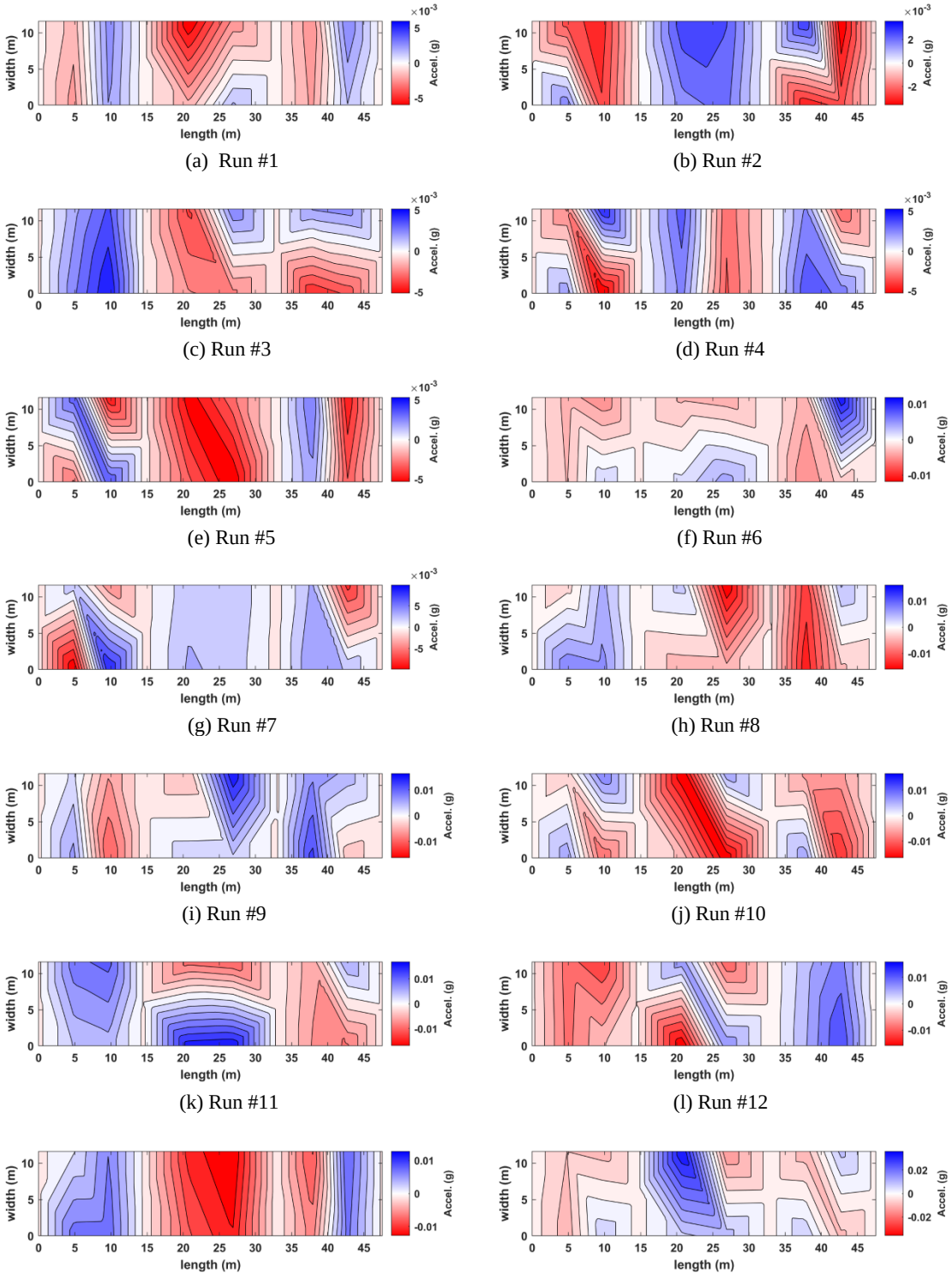

(a) Run #1 (b) Run #2

(c) Run #3 (d) Run #4

(e) Run #5 (f) Run #6

(g) Run #7 (h) Run #8

(i) Run #9 (j) Run #10

(k) Run #11 (l) Run #12

(m) Run # 13 (n) Run #14

Figure 4.10. Interpolated acceleration in plan view for 14 trucks passing at the NOBL North. Note the bridge is oriented to the north direction (up on the page is north).

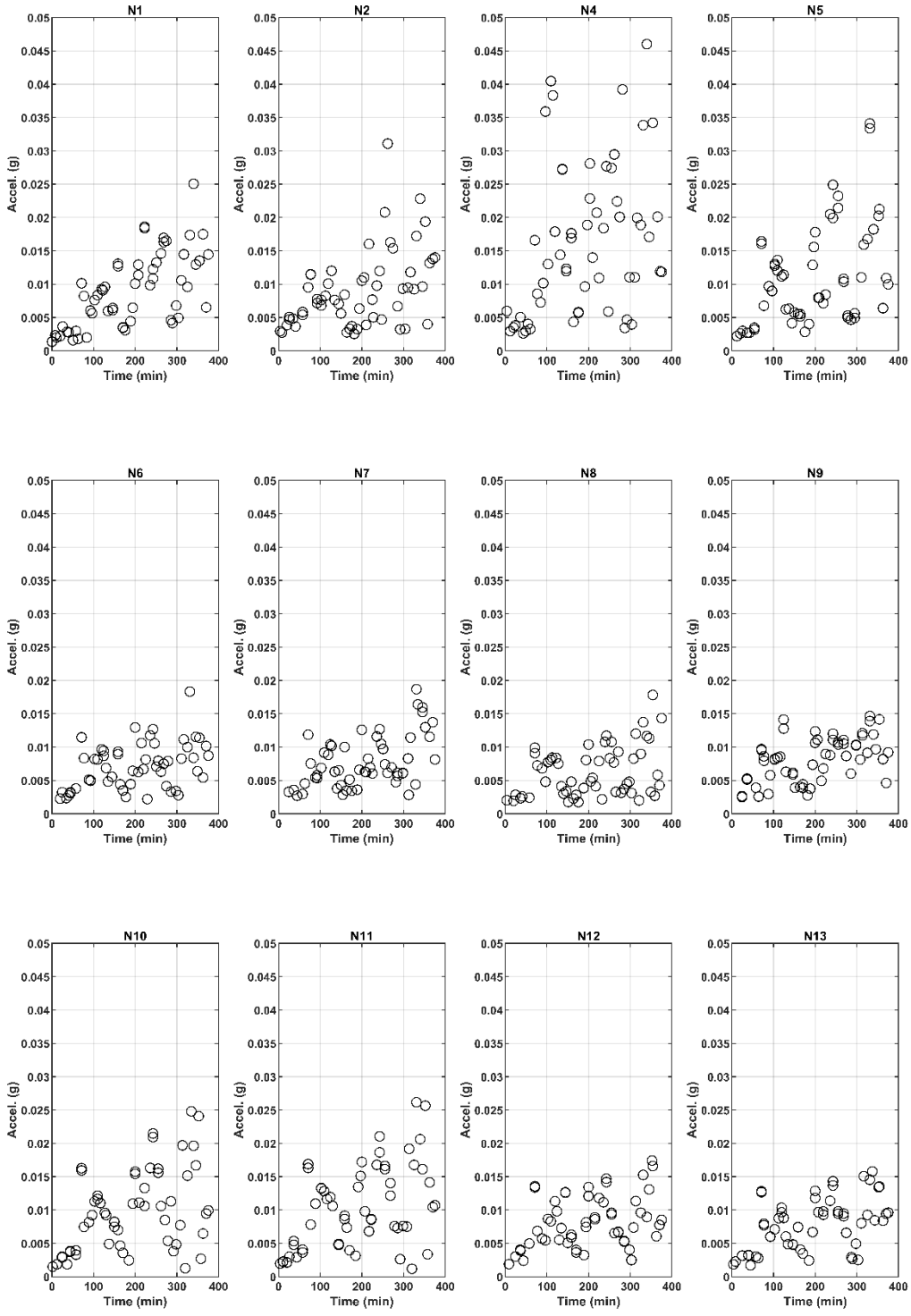

Figure 4.11. Absolute maximum acceleration values for each truck pass at the NOBL North.

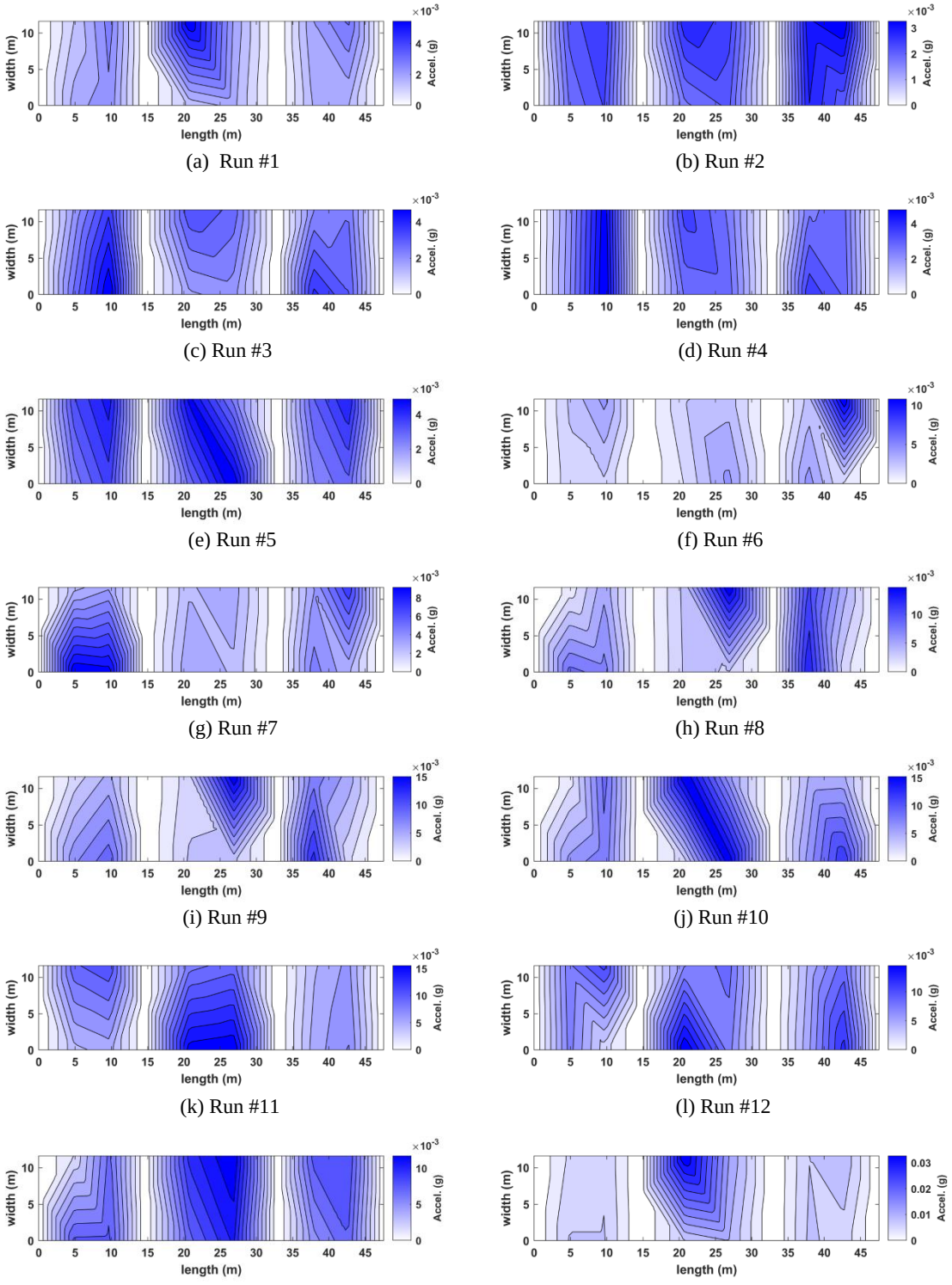

(a) Run #1 (b) Run #2

(c) Run #3 (d) Run #4

(e) Run #5 (f) Run #6

(g) Run #7 (h) Run #8

(i) Run #9 (j) Run #10

(k) Run #11 (l) Run #12

(m) Run # 13 (n) Run #14

Figure 4.12. Interpolated absolute-valued acceleration in plan view for 14 truck passings at the NOBL North. Note the bridge is oriented to the north direction (up on the page is north).

5 Strain gauge and updated FE models

5.1 Overview

This chapter provides a brief overview of load testing and analytical modeling performed for NOBL North at Omaha with a particular focus on strain gauges. Refer to Appendix C for additional data and discussion related to testing and modeling for this bridge supplementary to the information provided in this chapter. This chapter is included as a stand-alone given its detailed focus on the NOBL North site.

Strains measured during field tests were compared with analytical calculations. Finite element models (FEMs) in 2D and 3D were developed for this bridge using SAP2000, CSiBridg, AASHTOWare BrR, and COMSOL. Construction plans, initial site characterization geometric data, and supplementary correspondence provided by the Nebraska Department of Transportation (NDOT) primarily guided the geometry and material properties implemented in the bridge models. The analytical studies included explorations of various modeling assumptions, such as rotational restraint applied to the girder superstructure by abutments and piers.

Girder distribution factors (GDFs) quantify the proportion of live load carried by individual girders and are a common focus of field testing evaluations. The load test results were compared to AASHTO LRFD (2020) and AASHTO Standard Specifications (2002) approximate GDFs, and to GDFs determined from 3D FEMs. This study included an investigation of actual dynamic load amplification factors by comparing bridge responses when subjected to trucks traveling at varying speeds.

5.2 Prestressed Concrete Bridge Details

NOBL North at Omaha has nominal span lengths of 48, 60, and 48 ft, as shown in Figure 5.1. The bridge is comprised of five Nebraska Type 3A girders spaced at 8 ft 8 in, as shown in Figure 5.2 with 0-degree skew. The average deck thickness is 7.5 in., and the overhang is 3 ft-10 in. Refer to Chapter 2 for additional details.

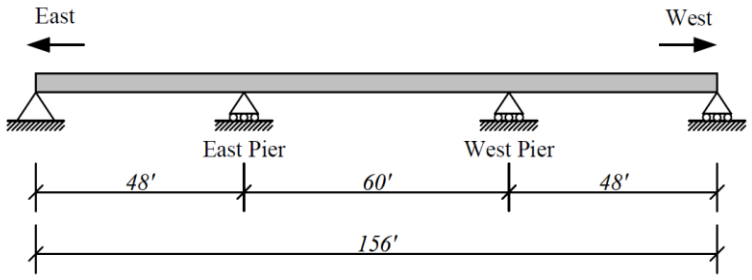

Figure 5.1. Schematic elevation of the bridge.

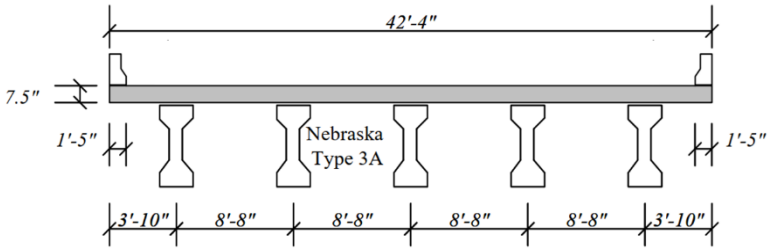

Figure 5.2. Schematic cross-section of the bridge.

5.3 Instrumentation

ST350 strain transducers from Bridge Diagnostics Inc (BDI) were installed on four cross-sections of the bridge, as shown in Figure 5.3. ST350 data was sampled at sufficiently high strain rates to capture dynamic strain amplification. Tests described herein were the short term and strain readings were zeroed at the start of each test run so that any thermally-induced strains were neglected.

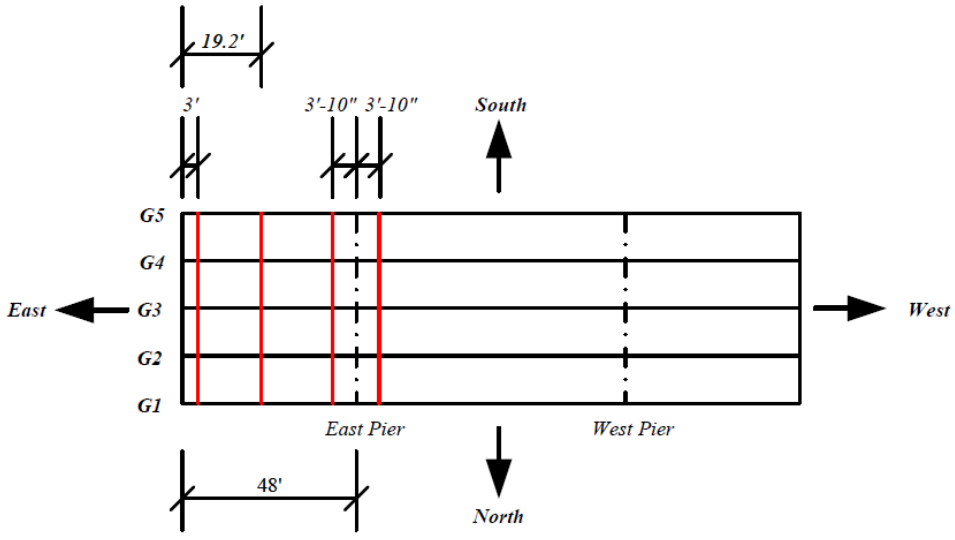

Figure 5.3. Strain transducers installation locations in the bridge.

The strain transducers were positioned 3 ft from the east abutment bearings' centerline. Similarly, maximum negative bending moments of the simple-made-continuous bridge were anticipated and investigated near the piers by installing strain transducers 3 ft away from the bearing centerlines on the east and west sides of the east pier. Each bearing centerline was offset 10 inches from the pier centerline, so that strain gages were located 3 ft-10 in. from the pier centerline. The positive moment was monitored at 0.4L of the east end span (19.2 ft to the east abutment centerline).

A total of forty-four (44) strain transducers were attached at the four selected cross-sections. Figure 5.4 shows the strain locations on the girder and the bottom of the concrete deck. On each girder, strain transducers were attached to the center of the bottom flange. Additionally, girder web strain transducers were installed to determine the neutral axis and evaluate the bridge behavior of non-composite and composite sections. A strain transducer was attached to the bottom of the concrete deck 2 in. from the side of the top flange of the center girder (G3) for each cross section. Transducers were attached to the concrete with adhesively bonded metal tabs, as shown in Figure 5.5.

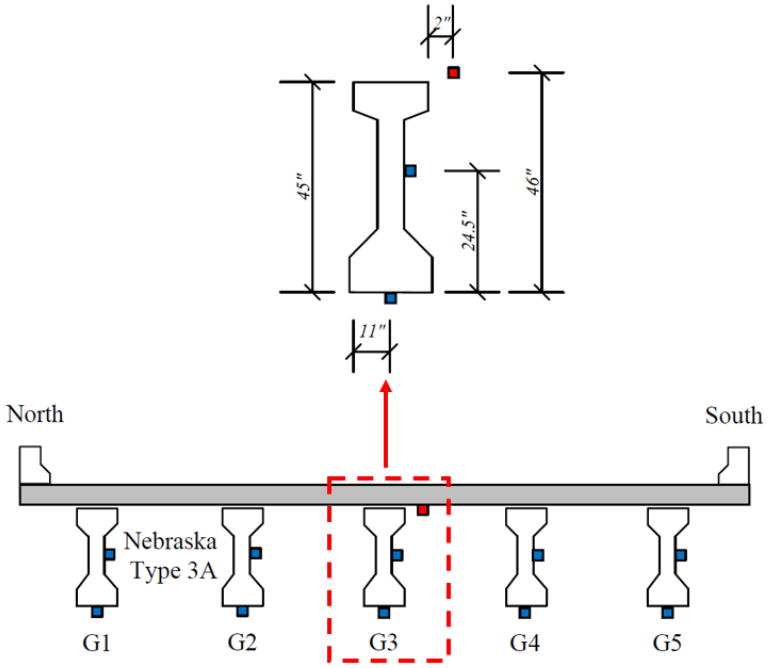

Figure 5.4. Strain transducers installation locations in the bridge cross-section.

Figure 5.5. Strain transducer attached to the bottom flange of girder.

5.4 Load Cases

Two 3-axle trucks (Legal Type 3 vehicles) were provided by NDOT for NOBL North loading. Figure 5.6 shows one of the trucks used in the load tests. Only total truck weight was supplied, not weight by axle or wheel, so each test truck axle load was assumed to be proportional to the Nebraska Legal Type 3 configuration. Girder distribution factors were evaluated by driving trucks across the bridge at various transverse locations, as illustrated in Figure 5.7. A total of 32 load tests were performed, with various combinations of one or both trucks, truck directions, truck transverse positions, and speeds from crawling (approximately 5 mph) up to about 60 mph. Refer to Appendix C for additional details.

Figure 5.6. Load test truck A.

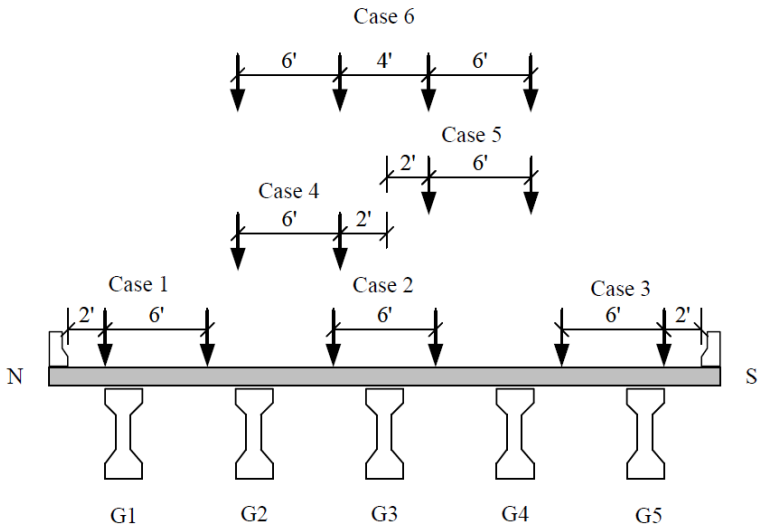

Figure 5.7. Transverse locations of trucks on the bridge.

5.5 Finite Element Analysis (FEA)

For this study, both two-dimensional (2D) and three-dimensional (3D) finite element analyses (FEA) were applied to investigate structural behavior. Analyses were performed using SAP2000™, CSiBridge™, AASHTOWare Bridge Rating™ (BrR), and COMSOL™ finite element programs. The following types of models were used:

Line-girder analysis:

- SAP2000 model with beam elements,

3D FEM analysis:

- 3D CSiBridge model with shell elements for slab and beam elements for girders,
- 3D AASHTOWare BrR model with shell elements for slab and beam elements for girders,
- 3D COMSOL model with solid elements for slab and girders.

Refer to Appendix C for additional details.

5.6 Load Test and FEM Results

CSiBridge results were used for comparison to the test results. To compare the test results with FEA models, the FEA values were taken at the locations where strain transducers were installed.

5.6.1 Load Test Strain Plotted with Time

Transducers located at 0.4L of the east end span measured the positive moment response and were used to quantify GDFs. As truck A crawls at approximately 5 mph from east to west at the center, Figure 5.8 shows the measured values for the transducers at 0.4L of the end span. Time (seconds) is shown on the x-axis, and microstrain ($\mu\varepsilon$) is shown on the y-axis. As expected for Run 1, peak strains occurred on the bridge's middle girder (G3). At the bottom of G3, the maximum strain value is about +32 $\mu\varepsilon$. Because of the intended

transverse symmetrical load position, the strains for G2 and G4 should be similar. However, G4 has greater strains than G2 presumably due to a slightly off-center transverse truck positioning.

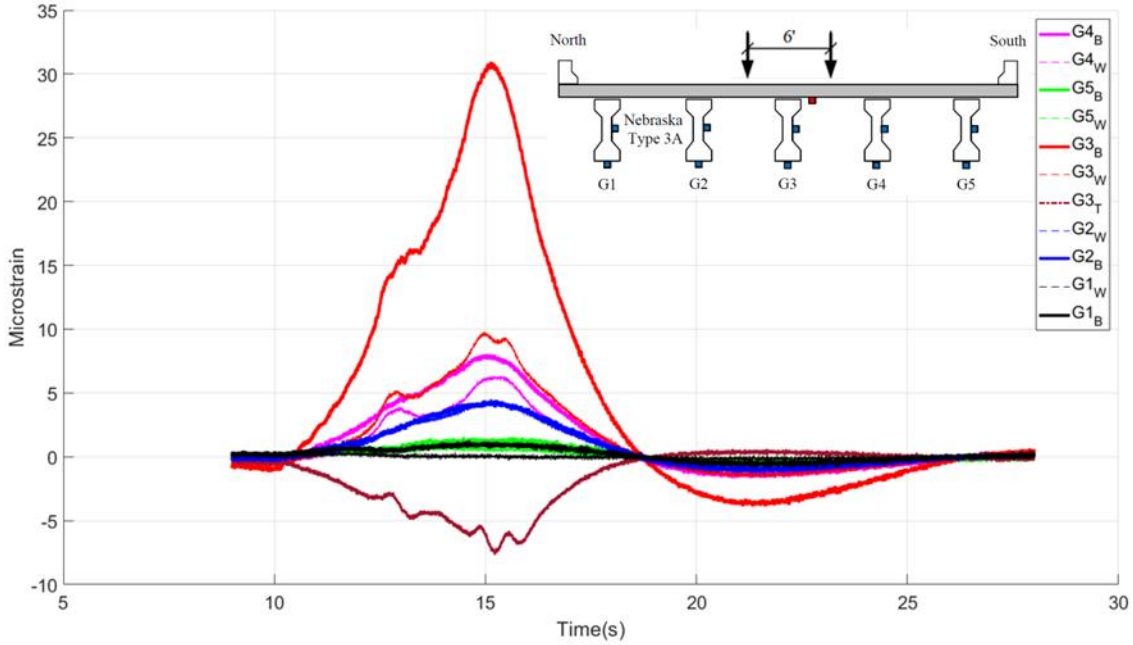

Figure 5.8. Strain transducer results at 0.4L end span for one truck A at the center from east to west.

Unexpectedly, the test strains at G2 are similar at the bottom flange and the web, implying axial rather than flexural deformation. This result does not seem reasonable, yet the recorded strains are nonzero and outside the noise band, suggesting that the data is real and not spurious noise. This abnormality may reflect torsional influences on the girder cross-section strains that could have obfuscated the primary flexural response. In situations where loads travel along the center of the bridge width, exterior girders G1 and G5, as expected, carried a lesser load. Refer to Appendix C for additional details.

5.6.2 Test and FEM Strain and GDF Results

GDFs were determined using strain data measured at the bottom of the girders. This project used the same GDF model as Stallings and Yoo (1993). The Wi was assumed to be one for both interior and exterior girders, which slightly overestimated interior girder GDFs and underestimated exterior girder GDFs. To

make comparisons with AASHTO LRFD GDFs, the GDF model has been modified to account for the number of lanes loaded.

The following load test GDFs are based on single or two trucks traveling at low speeds for various transverse locations. FEM GDFs were derived from CSiBridge models both with and without diaphragms. Figure 5.9 and Figure 5.10 show the bottom girder strains at 0.4L of the end span and corresponding GDFs for one truck traveling from east to west along the bridge centerline and 2 ft from the north and south barrier railings. Figure 5.9 shows that, as expected, the maximum strain occurred at G3 for center lane cases and exterior girders (G1 or G5) for trucks passing adjacent to barriers. However, there are some noticeable differences between strains from load tests and FEMs. With single-lane loading at the center, the maximum positive strain at G3 is about +31 με, close to the FEM at G3 for the model without diaphragms. However, other girders exhibit lower load test strain results than FEM. The bottom flange load test strain sum in Figure 5.9 is about half that of FEM.

Possible reasons for the lower strains observed in load tests than in FEMs include partial fixity conditions at supports (although test data did not indicate this effect to be significant for this bridge), higher concrete moduli of elasticity than expected according to AASHTO, and potential stiffening from barriers. Figure 5.10 shows that the load test GDFs at 0.4L of the end span were more similar to the results of the FEM without diaphragms, which indicates that the diaphragms are not acting with transverse flexural continuity through the girders. On close inspection of the NOBL North bridge at Omaha drawings, the diaphragms are found to only interact with the girders through compression bearing. Reinforcing at the top of the diaphragms ties the diaphragms to the deck, but no reinforcing crosses the interfaces of diaphragms and girder flanges or webs. Therefore, complex torsional effects and compression-only contact interactions may also be influencing both flange and web strains that are currently unaccounted for in the 3D FEM models.

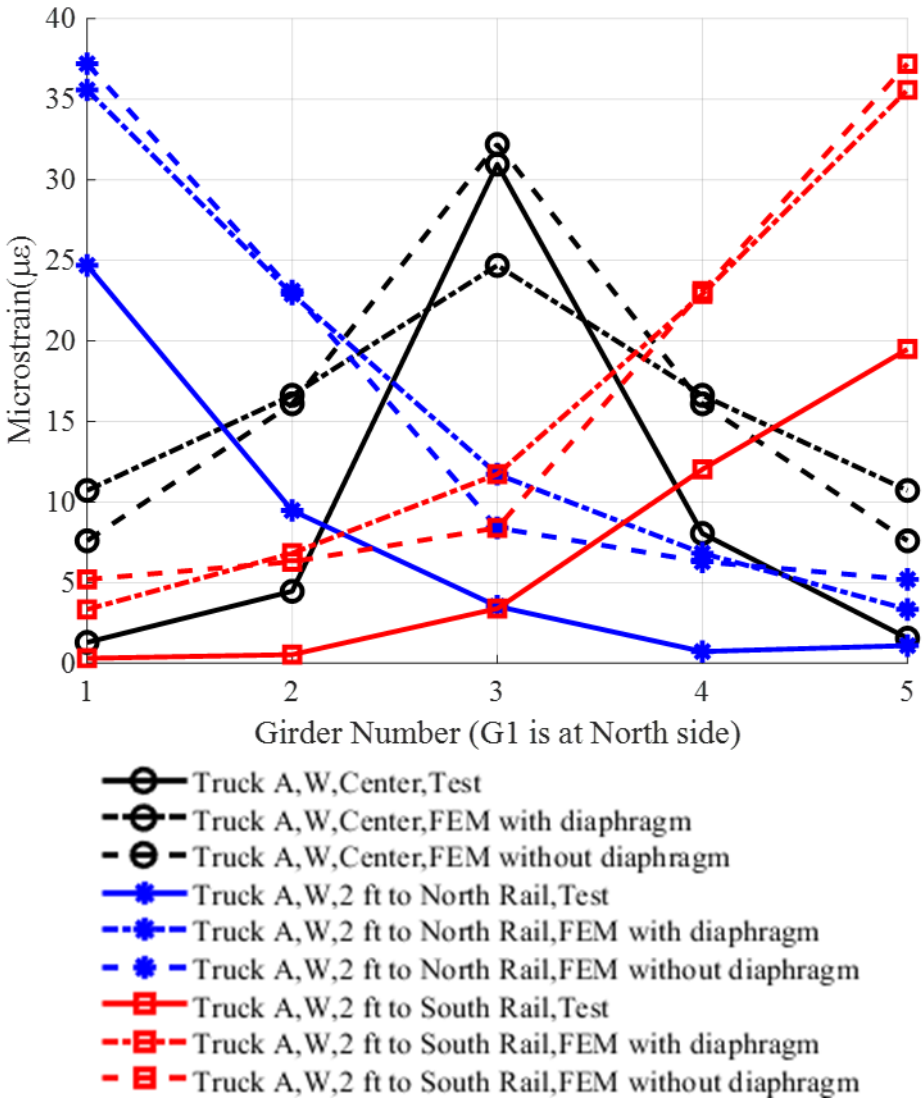

Figure 5.9. Positive strain at 0.4 L of east end Span, west direction loading.

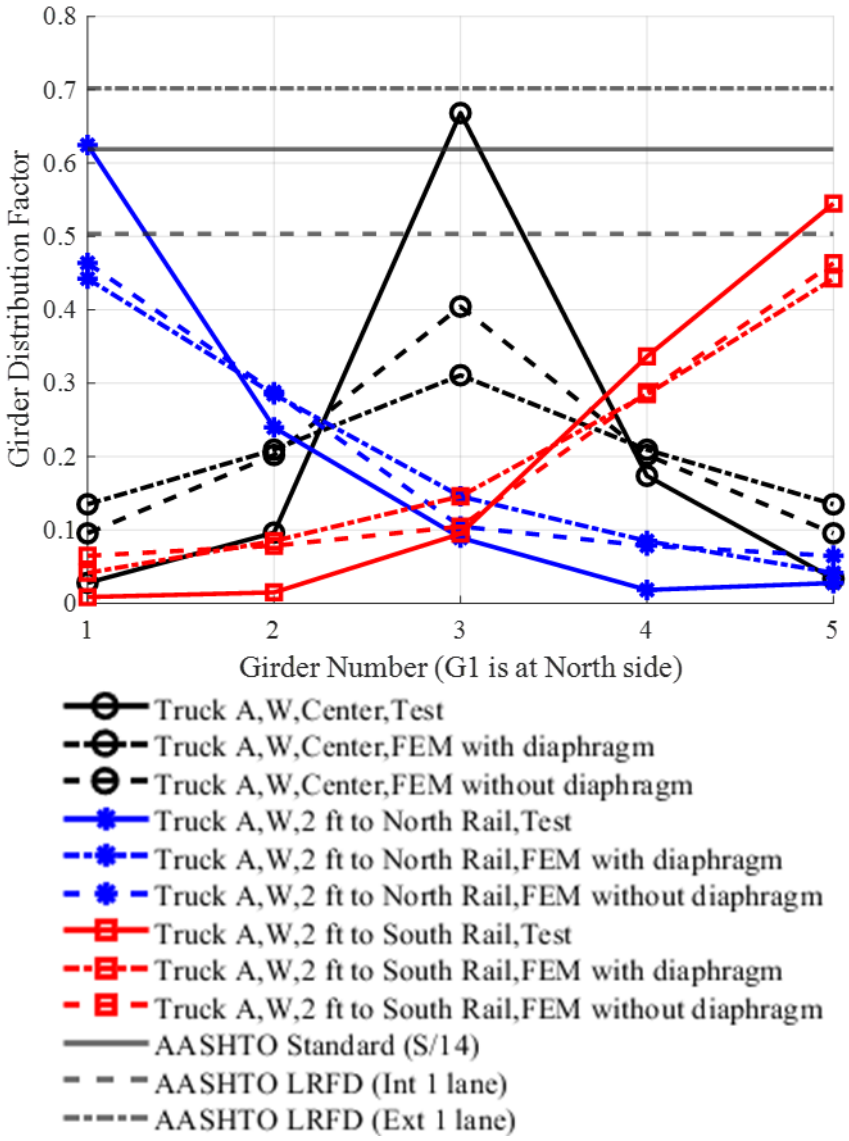

Figure 5.10. GDF from positive strain at 0.4 L of east end span, west direction loading.

5.6.3 Dynamic Load Allowance Results

Dynamic load factors (DLFs) were calculated as the ratio between the maximum dynamic strain and the maximum crawling speed (static) strain at the bottom of girders. DLFs were found to be negligible.

5.6.4 Neutral Axis Location

The neutral axis location was determined using an assumed linear strain profile through the depth of girders and pairs of strain measurements taken at the bottom flange and web. For Girder G3 at 0.4L along the end span, the neutral axis obtained from strain measurements was 36.22 in., only 3% lower than a theoretical composite section location of 37.39 in. obtained using as-built drawings for geometry and moduli of elasticity estimated according to AASHTO.

5.7 Intermediate conclusions

This stain gage task aimed to develop computational models representing the NOBL North bridge at Omaha (S036 02040L) and collect physical data to validate the FEM models. The models and load test data can be used by other researchers using the NOBL North site. During the field load tests, one-lane and two-lane loaded cases were taken into account to calculate the GDFs and DLFs and provide insight into the bridge behavior. NE Legal Type 3 trucks were used for the tests, and different locations, crawling speeds, and normal truck speeds were considered.

CSiBrdge, SAP2000, COMSOL, and AASHTOWare BrR were used to develop 2D line girder analysis and 3D FEMs. Shell, beam, and solid elements were used in the FEMs. CSiBridge models without barriers and with or without diaphragms were compared with load test results to determine if the model represents actual bridge behavior. Load tests and FEM analyses were also used to compare GDFs with AASHTO Standard (2002) and AASHTO LRFD (2020). Below are several takeaways from this chapter:

- The measured GDFs are generally close to those obtained from FEM analysis, but with some exceptions: For one truck or two trucks side-by-side in the center lane, GDF at G3 is higher than AASHTO interior GDFs (accounting for the Multiple Presence Factor (MPF)).
- Load test GDFs for exterior girders are smaller than AASHTO lever rule GDFs.
- For 0.4L of the end span, load test GDFs are more similar to computational results without diaphragms assumed continuous through girders.

- The sum of bottom girder load test strains is about half of the sum from FEM (potentially influenced by barrier participation, underestimated modulus of elasticity, partial fixity of supports in the natural bridge, and perturbation of measured strains by torsional effects).
- Load tests observed localized behavior near piers at the bottom of the concrete deck inconsistent with beam theory, likely a result of concentrated wheel loads near instrument locations.

The results indicate that the trends of strains and GDFs between load tests and FEMs are reasonably close; however, the magnitudes have some noticeable differences. The load tests recorded lower strains than predicted by the FEMs, possibly because some structural parameters (barriers at the middle span, diaphragms, modulus of elasticity, etc.) were not measured, complex torsional stress and strain fields perturbed the measurements, or due to hardware, software, or user errors with the strain transducer system. Future research would be beneficial to instrument diaphragms and barriers in positive moment regions to improve understanding of diaphragm behavior, update load distributions, estimate composite barrier participation, and more closely examine potential torsional effects in girders. Strain transducers could also be installed on one or both piers to investigate vertical strains associated with continuity participation and braking loads. It is also recommended that the load test be performed with heavier loads and that the modulus of elasticity be verified with non-destructive testing.

6 Future work and summary

6.1.1 Overview

The goal of this unique project was to establish the Nebraska Outdoor Bridge Lab (NOBL). The NOBL facility is located at two sites, Yutan and Omaha, Nebraska. It consists of three bridges, two steel bridges over the Platte River at Yutan as well as one concrete bridge over the Glenn Cunningham Reservoir at Omaha. All of these bridge sites are minimally not in regular service or completely out of service. The NOBL facility aims to become a national research and educational facility for bridge health and testing. This means supporting various stakeholders, including the University of Nebraska-Lincoln (UNL), other academic or research entities, the Nebraska Department of Transportation (NDOT), other transportation departments, practicing engineers, equipment/technology vendors, and the greater community. This facility aims to provide unique opportunities for students/future engineers, bridge engineers, bridge inspectors, and any other interested parties.

- To establish this facility, four tasks were completed and summarized in this document. Tasks included (1) Site Staging, (2) Site Characterization, (3) Facility Demonstration, and (4) Reporting. Within this project, the following key accomplishments were made:
- A safety and operational document summarize activities, procedures, and risks at this laboratory facility. This document is available on the NOBL project's website.
- The two steel bridge structures at Yutan were secured via fencing to create a safe laboratory environment.
- High-fidelity and high-detailed geometric surveys were conducted of all the bridge sites using lidar and uncrewed aerial systems. This provides accurate data at the centimeter level on the current condition of these structures. This data can be viewed on the NOBL project's website.
- Finite element analysis (FEA) models were constructed for all the bridge sites within the CSiBridge software platform.

- Ground penetrating radar surveys were conducted on all the bridge sites to quantify the condition of the bridge decks as well as the approach slabs.
- An extensive field demonstration was done at all three bridge sites. This involved an array of sensors to quantify the dynamic bridge behavior under various truckload combinations. Live loads included two 50-kip (nominal) weight triaxial trucks that loaded the bridges at various speeds, patterns, spacings, etc. Each bridge was subjected to approximately 60 different loading configurations. This data has been processed, filtered, compiled, and available for use by others upon request.
- A detailed strain gauge study was conducted at NOBL North and summarized as part of the site demonstration.
- The site demonstration was conducted in collaboration with external researchers from SC Solutions and its subaward grants to the University of Nevada-Reno and the University of California, Los Angeles. Ongoing collaborative work continues in publishing and marketing this data which will also increase the visibility of the site.

6.1.2 Online presence and available data

A critical part of this project is marketing and establishing a baseline set of data for use by others. To this end, the NOBL project has a dedicated website at http://nobl.unl.edu. This webpage exists at the University of Nebraska-Lincoln College of Engineering level for an extended lifespan. This website provides an overview of the project, the site, and describes some of the data available. This site will also host the final report for this project as well. Moreover, the generated datasets from this project are available for use by others by request. The available data includes for all bridge sites:

- Plan drawings.
- High-fidelity and high-detailed geospatial datasets in terms of three-dimensional point clouds and 2D orthomosaic images.

- Constructed finite element analysis (FEA) models in CSiBridge.
- Constructed FEA models in other platforms for the NOBL North bridge site only. This includes SAP2000, CSiBridg, AASHTOWare BrR, and COMSOL.
- Ground penetrating radar survey data and (likely) delamination maps.
- Extensive accelerometer and strain gage data from the experimental campaign (as detailed in Chapters 4 and 5)

For interested parties concerning NOBL site usage or data availability/sharing, please use one of the following methods:

- Online form submission (google forms) at: **https://forms.gle/4SgMcpUoPCQgMyCt7/**
- Email the site principal investigator, Prof. Richard L. Wood at: **rwood@unl.edu**
- If the above two methods do not provide a response within a week or so, please call or send an email inquiry to the UNL Department of Civil and Environmental Engineering

6.1.3 Future site usage plans

Since the establishment of this site, the site has been used by non-UNL personnel including NDOT, NSP, Omaha Police Department, and the Nebraska Wing of Civil Air Patrol (Fremont Cadet Squadron) . Some of the current plans for the use of this site include current and pending research projects at UNL as well as potentially at least six courses:

- CIVE 102 – Introduction to Geomatics for Civil Engineers
- CIVE 441 – Steel Design I
- CIVE 443/843 – Advanced Structural Analysis
- CIVE 839 – Bridge Design
- CIVE 891 – Non-Destructive Testing Methods

- CIVE 891 – Infrastructure Assessment Techniques

6.1.4 Future research needs

As this project progressed and with conversations with internal and external stakeholders, some future research needs include:

- Coring of the deck at select locations to confirm deck delamination.
- Live load testing with large loads to confirm/verify the elastic modulus of various bridge elements.
- Verification of load redistribution by undoing various assemblies (inclusive of the pin and hanger connections at Yutan).
- Controlled scour simulations and the effect on the superstructures.
- Extreme loads (destructive in nature) that apply high temperature or river collision loads.
- Validation of various non-destructive/remote sensing technologies and methodologies.

7 References

1. American Association of State Highway and Transportation Officials (AASHTO). (2020). AASHTO LRFD Bridge Design Specifications, 9th Ed., Washington, DC.

2. American Association of State Highway and Transportation Officials (AASHTO). (2002) Standard Specification for Highway Bridges, 17th Ed, Washington, D.C.

3. Bose, S., Nozari, A., Mohammadi, M. E., Stavridis, A., Babak, M., Wood, R., ... & Barbosa, A. (2016). Structural assessment of a school building in Sankhu, Nepal damaged due to torsional response during the 2015 Gorkha earthquake. In Dynamics of Civil Structures, Volume 2 (pp. 31-41). Springer, Cham.

4. Döhler, M., Andersen, P., & Mevel, L. (2017, May). Variance computation of modal parameter estimates from UPC subspace identification. In *IOMAC-7th International Operational Modal Analysis Conference*.

5. Liao, Y., Mohammadi, M. E., Wood, R. L., & Kim, Y. R. (2020). *Improvement of Low Traffic Volume Gravel Roads in Nebraska* (No. SPR-P1 (16) M040).

6. Martindale, G., Watson, D., Kodsy, A. M. K., El-Khier, M. A., Wood, R. L., & Morcous, G. (2019). *Performance evaluation of inverted tee (IT) bridge system* (No. Report No. 2611214037-001). Nebraska. Department of Transportation.

7. NOBL. (n.d.). Retrieved from https://engineering.unl.edu/outdoorbridgelab/

8. Ocel, J. M. (2021). *Historical Changes to Steel Bridge Design, Composition, and Properties* (No. FHWA-HRT-21-020). United States. Federal Highway Administration. Office of Infrastructure Research and Development.

9. Pashoutani, S., & Zhu, J. (2020). Ground penetrating radar data processing for concrete bridge deck evaluation. J. Bridg. Eng, 25, 04020030.

10. SC Solutions. (n.d.). Retrieved from https://www.scsolutions.com/sc-solutions-awarded-phase-ii-of-the-small-business-innovative-research-sbir-program-to-develop-digital-twin-and-computer-vision-technology-for-operational-monitoring-and-maintenance-of-bridges/

11. Stallings, J. M., & Yoo, C. H. (1993). Tests and ratings of short-span steel bridges. *Journal of Structural Engineering*, 119(7), 2150-2168. https://doi.org/10.1061/(ASCE)0733-9445(1993)119:7(2150).

APPENDIX A.

NOBL Safety Protocol and Information

Table of contents

Nomenclature

Name	Description
ANSI	American National Standards Institute
ASTM	American Society for Testing and Materials
ATV	All-terrain vehicle
DHHS	Department of Health and Human Services
EHS	Environmental Health Services
EPA	Environmental Protection Agency
GFCI	Ground-fault circuit interrupters
NDOT	Nebraska Department of Transportation
NIOSH	National Institute for Occupational Safety and Health
NOBL	Nebraska Outdoor Bridge Laboratory
PFD	Personal flotation device
PPE	Personal protective equipment
SPF	Sun protection factor
OSHA	Occupational Safety and Health Administration
UNL	University of Nebraska-Lincoln
USGS	United States Geological Survey

1 Introduction

The Nebraska Outdoor Bridge Laboratory (NOBL) facility consisting of two decommissioned steel bridge structures near Yutan/Venice located on Highway N-92 and one decommissioned concrete bridge structure located on Highway N-36 in north Omaha. These structures are planned to be used for research, education, and outreach as a joint venture between the University of Nebraska and Nebraska Department of Transportation. The objective of the NOBL project is to transform the two bridge sites (for a total of three bridges) into a national research and educational facility for bridge health and testing, which allows accessing various nondestructive and destructive evaluation and test verifications. The project PI is Dr. Richard L. Wood and co-PIs are Drs. Christine E. Wittich, Joshua S. Steelman, Jinying Zhu, Daniel G. Linzell, and Jay A. Puckett. In addition, a total of 36 students and postdoctoral research associates as of Fall 2019, including Dr. Mohammad Ebrahim Mohammadi, are predicted to participate in this research project at various stages. Mr. Peter Hilsabeck will serve as the Department of Civil and Environmental Engineering lab manager. All the project participants, including students, lab staff, contractors, researchers, scientists, and engineers, shall refer to and comply with the procedures outlined within this document as well as their own institution or firm's health and safety policies for the minimum safety requirements.

2 Site Hazard Assessment and Safety Training

As laid out by the University of Nebraska-Lincoln (UNL) Environmental Health and Safety (EHS) Virtual Manual, it is essential to perform a site hazard assessment to identify potential hazards (EHS 2020a and b). This should be done prior to the beginning of the fieldwork each day and as the tasks or potential hazards change. Note that within this project, the bridge sites are planned only to be accessed for inspection or any fieldwork during the daylight hours and in non-inclement weather conditions. Members of the team will be dispatched in at least pairs. Members will not access the worksite(s) without at least one other team member in the immediate area.

Reading through this safety protocol does NOT substitute for taking the minimal required safety courses and reading thru the UNL EHS Virtual Manual resource that has been set up for the NOBL team. Individual

training and equipment records will be maintained by the NOBL team and available upon request. Note all interested parties should complete the NOBL Lab Interest Form available on the website or at https://go.unl.edu/nobl_form.

3 Equipment Description and Safety

The bridge structures span over the Platte River (two steel bridges outside of Yutan/Venice) and the Glenn Cunningham Reservoir (concrete bridge in north Omaha) and access to various elements of these bridge is required. Much of the observation and many of the tasks will be done from the ground, on a ladder, from an NDOT snooper truck (vehicle-mounted aerial lift), boat, or, if absolutely necessary, from a tube and clamp-style scaffolding temporarily erected at the site. An all-terrain vehicle (ATV) may also be used to transport tools and equipment to the site.

Snooper truck

3.1 Snooper truck

Within this project, aerial lifts are used to access girders and transverse beams, lower bridge deck parts to install sensors, collect images, lidar scans, or visual assessments. OSHA (2020) requires that operators of aerial lifts receive training and demonstrate competency. The operators of the aerial lifts within this project are supplied and trained by NDOT. The lab manager will train riders of the lift of the minimal equipment-specific training needed.

Within this project, the snooper truck will be used to access to hard to reach areas for data collection and visual assessments on a regular basis. The snooper truck(s) is provided by the Nebraska Department of Transportation (NDOT). In addition, NDOT provides the operators and organizes the transportation of the snooper to the project site. As these are decommissioned bridges, there is no need for traffic control considerations during the operation of snooper. Note that, in addition to instructions from the NDOT operator, the Department of Civil and Environmental Engineering lab manager, Mr. Peter Hilsabeck will

train personnel and researchers who are planning to work on the snooper truck (EHS 2020b). The following items are determined based on the NDOT regulations and procedures for using the snooper truck:

1. Maximum number of personnel on the platform
2. Fall protection type during working on the platform (as well as fitting of equipment)
3. Area of operation
4. Rescue plan

The following equipment will be used at various stages of the project to provide access or transport the needed equipment for tests:

1. Ladders
2. Boat
3. An all-terrain vehicle or ATV
4. Scaffolding, tube, and clamp-style

It is vital for project participants to review and follow the outlined safety regulations in regard to using a ladder, boat, ATV, and scaffolding installation and usage. Therefore, testing can be performed effectively in a safe manner. To use other means of transportation or access that is not listed here, please contact and consult with project PI, Dr. Richard L. Wood.

3.2 Ladder info

The following procedures must be considered when using ladders. For a more detailed explanation, please see OSHA publication 3124-12R 2003, Stairways and Ladders: A Guide to OSHA Rules provides additional guidance.

1. Select ladders based on anticipated use, surrounding hazards, and rated load capacity
2. Ladders should be tied off if it is anticipated that they could slide or gusty winds are anticipated. People should discontinue the use of a ladder if inclement weather approaches.

3. Do not exceed the safe working height of the ladder, or ascend the ladder higher than recommended by the manufacturer
4. Do not position a ladder in an area where it can be bumped or dislodged
5. Face the ladder while climbing and descending
6. Always maintain three points of contact

3.3 Boat

Within this project, a boat, likely a flat bottom Jon boat outfitted with a trolling motor, is used to access the structural and nonstructural elements of the bridges for various goals. This includes but is not limited to visual inspection, remote sensing data collection, and sensor installation. In general, the boat must be registered with the state of Nebraska and only used by an experienced operator who is trained and over the age of 18. The following rules listed below should be followed during boat operation. For more detailed information and description about these rules, please check the boat operation regulations detailed by the Nebraska Game and Parks.

1. Boat operators should not exceed a speed of more than 5 MPH (8.05 km/hr).
2. The boat should not operate in an area marked off or set aside as a prohibited area.
3. The boat should not be left in any public waters.
4. Boat operators born after 12/31/1985 must complete a Boating Safety Course and be in possession of a course certificate when operating the boat. The course is offered by Nebraska Game and Parks (www.outdoornebraska.gov/boatereducation).
5. The boat should be inspected before and when loaded. The boat must retain at least one-half of the total depth of the boat above the water when measured at the center of the boat and must meet the requirement of the manufacturer's capacity plate.
6. The following equipment is required to be onboard anytime your boat is afloat. Refer to the Nebraska Game and Parks guide for specific details:
    a. Life jackets/Flotation devices

b. Fire Extinguisher (if motorboat has enclosed fuel tank, enclosed space or enclosed engine)

c. Oars

d. Bailing bucket

e. Muffler

f. Whistle or bell

g. Backfire flame arrestor

h. Ventilating

7. Every boat (except sailboards) must carry one U.S. Coast Guard-approved Type I, II, III, or V life jacket of the suitable size for each person on board. Each vessel (except personal watercraft canoes, kayaks, and sailboards) must carry one U.S. Coast Guard-approved Type IV throwable device.

8. Boat in use from sunset to sunrise (at night), must display the following lights as specified. No other lights may be used, except a spotlight for difficult navigation.

   a. The white light must be visible for a distance of at least two miles. The red and green lights must be visible for a distance of at least one mile. The green light should be visible from the starboard side and the red from the port side.

   b. All sailboats, when mechanically powered, shall display the lights required for that class of a mechanically powered boat. All motorboats and sailboats must carry a lantern for a flashlight for emergencies. All vessels, while at anchor, must display the 360-degree white light (except while anchored in a docking or anchorage area).

3.4 All-terrain vehicle

Within this project, the ATV is used for a similar proposal to that of a boat that is used to access the structural and nonstructural elements of the bridges for various goals. This includes but is not limited to visual inspection, remote sensing data collection, and sensor installation. Within this project, it is planned

that only Mr. Peter Hilsabeck, Department of Civil and Environmental Engineering lab manager, will operate ATV to move tools and equipment. In addition, the following rules will be followed during the usage of ATV:

1. The area should be assessed for weather, road, soil, and water conditions before accessing the area on the ATV.
2. Anyone must wear a helmet when riding an ATV.
3. No riders, in addition to the operator, are allowed.
4. Tools and equipment should be properly restrained before moving the vehicle.
5. The ATV will be properly restrained and safely transported to the work sites.

More information on the safe operation of ATV's may be found in the UNL EHS All-Terrain Vehicle Safe Operating Procedure found at https://ehs.unl.edu/sop/s-atv.pdf. In the future, any authorized person who has not previously operated the ATV should learn and familiarize himself with the vehicle prior to operating using the online resources that provide free training. For example, www.ATVsaftey.org.

3.5 Scaffolding, tube and clamp-style

Within this project, tube and clamp-style scaffolding will be used as a last resort to access hard to reach areas of the bridges either for detailed inspection, data collection, or sensor installation. No suspended scaffolding will be used. The bridge lab manager will serve as the competent person and oversee the rental, design, installation, use, and tear down of the equipment.

OSHA (2020a) has specific and detailed requirements concerning the use of scaffolding to protect against injury resulting from falls, collapse, or failure of the support structure, falling tools, materials, or debris. Similar to portable ladders, the following general requirements apply:

1. The foundation upon which scaffolding rests must be firm, level, and capable of carrying the load without settling or displacement
2. Unstable objects such as boxes, rocks, bricks, etc. must not be used as supports or for leveling

3. Use must be consistent with the rated load, and the design must meet or exceed OSHA's standard planking must also adhere to OSHA design and use requirements, including overlap/securing and maximum spans. Scaffolding higher than 60 ft (18.2 m) in height must be designed by a Professional Engineer
4. Scaffolding must be inspected before each use
5. Damaged or defective scaffolding must be immediately removed from service
6. Guardrails or personal fall arrest systems are required
7. Using scaffolds is prohibited during storms and high winds and in near proximity to overhead electrical lines. (Note: No overhead power lines are currently installed in the areas)
8. Surfaces must be kept clean and free of excess debris, tools, or other trip hazards to ensure enough spacing for working

The scaffolding installation should meet the standards in several provisions, as described by OSHA (2020a):

1. Assess the work area, site conditions, and work to be performed.
2. Conduct a pre-operation inspection to verify that all scaffold components are functioning correctly and/or are correctly assembled.
3. Keep the platform free from tripping hazards such as hand tools, equipment, or materials.
4. No wheels will be used on the footings of the scaffolding.
5. Guardrail height—The height of the top rail for scaffolds manufactured and placed in service after January 1, 2000, must be between 38 inches (0.9 meters) and 45 inches (1.2 meters). The height of the top rail for scaffolds manufactured and placed in service before January 1, 2000, can be between 36 inches (0.9 meters) and 45 inches (1.2 meters)
6. Crossbracing—When the crosspoint of crossbracing is used as a top rail, it must be between 38 inches (0.97 m) and 48 inches (1.3 meters) above the work platform.

7. Midrails— Midrails must be installed approximately halfway between the top rail and the platform surface. When a crosspoint of crossbracing is used as a mid-rail, it must be between 20 inches (0.5 meters) and 30 inches (0.8 m) above the work platform.
8. Footings—Support scaffold footings shall be level and capable of supporting the loaded scaffold. The legs, poles, frames, and uprights shall bear on base plates and mudsills.
9. Platforms—Supported scaffold platforms shall be fully planked or decked.
10. Guying ties and braces—Supported scaffolds with a height-to-base of more than 4:1 shall be restrained from tipping by guying, tying, bracing, or the equivalent.
11. Capacity—Scaffolds and scaffold components must support at least four times the maximum intended load.
12. Training—Employers must train each employee who works on a scaffold on the hazards and the procedures to control the hazards.
13. Inspections—Before each work shift and after any occurrence that could affect structural integrity, a competent person must inspect the scaffold and scaffold components for visible defects, which could affect the structural integrity and to authorize prompt corrective actions.
14. Erecting and Dismantling—When erecting and dismantling supported scaffolds, a competent person must determine the feasibility of providing a safe means of access and fall protection for these operations.
15. To inspect manila or plastic (or other synthetic) rope being used for top rails or mid-rails.
16. Follow the manufacturer's allowable load limit for the scaffold components and platforms, along with recommended bracing to ensure a rigid and structurally-sound scaffold.

4 Safety Topics

4.1 Fall protection

This section discusses the fall protection safety details for personnel who will be at heights over six feet while using ladders, aerial lifts (snooper truck), and work on scaffolding. Working at heights poses the

hazard of falling; as a result, the safety precaution in regard to fall protection is 100% tie off at all times whenever personnel is working over 6 feet in height off of the ground or next highest structure. This will be accomplished using guardrails, if available and appropriate personal fall protection equipment, such as a harness and lanyard.

4.2 Personal protective equipment (PPE)

The project participants should use personal protective equipment (PPE) to enhances safety during the fieldwork. The PPE gear selected for personnel should be selected, fit, and maintained appropriately to protect workers according to their activity and reviewed by the lab bridge manager prior to being issued. In general, the PPE used should consist of the items listed below based ANSI, ASTM, and OSHA regulations/standards:

1. **High visibility apparel including vests, coats, hats, and pants** that meet ANSI/ISEA 107-2004ANSI Class II, III / ISEA "American National Standard for High-Visibility Safety Apparel."
2. **Long pants and sleeved shirts** other than high visibility apparel
3. **Footwear** to protect foot, ankle, and toes that meet ASTM F2413.
4. **Gloves** to protect hands.
5. **Hard hats** that meet the requirements specified by ANSI Z98.1.
6. **Safety glasses and goggles** to protect eyes that meet the requirements specified by ANSI Z87.1-1989.
7. **Hearing protection** must be used by personnel when working in high noise environments. If high noise levels are suspected, contact the EHS office to have a documented hazard assessment conducted. They can help identify less noisy methods, equipment and get UNL participants enrolled in the program, if necessary.
8. **Tyvek suits** should be used in case of general clean-up or if there is a potential to be exposed to an environmental hazard.

9. **Air-purifying respirators** that meet NIOSH approval with an oil-proof P class filter must be used by personnel if the fieldwork will involve exposure to airborne dust, toxic gaseous chemicals, or biological hazards. If this equipment is to be used, each participant must be enrolled in the UNL Respiratory Protection Program. Contact the UNL EHS office for further information and to set up an initial training session.
10. **Coast Guard-approved life jackets** that roll head up must be worn when working over water and not 100% tied off for fall protection. Life jackets will also be worn when in the boat or working near water or wading water.
11. During fieldwork, clothing to provide protection from the sun, including hats, sunglasses, light-colored long pants, and sleeve shirts, as well as routine use and frequent reapplication of sunscreen with at least a sun protection factor (or SPF) of 30, is advisable. Details about the heat stress can be found in the UNL EHS Virtual Manual (EHS 2020).
12. **To protect from cold stress, layered and loose clothing** can provide insulation, comfort, and proper blood circulation. In addition, to reduce body heat loss, the head, hands, face, and ears should be covered. Details about the cold stress can be found in the UNL EHS Virtual Manual (EHS 2020).
13. To avoid insect stings and bites, use **insect repellants** as directed on the label and wear long pants and sleeve shirts, gloves, closed-toed footwear that covers the ankle. In addition, do not wear perfumes, hairsprays, or other scented products that may attract insects. Details about insect stings and bites can be found in the UNL EHS Virtual Manual (EHS 2020).

4.3 Other potential site hazards

During the site survey for other hazards, personnel should also consider the environmental hazards as discussed by EHS (2020):

a. Traffic Control: All three of these bridges have been decommissioned by the State of Nebraska, meaning that there should be no active motor vehicle traffic in and on these bridges. Team members

working on-site will park vehicles in the designated spots away from traffic on active roadways and any other equipment being operated it the area. They will wear high visibility clothing and remain vigilant for moving equipment at all times.

b. Lack of Illumination: spotlights or flashlights should be provided to increase visibility.

c. Walking Sloped Surface Site Access: As the project sites potentially require the personnel and researchers to access and work on the sloped surfaces and grounds, the site assessment survey must also approximately identify these areas and plan to prepare appropriate access and egress. In addition, the plan should consider falling materials within the sloped areas, identify loose rocks or soil.

d. Overhead or Adjacent Area Hazards: There are no railroads, pipelines, or electrical lines over the site area.

e. Confined Space: At the Yutan site, there are utility boxes and manholes (utility or maintenance holes) that are considered "confined spaces" and which can partially be flooded, as seen in the past. Personnel and researchers are prohibited from working in any confined spaces unless adequate protection has been provided. If the entrance to a confined space is deemed necessary, personnel will contact the EHS office immediately before any work is performed. EHS will conduct a site audit and assist in the entry process.

f. Biological Hazards: The girders should be assessed for the presence of bats or pigeon droppings or fungus prior to any work within these areas. Due to potentially harmful consequences such as Histoplasmosis, personnel and researchers must use appropriate PPE as discussed in the earlier section of this report before work. In addition, the site assessment should consider potential dangers such as snakes and other wildlife. Personnel must use the appropriate PPE when working in areas of long grasses and dense vegetation. Lastly and more importantly, the site survey must plan to reduce the identified potential hazard by changing and modifying the test or data collection procedures or introduce administrative control to mitigate the risk. For more details about safety assessments, please see the Job Safety Assessment Procedures provided by EHS (2020).

4.4 Considerations for working near or wading water

Within this project, it is predicted that the team will potentially work near or wade a shallow body of water to collect data or inspect the bridge conditions. Here, the shallow water refers to a water body with a depth of one ft or less. In these conditions, the team should minimally follow procedures listed by the guide to safe field operations of the United States Geological Survey or USGS (2020):

1. The team should review the field plans to determine the best section for wading and if any potential risks are noted and the maximum velocity and depths that may be encountered.
2. The team should determine whether the river stage is rising or falling and should be aware of rapid rises in the river stage before wading and anticipate and allow for changes in water flow conditions. To determine raising or falling of water level, one practical idea is to select an object (such as rock, stump, mark along the bank, etc.) that is just above the water surface and keep watching it to determine if the river stage is rising or falling.
3. The personnel who are wading the water should always probe the stream bed ahead with a rod when moving in the water.
4. The personnel who are wading the water should keep their feet spread apart and alignment of legs parallel to the flow for better stability.
5. If the water velocity becomes too high for safe wading, personnel in the water must not turn around as when the greater area of the front or back of the body is exposed to the current, sweeping downstream becomes more likely. The best practice for the personnel is to back out carefully and bracing themselves with the wading rod.
6. Personnel should wear a personal flotation device (PFD) or coast guard-approved life jackets when wading water.
7. Personnel who are wading the water should not wear boots or waders that are too tight or too loose.
8. Personnel who are wading the water should be aware of sand channels where potholes, quicksand, and scour can be hazardous; in particular, the areas close to bridge piers are prone to scour.

9. Personnel who are wading the water should be aware of slick, steep banks, and swampy areas and watch for debris and ice drifting.

5 Chemical Safety

As OSHA (2020c) described, the chemical hazards and toxic substances introduce various types of health hazards, including but not limited to irritation, sensitization, and physical hazards (e.g., flammability, corrosion, and explosibility). It is anticipated that very few chemicals (spray paint, adhesives, adhesive remover such as acetone and gasoline as a fuel source) will be introduced to the work sites. All empty containers, visible waste, contaminated rags, paper, and PPE will be collected and properly disposed of in the engineering bridge lab in Lincoln.

Other chemical hazards pertain to the possibility of an exposure to lead, crystalline silica, and/or asbestos that is already in use on the bridges as lead paint, concrete, and construction material (e.g., concrete, sprayed-on insulation or fireproofing). It is anticipated that areas on existing structures will be minimally disturbed on the surface in an area of one square inch to ensure that the sensor will properly adhere to the structure. If any greater disturbance (including surface painting (in excess of routine sensor marking), grinding, sanding, welding, etc.) to an area of the structure is planned, personnel must contact the EHS office immediately before any work is performed for a complete hazard assessment. Power tools used on site should be equipped with a HEPA-filtered method of dust collection.

Information on how personnel and researchers possibly are exposed to the lead, silica, and asbestos is provided in this section.

- Asbestos and crystalline silica are naturally occurring minerals, while lead is a naturally occurring metal whose use and removal is highly regulated by OSHA and the EPA.
- All three are known or probably human carcinogens.
- Other potential health hazards:

    - Asbestos has shown effects including asbestosis (inflammation and permanent damage to the lungs) and other nonmalignant lung and pleural disorders.
    - Respirable crystalline silica also has shown permanent damage to the lungs, an increased presence of tuberculosis (in those with silicosis), chronic pulmonary disease (COPD), and other illnesses such as renal disease.
    - Lead has shown effects on the blood, kidneys, and nervous, immune, and cardiovascular systems.
- Potential routes of exposure to the body are primarily achieved thru inhalation of dust or fumes and ingestion.
- Good personal hygiene and handwashing should be practiced. No smoking, eating, or drinking should occur in areas where these substances may be present.

6 Tools

Throughout the project, various tools may be used by researchers and personnel to collect data, plan, and conduct tests. Researchers not only have to be trained to use the equipment properly but also must follow the standard procedures to use the equipment as detailed by the equipment manufacturer. In addition, if equipment requires training, the users must participate the required training prior to using the equipment.

6.1 Communication

Within this project, the researchers and team must plan in regard to communication devices depending on the scope of the fieldwork during testing or data collection. All the researchers and personnel that are present within the project site during site visits, tests, or data collections must be equipped with a communication means and be able to communicate with each other directly. The communication can be through two-way walkie-talkies or cell phones.

6.2 Power tools, electrical safety and extension cords

As laid out by OSHA (2020g), the cordless, battery powered tools used within this project must be equipped with safety switches and guards. Power tools should be equipped with HEPA-filtered dust collection systems, or additional safeguards should be in place. Contact EHS for more information. In addition, a workspace where the equipment is used and wires are routed should be kept as dry as possible to prevent accidents. All extension cords should be rated for outdoor use, equipped with GFCI protection and regularly inspected to ensure that they are in good condition. Any damage to the insulation, prongs or wiring and the extension cord should immediately be removed from service and properly discarded. Only double insulated power tools should be used on site.

To prevent hazards associated with the use of power tools, OSHA (2020g) recommends the following precautions listed below. For more detail about the power tools, please visit the OSHA (2020g).

1. Users must not carry or hold a power tool by the cord
2. Users must not yank the cord to detach the power tool cord from the receptacle
3. The cords and wires must be placed and stored away from heat, oil, and particularly sharp edges
4. The power tools should be disconnected during storage
5. The power tools should be disconnected from power prior to servicing and cleaning, and when changing accessories such as blades, bits, and cutters
6. Personnel that are not involved in using the power tools must remain at a safe distance from the work area
7. If needed, the operator of the power tools should secure the working area with C-clamps or a vise
8. The operator of the power tools must avoid accidental starting by not hold fingers on the switch button while carrying a plugged-in tool
9. The operators must follow the equipment's user manual instructions for charging and maintaining the equipment including but not limited to lubricating and changing accessories
10. The operators must be positioned comfortably and balanced when operating power tools

11. The operators must be equipped with appropriate PPE when operating the power tools such as portable hand grinder or drill.
12. The operators of power tools must remove all damaged power tools from use and tag the damaged equipment appropriately
13. If extension cords are used within the project, the outlets they are plugged into such as on the snooper truck or the cords themselves must be equipped with ground-fault circuit interrupters (GFCI) as described by OSHA (2020h)

7 Emergency Response Action Plans

Each team will be trained on the proper way to contact authorities in case of an emergency. The information will be specific to each worksite and contain the proper street address to give to the 911 dispatcher. Written information will be available at each site and to each member of the team. A basic first aid kit will be present at the worksite as a part of the regular tools and equipment taken to the worksite. It will be inspected and maintained by the NOBL team.

- **Yutan/Venice:**
    - The site is referred to as "Highway 92 (or West Center Road) and Platte River **Decommissioned** Bridges". It will be necessary to state which bridge (east or west) as well as the location on/under the bridge.
    - Depending on which bridge (east or west), either the Yutan or Waterloo Volunteer Fire Department will be dispatched to respond. Both have the equipment, trained members on the regional dive team and are trained to perform over the water and swift water rescues.
    - Yutan Volunteer Fire Department may be contacted at the non-emergency message phone (402) 625-2273 or by email at **yutanvfd@yutanvfd.org**. Their website is http://yutanvfd.org/default.htm.
    - Waterloo Volunteer Fire Department may be contacted at the non-emergency message phone (402) 779-4250. Their website is http://www.waterloofire.ne.gov/.

- **Highway 36 – Glenn Cunningham Reservoir:**
    - The site is temporarily referred to as "Highway 36 and Glenn Cunningham Reservoir **Decommissioned** Bridge". It will be necessary to state which side of the bridge as well as the location on/under the bridge.
    - Further investigation and outreach need to be done with the Douglas County Department of Roads Engineer to determine which of four area volunteer and paid fire departments would be responding to the site and the official street address. Depending on the exact location, it is possible that the Irvington, Bennington or Ponca Hills Volunteer Fire Departments or the Omaha Fire Department (paid) may respond. Confirmation will be made that each of these departments has the proper equipment, trained members on the regional dive team, and are trained to perform over the water and swift water rescues.
    - Douglas County Engineer's office may be contacted at (402) 444-6372. Their website is https://www.dcengineer.org/.

Details on contacting the responding volunteer fire department for each site will be established and an effort will be made to contact each one to review possible needs for emergency rescue on site will be made in the future.

8 Safety Resources and References

Environmental Health and Safety (EHS). (2020a) Online manual of Environmental Health and Safety, University of Nebraska-Lincoln, https://scsapps.unl.edu/VirtualManual/ProfileContents.aspx, (Jan 2, 2020). ***(To access, please use the email address rwood@unl.edu.)***

Environmental Health and Safety (EHS). (2020b) Training Needs Assessment for EHS-Related Topics, University of Nebraska-Lincoln, https://ehs.unl.edu/web-based-training, (Jan. 9, 2020)

National Institute of Occupational Safety and Health (NIOSH). (2005). *NIOSH pocket guide to chemical hazards*, Department of Health and Human Services (DHHS), DHHS (NIOSH) Publication No. 2005-149.

Occupational Safety and Health Administration (OSHA) (2020a). Scaffolding Standards, United States Department of Labor, https://www.osha.gov/SLTC/etools/scaffolding/faq.html, (Jan. 3, 2020).

Occupational Safety and Health Administration (OSHA) (2020b). Chemical hazards and toxic substances, United States Department of Labor, https://www.osha.gov/SLTC/hazardoustoxicsubstances/, (Jan. 4, 2020).

Occupational Safety and Health Administration (OSHA) (2020e) Asbestos, United States Department of Labor, https://www.osha.gov/ SLTC/asbestos/index.html, (Jan. 4, 2020).

Occupational Safety and Health Administration (OSHA) (2020f). Lead, United States Department of Labor, https://www.osha.gov/SLTC/ lead/index.html, (Jan. 4, 2020).

Occupational Safety and Health Administration (OSHA) (2020g) Silica, United States Department of Labor, Crystalline, https://www.osha. gov/dsg/topics/silicacrystalline/index.html, (Jan. 4, 2020).

Occupational Safety and Health Administration (OSHA) (2020h). Hand and power tools, United States Department of Labor, https://www .osha.gov/Publications/osha3080.pdf, (Jan. 3, 2020).

Occupational Safety and Health Administration (OSHA) (2020i). Electrical Incidents, Ground-Fault Circuit Interrupters (GFCI), United States Department of Labor, https://www.osha.gov/SLTC/electrical/hazards/gfci.html (Jan. 2, 2020).

United States Geological Survey (USGS) (2020). Surface-water activities, U.S. Geological Survey Open-File Report 95-777, https://pubs.usgs.gov/of/1995/ of95-777/sw_act.html, (Aug. 19, 2020).

APPENDIX B.

Processed Data

List of Figures

List of Tables

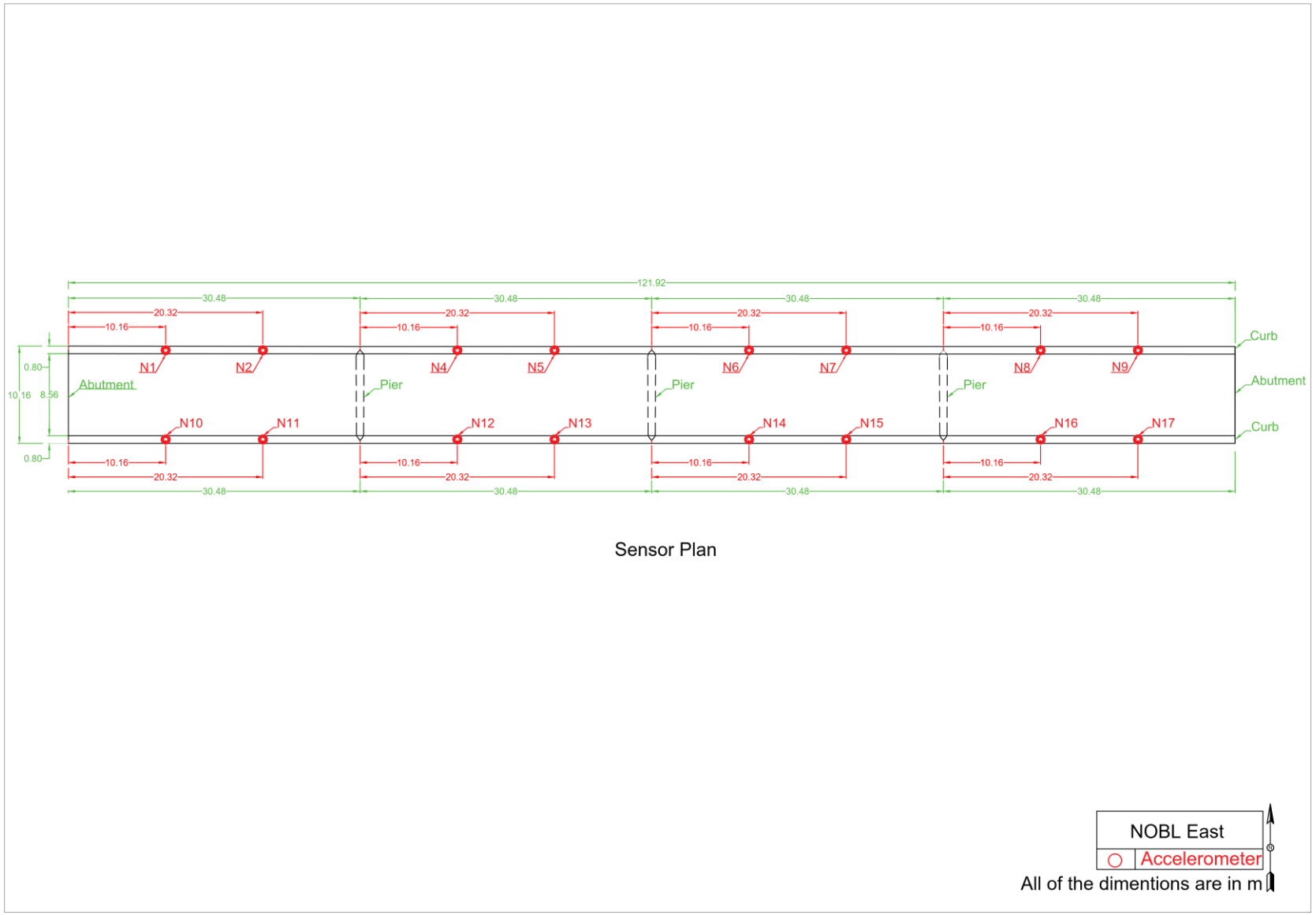

Figure B.1. Locations of the accelerometer instrumented for NOBL East

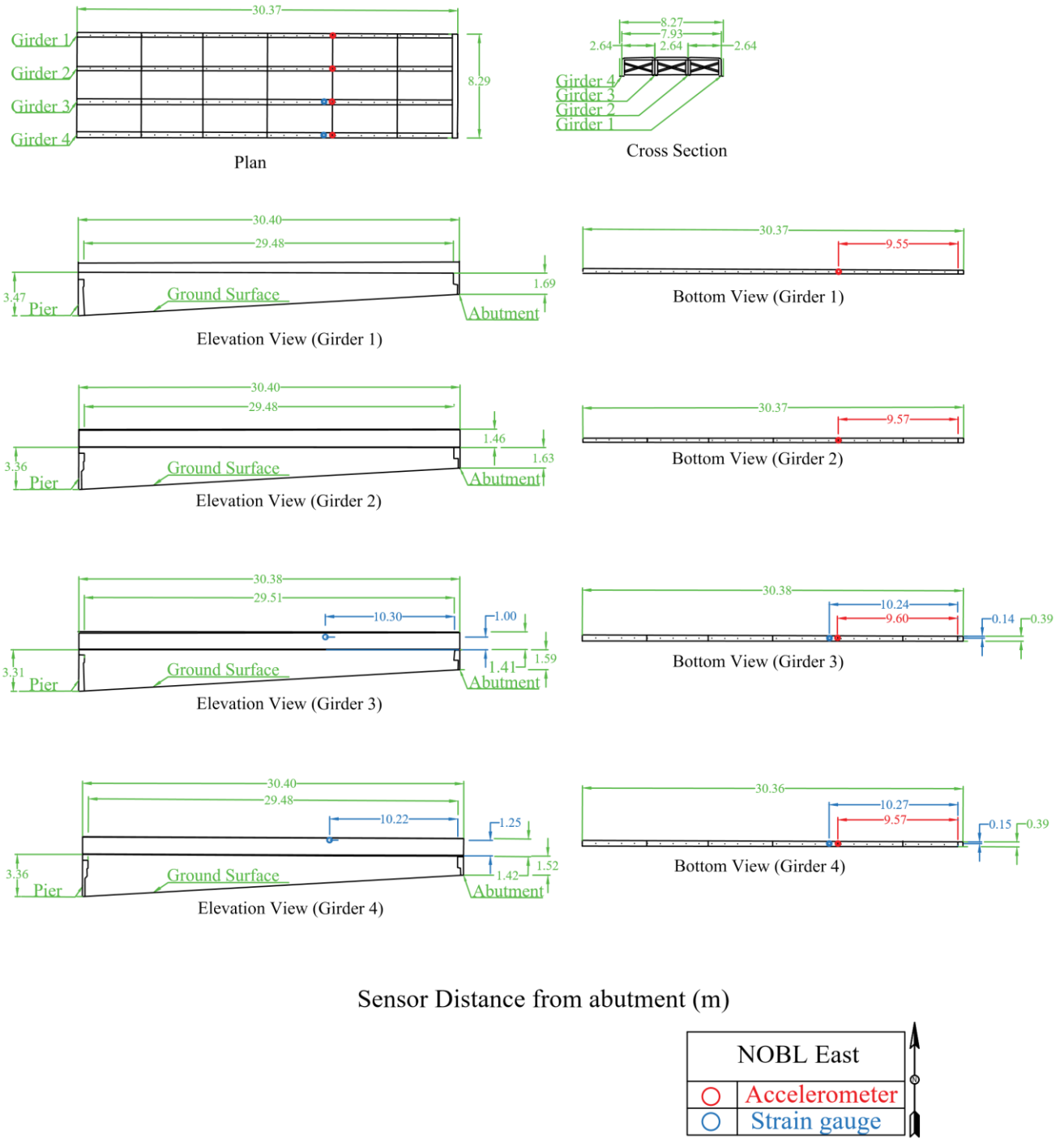

Figure B.2. Locations of the accelerometers instrumented to girders for NOBL East

Table B.1. Live load test for NOBL EastRun #	Dir.	Speed (mph)	Truck #	Lane
1	W[1]	5	1	C [3]
2	E [2]	5	1	C
3	W	5	1	C
4	E	5	1	C
5	W	10	1	C
6	E	10	1	C
7	W	20	1	C
8	E	20	1	C
9	W	20	1	C
10	E	20	1	C
11	W	40	1	C
12	E	40	1	C
13	W	40	1	C
14	E	40	1	C
15	W	45	1	C
16	E	55	1	C
17	W	45	2	C
18	E	55	2	C
19	W	45	2	C
20	E	55	2	C
21	W	5	1	N^+
22	E	5	1	N^+
23	W	5	1	N^+
24	E	5	1	N^+
25	W	5	1	S^+
26	E	5	1	S^+
27	W	10	1	N
28	E	10	1	N
29	W	40	1	N
30	E	40	1	N
31	W	10	1	S
32	E	10	1	S
33	W	40	1	S
34	E	40	1	S
35	W-W [4]	10-10	2-1	S-N [5]
36	E-E [6]	10-10	2-1	S-N
37	W-W	10-10	2-1	S-N
38	E-E	10-10	2-1	S-N
39	W-W	40-40	2-1	S-N

40	E-E	40-40	2-1	S-N
41	W-W	40-40	2-1	S-N
42	E-E	40-40	2-1	S-N
43	W/W	10/10	1/2	N/N [7]
44	E/E	10/10	1/2	N/N
45	W/W	40/40	1/2	N/N
46	E/E	40/40	1/2	N/N
47	W/W	10/10	1/2	S/S [8]
48	E/E	10/10	1/2	S/S
49	W/W	40/40	1/2	S/S
50	E/E	40/40	1/2	S/S
51	W/W	30/30	1/2	C/C
52	E/E	30/30	1/2	C/C
53	W	Braking (40 mph to 0 at abutment)	1	C
54	E	Braking (40 mph to 0 at abutment)	1	C
55	W	Braking (40 mph to 0 at pier)	1	C
56	E	Braking (40 mph to 0 at pier)	1	C
57	W-W	Varying speed	2-1	S-N
58	E-E	Varying speed	2-1	S-N
59	E-W	Varying speed	1-2	S-N
60	E-W	Varying speed	1-2	N-S

1. Truck pass from East to West direction.
2. Truck pass from West to East direction.
3. Truck pass through the center of the bridge.
4. Trucks pass side-by-side from East to West direction.
5. Trucks pass side-by-side in North and South Lane.
6. Trucks pass side-by-side from West to East direction.
7. Trucks pass back-to-back in the North Lane.
8. Trucks pass back-to-back in the South Lane.

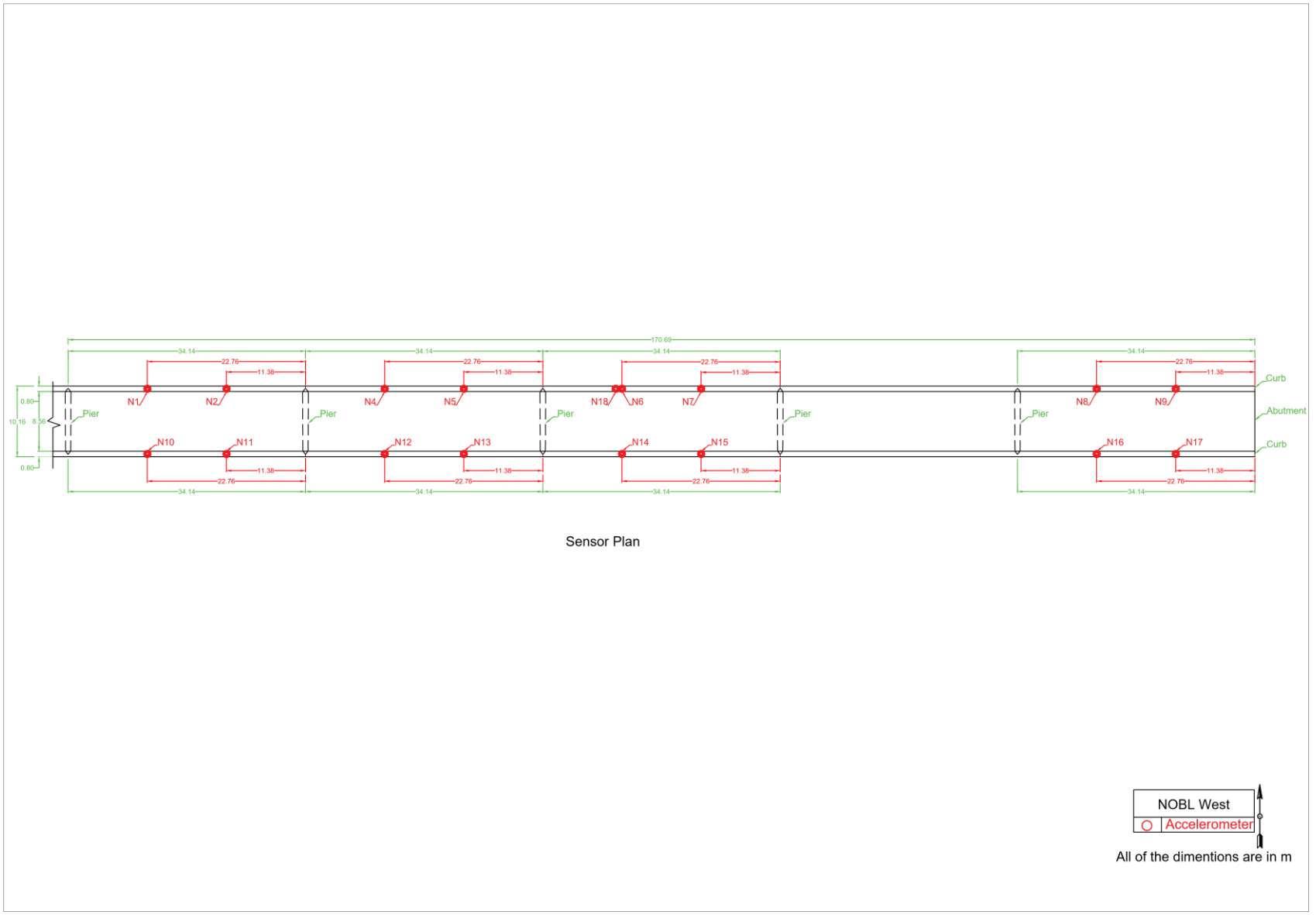

Figure B.3. Locations of the accelerometer instrumented for NOBL West

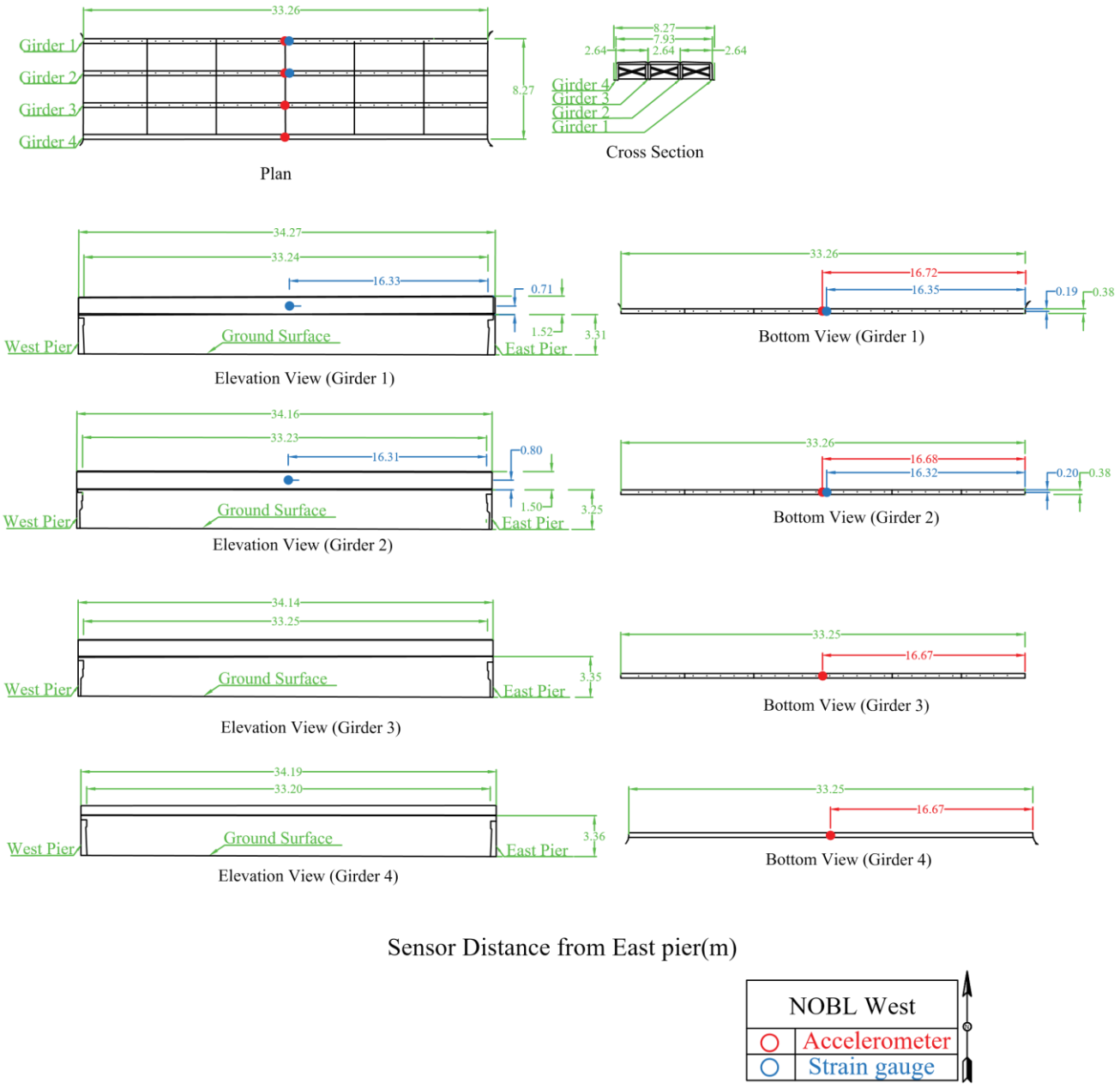

Figure B.4. Locations of the accelerometers instrumented to girders for NOBL West

Table B.2. Live load test for NOBL West

Run #	Dir.	Speed (mph)	Truck	Lane
1	W [1]	5	1	Center [2]
2	E [3]	5	1	Center
3	W	5	1	Center
4	E	5	1	Center
5	W	20	1	Center
6	E	20	1	Center
7	W	20	1	Center
8	E	20	1	Center
9	W	40	1	Center
10	E	40*	1	Center
11	W	40	1	Center
12	E	40*	1	Center
13	W	5	2	N^+ [4]
14	E	5	2	N^+
15	W	5	2	S^+ [5]
16	E	5	2	S^+
17	W	10	2	Center
18	E	10	2	Center
19	W	10	2	North
20	E	10	2	North
21	W	40	2	North
22	E	40*	2	North
23	W	10	2	South
24	E	10	2	South
25	W	40	2	South
26	E	40*	2	South
27	W-W [6]	10	1-2	N-S [8]
28	E-E [7]	10	1-2	N-S
29	W-W	10	1-2	N-S
30	E-E	10	1-2	N-S
31	W-W	30	1-2	N-S
32	E-E	30	1-2	N-S
33	W-W	30	1-2	N-S
34	E-E	30	1-2	N-S
35	W/W [9]	10	1/2	North
36	E/E [10]	10	1/2	North
37	W/W	10	1/2	South
38	E/E	10	1/2	South
39	W/W	40	1/2	North

40	E/E	40*	1/2	North
41	W/W	50	1/2	South
42	E/E	40*	1/2	South
43	W	40	Comb A[11]	-
44	E	30*	Comb B [12]	-
45	W	40	Comb A	-
46	E	30*	Comb B	-
47	W	var	Comb A-Rev [12]	-
48	E/E	30*	112 ft spacing	-
49	W	20	Comb A-Rev	-
50	E/E	var*	112 ft spacing	-
51	W	var	Comb A-Rev	-
52	E	var*	Comb C [14]	-
53	W	var	Comb F [15]	Center
54	cross	30	Comb D [16]	Both
55	cross	30	Comb E [17]	Both
56	cross	30	Comb D	Both
57	cross	30	Comb E	Both
58	W	var	Comb G [18]	Center
59	E	var*	Comb H [19]	Both

1. Truck pass from East to West direction.

2. Truck pass through the center of the bridge.

3. Truck pass from West to East direction.

4. 2 [ft] away from the North edge of the North edge.

5. 2[ft] away from the South edge of the South edge.

6. Trucks pass side-by-side from East to West direction.

7. Trucks pass side-by-side from West to East direction.

8. Trucks pass side-by-side in South and North Lane.

9. Trucks pass back-to-back from East to West direction.

10. Trucks pass back-to-back from West to East direction.

11. Truck one in North Lane with speed 40 mph and truck 2 in South Lane with speed 20 mph.

12. Truck one passed in the front and in the North Lane, second truck has 200 ft space with the first truck and passed through the south Lane.

13. Truck two in North Lane with speed 20 mph and truck 1 in South Lane with speed 40 mph.

14. Truck one passed in the South Lane, second truck has 200 ft space with the first truck and passed through the North Lane.

15. Braking test, truck one pressed brake at the speed of 40 mph and reduced it speed to 0.

16. Truck one pass from East to West direction in south Lane and truck two pass from West to East direction in North Lane.

17. Truck one pass from West to East direction in North Lane and truck two pass from East to West direction in South Lane.

18. Braking test, truck two pressed brake at the speed of 40 mph and reduced it speed to 0.

19. Braking test, truck one pressed brake at the speed of 40 mph and reduced it speed to 0 in North lane and truck two pressed brake at the speed of 20 mph and reduced it speed to 0 in South Lane.

*East bound trucks started less than target speed

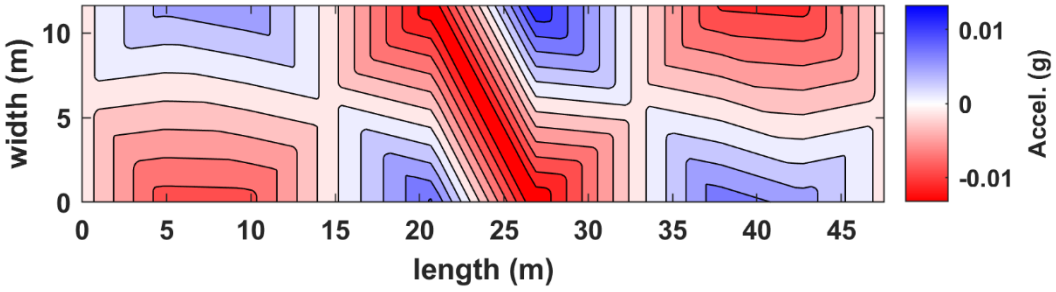

Figure B.5. Interpolated acceleration in plan view for truck pass 15 at the NOBL North bridge structure.

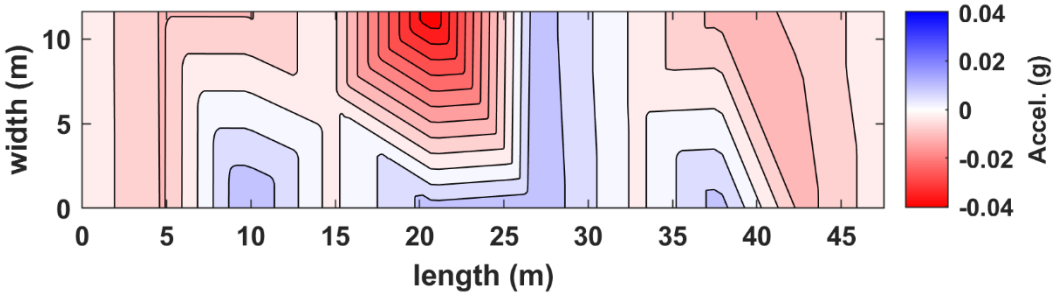

Figure B.6. Interpolated acceleration in plan view for truck pass 16 at the NOBL North bridge structure.

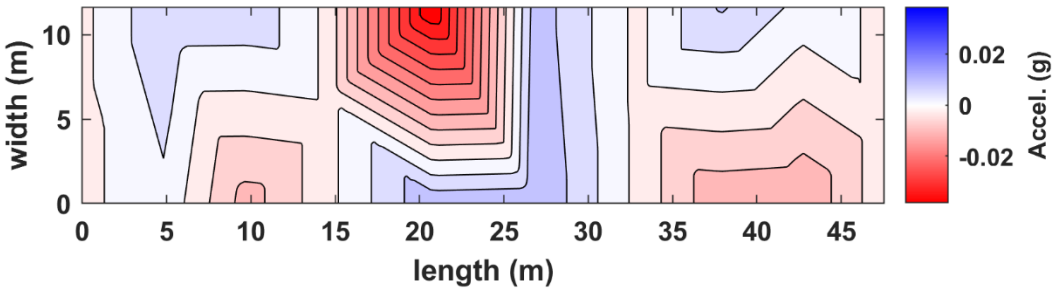

Figure B.7. Interpolated acceleration in plan view for truck pass 17 at the NOBL North bridge structure.

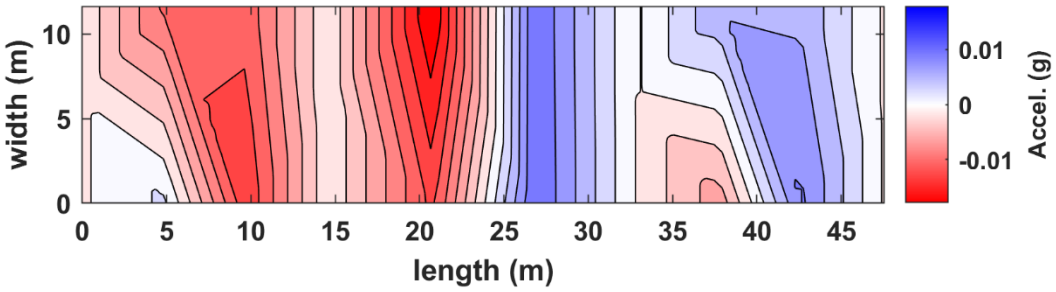

Figure B.8. Interpolated acceleration in plan view for truck pass 18 at the NOBL North bridge structure.

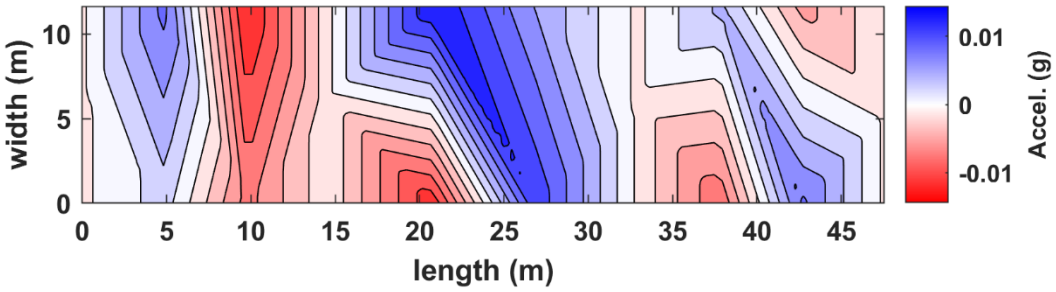

Figure B.9. Interpolated acceleration in plan view for truck pass 19 at the NOBL North bridge structure.

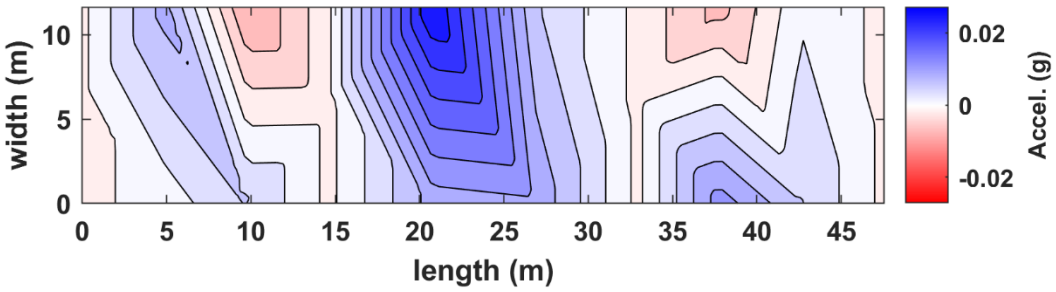

Figure B.10. Interpolated acceleration in plan view for truck pass 20 at the NOBL North bridge structure.

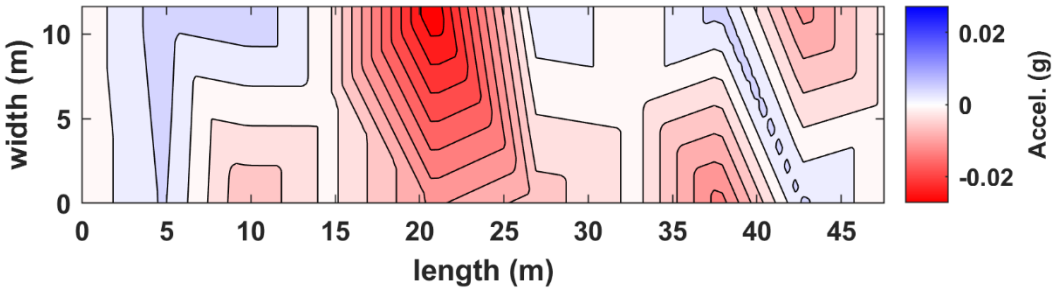

Figure B.11. Interpolated acceleration in plan view for truck pass 21 at the NOBL North bridge structure.

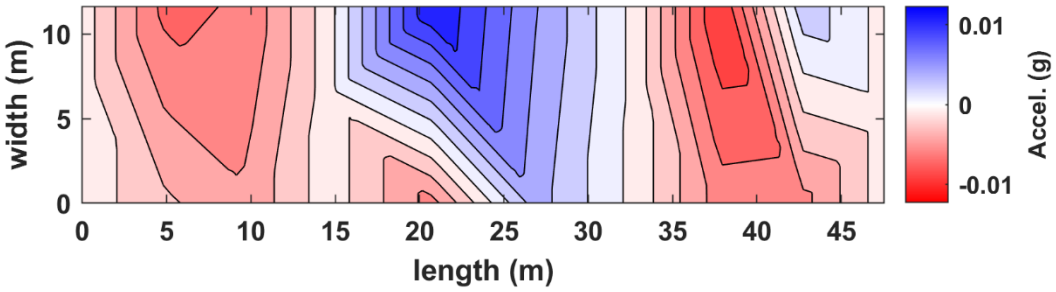

Figure B.12. Interpolated acceleration in plan view for truck pass 22 at the NOBL North bridge structure.

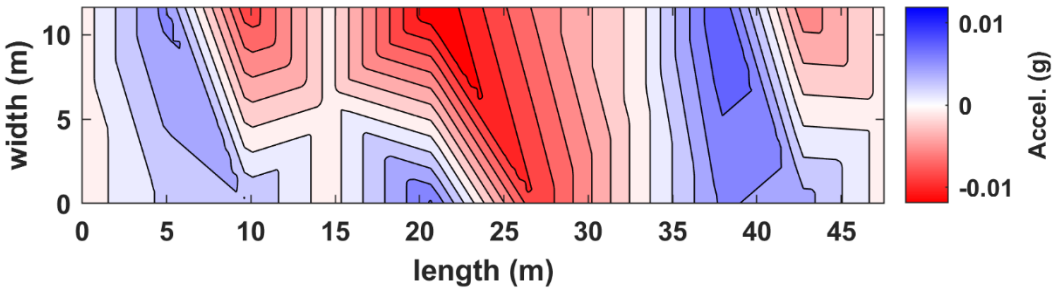

Figure B.13. Interpolated acceleration in plan view for truck pass 23 at the NOBL North bridge structure.

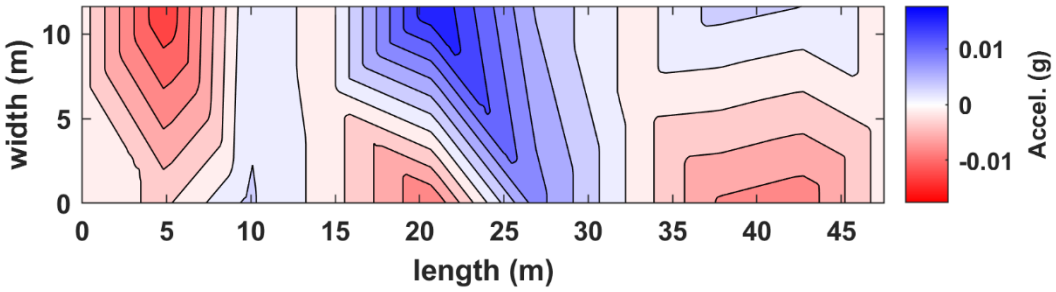

Figure B.14. Interpolated acceleration in plan view for truck pass 24 at the NOBL North bridge structure.

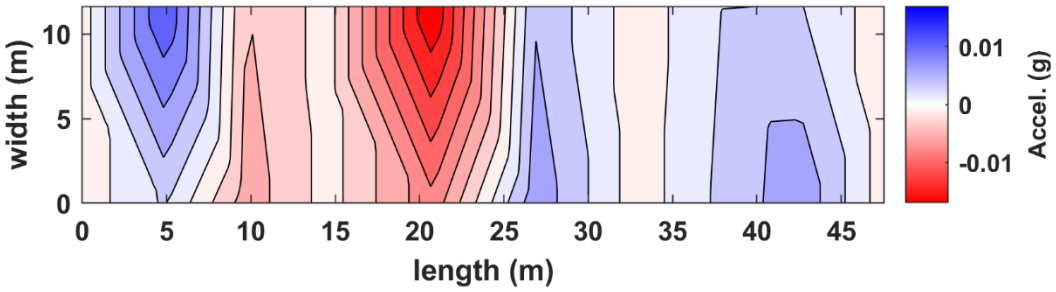

Figure B.15. Interpolated acceleration in plan view for truck pass 25 at the NOBL North bridge structure.

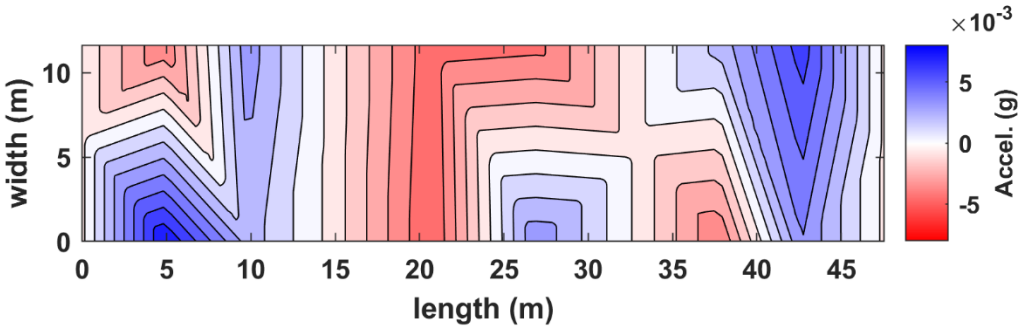

Figure B.16. Interpolated acceleration in plan view for truck pass 26 at the NOBL North bridge structure.

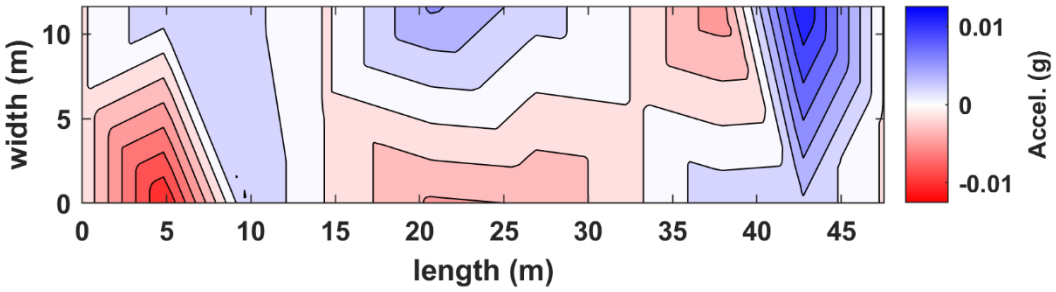

Figure B.17. Interpolated acceleration in plan view for truck pass 27 at the NOBL North bridge structure.

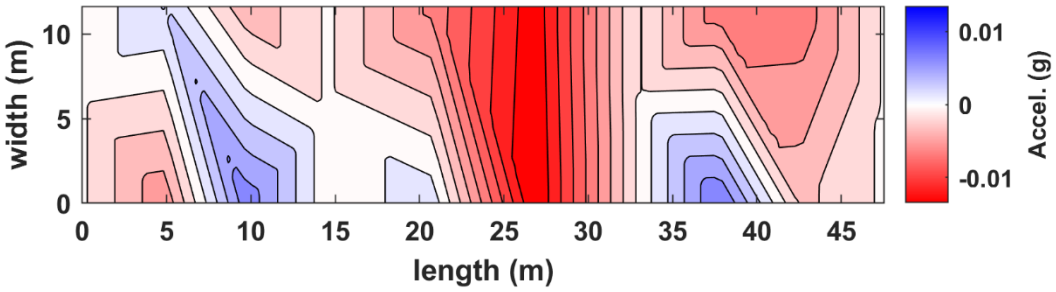

Figure B.18. Interpolated acceleration in plan view for truck pass 28 at the NOBL North bridge structure.

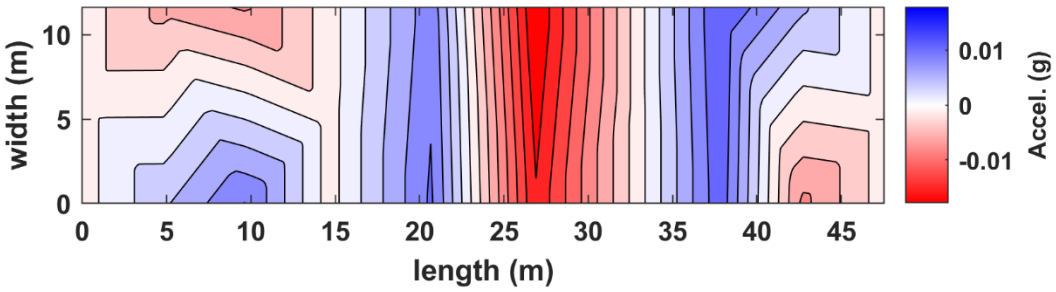

Figure B.19. Interpolated acceleration in plan view for truck pass 29 at the NOBL North bridge structure.

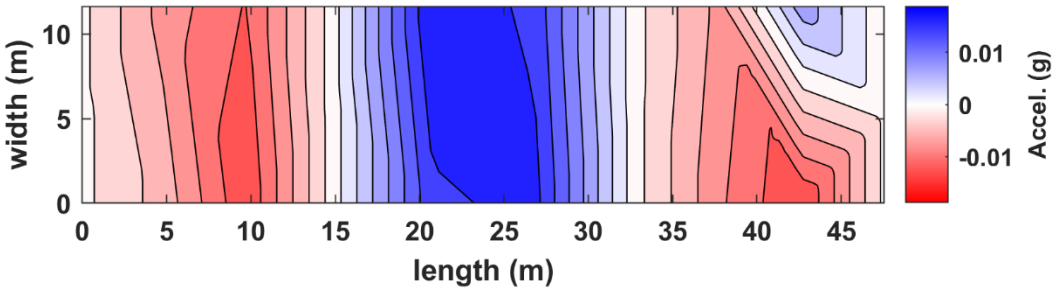

Figure B.20. Interpolated acceleration in plan view for truck pass 30 at the NOBL North bridge structure.

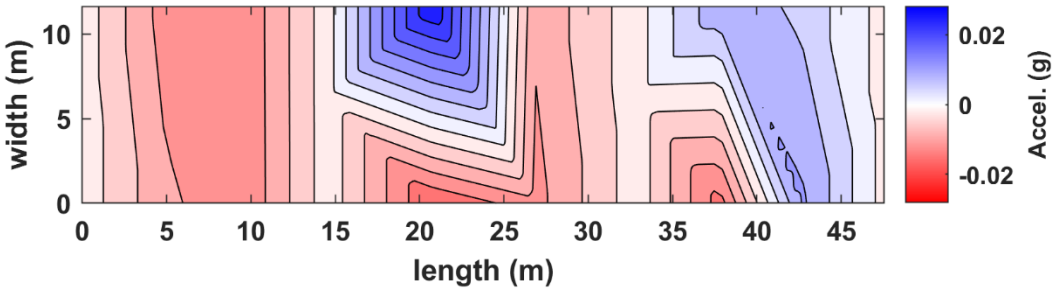

Figure B.21. Interpolated acceleration in plan view for truck pass 31 at the NOBL North bridge structure.

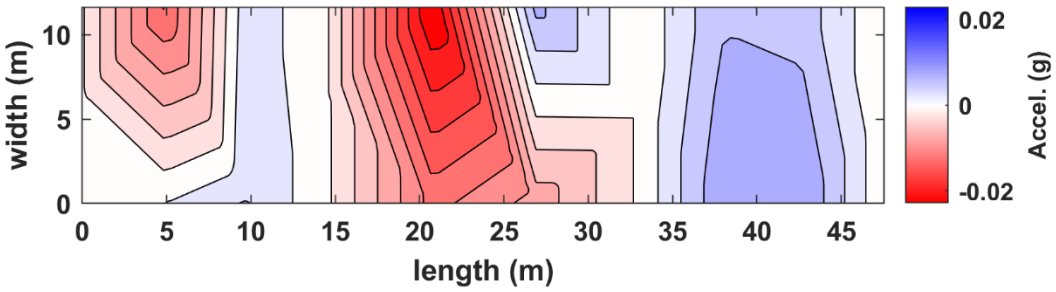

Figure B.22. Interpolated acceleration in plan view for truck pass 32 at the NOBL North bridge structure.

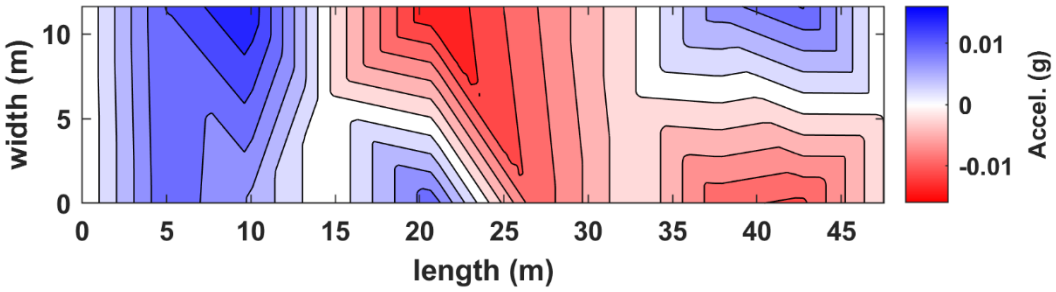

Figure B.23. Interpolated acceleration in plan view for truck pass 33 at the NOBL North bridge structure.

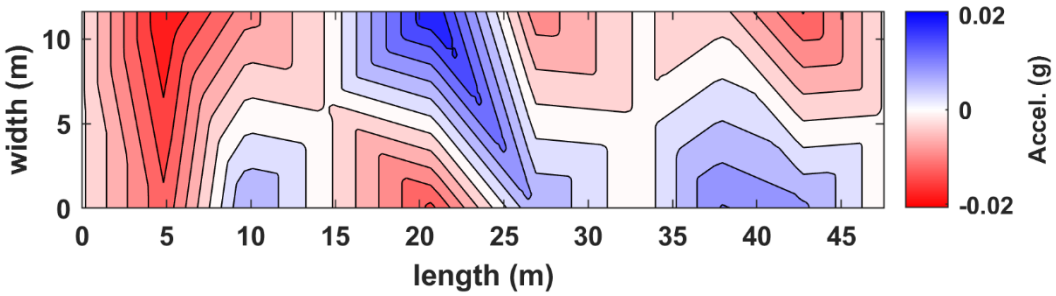

Figure B.24. Interpolated acceleration in plan view for truck pass 34 at the NOBL North bridge structure.

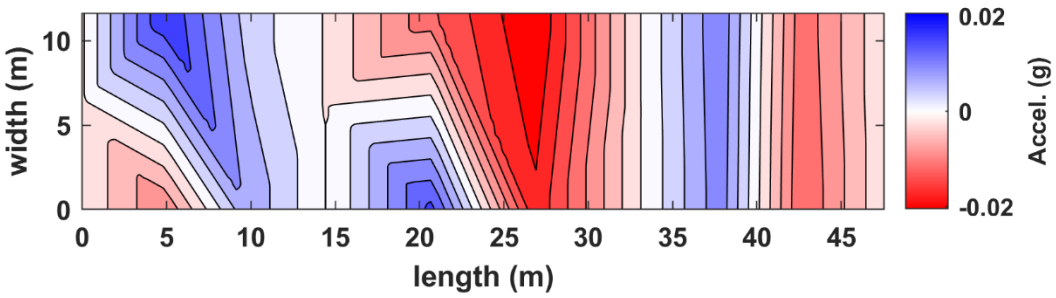

Figure B.25. Interpolated acceleration in plan view for truck pass 35 at the NOBL North bridge structure.

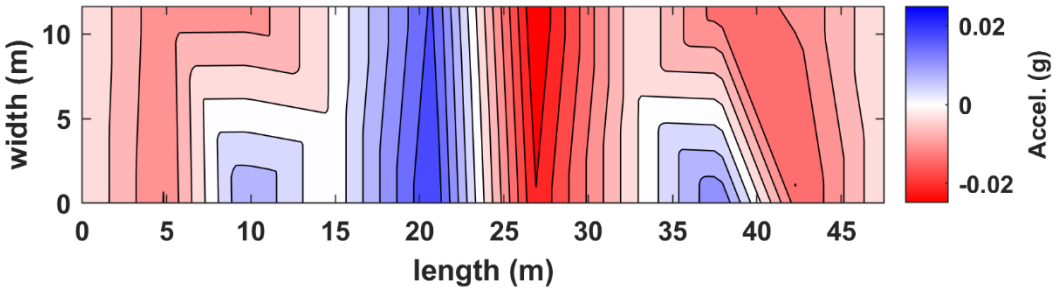

Figure B.26. Interpolated acceleration in plan view for truck pass 36 at the NOBL North bridge structure.

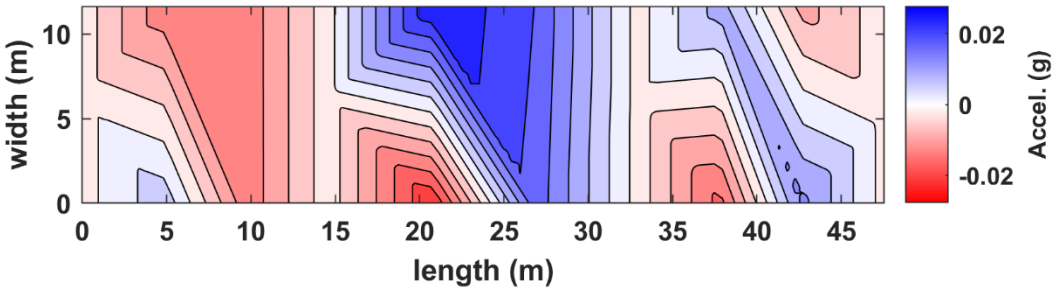

Figure B.27. Interpolated acceleration in plan view for truck pass 37 at the NOBL North bridge structure.

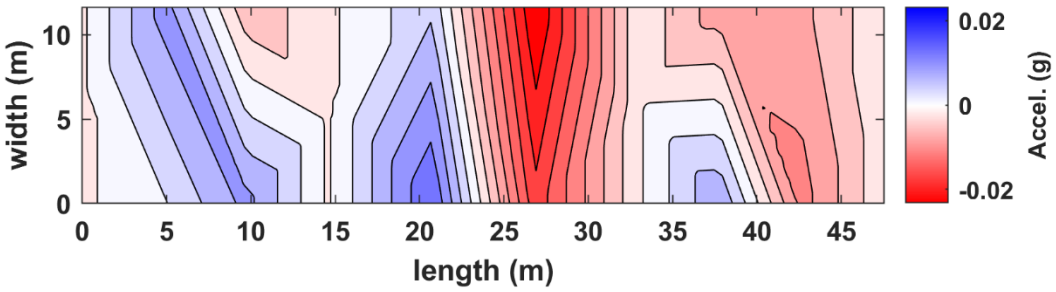

Figure B.28. Interpolated acceleration in plan view for truck pass 38 at the NOBL North bridge structure.

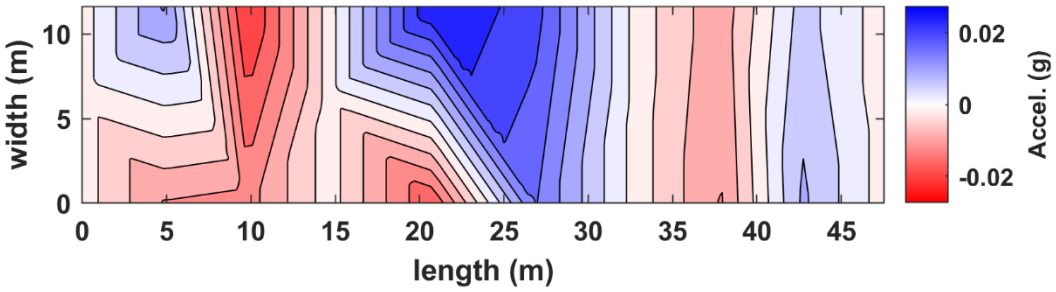

Figure B.29. Interpolated acceleration in plan view for truck pass 39 at the NOBL North bridge structure.

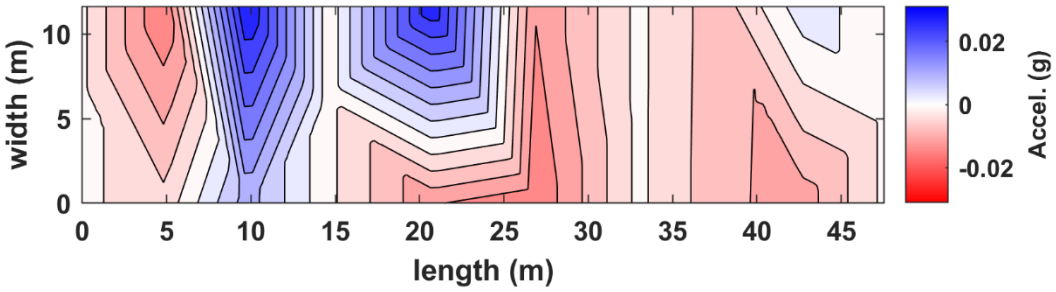

Figure B.30. Interpolated acceleration in plan view for truck pass 40 at the NOBL North bridge structure.

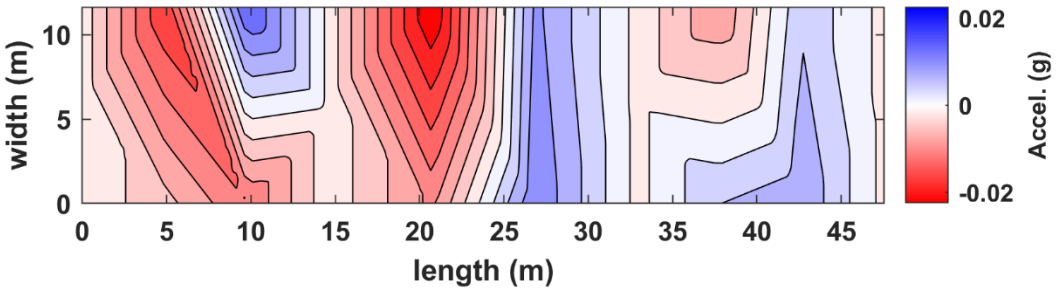

Figure B.31. Interpolated acceleration in plan view for truck pass 41 at the NOBL North bridge structure.

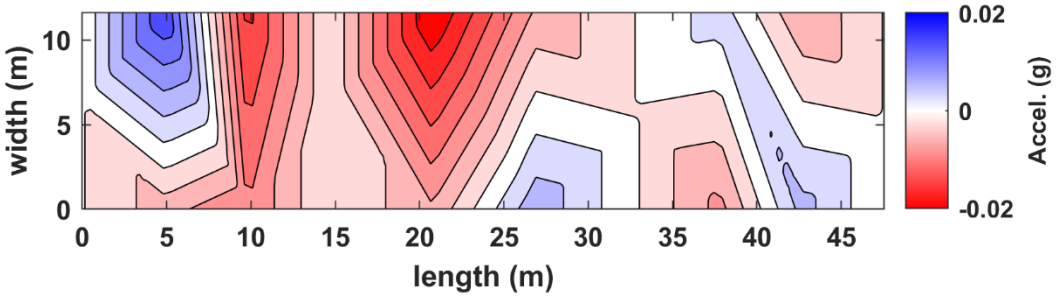

Figure B.32. Interpolated acceleration in plan view for truck pass 42 at the NOBL North bridge structure.

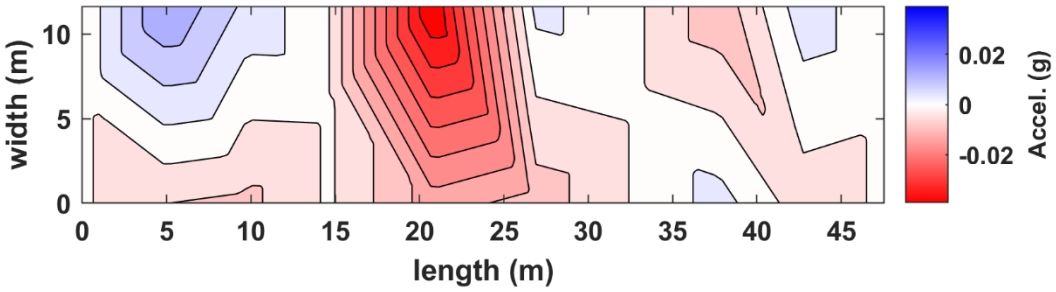

Figure B.33. Interpolated acceleration in plan view for truck pass 43 at the NOBL North bridge structure.

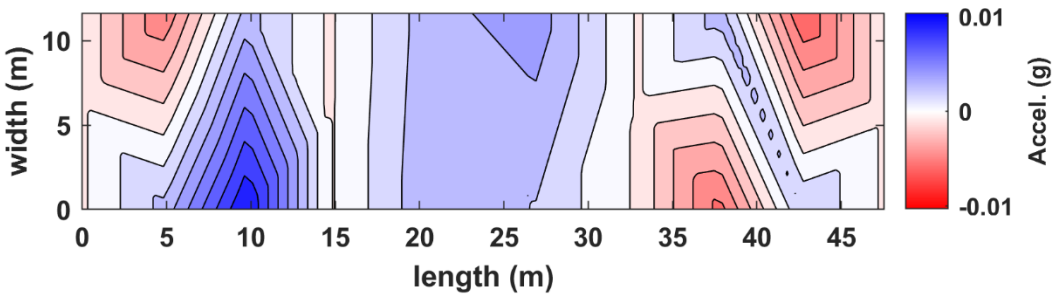

Figure B.34. Interpolated acceleration in plan view for truck pass 44 at the NOBL North bridge structure.

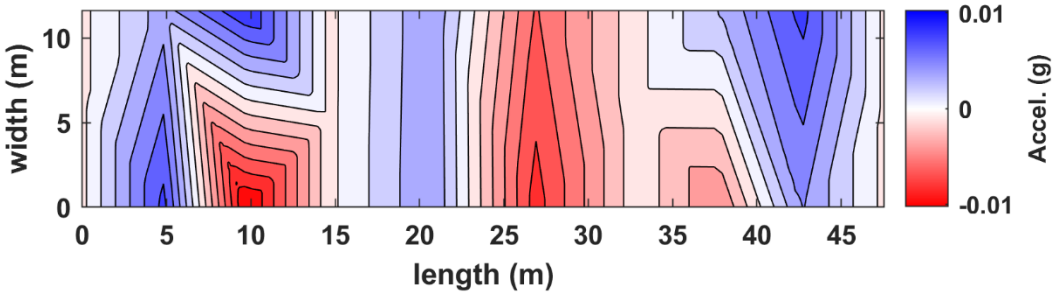

Figure B.35. Interpolated acceleration in plan view for truck pass 45 at the NOBL North bridge structure.

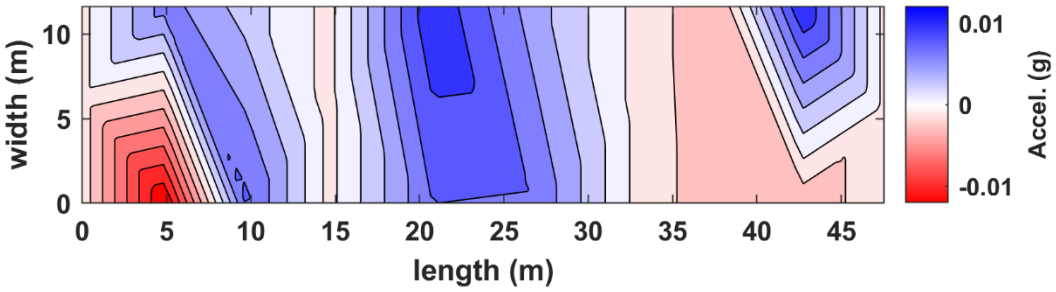

Figure B.36. Interpolated acceleration in plan view for truck pass 46 at the NOBL North bridge structure.

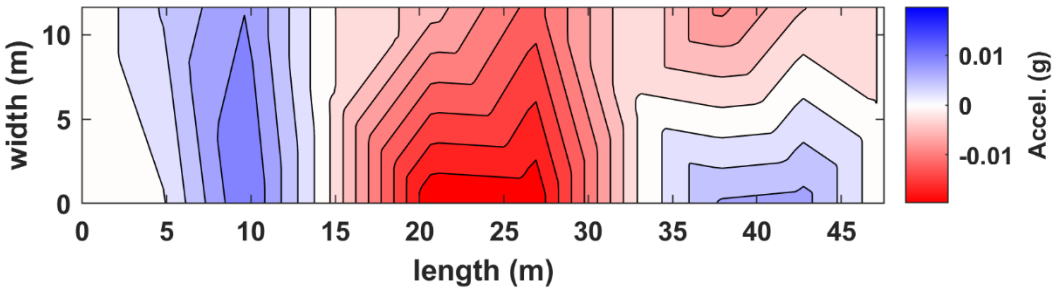

Figure B.37. Interpolated acceleration in plan view for truck pass 47 at the NOBL North bridge structure.

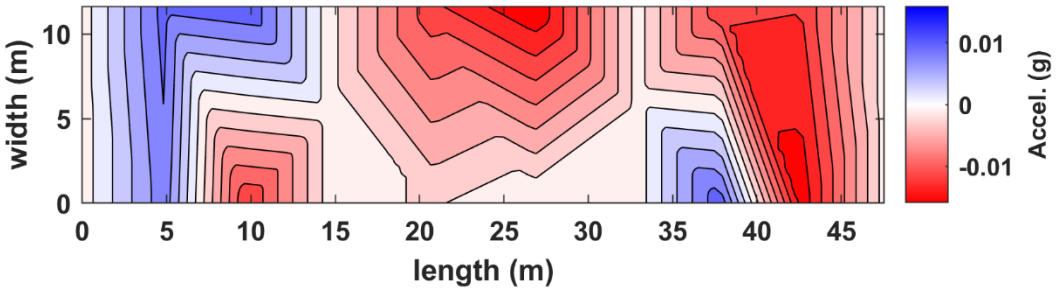

Figure B.38. Interpolated acceleration in plan view for truck pass 48 at the NOBL North bridge structure.

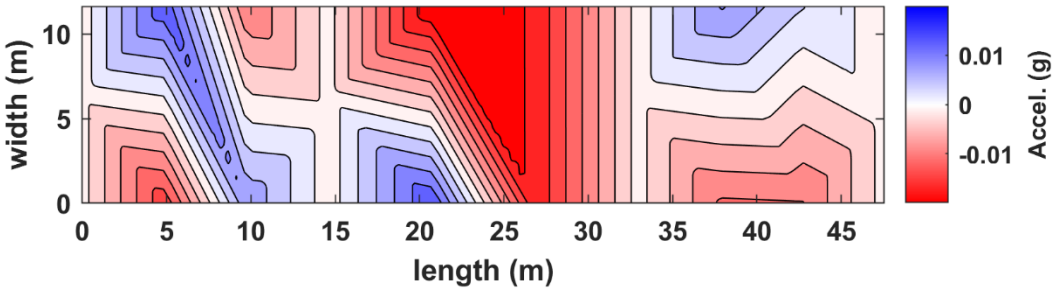

Figure B.39. Interpolated acceleration in plan view for truck pass 49 at the NOBL North bridge structure.

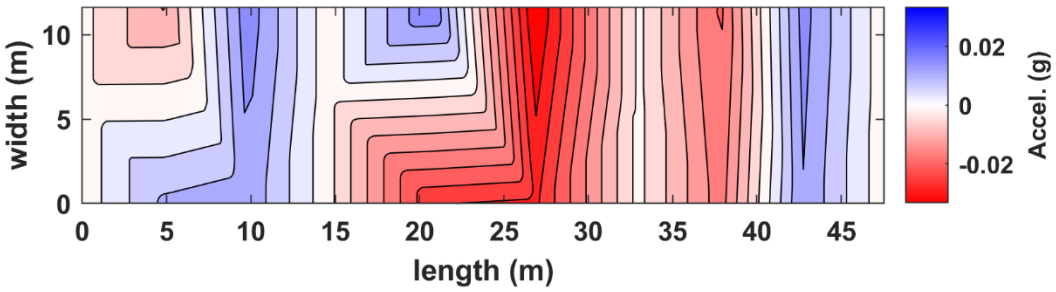

Figure B.40. Interpolated acceleration in plan view for truck pass 50 at the NOBL North bridge structure.

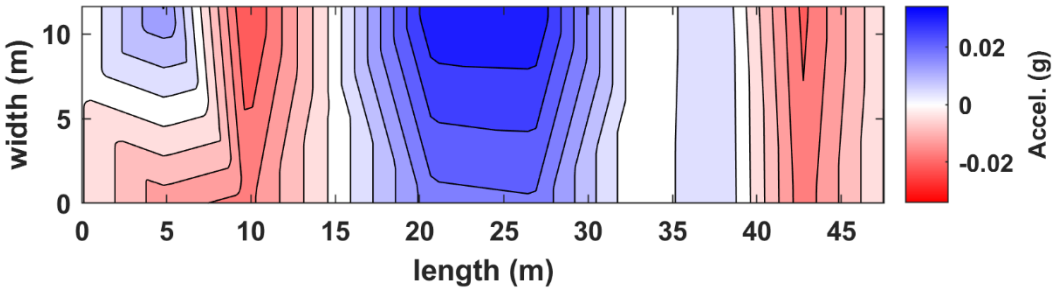

Figure B.41. Interpolated acceleration in plan view for truck pass 51 at the NOBL North bridge structure.

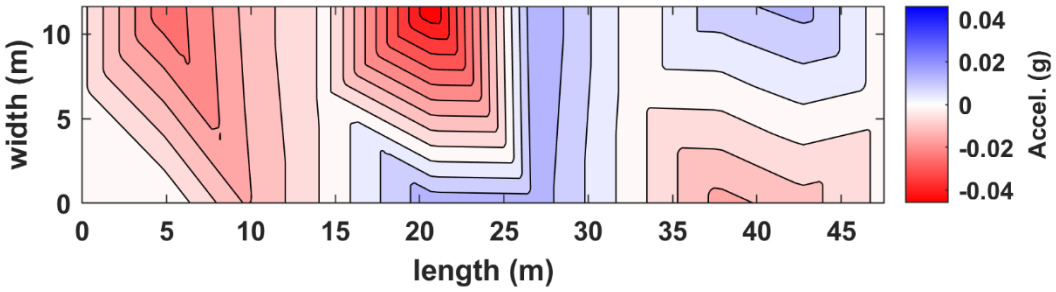

Figure B.42. Interpolated acceleration in plan view for truck pass 52 at the NOBL North bridge structure.

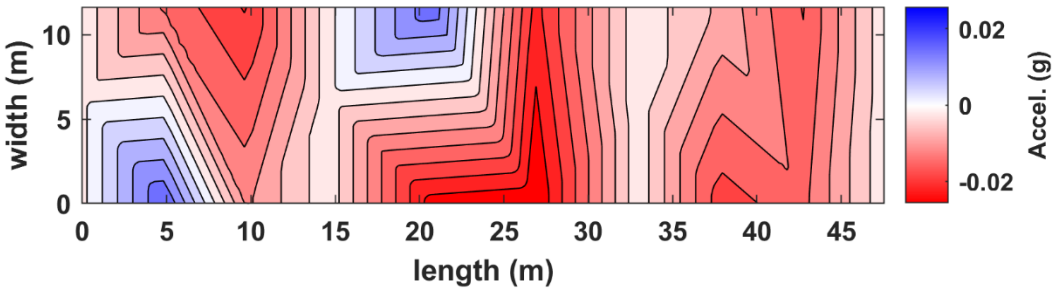

Figure B.43. Interpolated acceleration in plan view for truck pass 53 at the NOBL North bridge structure.

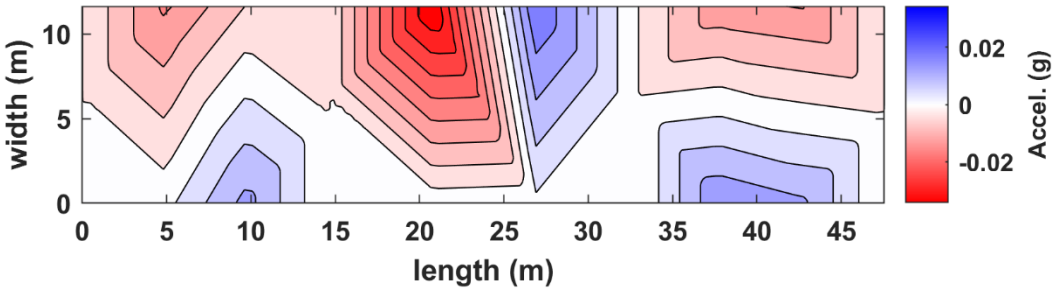

Figure B.44. Interpolated acceleration in plan view for truck pass 54 at the NOBL North bridge structure.

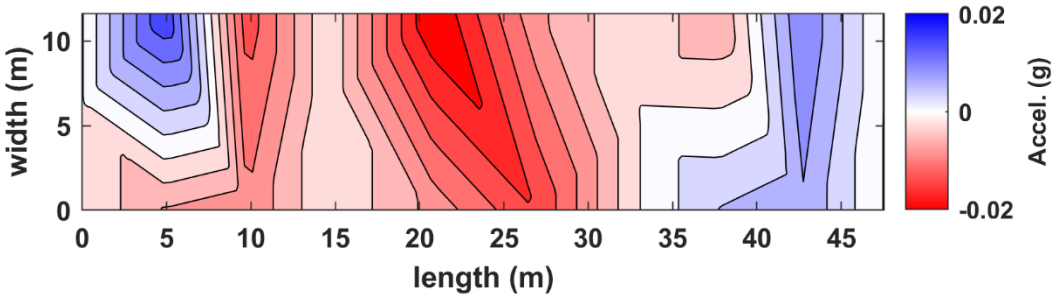

Figure B.45. Interpolated acceleration in plan view for truck pass 55 at the NOBL North bridge structure.

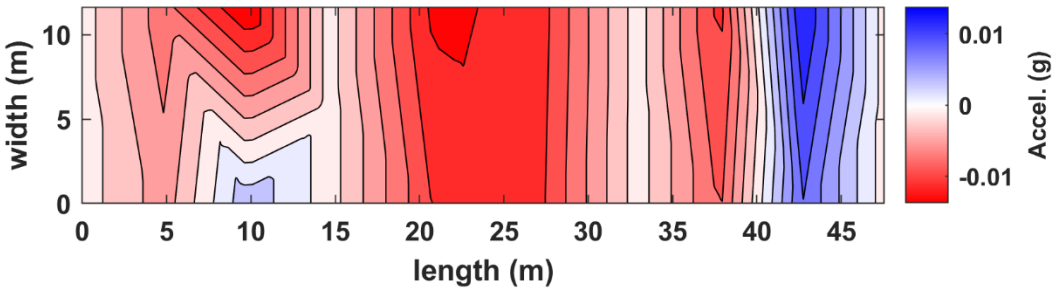

Figure B.46. Interpolated acceleration in plan view for truck pass 56 at the NOBL North bridge structure.

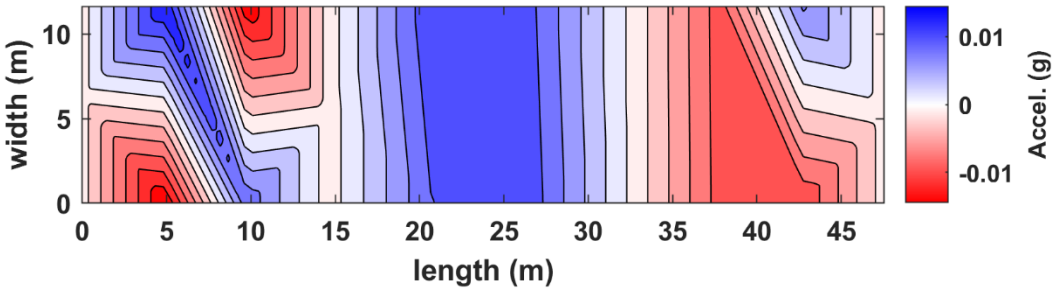

Figure B.47. Interpolated acceleration in plan view for truck pass 57 at the NOBL North bridge structure.

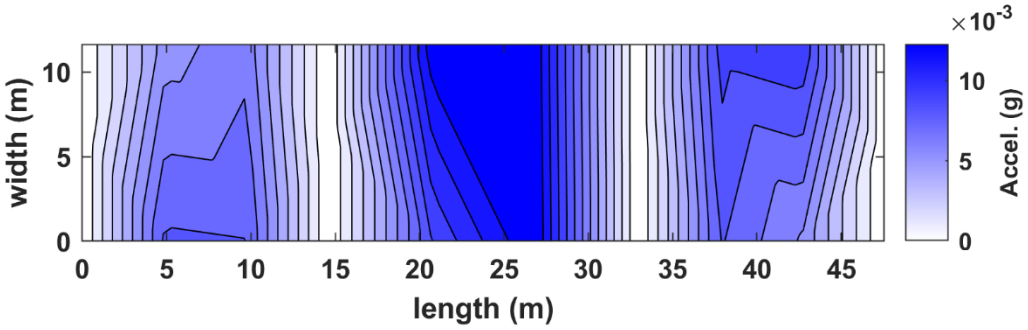

Figure B.48. Interpolated absolute-valued acceleration in plan view for truck pass 15 at the NOBL North bridge structure.

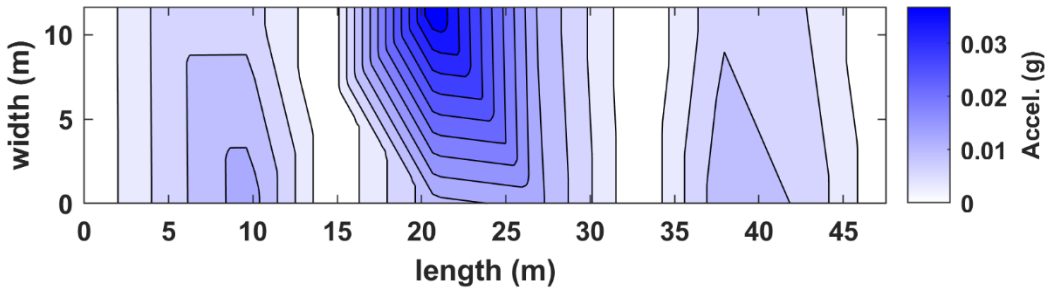

Figure B.49. Interpolated absolute-valued acceleration in plan view for truck pass 16 at the NOBL North bridge structure.

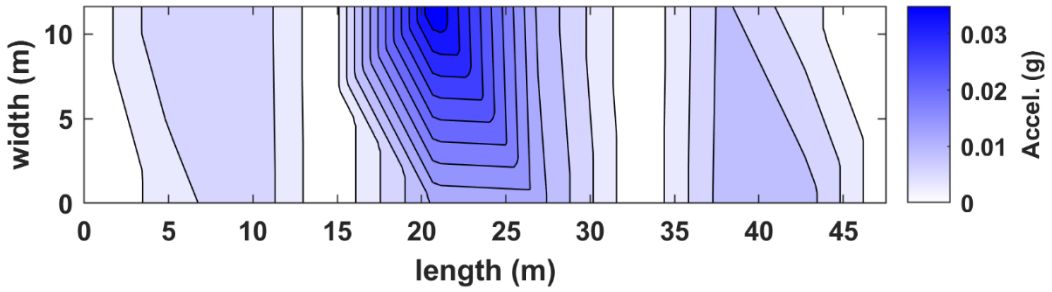

Figure B.50. Interpolated absolute-valued acceleration in plan view for truck pass 17 at the NOBL North bridge structure.

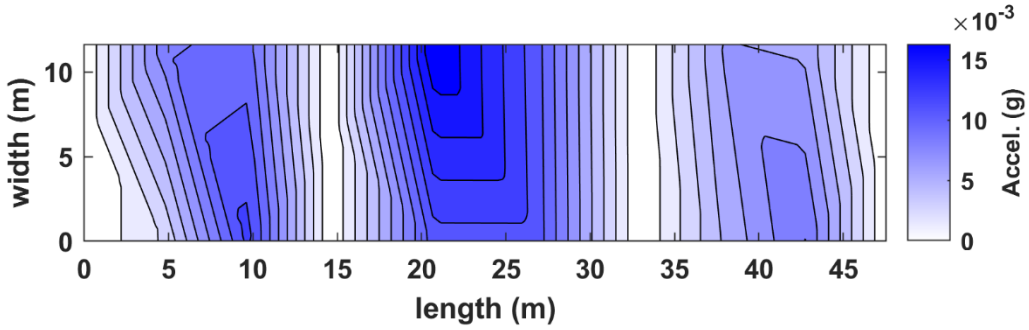

Figure B.51. Interpolated absolute-valued acceleration in plan view for truck pass 18 at the NOBL North bridge structure.

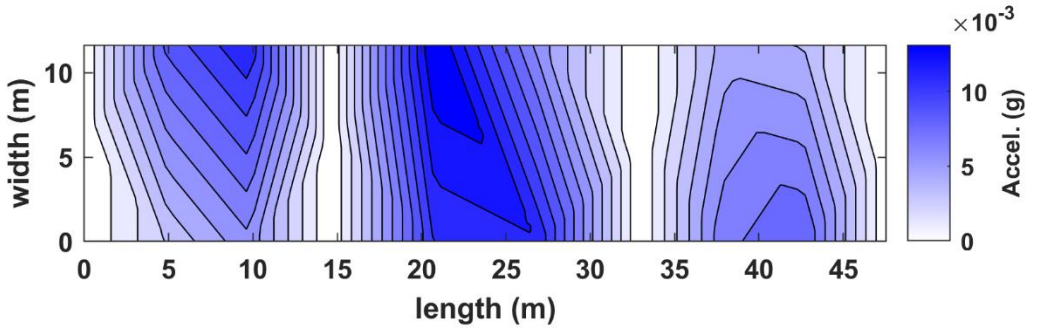

Figure B.52. Interpolated absolute-valued acceleration in plan view for truck pass 19 at the NOBL North bridge structure.

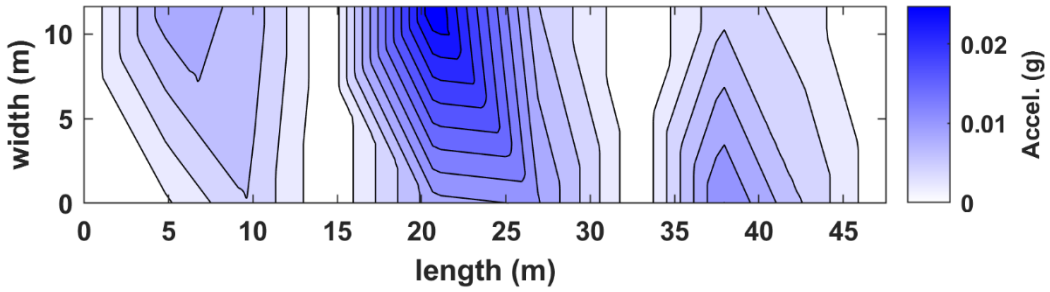

Figure B.53. Interpolated absolute-valued acceleration in plan view for truck pass 20 at the NOBL North bridge structure.

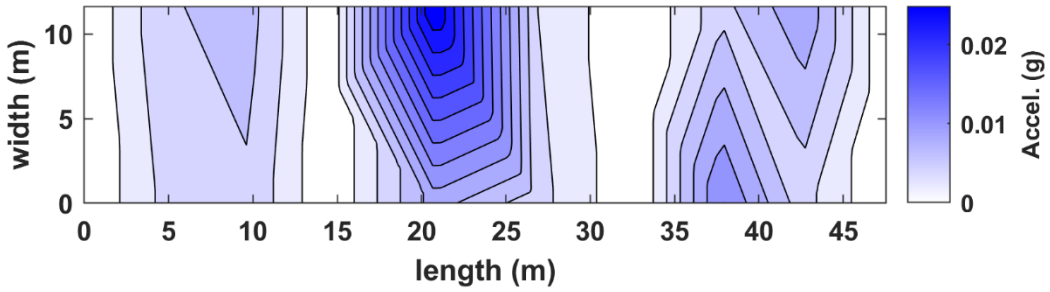

Figure B.54. Interpolated absolute-valued acceleration in plan view for truck pass 21 at the NOBL North bridge structure.

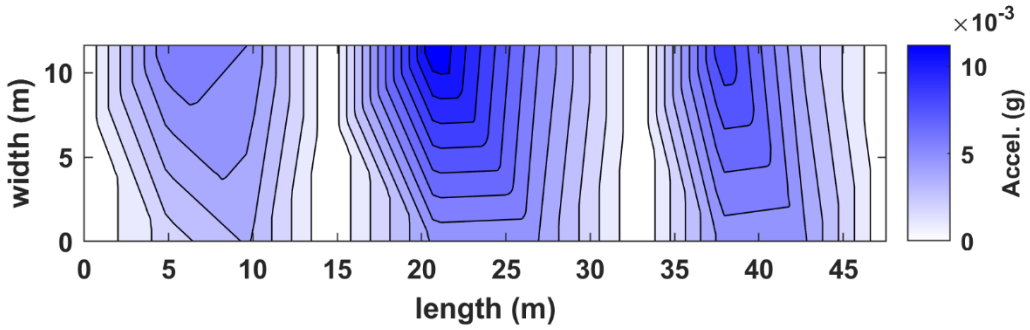

Figure B.55. Interpolated absolute-valued acceleration in plan view for truck pass 22 at the NOBL North bridge structure.

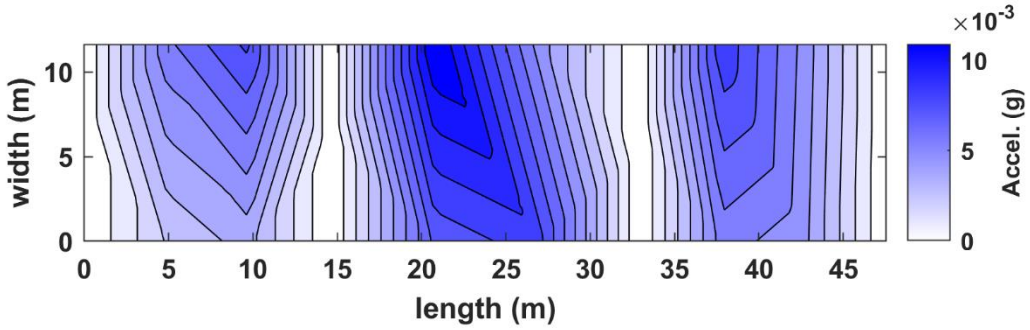

Figure B.56. Interpolated absolute-valued acceleration in plan view for truck pass 23 at the NOBL North bridge structure.

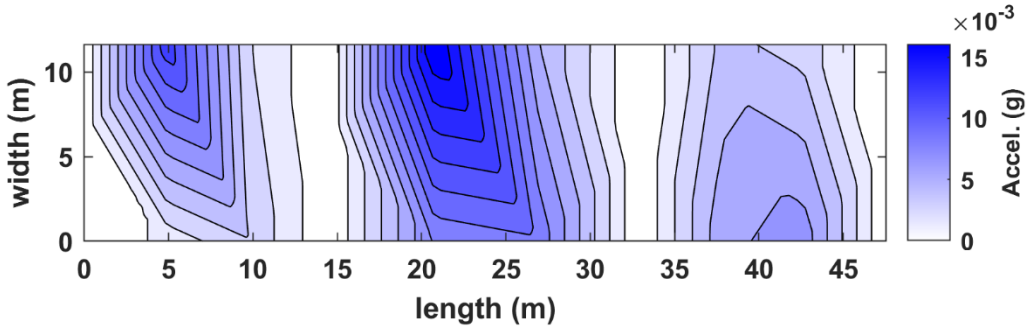

Figure B.57. Interpolated absolute-valued acceleration in plan view for truck pass 24 at the NOBL North bridge structure.

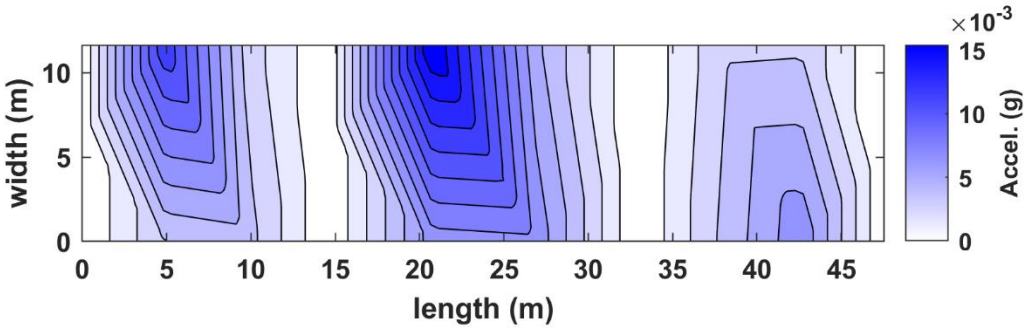

Figure B.58. Interpolated absolute-valued acceleration in plan view for truck pass 25 at the NOBL North bridge structure.

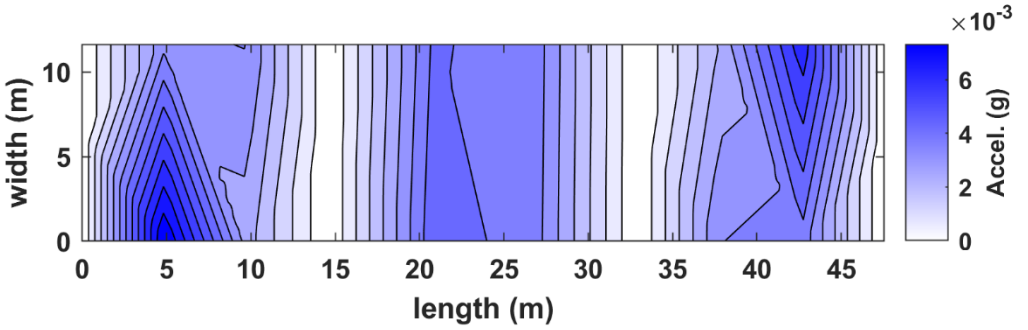

Figure B.59. Interpolated absolute-valued acceleration in plan view for truck pass 26 at the NOBL North bridge structure.

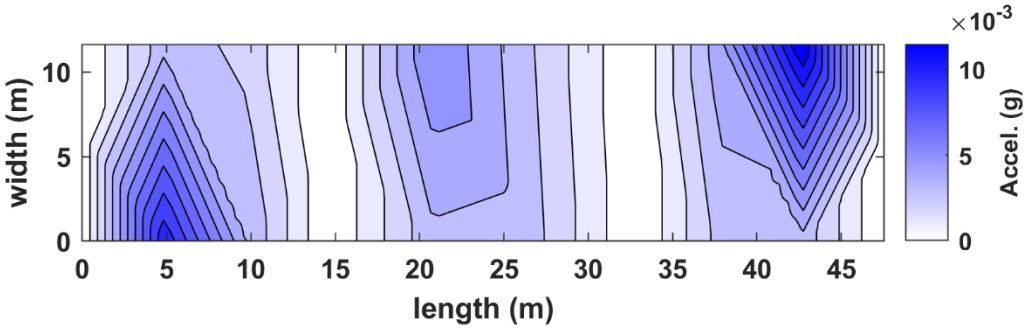

Figure B.60. Interpolated absolute-valued acceleration in plan view for truck pass 27 at the NOBL North bridge structure.

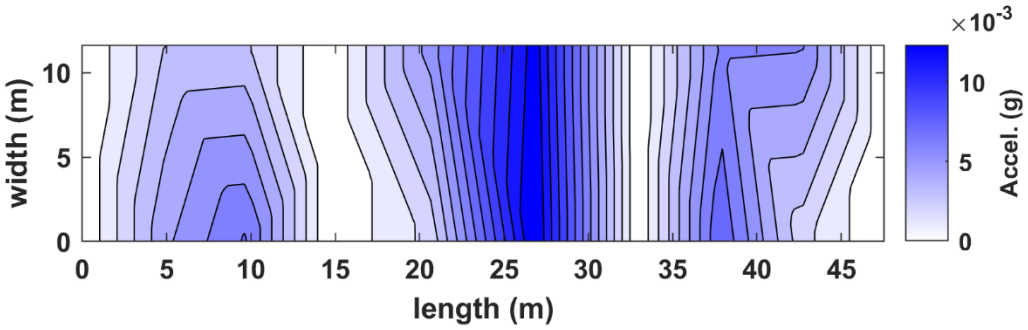

Figure B.61. Interpolated absolute-valued acceleration in plan view for truck pass 28 at the NOBL North bridge structure.

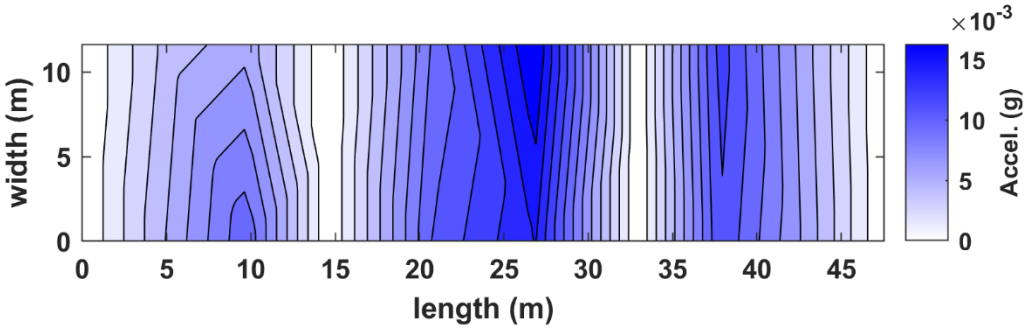

Figure B.62. Interpolated absolute-valued acceleration in plan view for truck pass 29 at the NOBL North bridge structure.

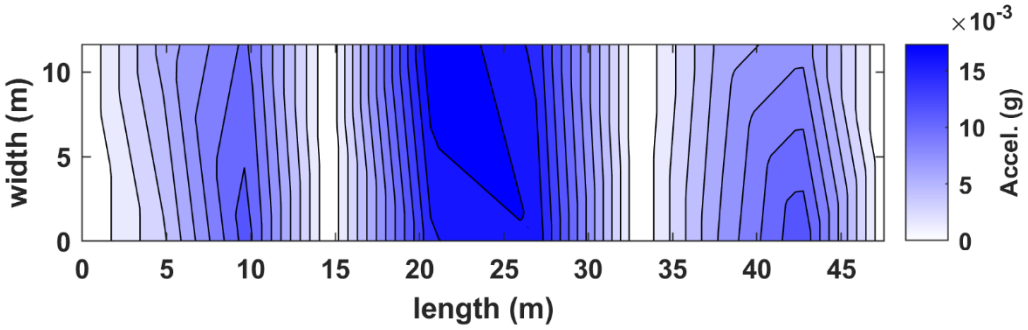

Figure B.63. Interpolated absolute-valued acceleration in plan view for truck pass 30 at the NOBL North bridge structure.

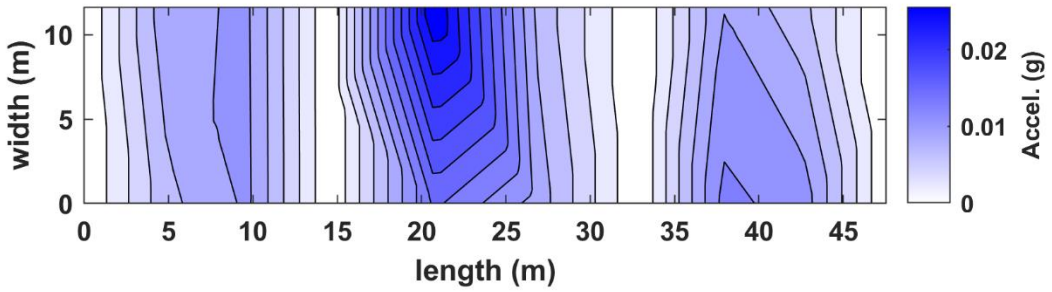

Figure B.64. Interpolated absolute-valued acceleration in plan view for truck pass 31 at the NOBL North bridge structure.

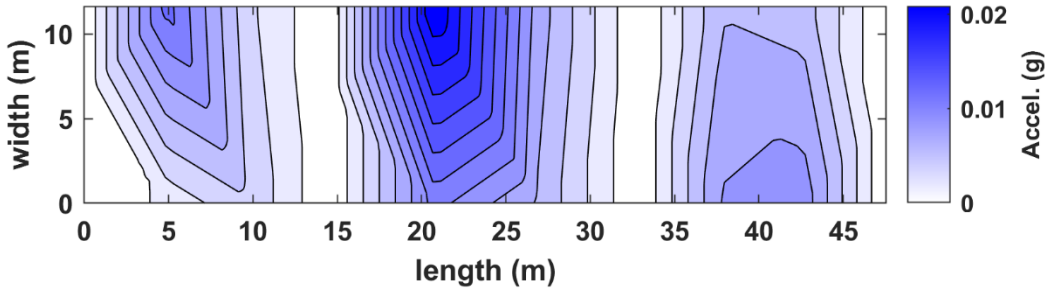

Figure B.65. Interpolated absolute-valued acceleration in plan view for truck pass 32 at the NOBL North bridge structure.

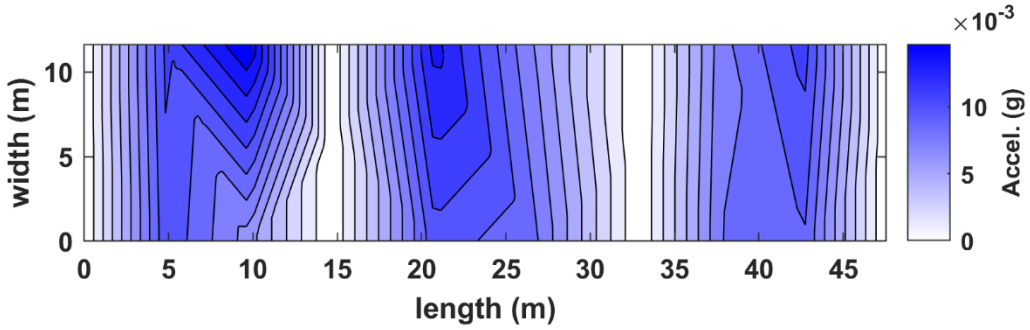

Figure B.66. Interpolated absolute-valued acceleration in plan view for truck pass 33 at the NOBL North bridge structure.

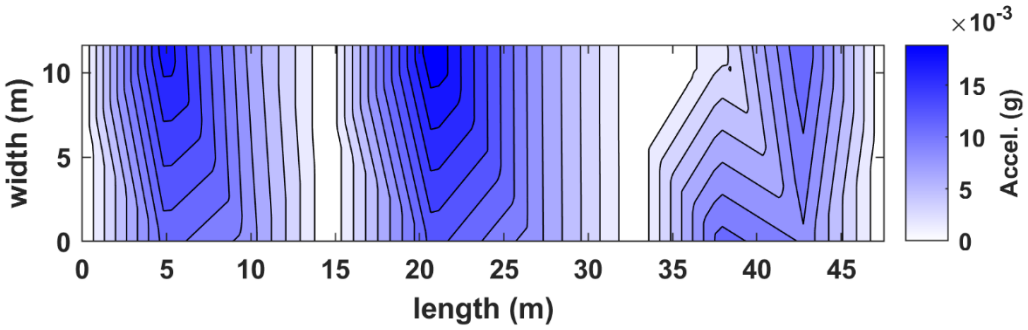

Figure B.67. Interpolated absolute-valued acceleration in plan view for truck pass 34 at the NOBL North bridge structure.

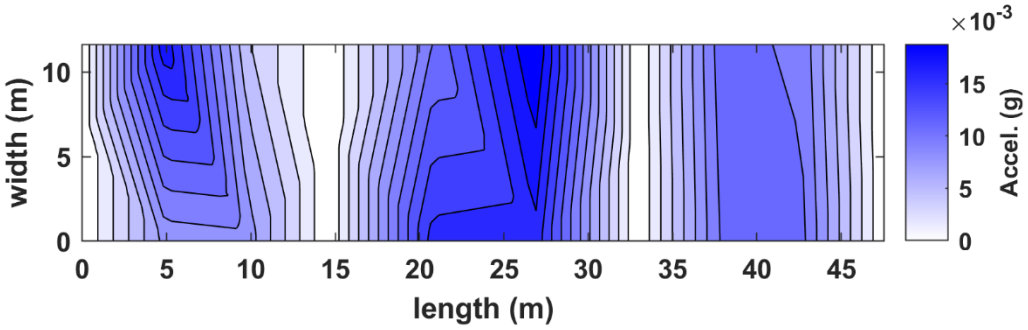

Figure B.68. Interpolated absolute-valued acceleration in plan view for truck pass 35 at the NOBL North bridge structure.

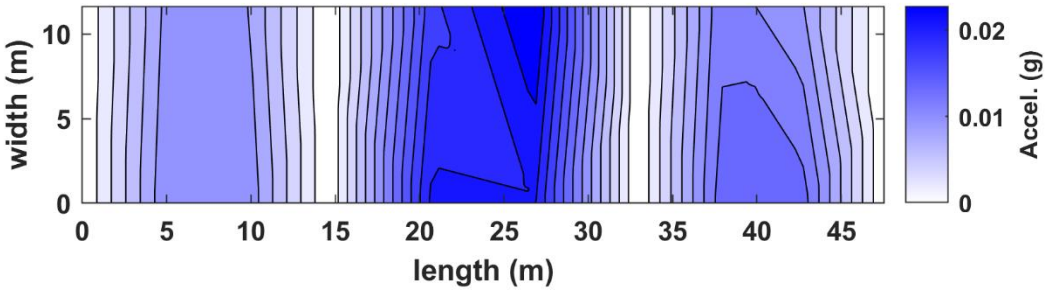

Figure B.69. Interpolated absolute-valued acceleration in plan view for truck pass 36 at the NOBL North bridge structure.

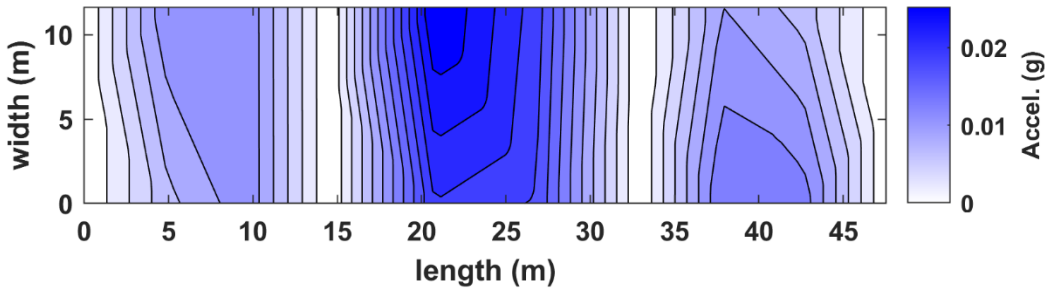

Figure B.70. Interpolated absolute-valued acceleration in plan view for truck pass 37 at the NOBL North bridge structure.

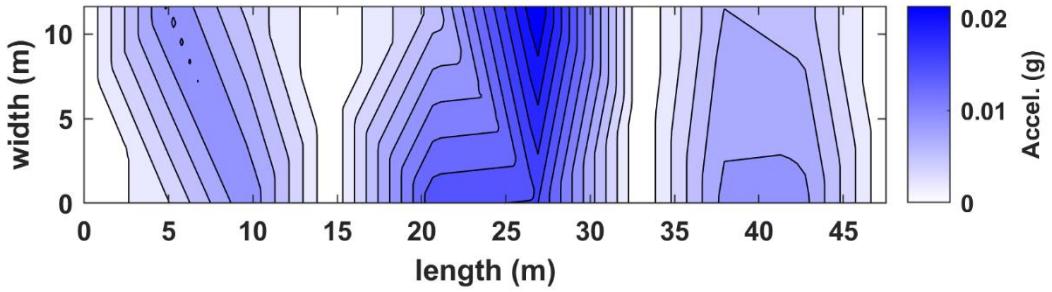

Figure B.71. Interpolated absolute-valued acceleration in plan view for truck pass 38 at the NOBL North bridge structure.

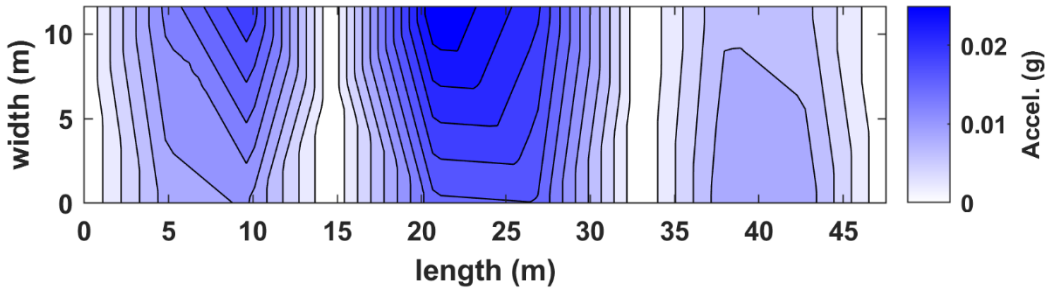

Figure B.72. Interpolated absolute-valued acceleration in plan view for truck pass 39 at the NOBL North bridge structure.

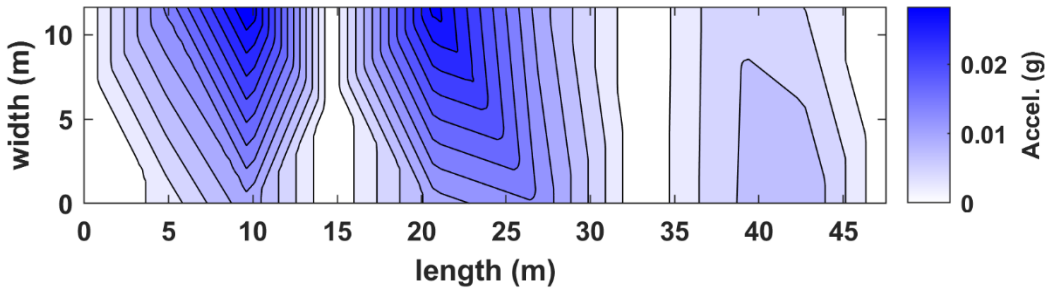

Figure B.73. Interpolated absolute-valued acceleration in plan view for truck pass 40 at the NOBL North bridge structure.

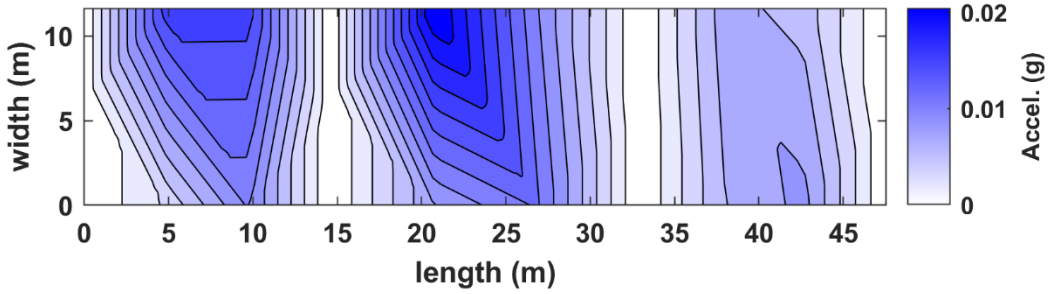

Figure B.74. Interpolated absolute-valued acceleration in plan view for truck pass 41 at the NOBL North bridge structure.

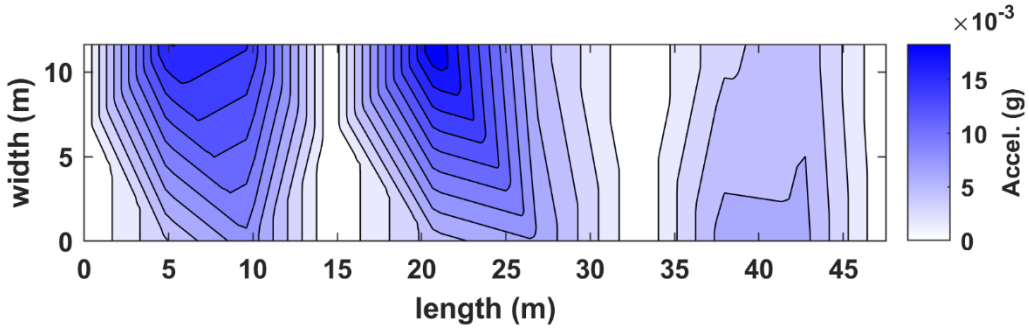

Figure B.75. Interpolated absolute-valued acceleration in plan view for truck pass 42 at the NOBL North bridge structure.

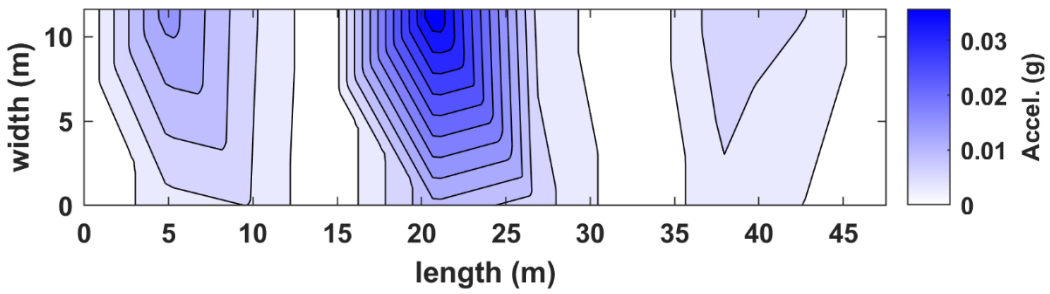

Figure B.76. Interpolated absolute-valued acceleration in plan view for truck pass 43 at the NOBL North bridge structure.

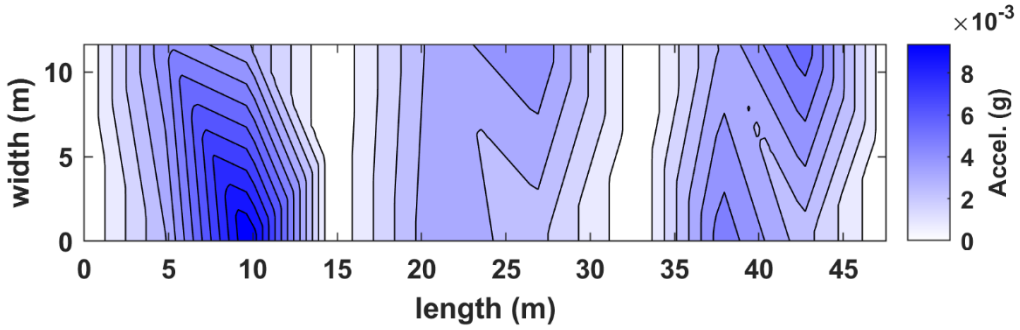

Figure B.77. Interpolated absolute-valued acceleration in plan view for truck pass 44 at the NOBL North bridge structure.

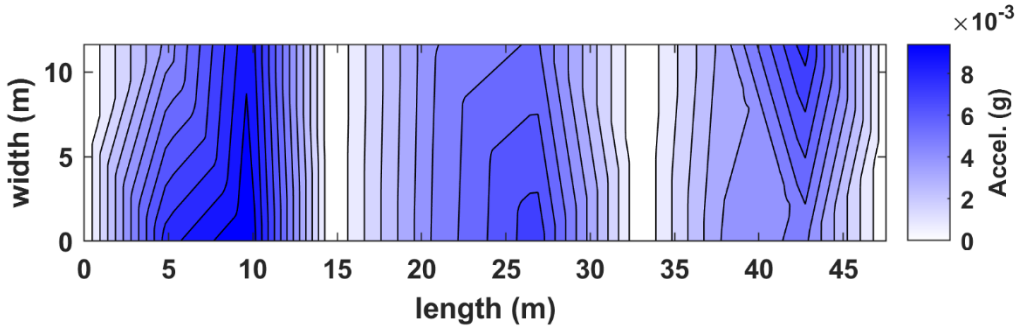

Figure B.78. Interpolated absolute-valued acceleration in plan view for truck pass 45 at the NOBL North bridge structure.

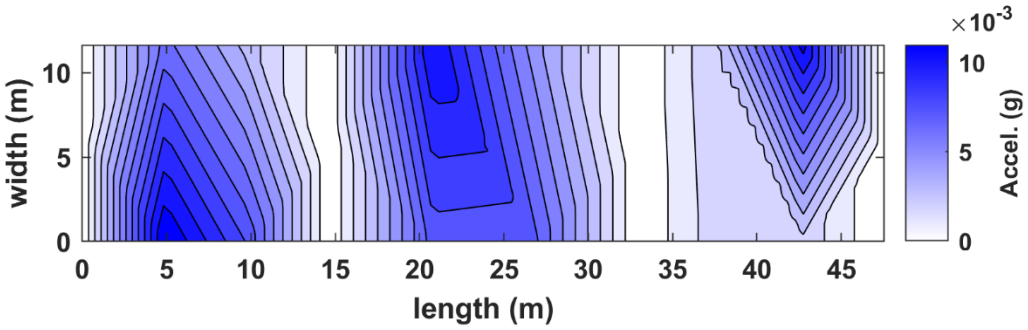

Figure B.79. Interpolated absolute-valued acceleration in plan view for truck pass 46 at the NOBL North bridge structure.

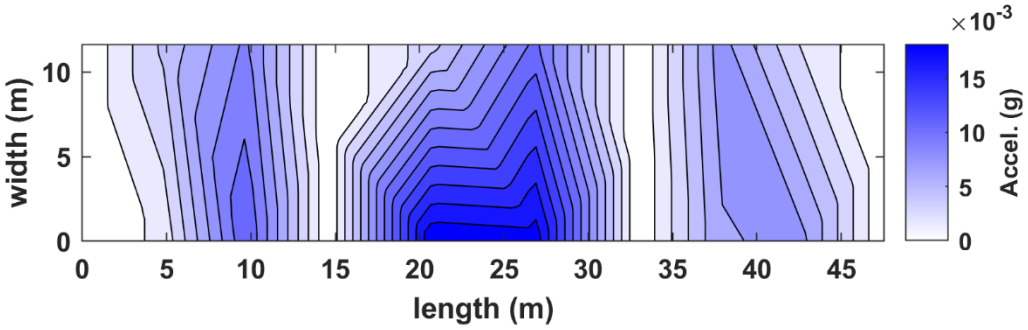

Figure B.80. Interpolated absolute-valued acceleration in plan view for truck pass 47 at the NOBL North bridge structure.

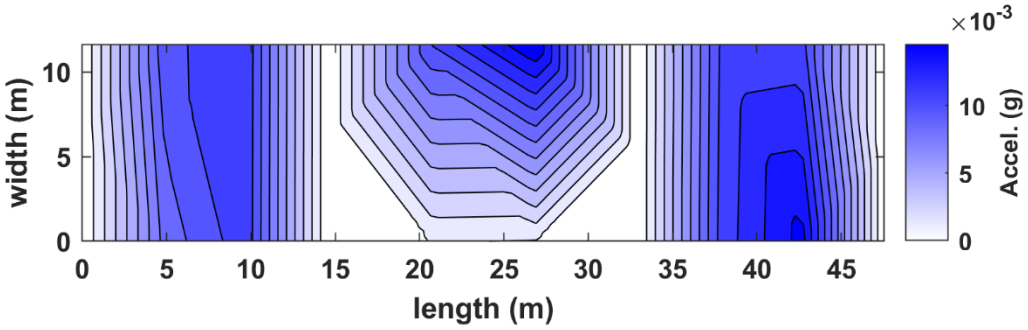

Figure B.81. Interpolated absolute-valued acceleration in plan view for truck pass 48 at the NOBL North bridge structure.

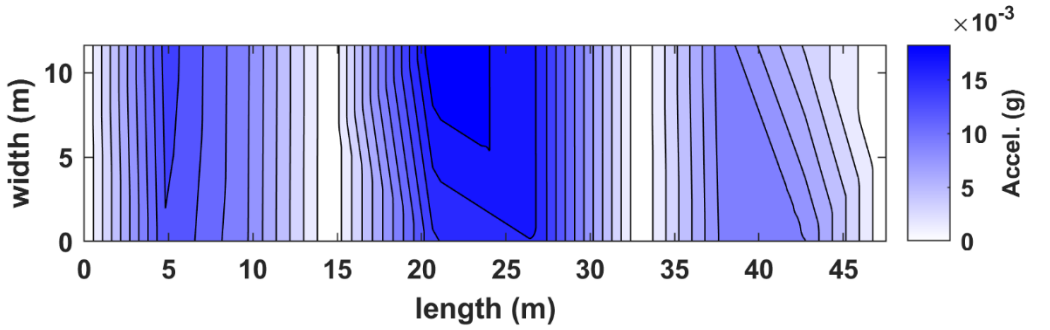

Figure B.82. Interpolated absolute-valued acceleration in plan view for truck pass 49 at the NOBL North bridge structure.

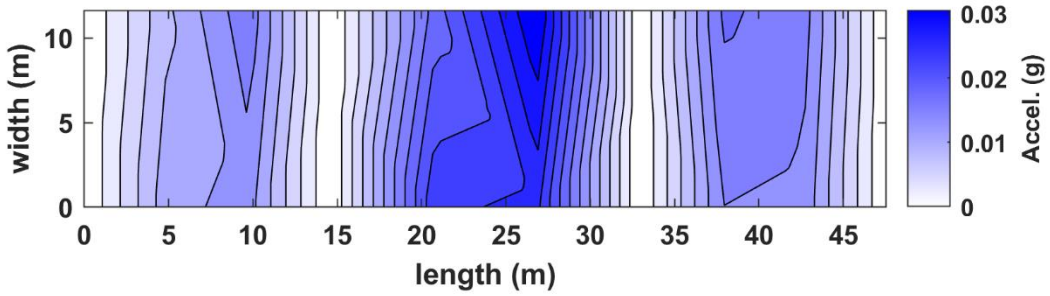

Figure B.83. Interpolated absolute-valued acceleration in plan view for truck pass 50 at the NOBL North bridge structure.

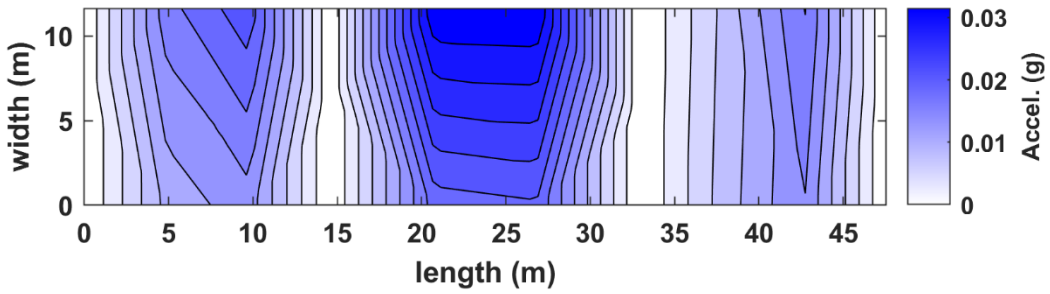

Figure B.84. Interpolated absolute-valued acceleration in plan view for truck pass 51 at the NOBL North bridge structure.

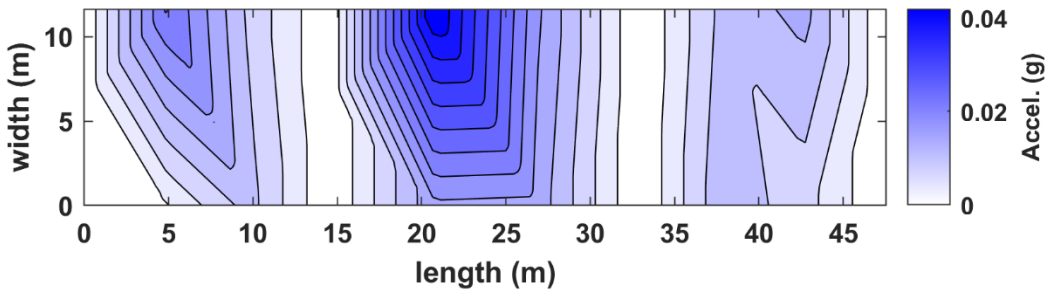

Figure B.85. Interpolated absolute-valued acceleration in plan view for truck pass 52 at the NOBL North bridge structure.

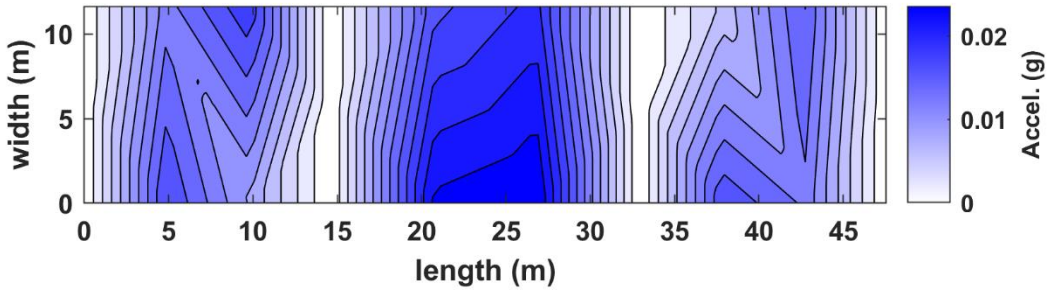

Figure B.86. Interpolated absolute-valued acceleration in plan view for truck pass 53 at the NOBL North bridge structure.

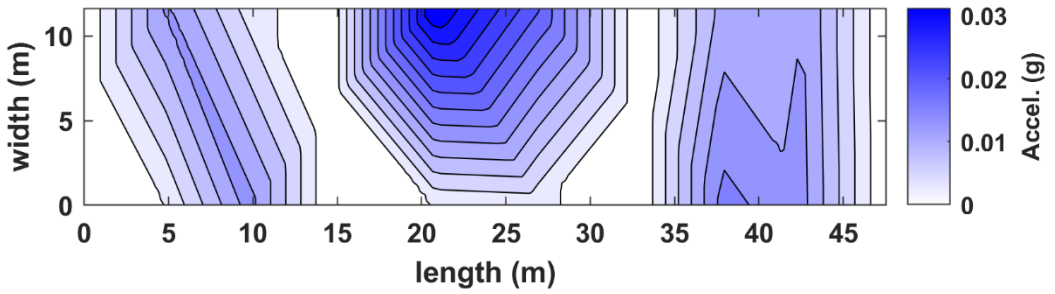

Figure B.87. Interpolated absolute-valued acceleration in plan view for truck pass 54 at the NOBL North bridge structure.

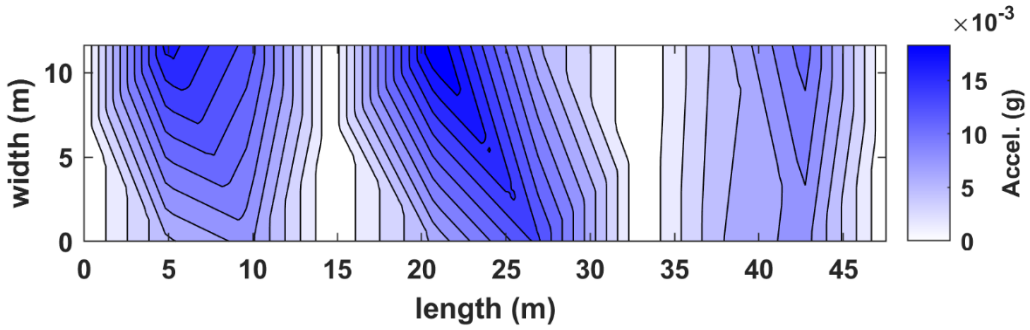

Figure B.88. Interpolated absolute-valued acceleration in plan view for truck pass 55 at the NOBL North bridge structure.

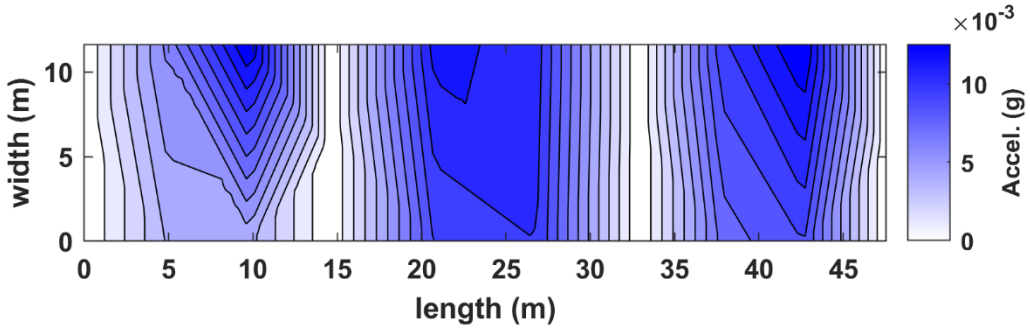

Figure B.89. Interpolated absolute-valued acceleration in plan view for truck pass 56 at the NOBL North bridge structure.

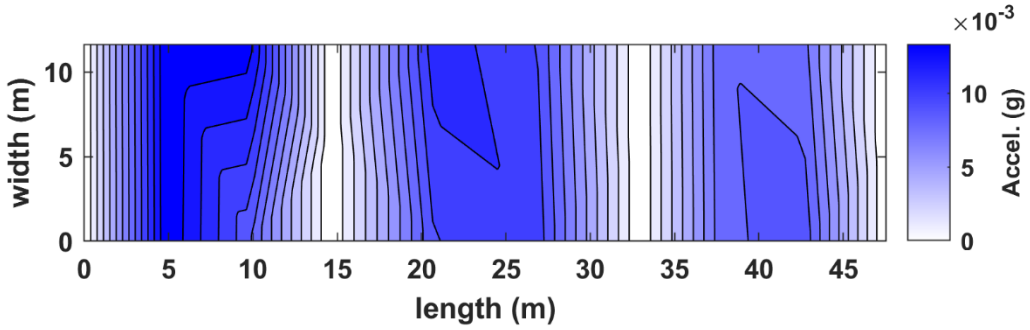

Figure B.90. Interpolated absolute-valued acceleration in plan view for truck pass 57 at the NOBL North bridge structure.

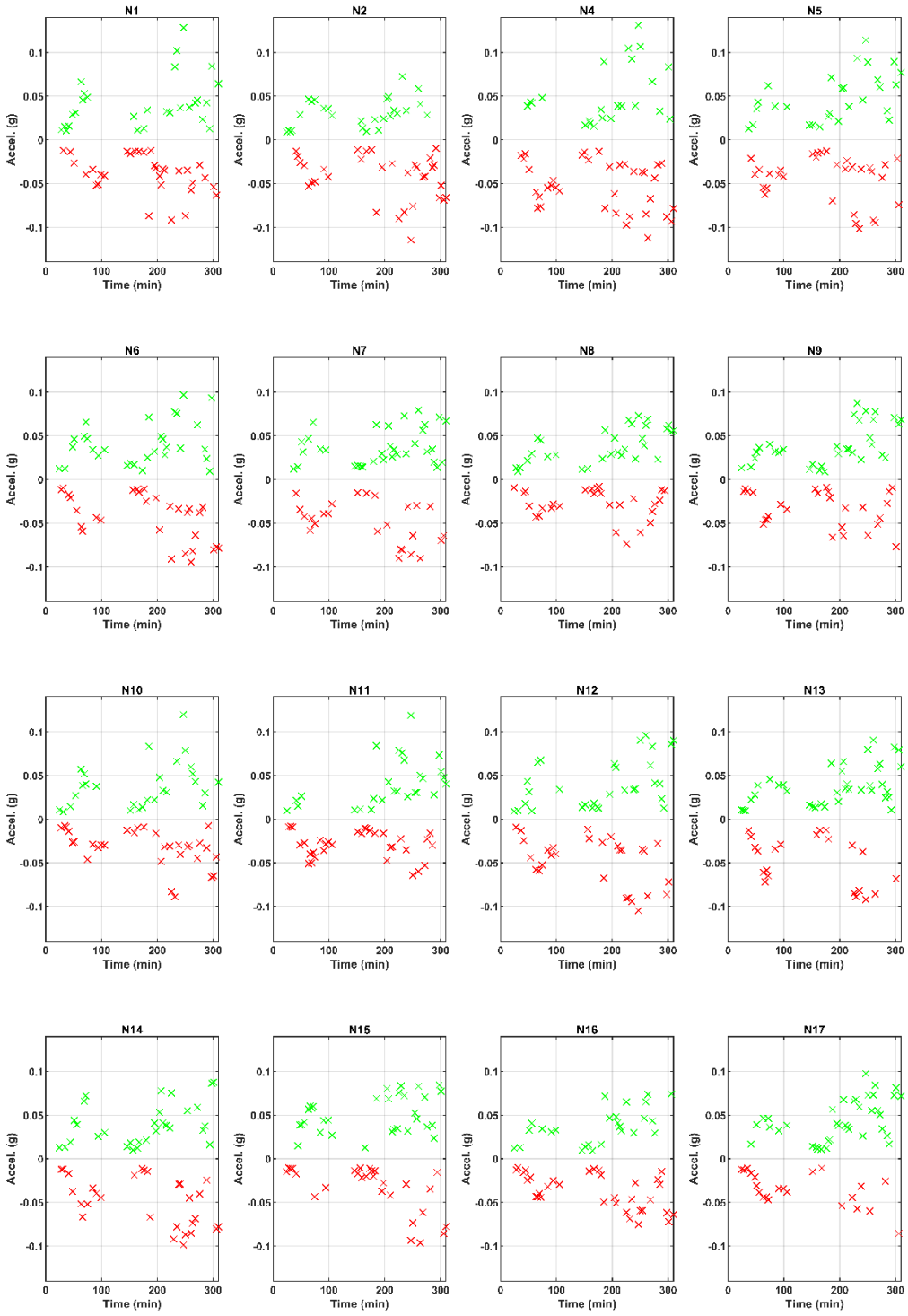

Figure B.91. Maximum acceleration values for each truck pass at the NOBL East Yutan bridge structure.

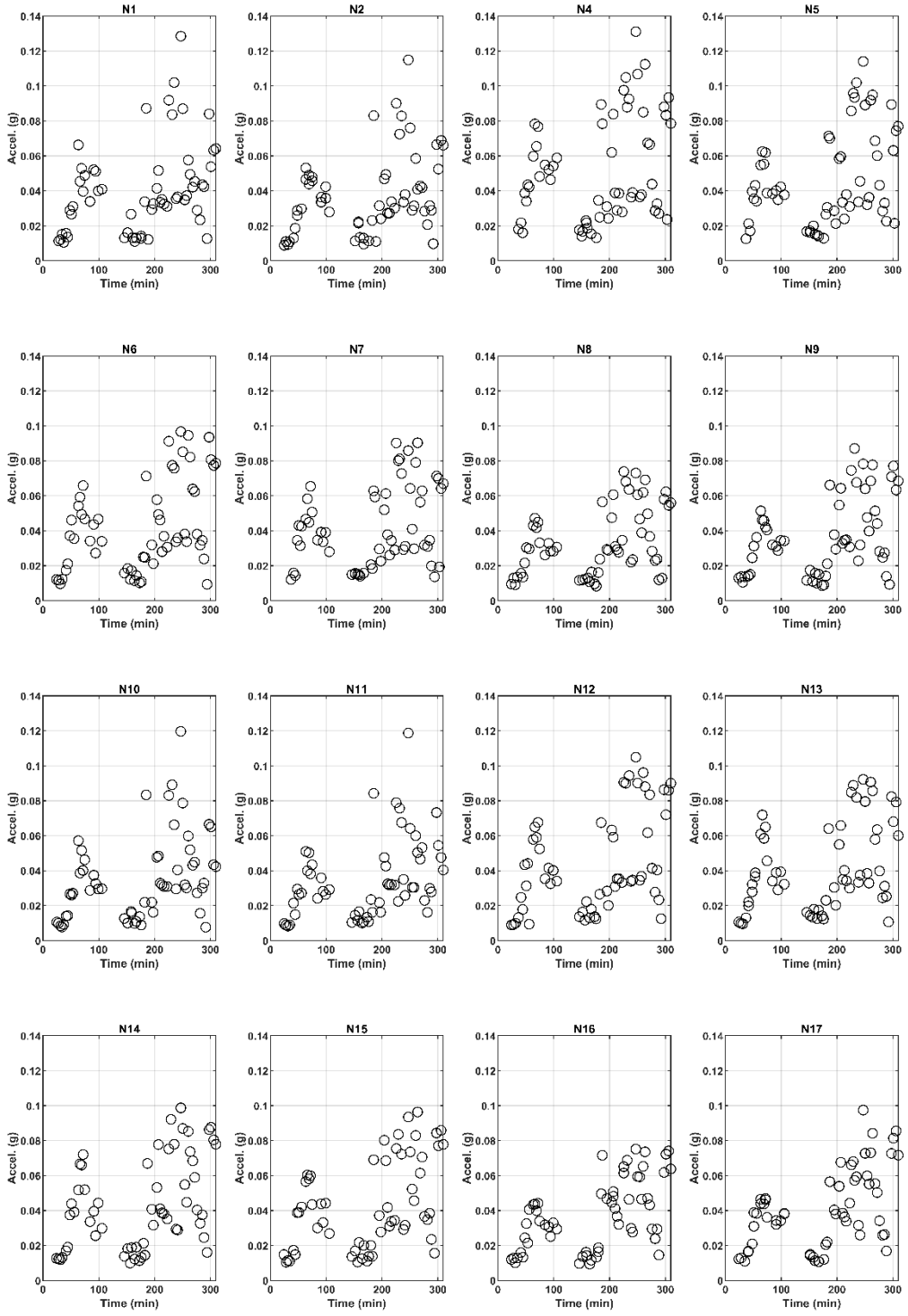

Figure B.92. Absolute maximum acceleration values for each truck pass at the NOBL East Yutan bridge structure.

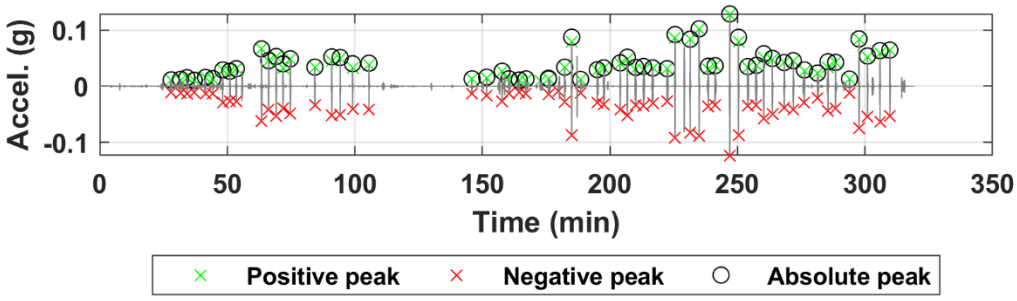

Figure B.93. Acceleration time history of sensor N01 for all truck passes at the NOBL East Yutan bridge structure.

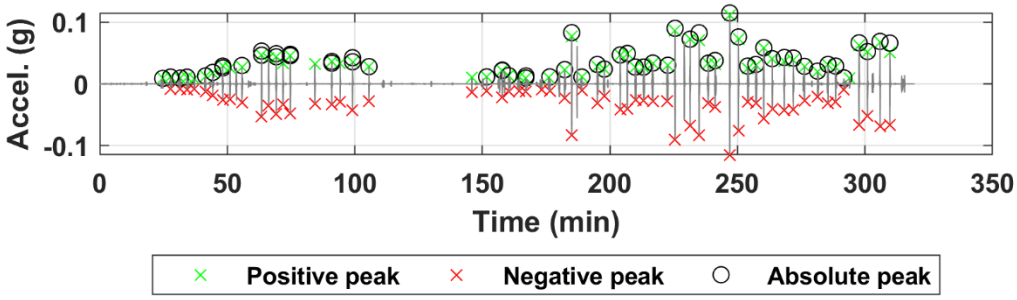

Figure B.94. Acceleration time history of sensor N02 for all truck passes at the NOBL East Yutan bridge structure.

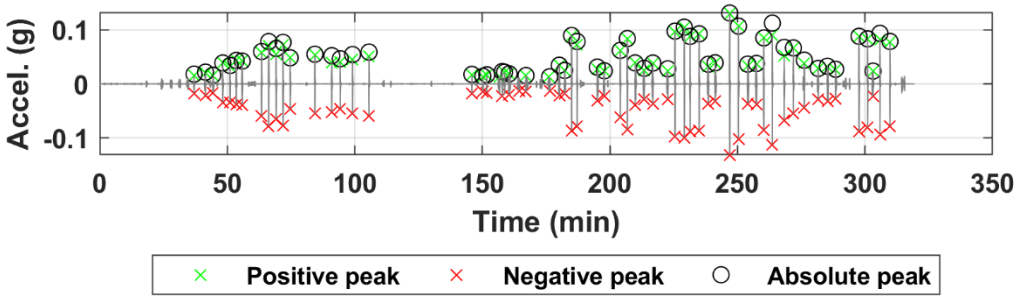

Figure B.95. Acceleration time history of sensor N04 for all truck passes at the NOBL East Yutan bridge structure.

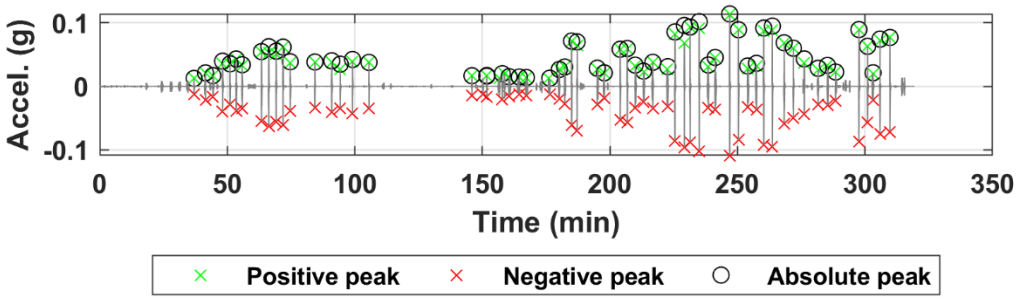

Figure B.96. Acceleration time history of sensor N05 for all truck passes at the NOBL East Yutan bridge structure.

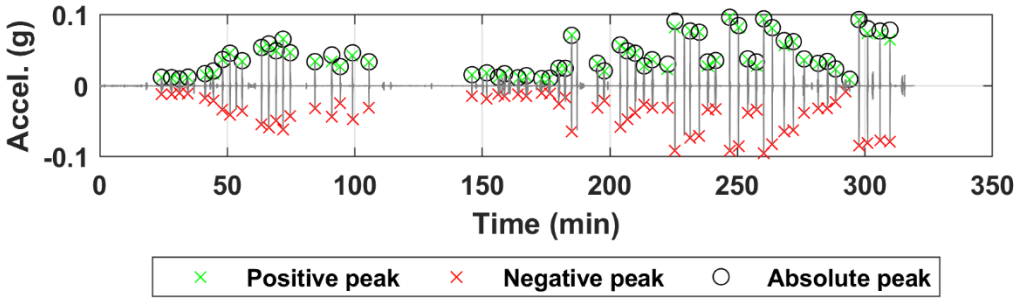

Figure B.97. Acceleration time history of sensor N06 for all truck passes at the NOBL East Yutan bridge structure.

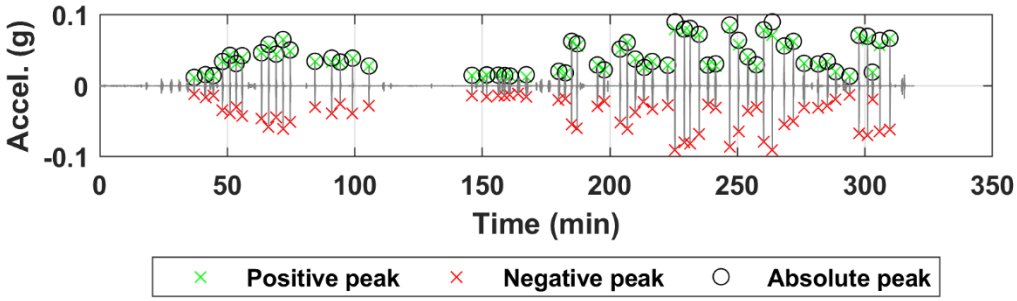

Figure B.98. Acceleration time history of sensor N07 for all truck passes at the NOBL East Yutan bridge structure.

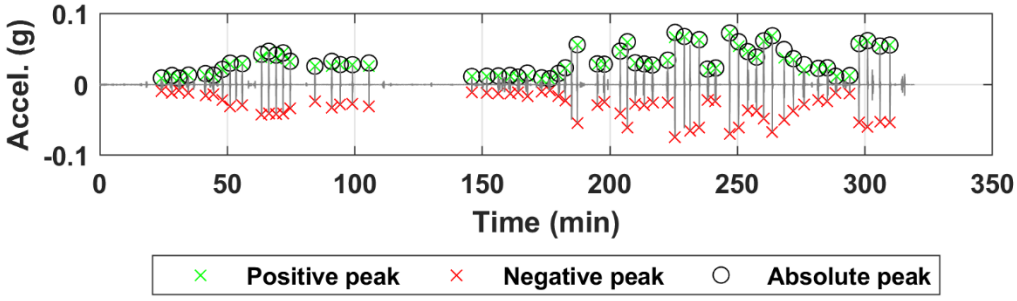

Figure B.99. Acceleration time history of sensor N08 for all truck passes at the NOBL East Yutan bridge structure.

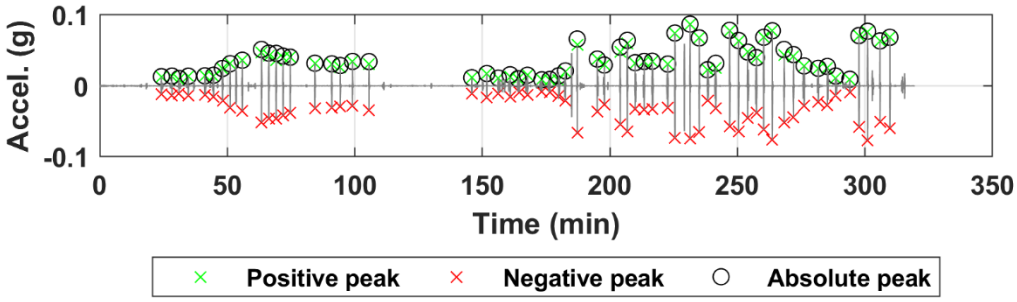

Figure B.100. Acceleration time history of sensor N09 for all truck passes at the NOBL East Yutan bridge structure.

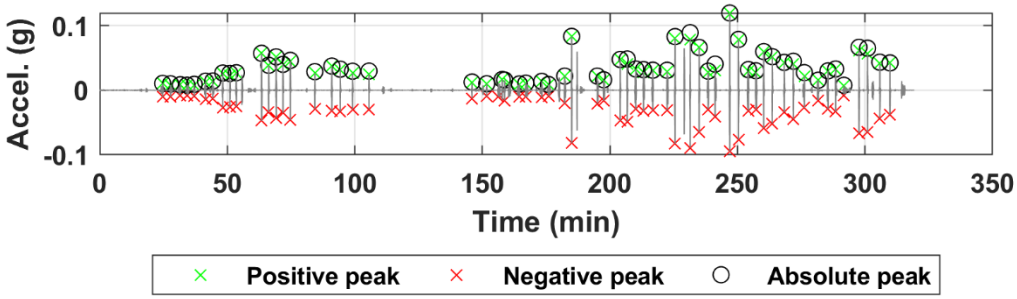

Figure B.101. Acceleration time history of sensor N10 for all truck passes at the NOBL East Yutan bridge structure.

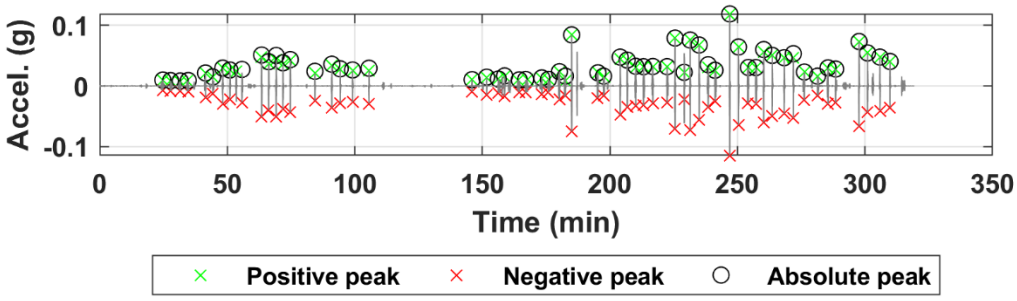

Figure B.102. Acceleration time history of sensor N11 for all truck passes at the NOBL East Yutan bridge structure.

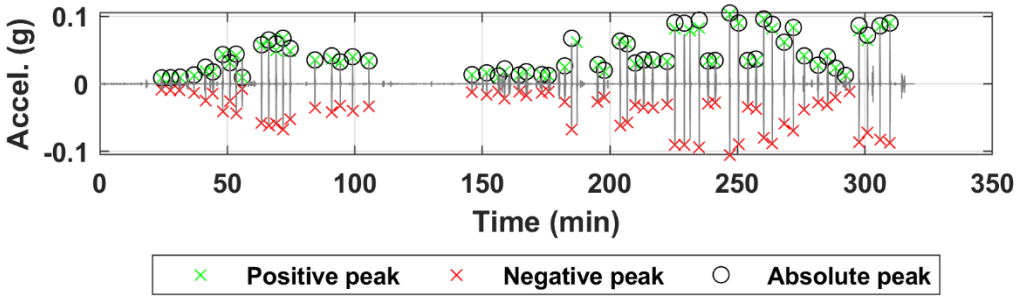

Figure B.103. Acceleration time history of sensor N12 for all truck passes at the NOBL East Yutan bridge structure.

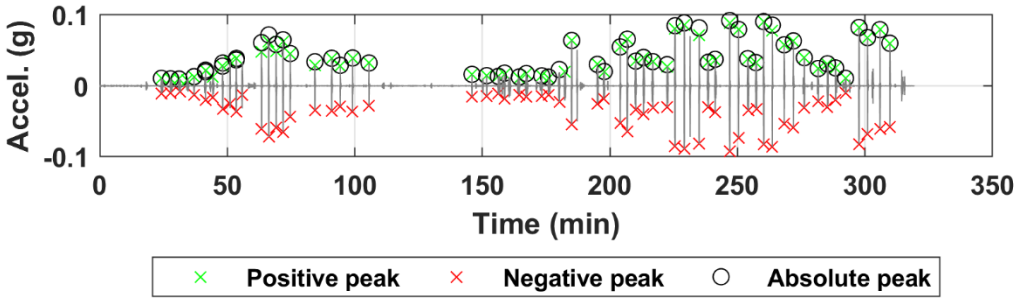

Figure B.104. Acceleration time history of sensor N13 for all truck passes at the NOBL East Yutan bridge structure.

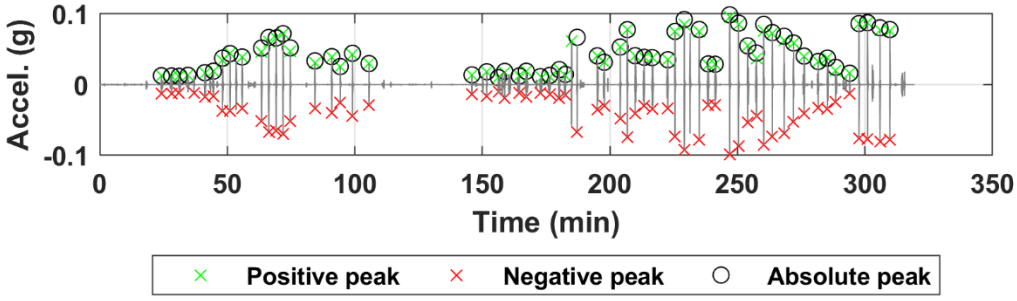

Figure B.105. Acceleration time history of sensor N14 for all truck passes at the NOBL East Yutan bridge structure.

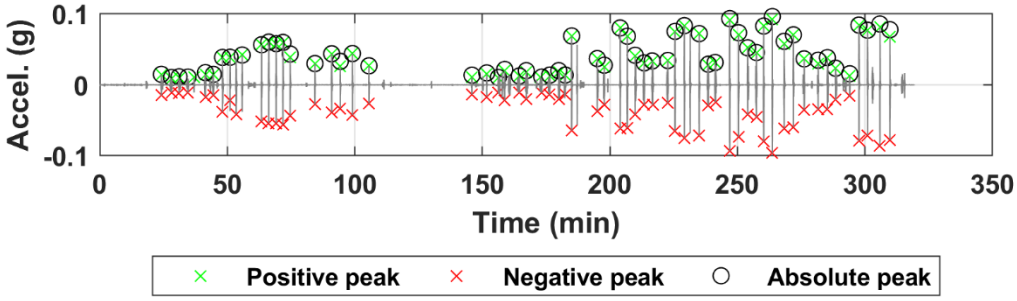

Figure B.106. Acceleration time history of sensor N15 for all truck passes at the NOBL East Yutan bridge structure.

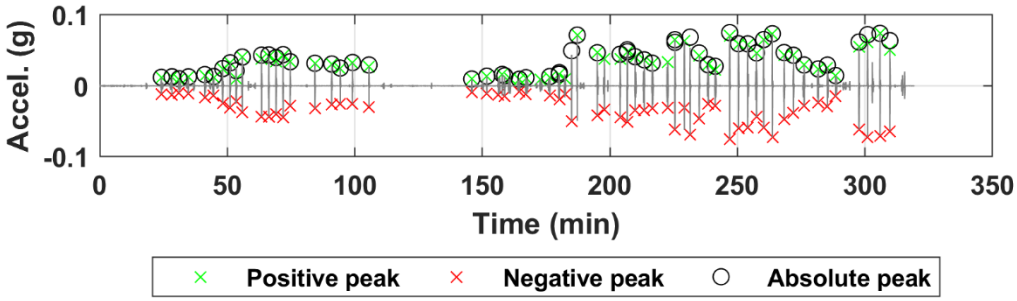

Figure B.107. Acceleration time history of sensor N16 for all truck passes at the NOBL East Yutan bridge structure.

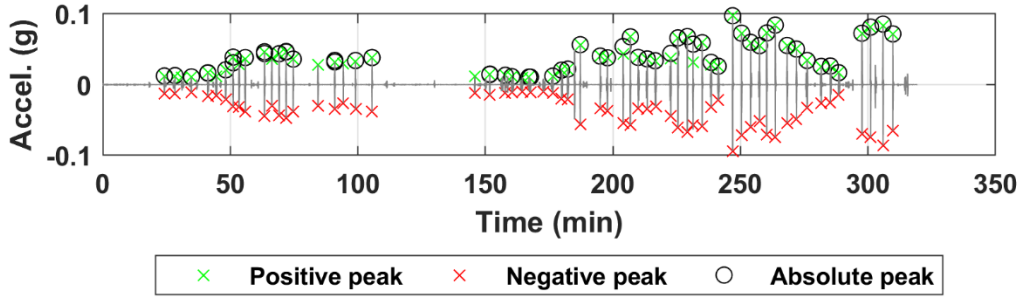

Figure B.108. Acceleration time history of sensor N17 for all truck passes at the NOBL East Yutan bridge structure.

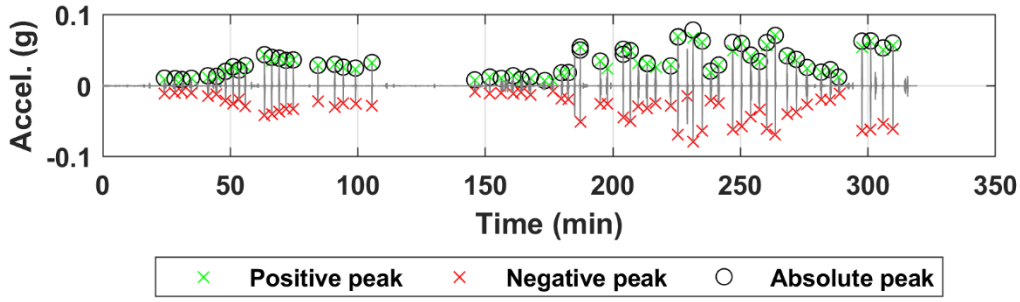

Figure B.109. Acceleration time history of sensor N18 for all truck passes at the NOBL East Yutan bridge structure.

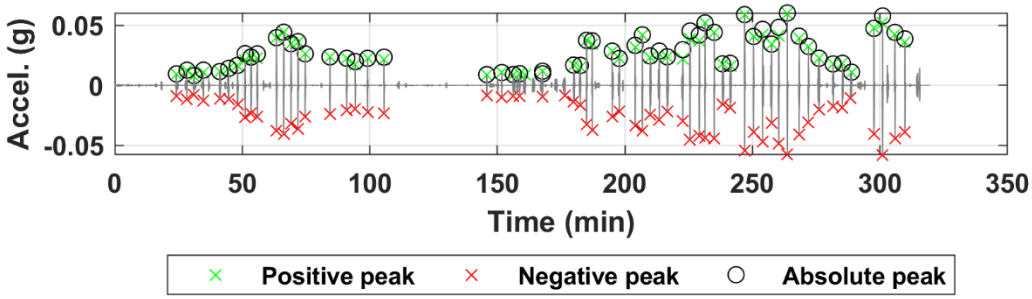

Figure B.110. Acceleration time history of sensor N19 for all truck passes at the NOBL East Yutan bridge structure.

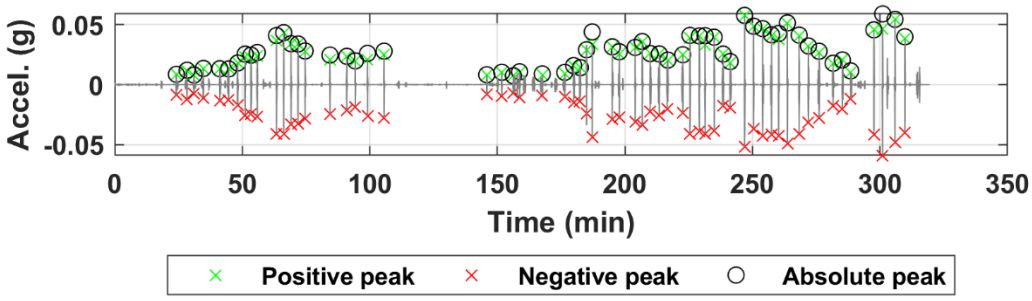

Figure B.111. Acceleration time history of sensor N20 for all truck passes at the NOBL East Yutan bridge structure.

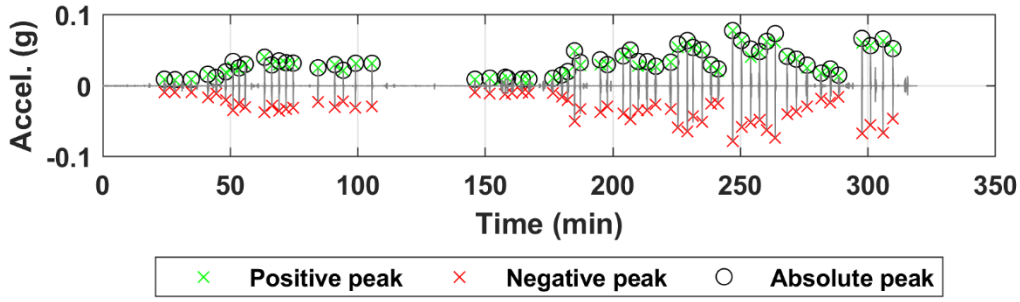

Figure B.112. Acceleration time history of sensor N21 for all truck passes at the NOBL East Yutan bridge structure.

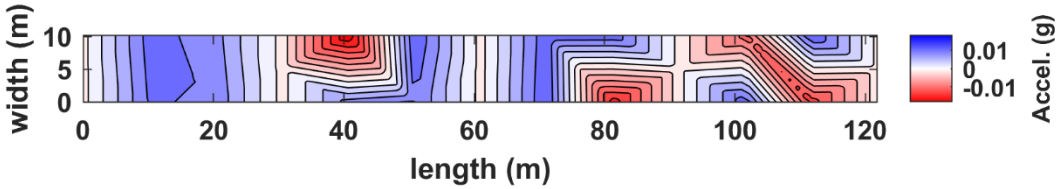

Figure B.113. Interpolated acceleration in plan view for truck pass 01 at the NOBL East Yutan bridge structure.

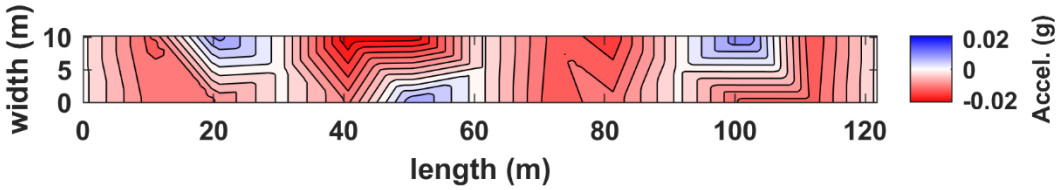

Figure B.114. Interpolated acceleration in plan view for truck pass 02 at the NOBL East Yutan bridge structure.

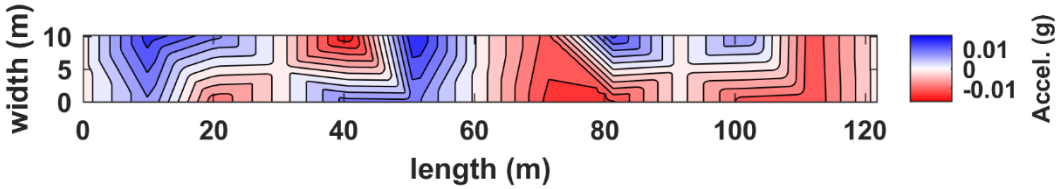

Figure B.115. Interpolated acceleration in plan view for truck pass 03 at the NOBL East Yutan bridge structure.

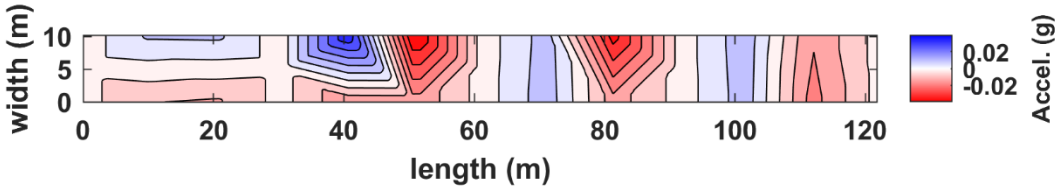

Figure B.116. Interpolated acceleration in plan view for truck pass 04 at the NOBL East Yutan bridge structure.

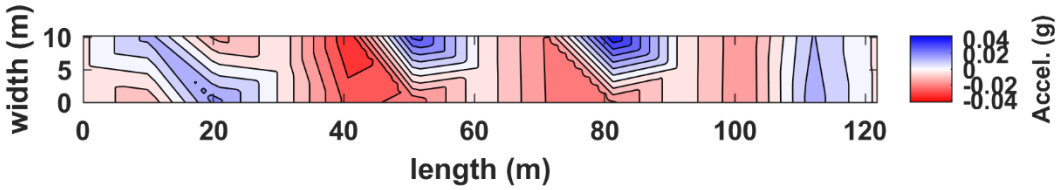

Figure B.117. Interpolated acceleration in plan view for truck pass 05 at the NOBL East Yutan bridge structure.

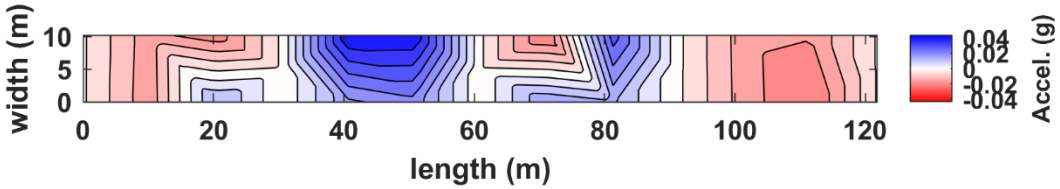

Figure B.118. Interpolated acceleration in plan view for truck pass 06 at the NOBL East Yutan bridge structure.

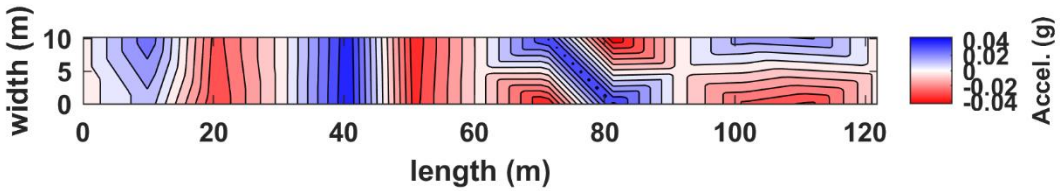

Figure B.119. Interpolated acceleration in plan view for truck pass 07 at the NOBL East Yutan bridge structure.

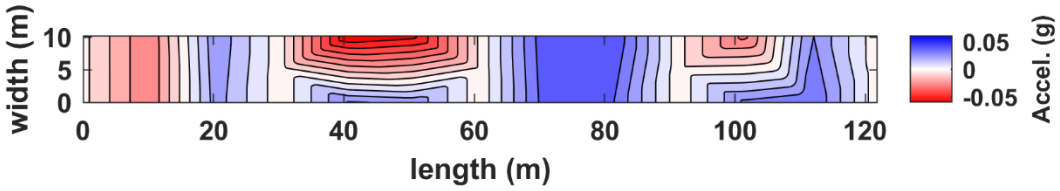

Figure B.120. Interpolated acceleration in plan view for truck pass 08 at the NOBL East Yutan bridge structure.

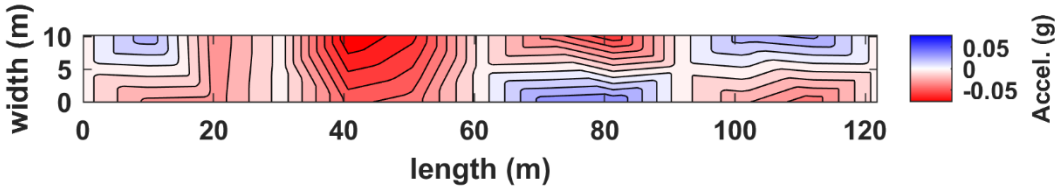

Figure B.121. Interpolated acceleration in plan view for truck pass 09 at the NOBL East Yutan bridge structure.

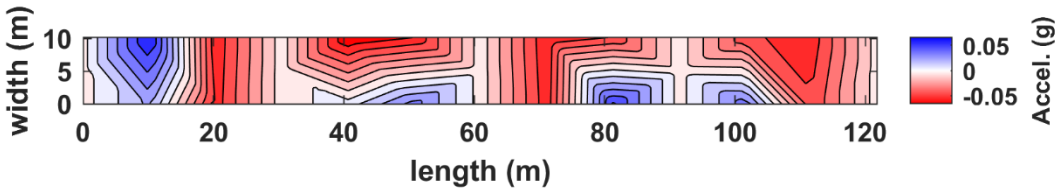

Figure B.122. Interpolated acceleration in plan view for truck pass 10 at the NOBL East Yutan bridge structure.

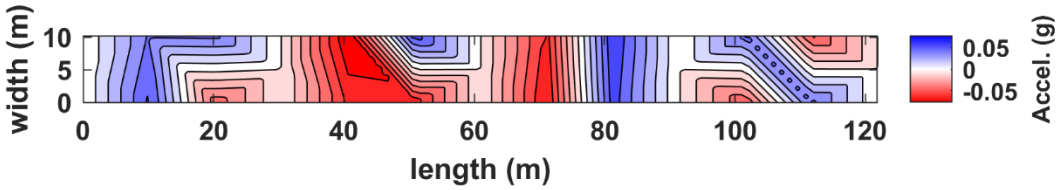

Figure B.123. Interpolated acceleration in plan view for truck pass 11 at the NOBL East Yutan bridge structure.

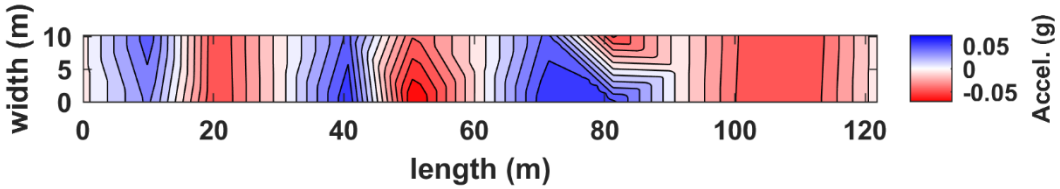

Figure B.124. Interpolated acceleration in plan view for truck pass 12 at the NOBL East Yutan bridge structure.

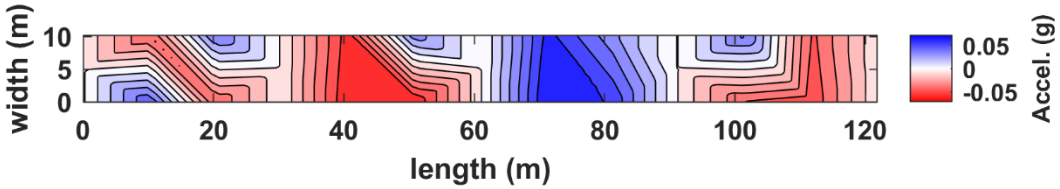

Figure B.125. Interpolated acceleration in plan view for truck pass 13 at the NOBL East Yutan bridge structure.

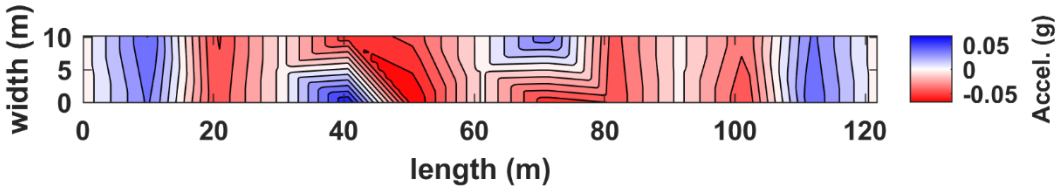

Figure B.126. Interpolated acceleration in plan view for truck pass 14 at the NOBL East Yutan bridge structure.

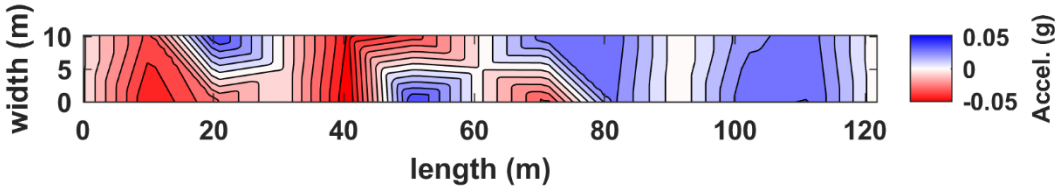

Figure B.127. Interpolated acceleration in plan view for truck pass 15 at the NOBL East Yutan bridge structure.

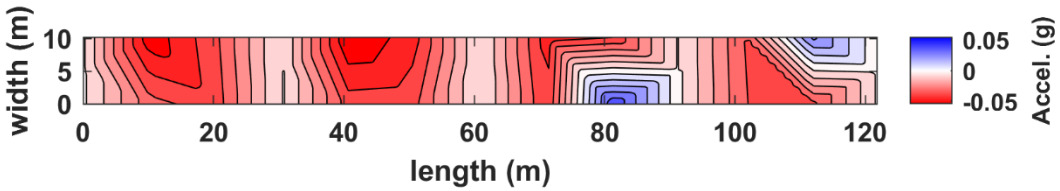

Figure B.128. Interpolated acceleration in plan view for truck pass 16 at the NOBL East Yutan bridge structure.

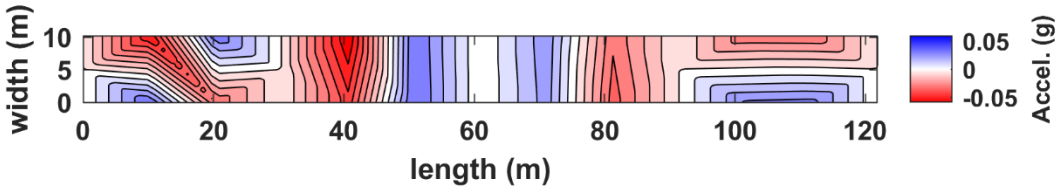

Figure B.129. Interpolated acceleration in plan view for truck pass 17 at the NOBL East Yutan bridge structure.

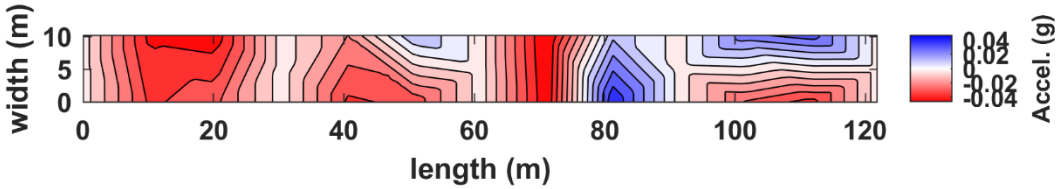

Figure B.130. Interpolated acceleration in plan view for truck pass 18 at the NOBL East Yutan bridge structure.

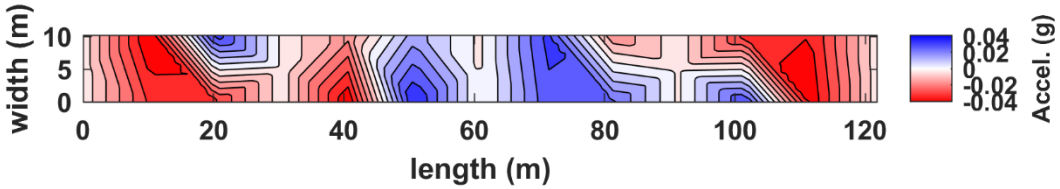

Figure B.131. Interpolated acceleration in plan view for truck pass 19 at the NOBL East Yutan bridge structure.

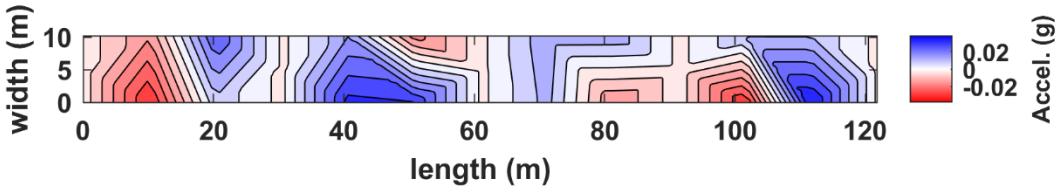

Figure B.132. Interpolated acceleration in plan view for truck pass 20 at the NOBL East Yutan bridge structure.

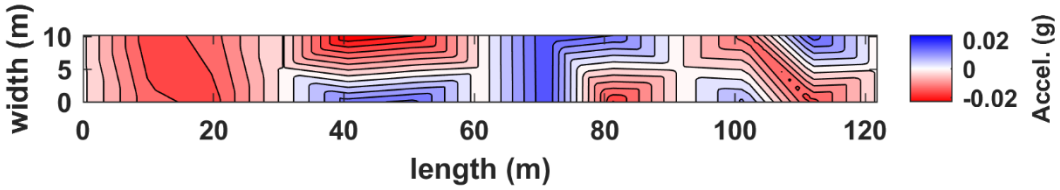

Figure B.133. Interpolated acceleration in plan view for truck pass 21 at the NOBL East Yutan bridge structure.

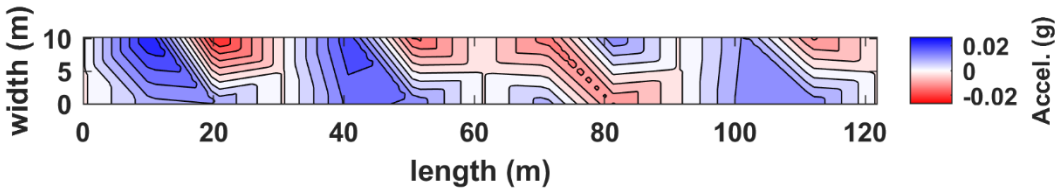

Figure B.134. Interpolated acceleration in plan view for truck pass 22 at the NOBL East Yutan bridge structure.

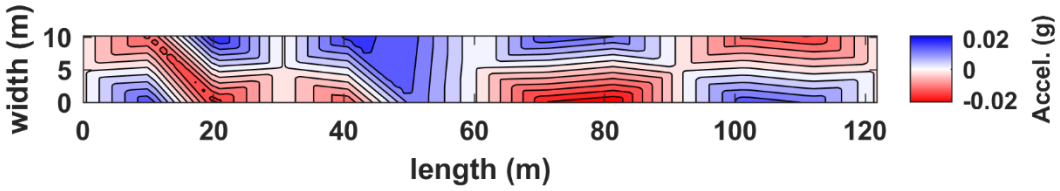

Figure B.135. Interpolated acceleration in plan view for truck pass 23 at the NOBL East Yutan bridge structure.

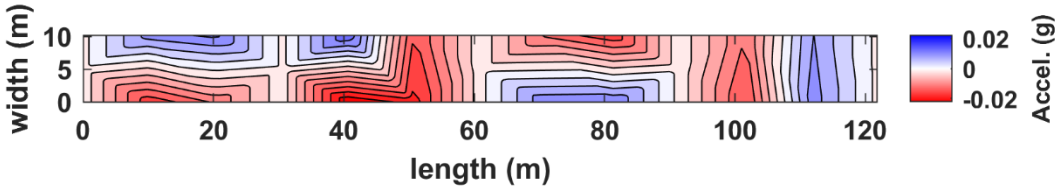

Figure B.136. Interpolated acceleration in plan view for truck pass 24 at the NOBL East Yutan bridge structure.

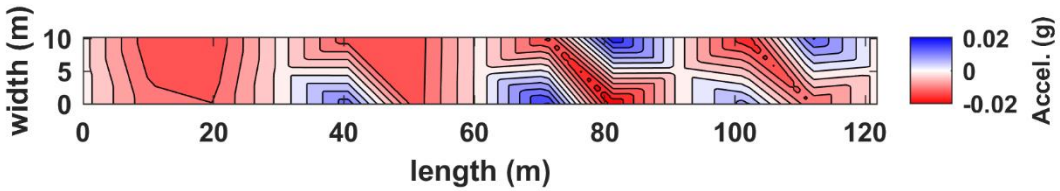

Figure B.137. Interpolated acceleration in plan view for truck pass 25 at the NOBL East Yutan bridge structure.

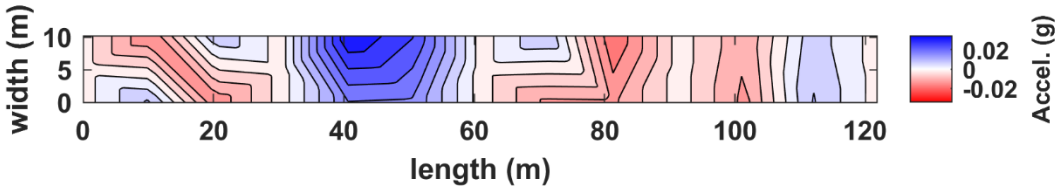

Figure B.138. Interpolated acceleration in plan view for truck pass 26 at the NOBL East Yutan bridge structure.

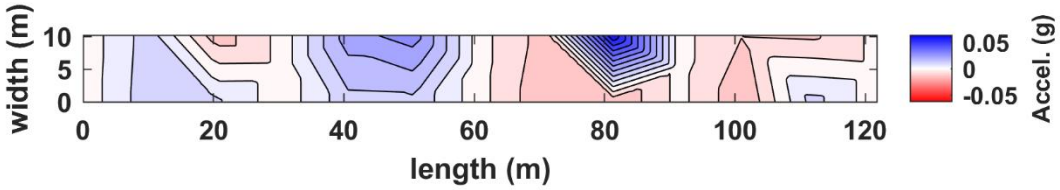

Figure B.139. Interpolated acceleration in plan view for truck pass 27 at the NOBL East Yutan bridge structure.

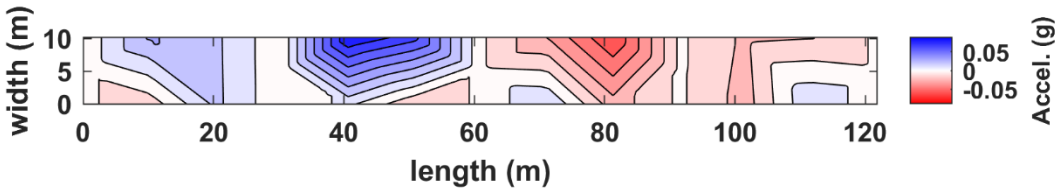

Figure B.140. Interpolated acceleration in plan view for truck pass 28 at the NOBL East Yutan bridge structure.

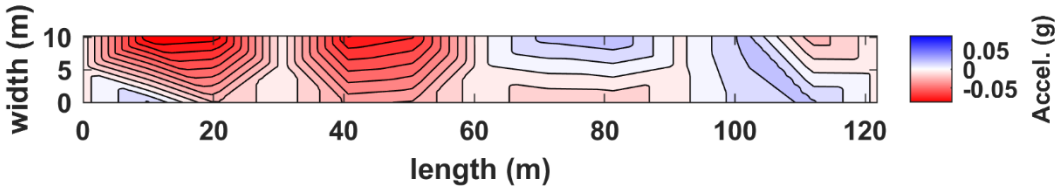

Figure B.141. Interpolated acceleration in plan view for truck pass 29 at the NOBL East Yutan bridge structure.

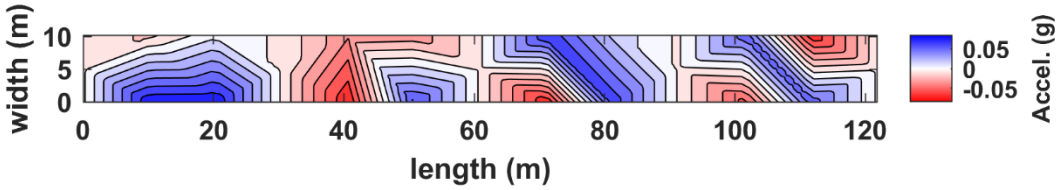

Figure B.142. Interpolated acceleration in plan view for truck pass 30 at the NOBL East Yutan bridge structure.

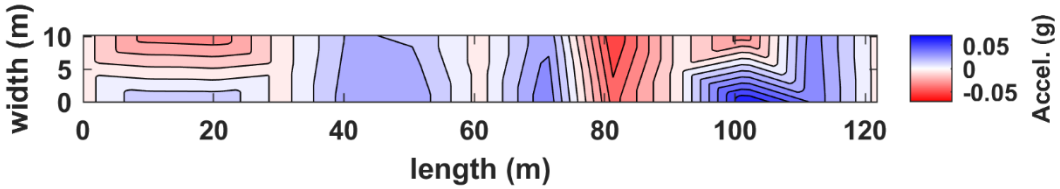

Figure B.143. Interpolated acceleration in plan view for truck pass 31 at the NOBL East Yutan bridge structure.

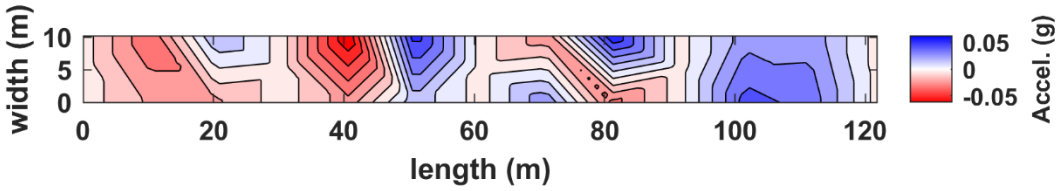

Figure B.144. Interpolated acceleration in plan view for truck pass 32 at the NOBL East Yutan bridge structure.

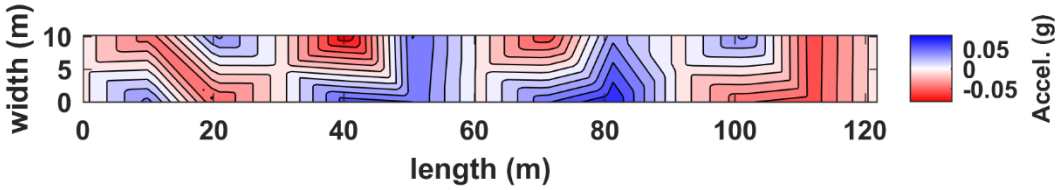

Figure B.145. Interpolated acceleration in plan view for truck pass 33 at the NOBL East Yutan bridge structure.

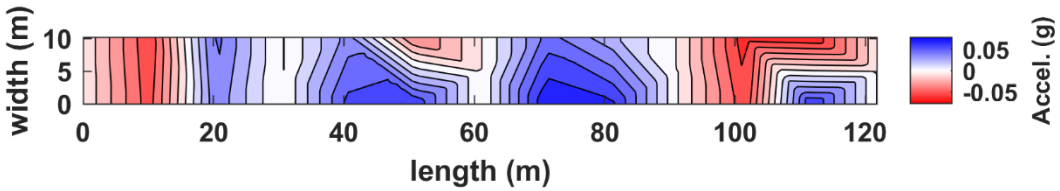

Figure B.146. Interpolated acceleration in plan view for truck pass 34 at the NOBL East Yutan bridge structure.

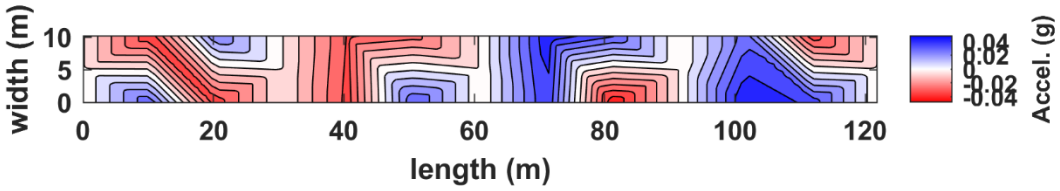

Figure B.147. Interpolated acceleration in plan view for truck pass 35 at the NOBL East Yutan bridge structure.

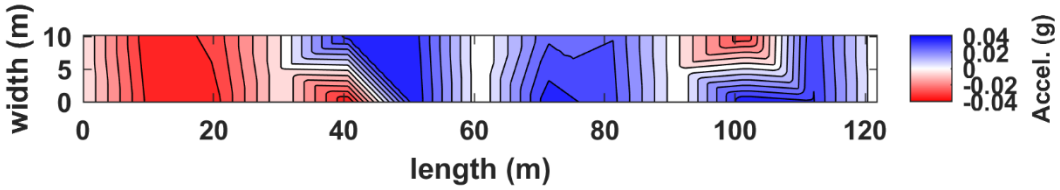

Figure B.148. Interpolated acceleration in plan view for truck pass 36 at the NOBL East Yutan bridge structure.

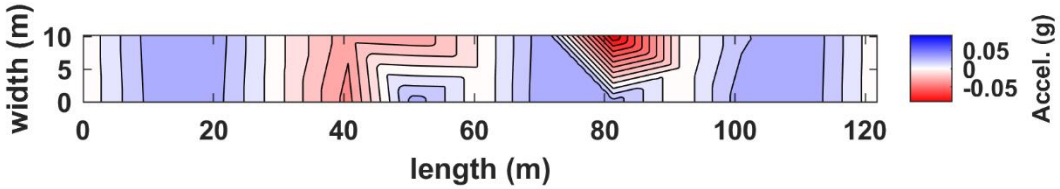

Figure B.149. Interpolated acceleration in plan view for truck pass 37 at the NOBL East Yutan bridge structure.

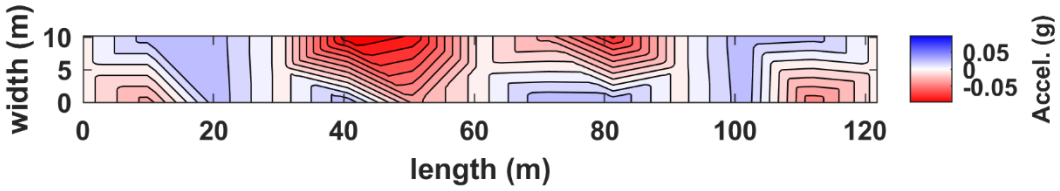

Figure B.150. Interpolated acceleration in plan view for truck pass 38 at the NOBL East Yutan bridge structure.

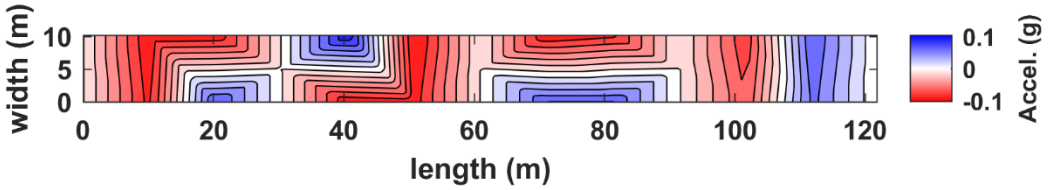

Figure B.151. Interpolated acceleration in plan view for truck pass 39 at the NOBL East Yutan bridge structure.

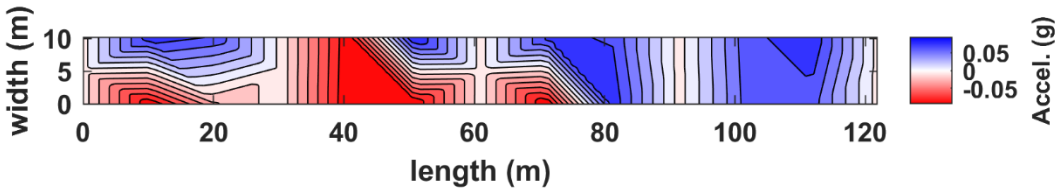

Figure B.152. Interpolated acceleration in plan view for truck pass 40 at the NOBL East Yutan bridge structure.

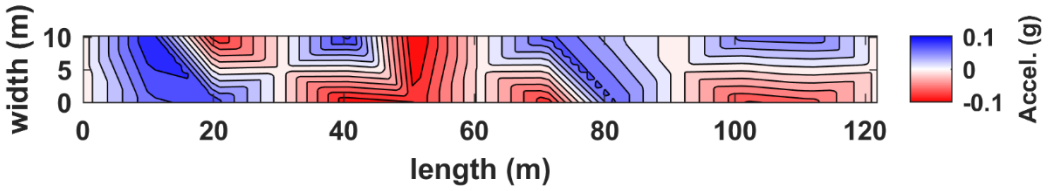

Figure B.153. Interpolated acceleration in plan view for truck pass 41 at the NOBL East Yutan bridge structure.

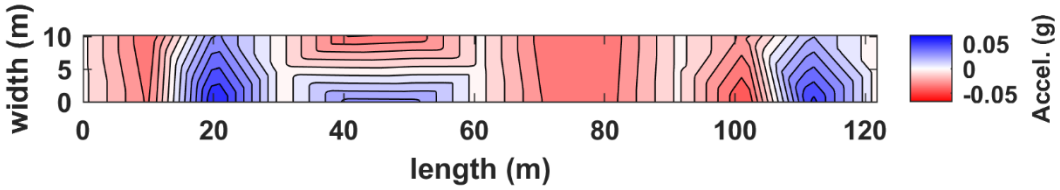

Figure B.154. Interpolated acceleration in plan view for truck pass 42 at the NOBL East Yutan bridge structure.

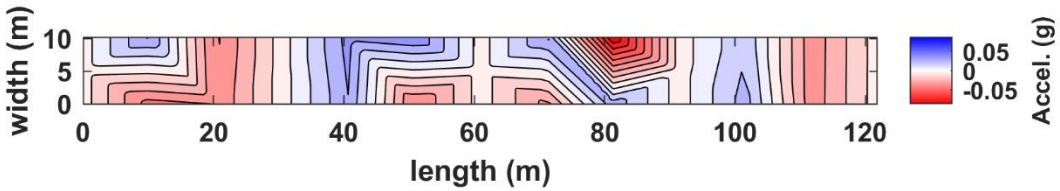

Figure B.155. Interpolated acceleration in plan view for truck pass 43 at the NOBL East Yutan bridge structure.

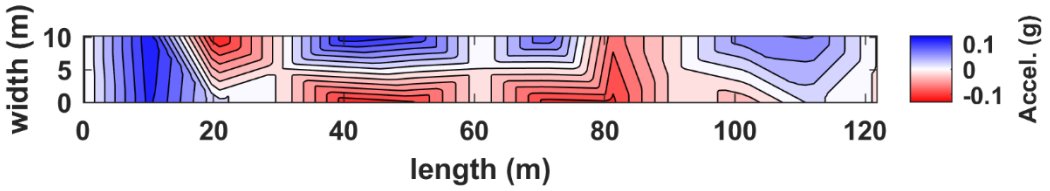

Figure B.156. Interpolated acceleration in plan view for truck pass 44 at the NOBL East Yutan bridge structure.

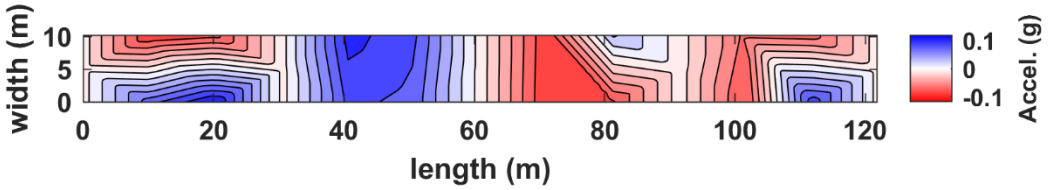

Figure B.157. Interpolated acceleration in plan view for truck pass 45 at the NOBL East Yutan bridge structure.

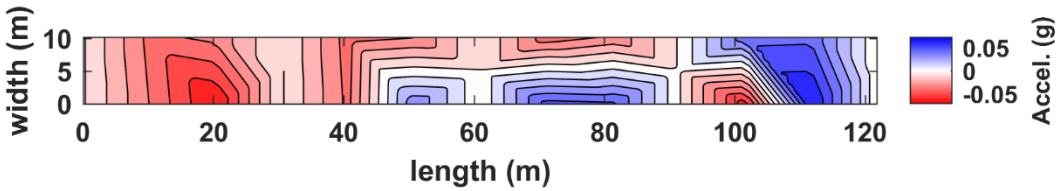

Figure B.158. Interpolated acceleration in plan view for truck pass 46 at the NOBL East Yutan bridge structure.

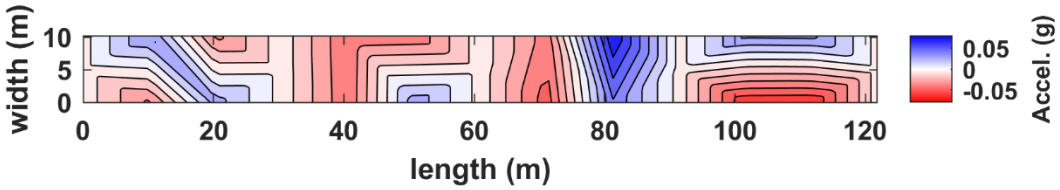

Figure B.159. Interpolated acceleration in plan view for truck pass 47 at the NOBL East Yutan bridge structure.

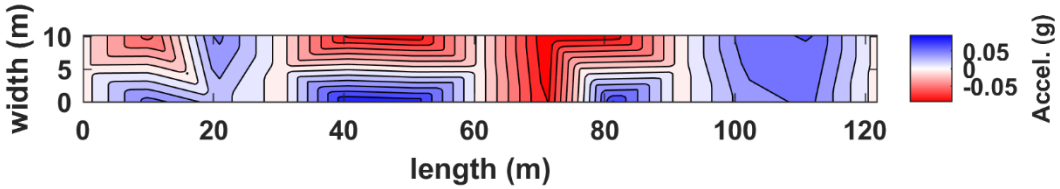

Figure B.160. Interpolated acceleration in plan view for truck pass 48 at the NOBL East Yutan bridge structure.

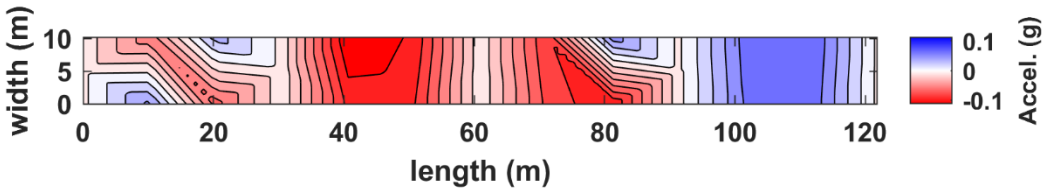

Figure B.161. Interpolated acceleration in plan view for truck pass 49 at the NOBL East Yutan bridge structure.

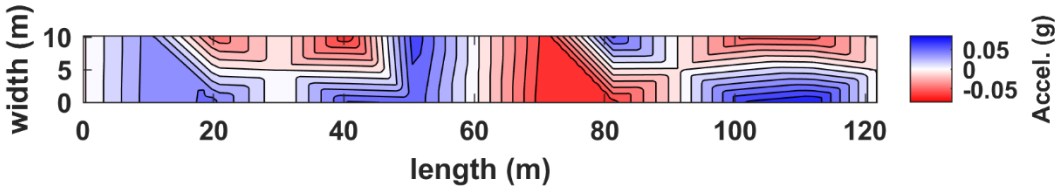

Figure B.162. Interpolated acceleration in plan view for truck pass 50 at the NOBL East Yutan bridge structure.

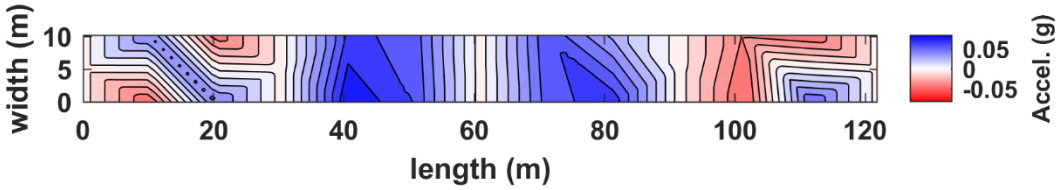

Figure B.163. Interpolated acceleration in plan view for truck pass 51 at the NOBL East Yutan bridge structure.

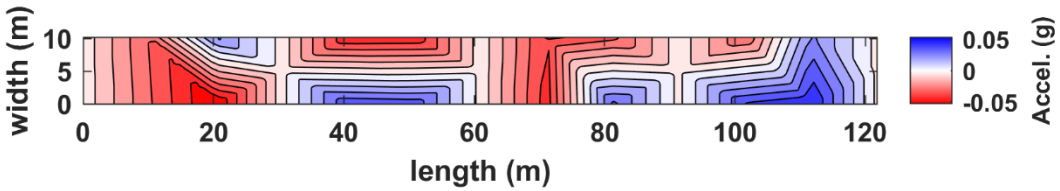

Figure B.164. Interpolated acceleration in plan view for truck pass 52 at the NOBL East Yutan bridge structure.

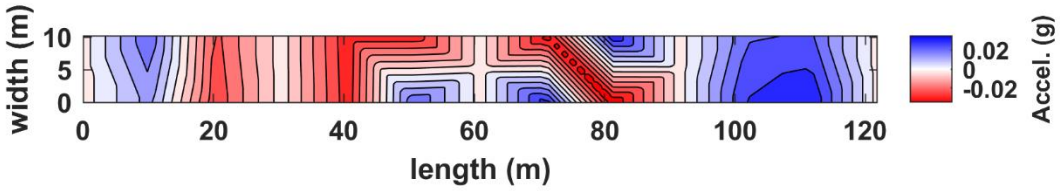

Figure B.165. Interpolated acceleration in plan view for truck pass 53 at the NOBL East Yutan bridge structure.

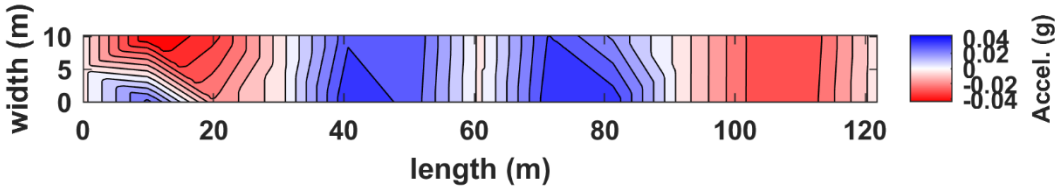

Figure B.166. Interpolated acceleration in plan view for truck pass 54 at the NOBL East Yutan bridge structure.

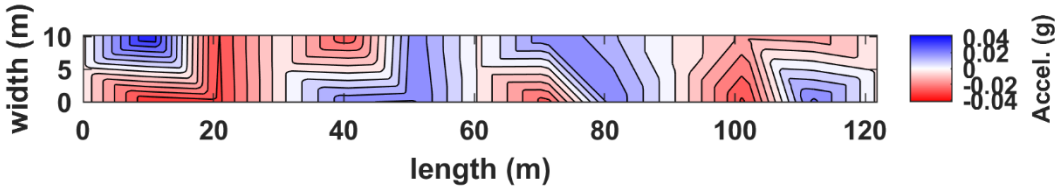

Figure B.167. Interpolated acceleration in plan view for truck pass 55 at the NOBL East Yutan bridge structure.

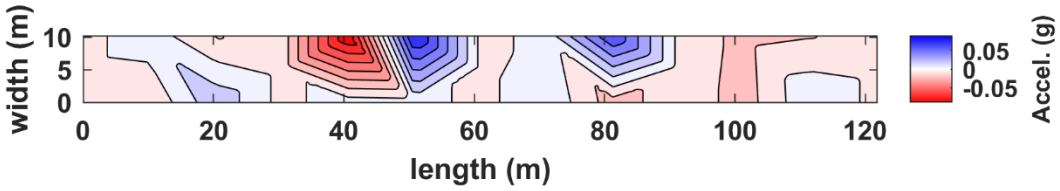

Figure B.168. Interpolated acceleration in plan view for truck pass 56 at the NOBL East Yutan bridge structure.

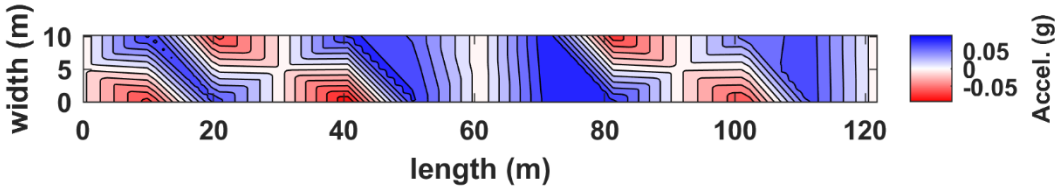

Figure B.169. Interpolated acceleration in plan view for truck pass 57 at the NOBL East Yutan bridge structure.

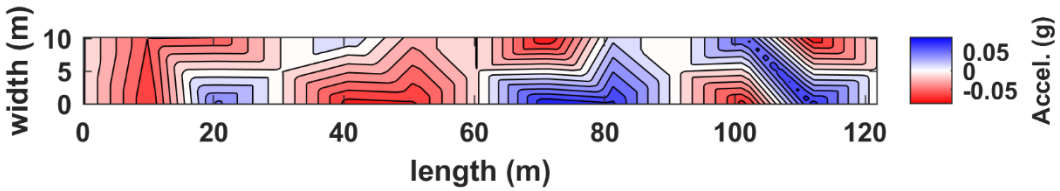

Figure B.170. Interpolated acceleration in plan view for truck pass 58 at the NOBL East Yutan bridge structure.

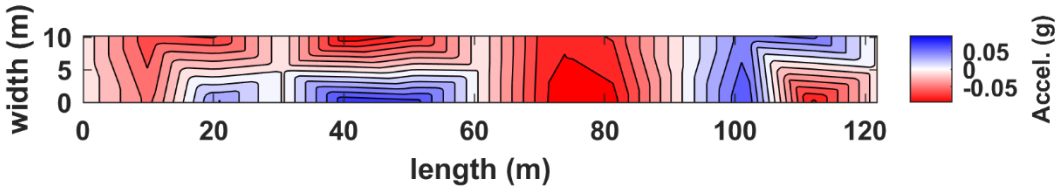

Figure B.171. Interpolated acceleration in plan view for truck pass 59 at the NOBL East Yutan bridge structure.

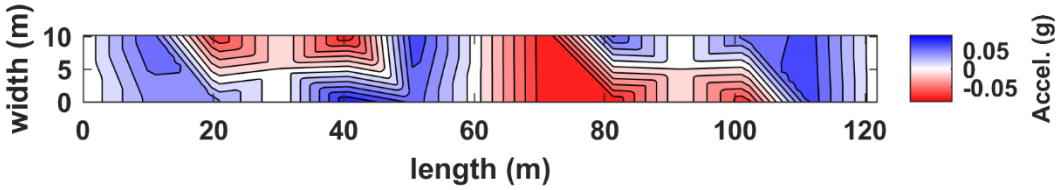

Figure B.172. Interpolated acceleration in plan view for truck pass 60 at the NOBL East Yutan bridge structure.

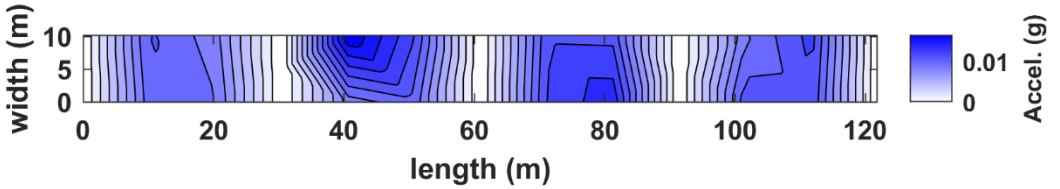

Figure B.173. Interpolated absolute-valued acceleration in plan view for truck pass 01 at the NOBL East Yutan bridge structure.

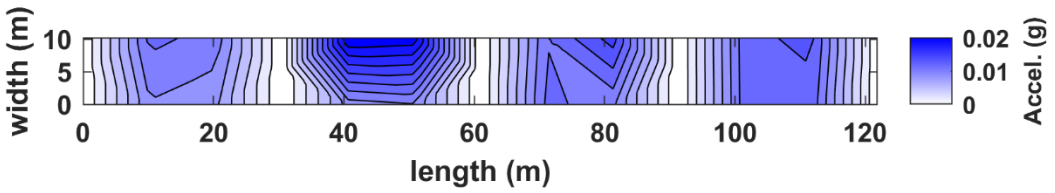

Figure B.174. Interpolated absolute-valued acceleration in plan view for truck pass 02 at the NOBL East Yutan bridge structure.

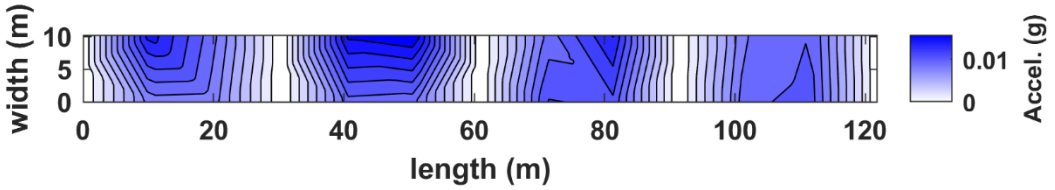

Figure B.175. Interpolated absolute-valued acceleration in plan view for truck pass 03 at the NOBL East Yutan bridge structure.

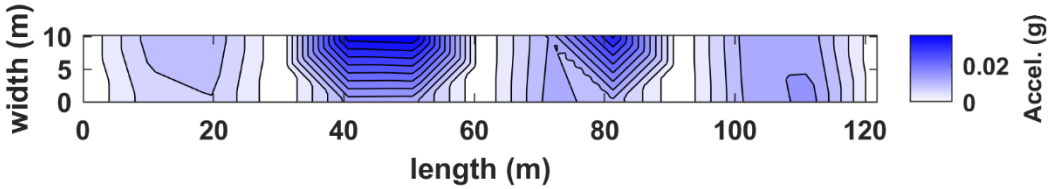

Figure B.176. Interpolated absolute-valued acceleration in plan view for truck pass 04 at the NOBL East Yutan bridge structure.

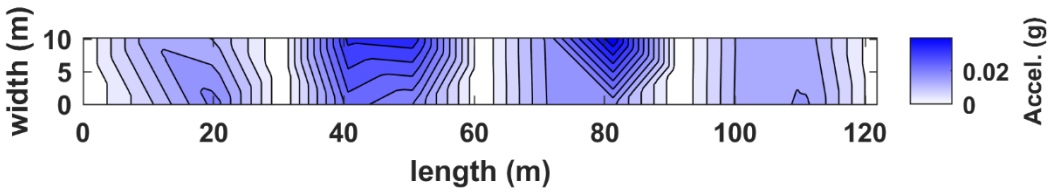

Figure B.177. Interpolated absolute-valued acceleration in plan view for truck pass 05 at the NOBL East Yutan bridge structure.

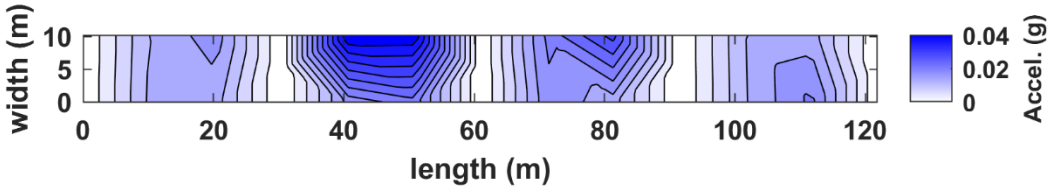

Figure B.178. Interpolated absolute-valued acceleration in plan view for truck pass 06 at the NOBL East Yutan bridge structure.

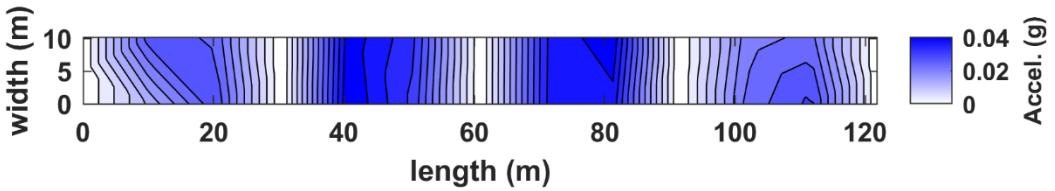

Figure B.179. Interpolated absolute-valued acceleration in plan view for truck pass 07 at the NOBL East Yutan bridge structure.

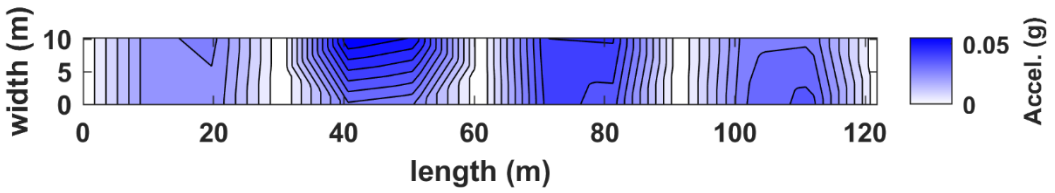

Figure B.180. Interpolated absolute-valued acceleration in plan view for truck pass 08 at the NOBL East Yutan bridge structure.

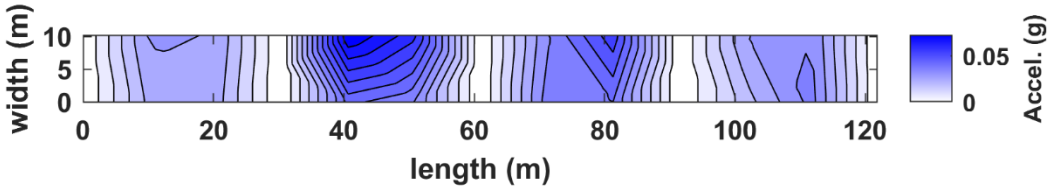

Figure B.181. Interpolated absolute-valued acceleration in plan view for truck pass 09 at the NOBL East Yutan bridge structure.

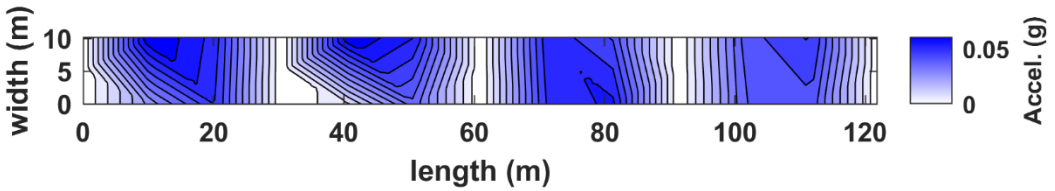

Figure B.182. Interpolated absolute-valued acceleration in plan view for truck pass 10 at the NOBL East Yutan bridge structure.

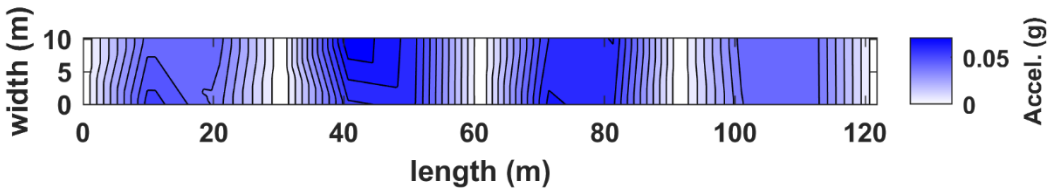

Figure B.183. Interpolated absolute-valued acceleration in plan view for truck pass 11 at the NOBL East Yutan bridge structure.

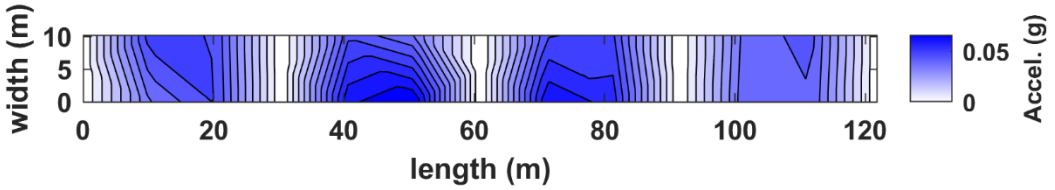

Figure B.184. Interpolated absolute-valued acceleration in plan view for truck pass 12 at the NOBL East Yutan bridge structure.

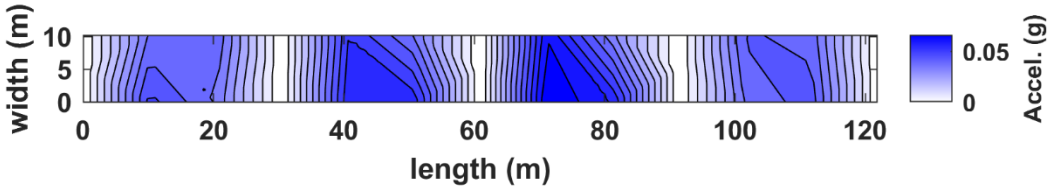

Figure B.185. Interpolated absolute-valued acceleration in plan view for truck pass 13 at the NOBL East Yutan bridge structure.

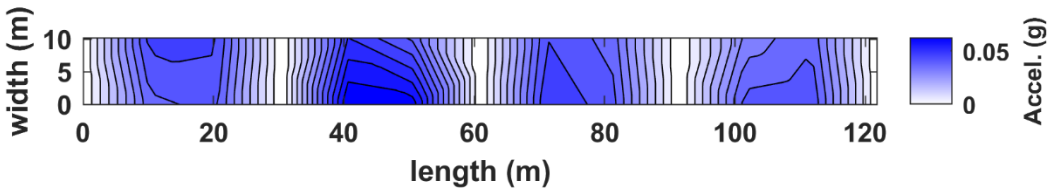

Figure B.186. Interpolated absolute-valued acceleration in plan view for truck pass 14 at the NOBL East Yutan bridge structure.

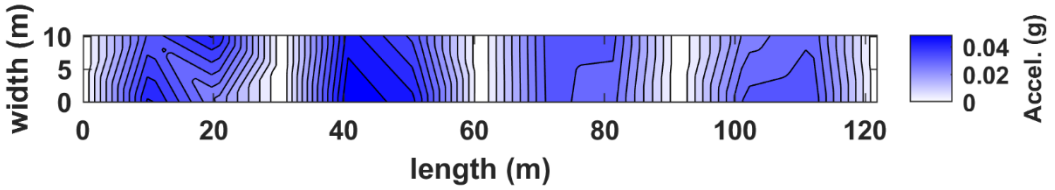

Figure B.187. Interpolated absolute-valued acceleration in plan view for truck pass 15 at the NOBL East Yutan bridge structure.

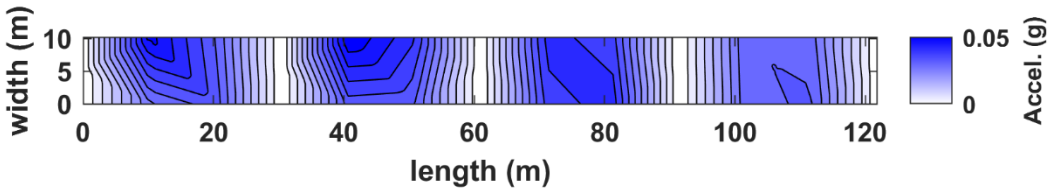

Figure B.188. Interpolated absolute-valued acceleration in plan view for truck pass 16 at the NOBL East Yutan bridge structure.

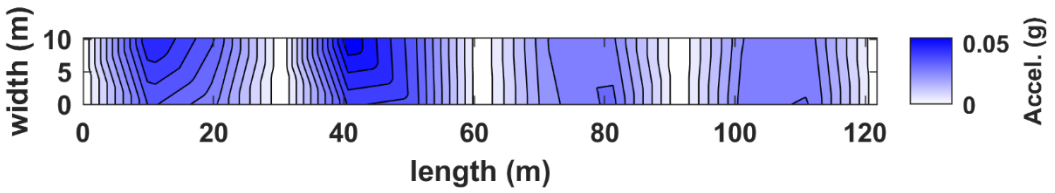

Figure B.189. Interpolated absolute-valued acceleration in plan view for truck pass 17 at the NOBL East Yutan bridge structure.

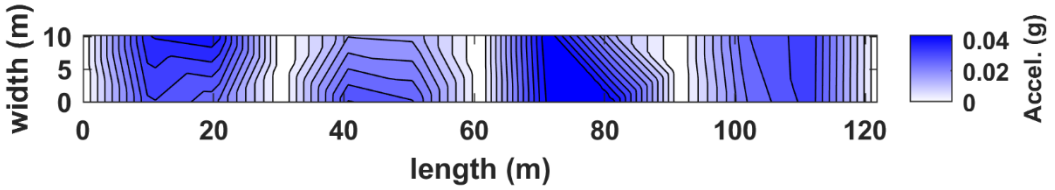

Figure B.190. Interpolated absolute-valued acceleration in plan view for truck pass 18 at the NOBL East Yutan bridge structure.

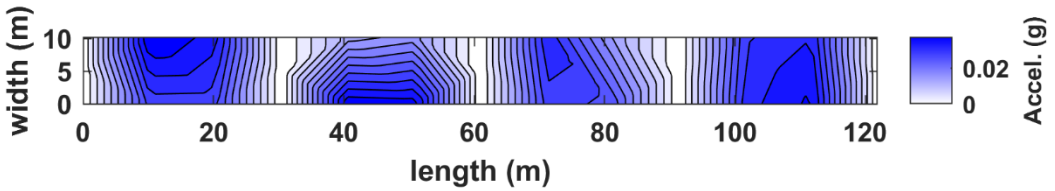

Figure B.191. Interpolated absolute-valued acceleration in plan view for truck pass 19 at the NOBL East Yutan bridge structure.

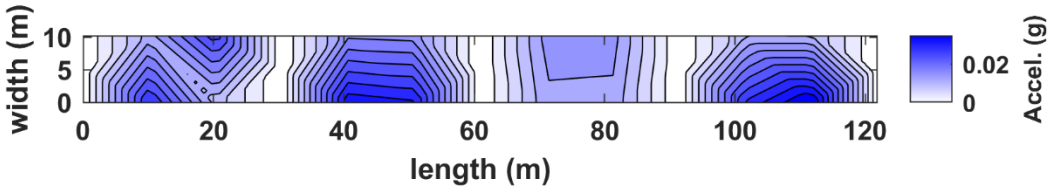

Figure B.192. Interpolated absolute-valued acceleration in plan view for truck pass 20 at the NOBL East Yutan bridge structure.

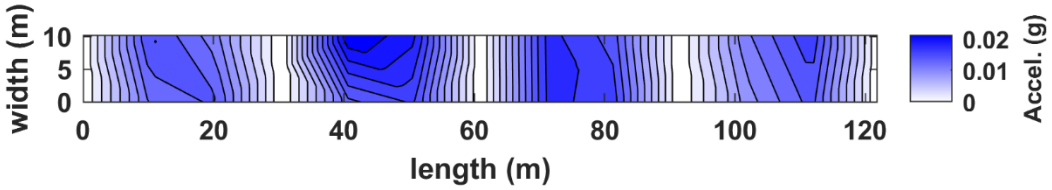

Figure B.193. Interpolated absolute-valued acceleration in plan view for truck pass 21 at the NOBL East Yutan bridge structure.

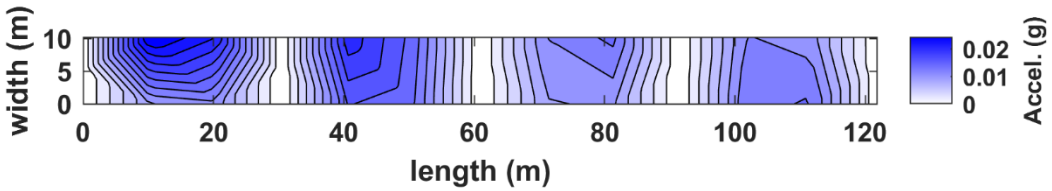

Figure B.194. Interpolated absolute-valued acceleration in plan view for truck pass 22 at the NOBL East Yutan bridge structure.

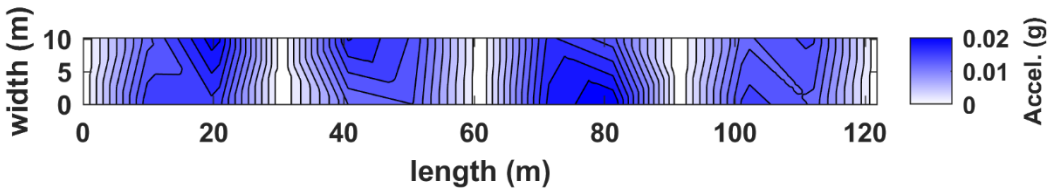

Figure B.195. Interpolated absolute-valued acceleration in plan view for truck pass 23 at the NOBL East Yutan bridge structure.

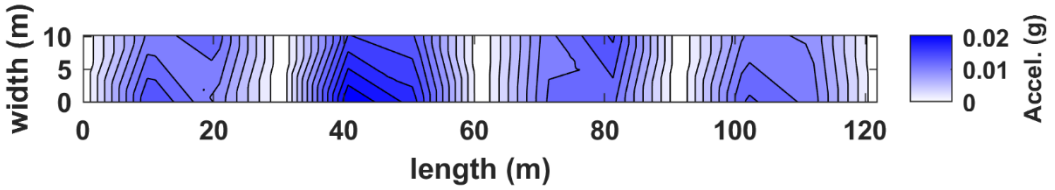

Figure B.196. Interpolated absolute-valued acceleration in plan view for truck pass 24 at the NOBL East Yutan bridge structure.

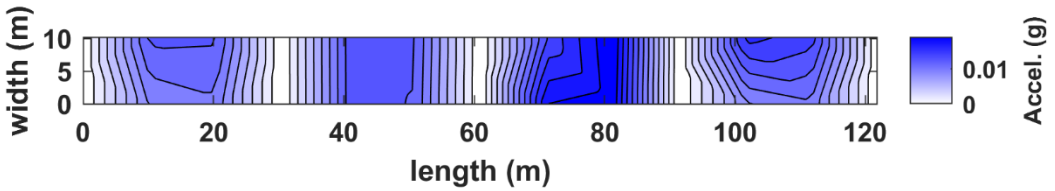

Figure B.197. Interpolated absolute-valued acceleration in plan view for truck pass 25 at the NOBL East Yutan bridge structure.

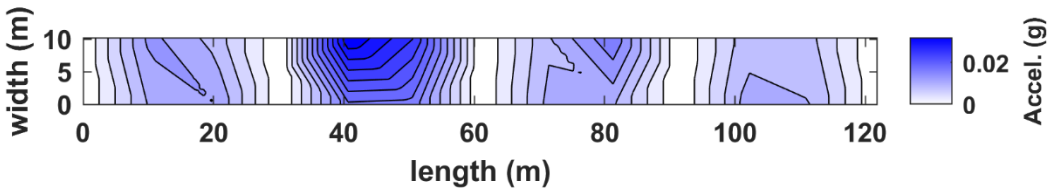

Figure B.198. Interpolated absolute-valued acceleration in plan view for truck pass 26 at the NOBL East Yutan bridge structure.

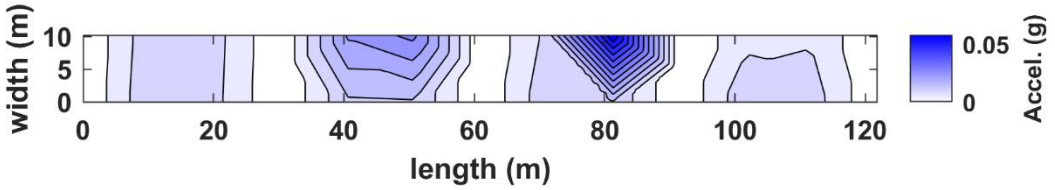

Figure B.199. Interpolated absolute-valued acceleration in plan view for truck pass 27 at the NOBL East Yutan bridge structure.

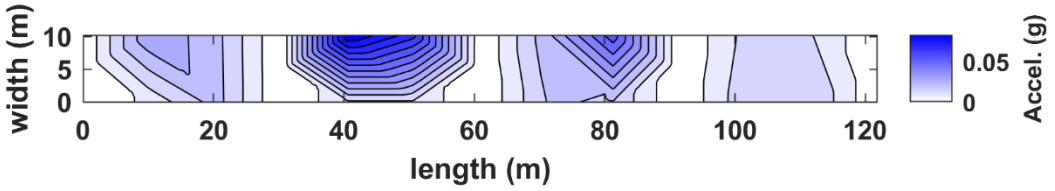

Figure B.200. Interpolated absolute-valued acceleration in plan view for truck pass 28 at the NOBL East Yutan bridge structure.

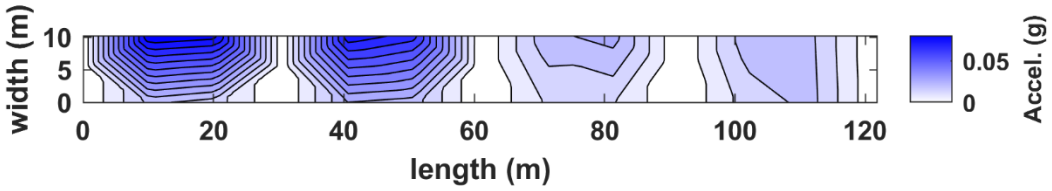

Figure B.201. Interpolated absolute-valued acceleration in plan view for truck pass 29 at the NOBL East Yutan bridge structure.

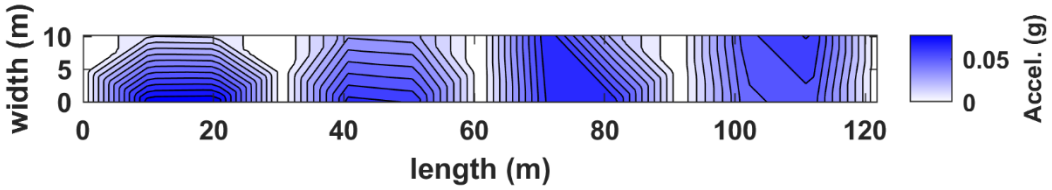

Figure B.202. Interpolated absolute-valued acceleration in plan view for truck pass 30 at the NOBL East Yutan bridge structure.

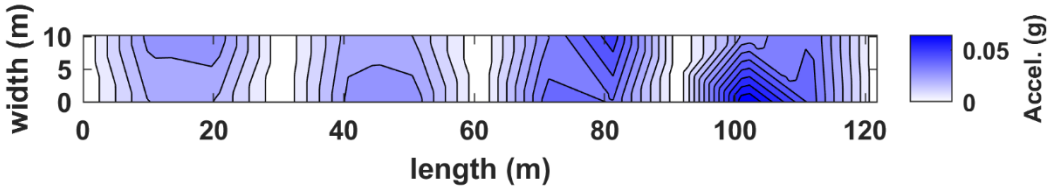

Figure B.203. Interpolated absolute-valued acceleration in plan view for truck pass 31 at the NOBL East Yutan bridge structure.

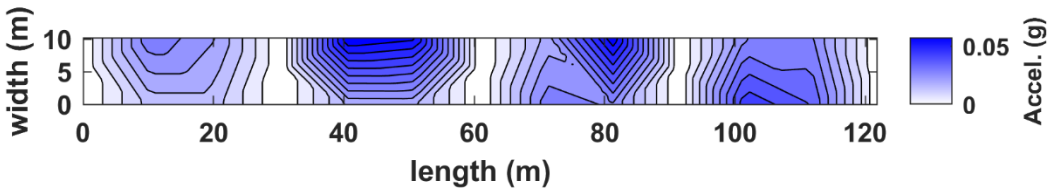

Figure B.204. Interpolated absolute-valued acceleration in plan view for truck pass 32 at the NOBL East Yutan bridge structure.

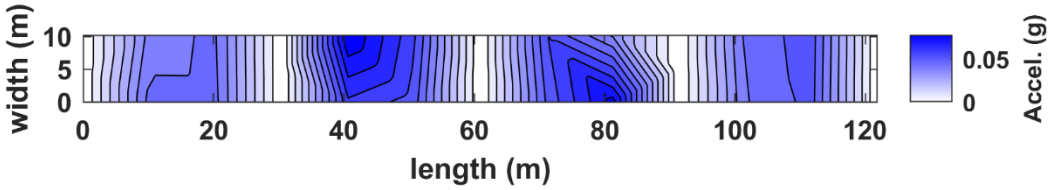

Figure B.205. Interpolated absolute-valued acceleration in plan view for truck pass 33 at the NOBL East Yutan bridge structure.

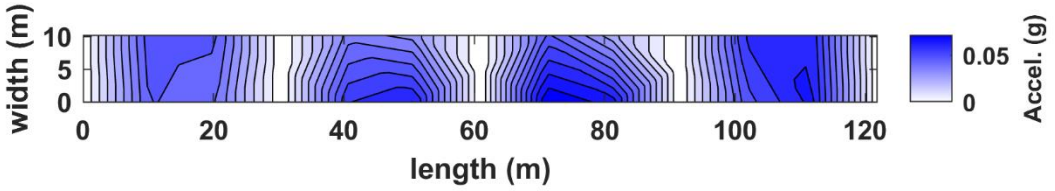

Figure B.206. Interpolated absolute-valued acceleration in plan view for truck pass 34 at the NOBL East Yutan bridge structure.

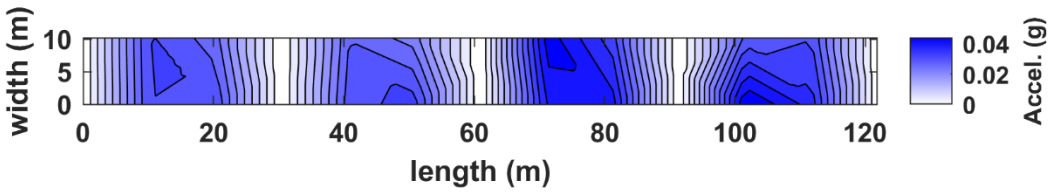

Figure B.207. Interpolated absolute-valued acceleration in plan view for truck pass 35 at the NOBL East Yutan bridge structure.

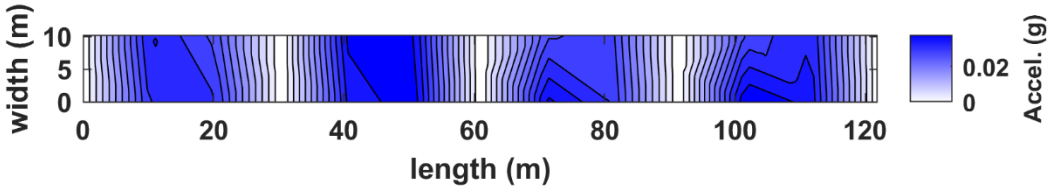

Figure B.208. Interpolated absolute-valued acceleration in plan view for truck pass 36 at the NOBL East Yutan bridge structure.

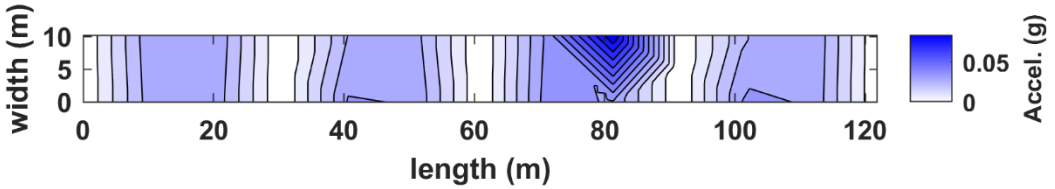

Figure B.209. Interpolated absolute-valued acceleration in plan view for truck pass 37 at the NOBL East Yutan bridge structure.

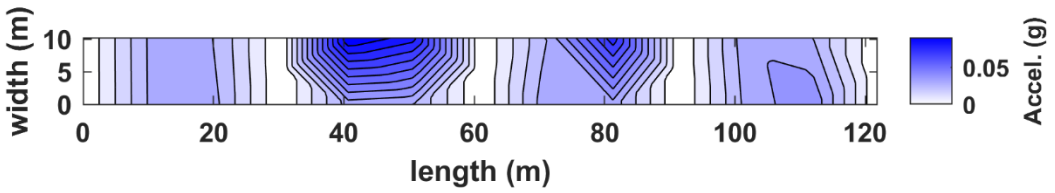

Figure B.210. Interpolated absolute-valued acceleration in plan view for truck pass 38 at the NOBL East Yutan bridge structure.

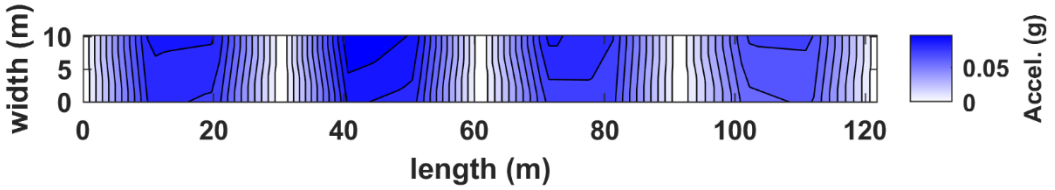

Figure B.211. Interpolated absolute-valued acceleration in plan view for truck pass 39 at the NOBL East Yutan bridge structure.

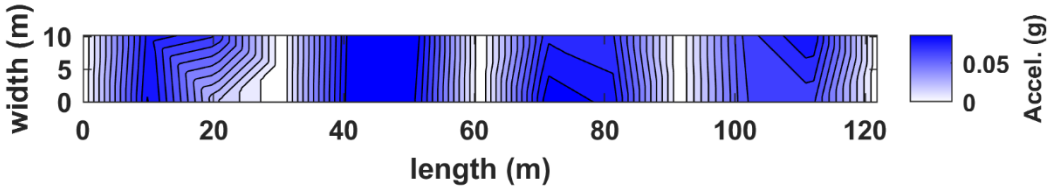

Figure B.212. Interpolated absolute-valued acceleration in plan view for truck pass 40 at the NOBL East Yutan bridge structure.

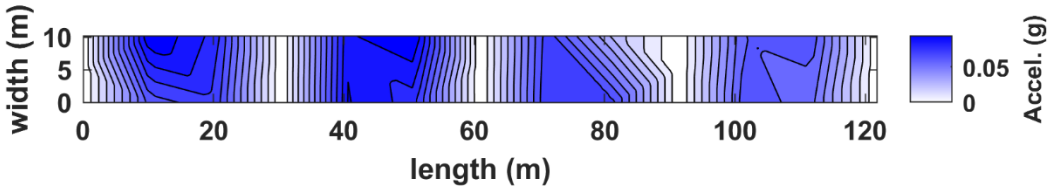

Figure B.213. Interpolated absolute-valued acceleration in plan view for truck pass 41 at the NOBL East Yutan bridge structure.

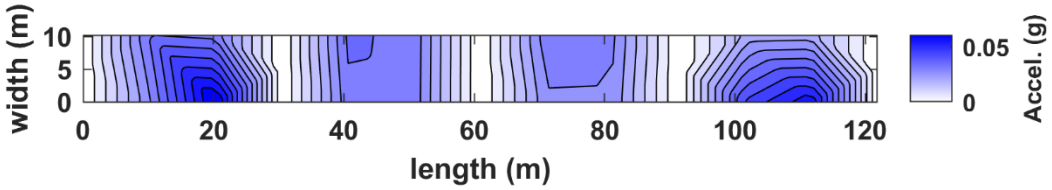

Figure B.214. Interpolated absolute-valued acceleration in plan view for truck pass 42 at the NOBL East Yutan bridge structure.

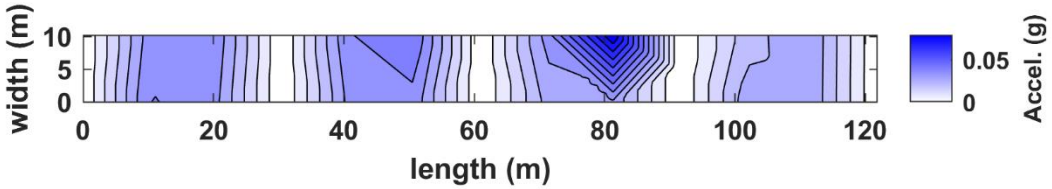

Figure B.215. Interpolated absolute-valued acceleration in plan view for truck pass 43 at the NOBL East Yutan bridge structure.

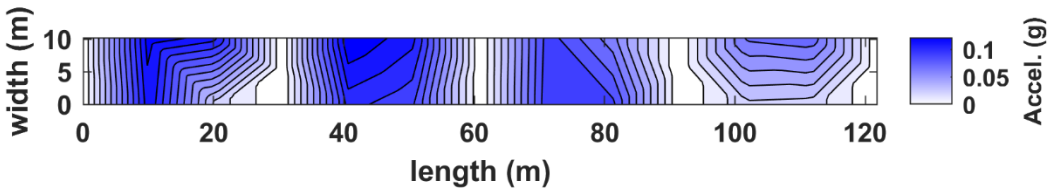

Figure B.216. Interpolated absolute-valued acceleration in plan view for truck pass 44 at the NOBL East Yutan bridge structure.

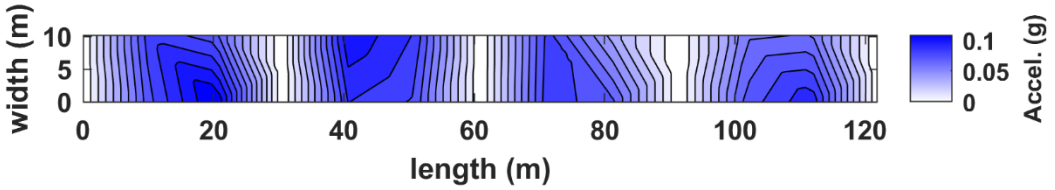

Figure B.217. Interpolated absolute-valued acceleration in plan view for truck pass 45 at the NOBL East Yutan bridge structure.

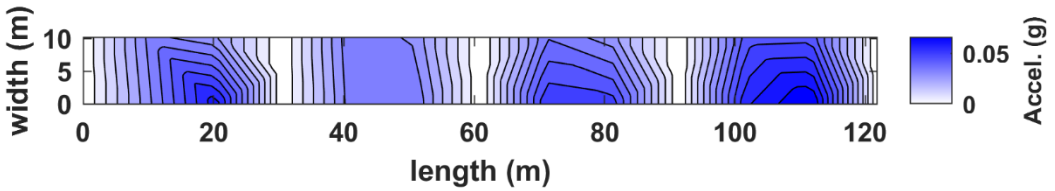

Figure B.218. Interpolated absolute-valued acceleration in plan view for truck pass 46 at the NOBL East Yutan bridge structure.

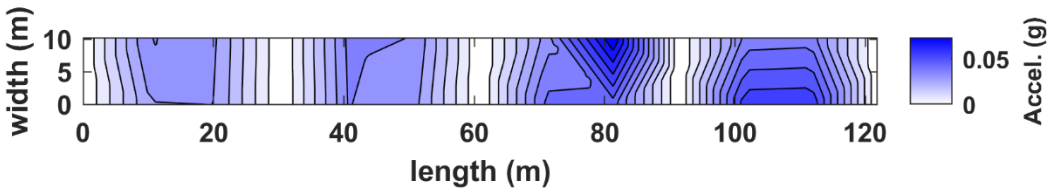

Figure B.219. Interpolated absolute-valued acceleration in plan view for truck pass 47 at the NOBL East Yutan bridge structure.

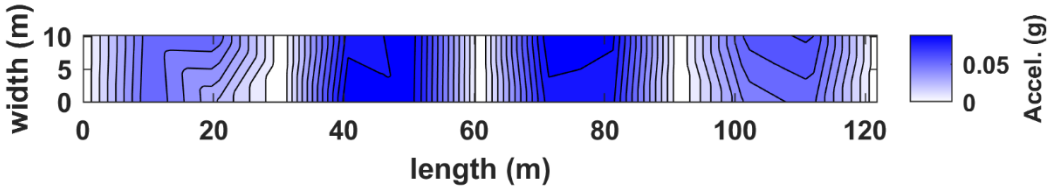

Figure B.220. Interpolated absolute-valued acceleration in plan view for truck pass 48 at the NOBL East Yutan bridge structure.

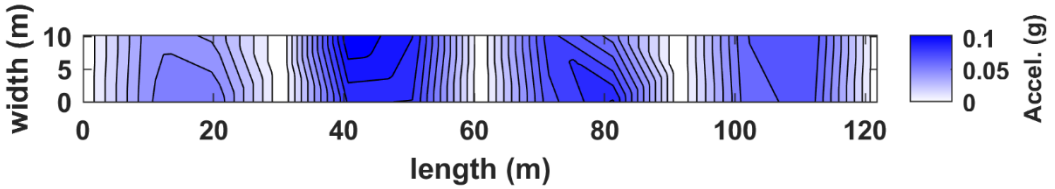

Figure B.221. Interpolated absolute-valued acceleration in plan view for truck pass 49 at the NOBL East Yutan bridge structure.

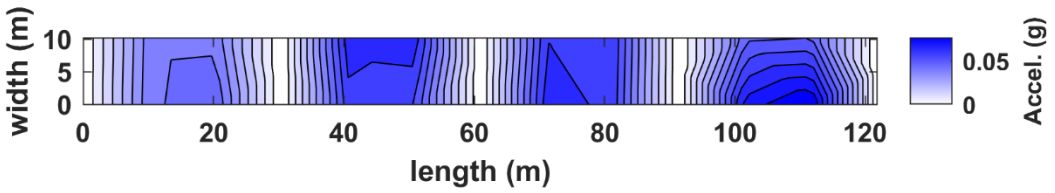

Figure B.222. Interpolated absolute-valued acceleration in plan view for truck pass 50 at the NOBL East Yutan bridge structure.

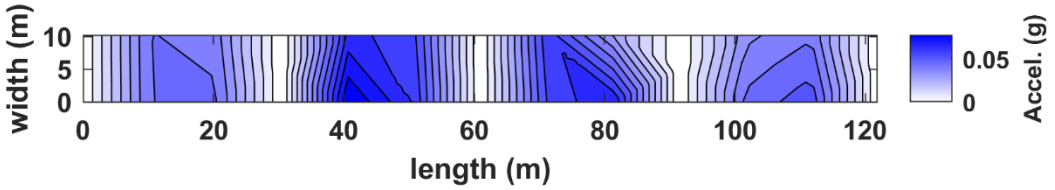

Figure B.223. Interpolated absolute-valued acceleration in plan view for truck pass 51 at the NOBL East Yutan bridge structure.

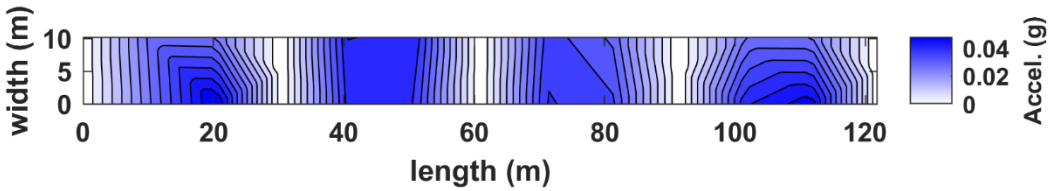

Figure B.224. Interpolated absolute-valued acceleration in plan view for truck pass 52 at the NOBL East Yutan bridge structure.

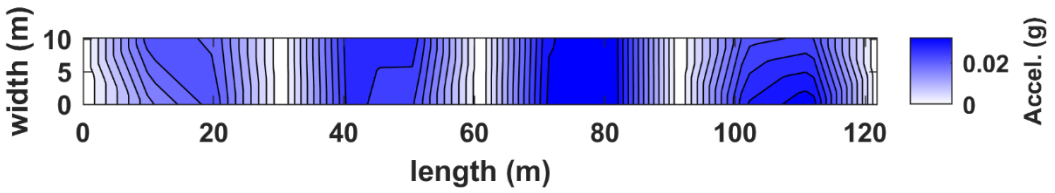

Figure B.225. Interpolated absolute-valued acceleration in plan view for truck pass 53 at the NOBL East Yutan bridge structure.

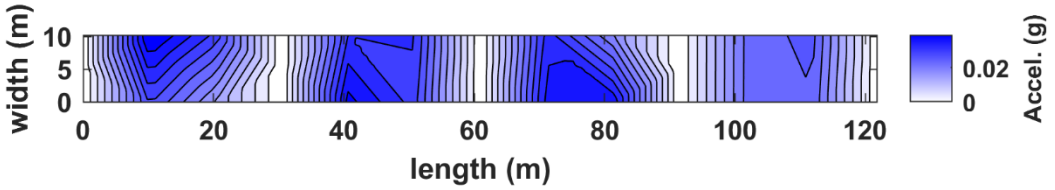

Figure B.226. Interpolated absolute-valued acceleration in plan view for truck pass 54 at the NOBL East Yutan bridge structure.

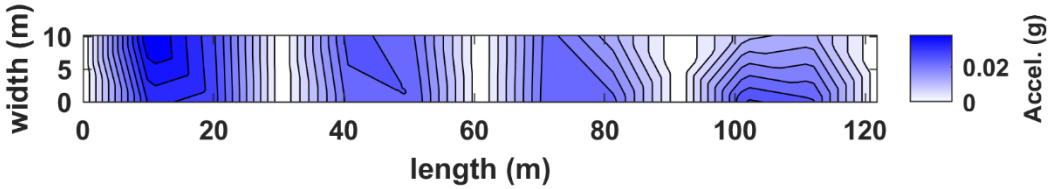

Figure B.227. Interpolated absolute-valued acceleration in plan view for truck pass 55 at the NOBL East Yutan bridge structure.

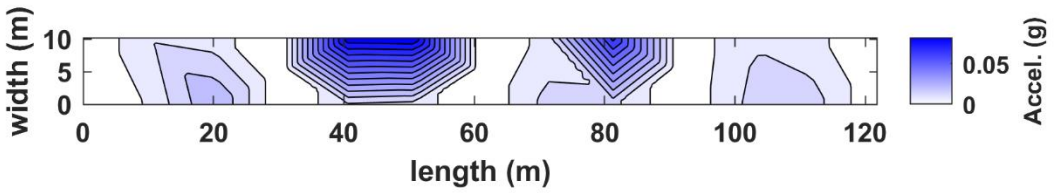

Figure B.228. Interpolated absolute-valued acceleration in plan view for truck pass 56 at the NOBL East Yutan bridge structure.

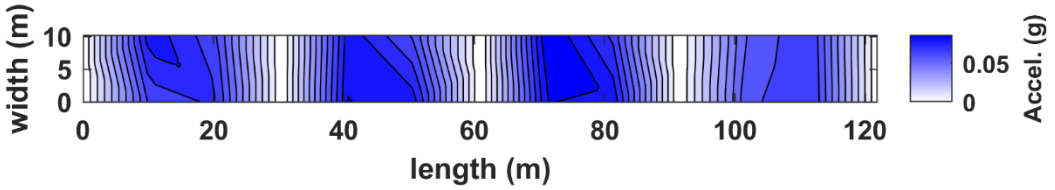

Figure B.229. Interpolated absolute-valued acceleration in plan view for truck pass 57 at the NOBL East Yutan bridge structure.

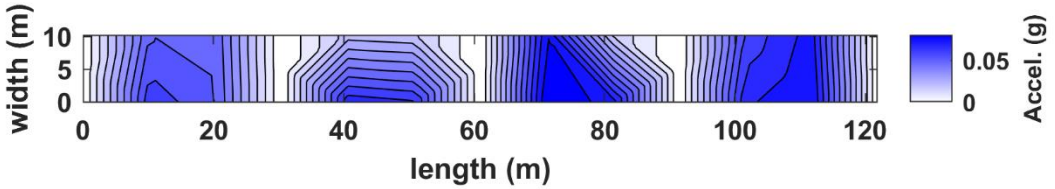

Figure B.230. Interpolated absolute-valued acceleration in plan view for truck pass 58 at the NOBL East Yutan bridge structure.

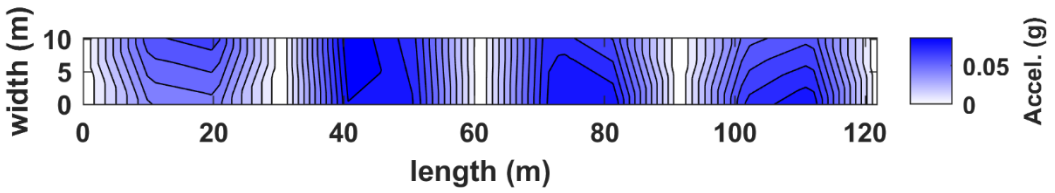

Figure B.231. Interpolated absolute-valued acceleration in plan view for truck pass 59 at the NOBL East Yutan bridge structure.

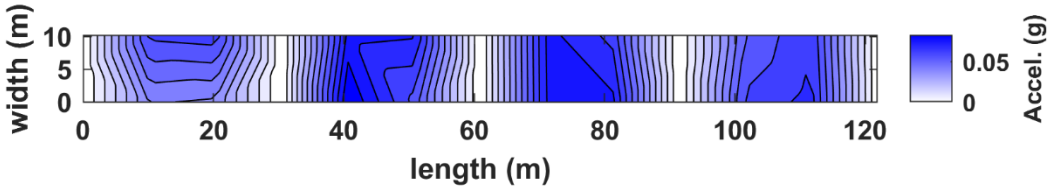

Figure B.232. Interpolated absolute-valued acceleration in plan view for truck pass 60 at the NOBL East Yutan bridge structure.

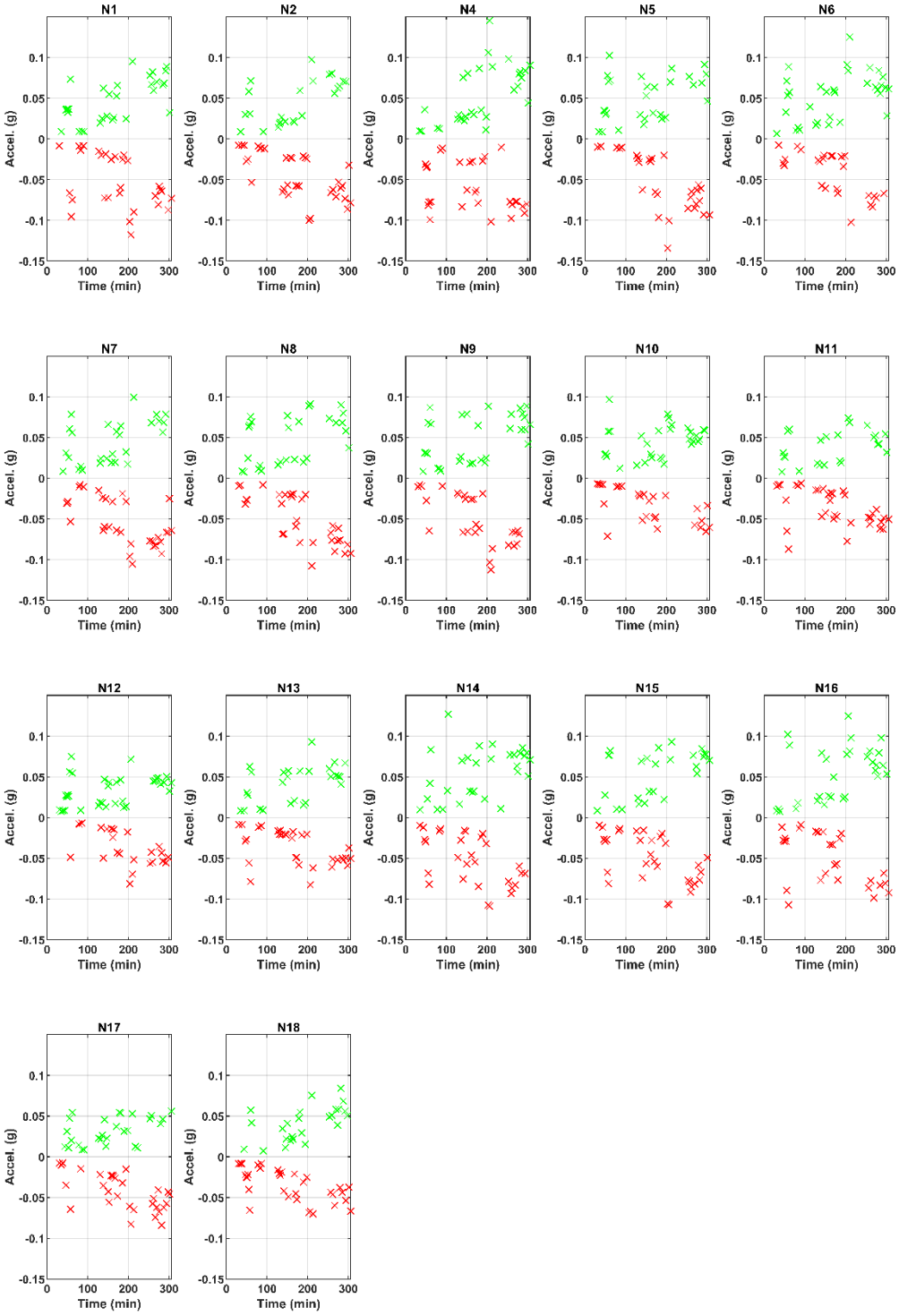

Figure B.233. Maximum acceleration values for each truck pass at the NOBL West Yutan bridge structure.

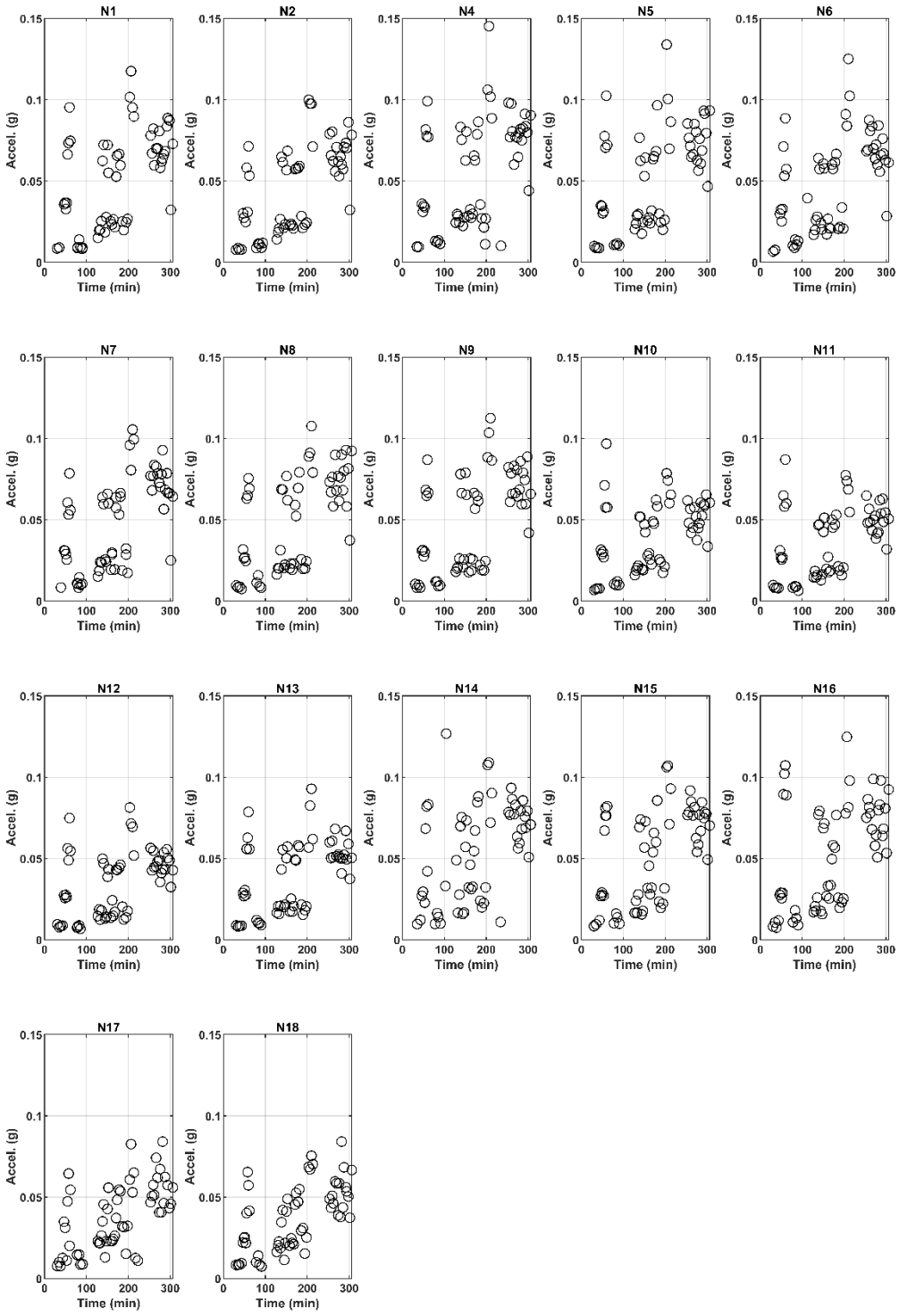

Figure B.234. Absolute maximum acceleration values for each truck pass at the NOBL West Yutan bridge structure.

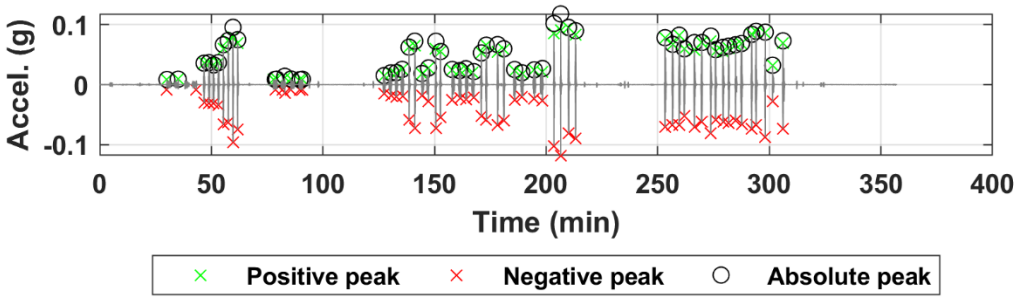

Figure B.235. Acceleration time history of sensor N01 for all truck passes at the NOBL West Yutan bridge structure.

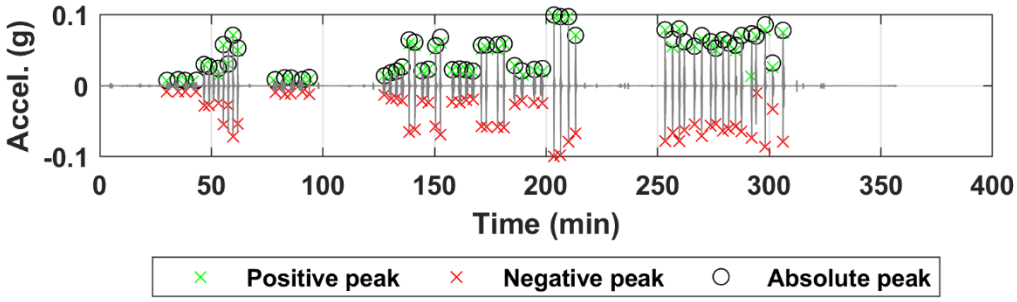

Figure B.236. Acceleration time history of sensor N02 for all truck passes at the NOBL West Yutan bridge structure.

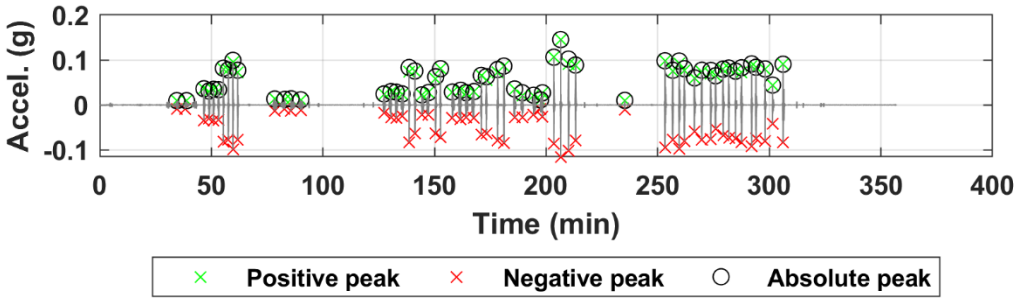

Figure B.237. Acceleration time history of sensor N04 for all truck passes at the NOBL West Yutan bridge structure.

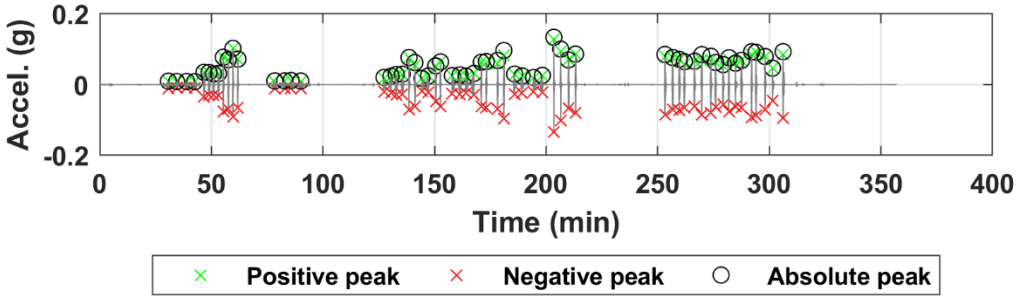

Figure B.238. Acceleration time history of sensor N05 for all truck passes at the NOBL West Yutan bridge structure.

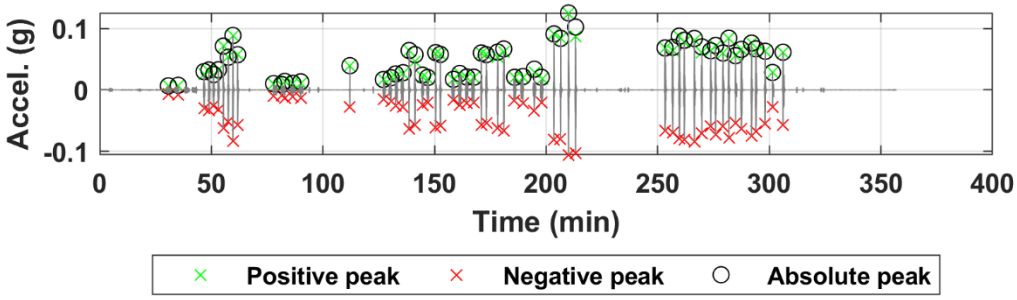

Figure B.239. Acceleration time history of sensor N06 for all truck passes at the NOBL West Yutan bridge structure.

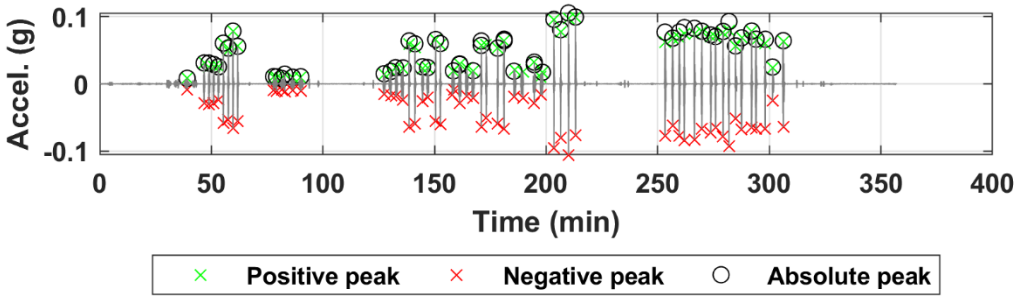

Figure B.240. Acceleration time history of sensor N07 for all truck passes at the NOBL West Yutan bridge structure.

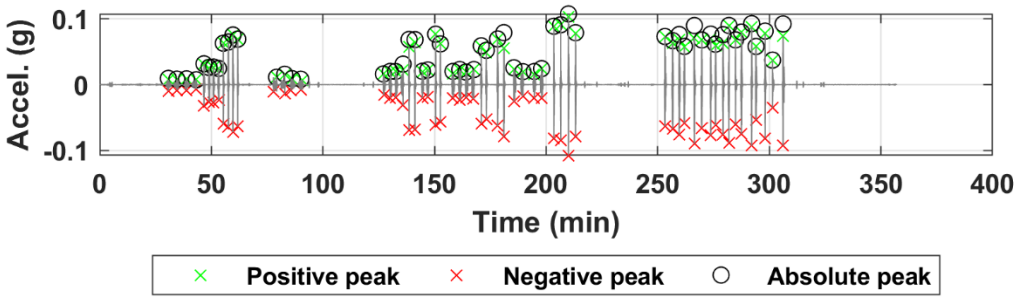

Figure B.241. Acceleration time history of sensor N08 for all truck passes at the NOBL West Yutan bridge structure.

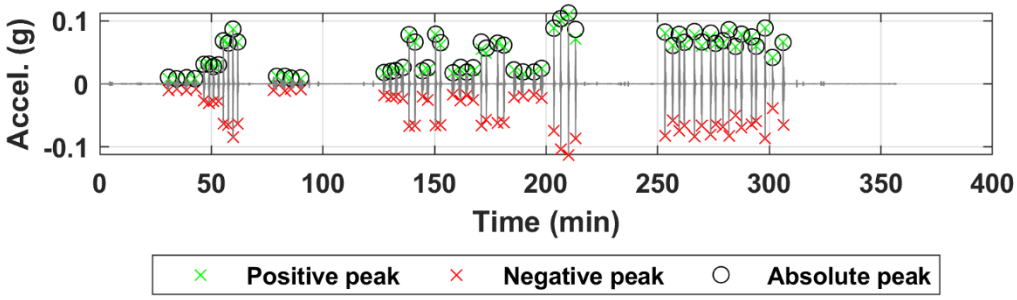

Figure B.242. Acceleration time history of sensor N09 for all truck passes at the NOBL West Yutan bridge structure.

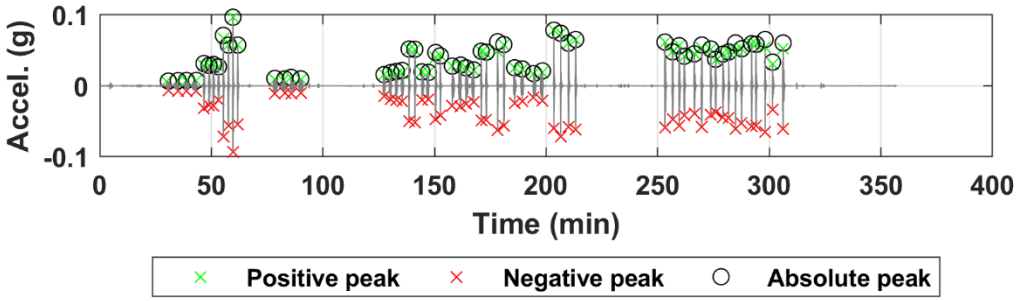

Figure B.243. Acceleration time history of sensor N10 for all truck passes at the NOBL West Yutan bridge structure.

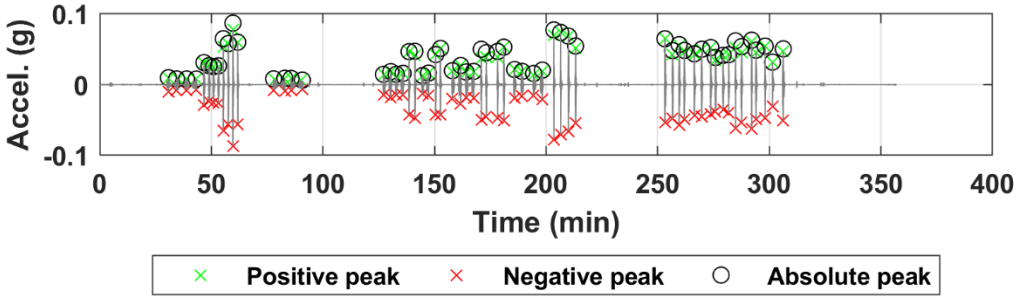

Figure B.244. Acceleration time history of sensor N11 for all truck passes at the NOBL West Yutan bridge structure.

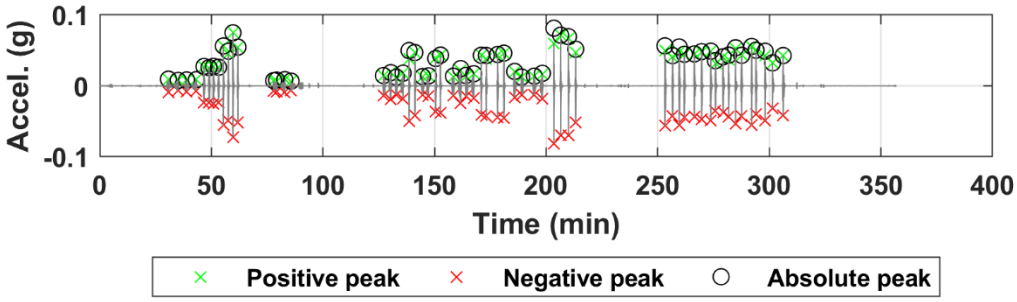

Figure B.245. Acceleration time history of sensor N12 for all truck passes at the NOBL West Yutan bridge structure.

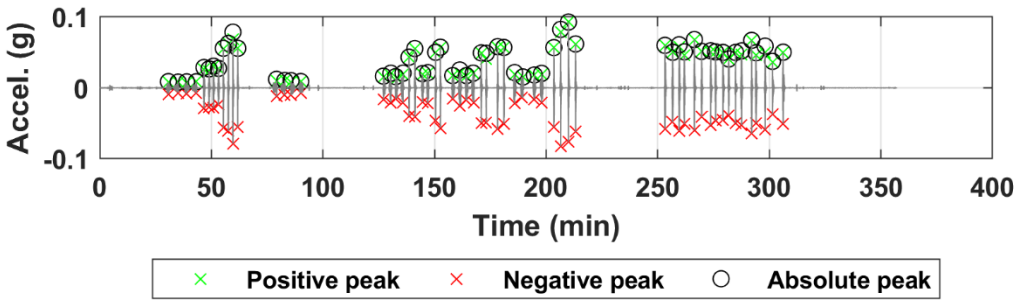

Figure B.246. Acceleration time history of sensor N13 for all truck passes at the NOBL West Yutan bridge structure.

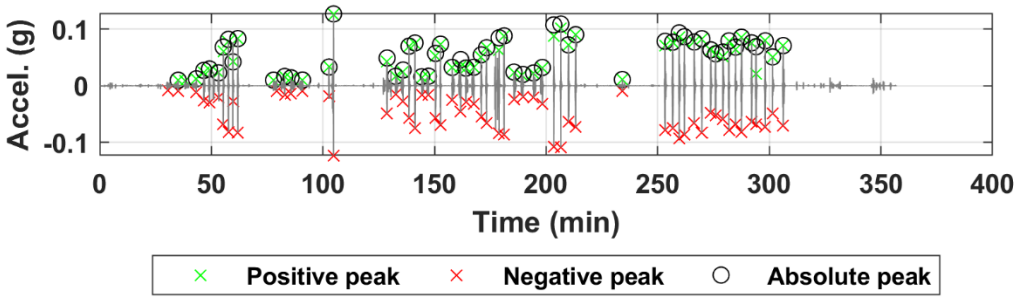

Figure B.247. Acceleration time history of sensor N14 for all truck passes at the NOBL West Yutan bridge structure.

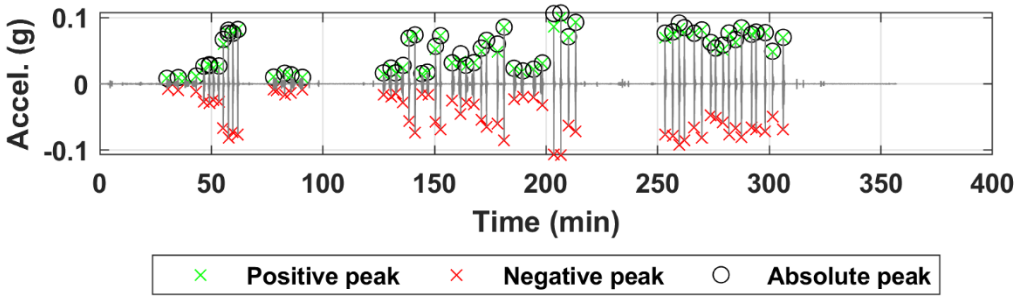

Figure B.248. Acceleration time history of sensor N15 for all truck passes at the NOBL West Yutan bridge structure.

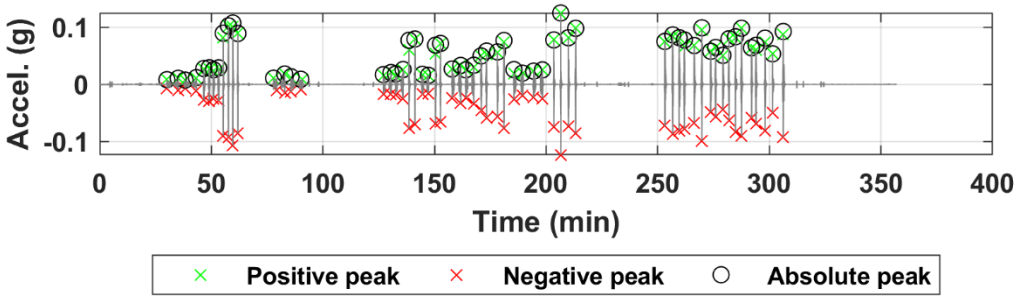

Figure B.249. Acceleration time history of sensor N16 for all truck passes at the NOBL West Yutan bridge structure.

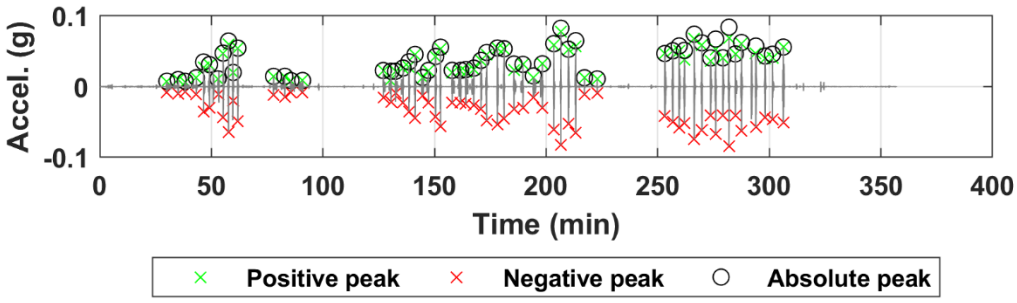

Figure B.250. Acceleration time history of sensor N17 for all truck passes at the NOBL West Yutan bridge structure.

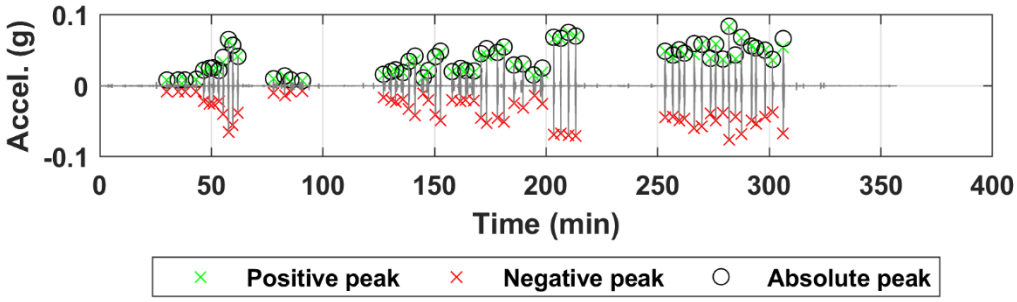

Figure B.251. Acceleration time history of sensor N18 for all truck passes at the NOBL West Yutan bridge structure.

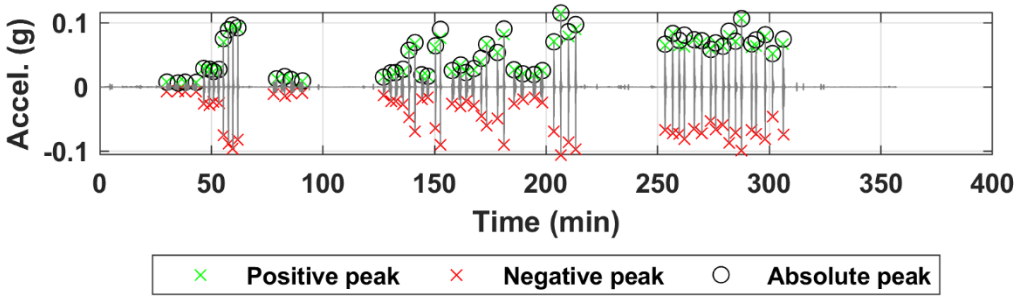

Figure B.252. Acceleration time history of sensor N19 for all truck passes at the NOBL West Yutan bridge structure.

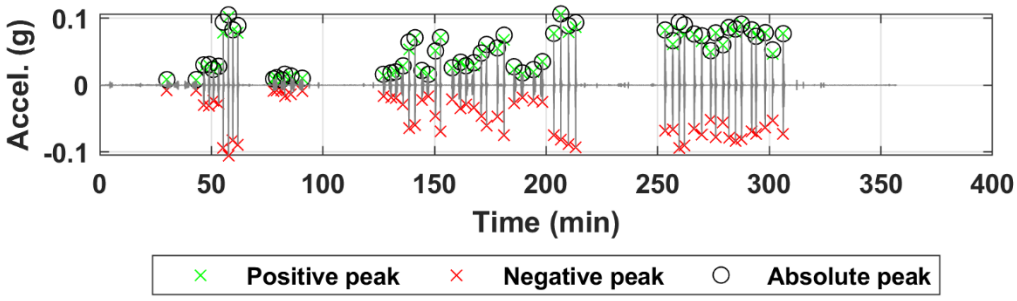

Figure B.253. Acceleration time history of sensor N20 for all truck passes at the NOBL West Yutan bridge structure.

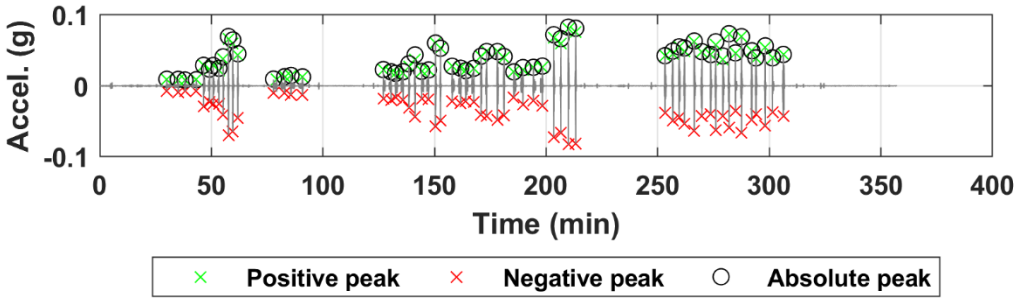

Figure B.254. Acceleration time history of sensor N21 for all truck passes at the NOBL West Yutan bridge structure.

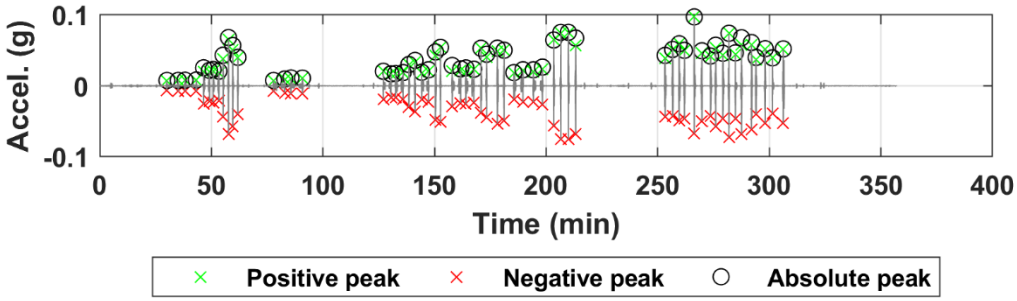

Figure B.255. Acceleration time history of sensor N22 for all truck passes at the NOBL West Yutan bridge structure.

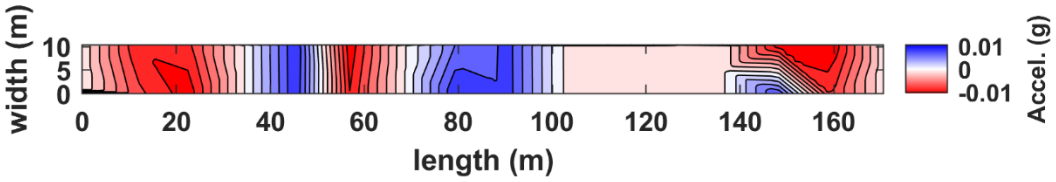

Figure B.256. Interpolated acceleration in plan view for truck pass 01 at the NOBL West Yutan bridge structure.

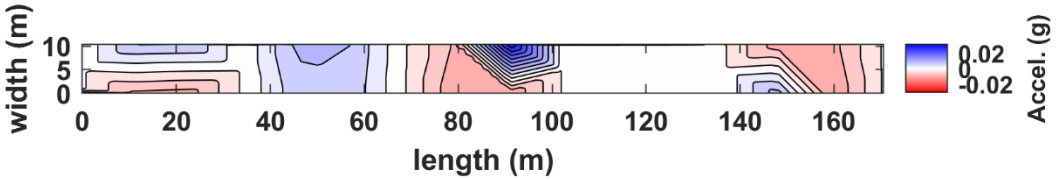

Figure B.257. Interpolated acceleration in plan view for truck pass 02 at the NOBL West Yutan bridge structure.

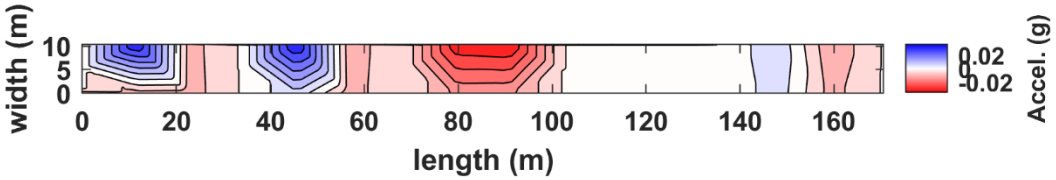

Figure B.258. Interpolated acceleration in plan view for truck pass 03 at the NOBL West Yutan bridge structure.

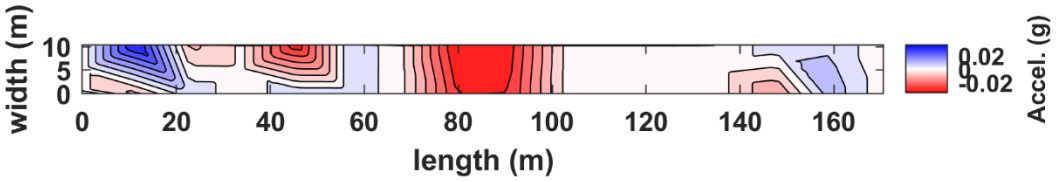

Figure B.259. Interpolated acceleration in plan view for truck pass 04 at the NOBL West Yutan bridge structure.

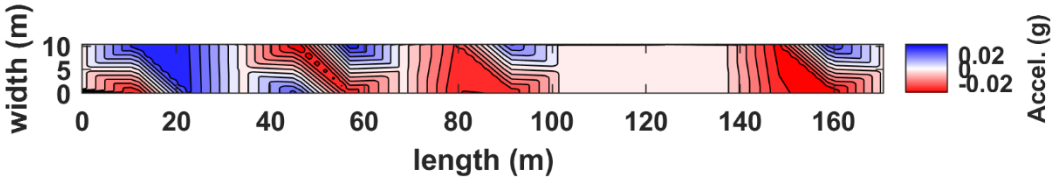

Figure B.260. Interpolated acceleration in plan view for truck pass 05 at the NOBL West Yutan bridge structure.

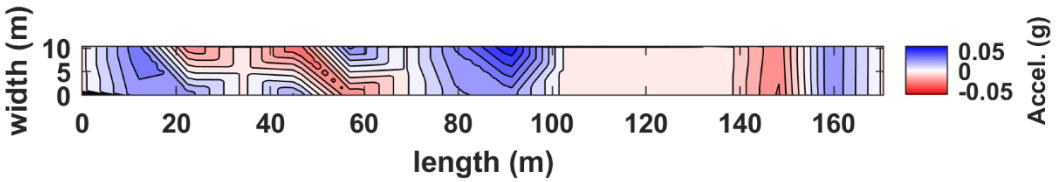

Figure B.261. Interpolated acceleration in plan view for truck pass 06 at the NOBL West Yutan bridge structure.

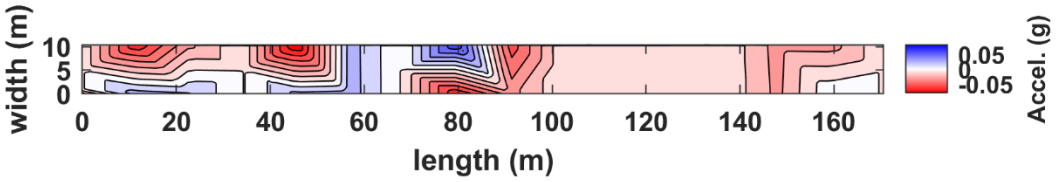

Figure B.262. Interpolated acceleration in plan view for truck pass 07 at the NOBL West Yutan bridge structure.

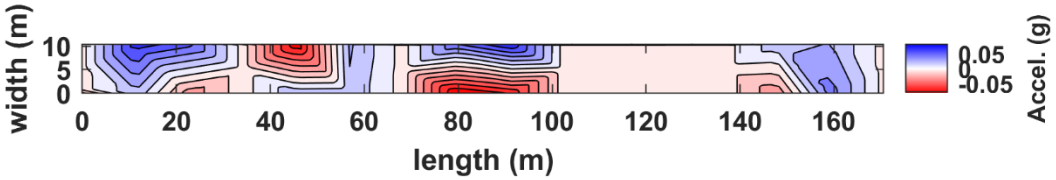

Figure B.263. Interpolated acceleration in plan view for truck pass 08 at the NOBL West Yutan bridge structure.

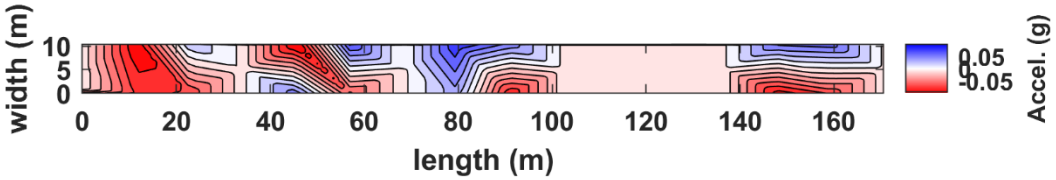

Figure B.264. Interpolated acceleration in plan view for truck pass 09 at the NOBL West Yutan bridge structure.

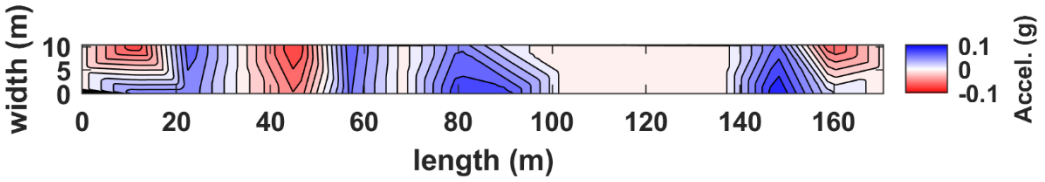

Figure B.265. Interpolated acceleration in plan view for truck pass 10 at the NOBL West Yutan bridge structure.

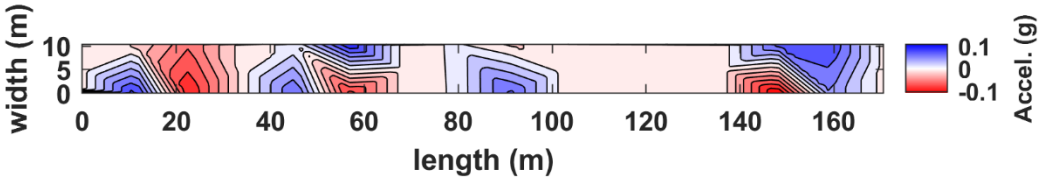

Figure B.266. Interpolated acceleration in plan view for truck pass 11 at the NOBL West Yutan bridge structure.

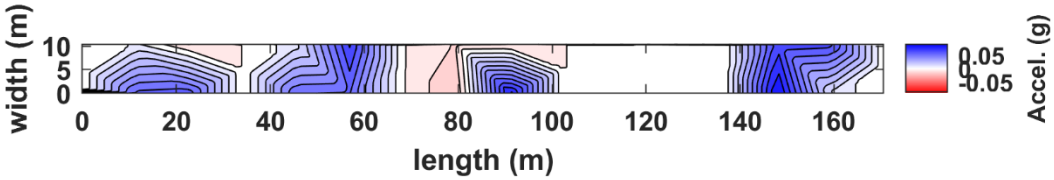

Figure B.267. Interpolated acceleration in plan view for truck pass 12 at the NOBL West Yutan bridge structure.

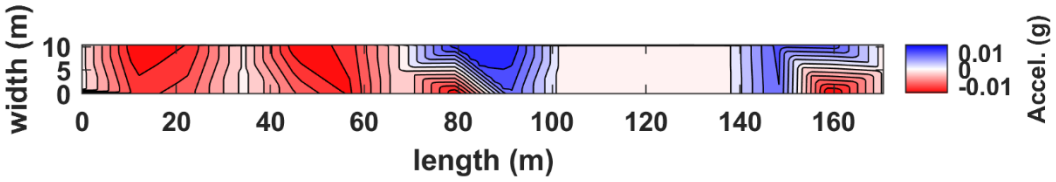

Figure B.268. Interpolated acceleration in plan view for truck pass 13 at the NOBL West Yutan bridge structure.

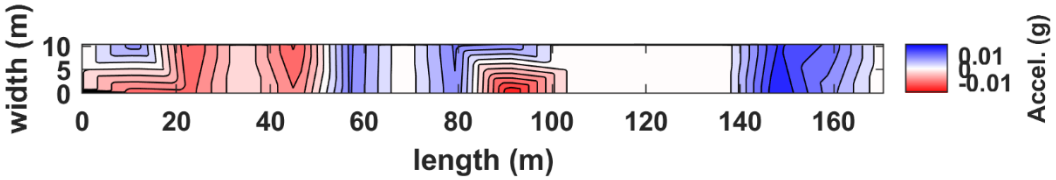

Figure B.269. Interpolated acceleration in plan view for truck pass 14 at the NOBL West Yutan bridge structure.

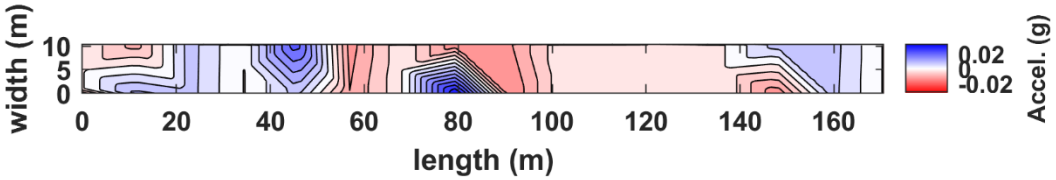

Figure B.270. Interpolated acceleration in plan view for truck pass 15 at the NOBL West Yutan bridge structure.

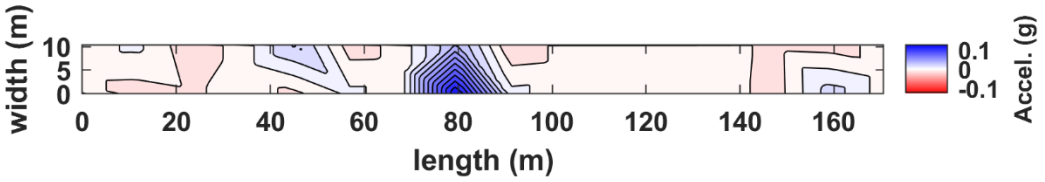

Figure B.271. Interpolated acceleration in plan view for truck pass 16 at the NOBL West Yutan bridge structure.

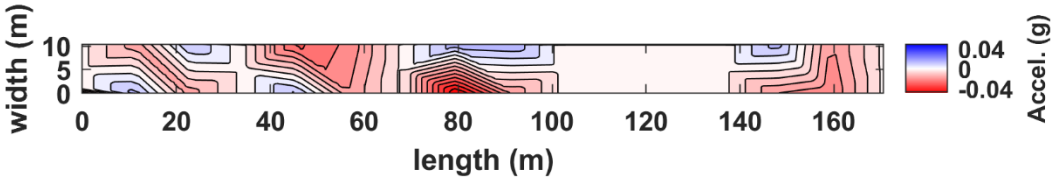

Figure B.272. Interpolated acceleration in plan view for truck pass 17 at the NOBL West Yutan bridge structure.

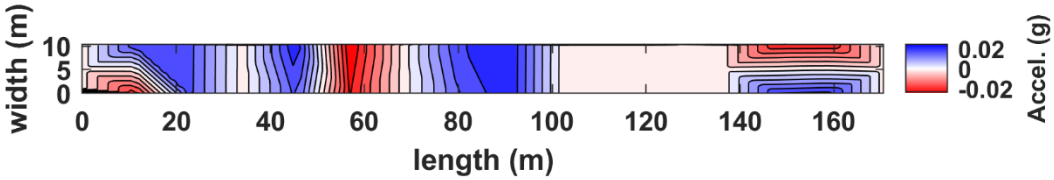

Figure B.273. Interpolated acceleration in plan view for truck pass 18 at the NOBL West Yutan bridge structure.

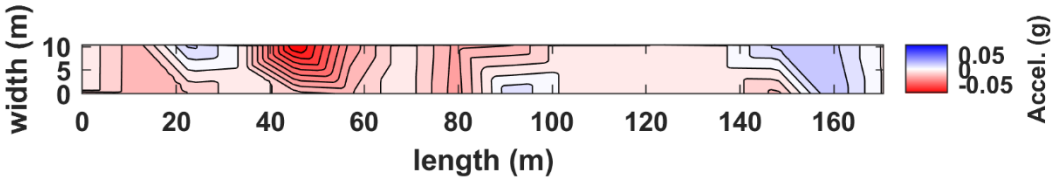

Figure B.274. Interpolated acceleration in plan view for truck pass 19 at the NOBL West Yutan bridge structure.

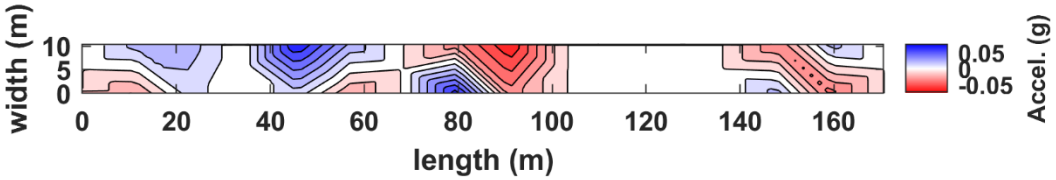

Figure B.275. Interpolated acceleration in plan view for truck pass 20 at the NOBL West Yutan bridge structure.

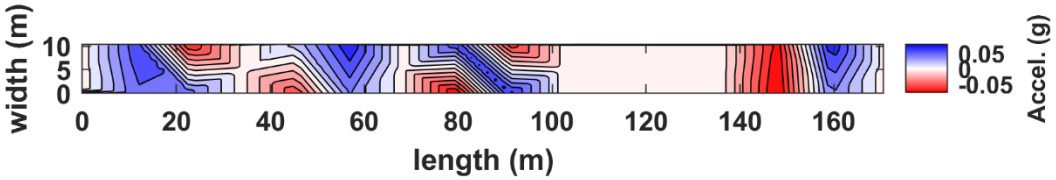

Figure B.276. Interpolated acceleration in plan view for truck pass 21 at the NOBL West Yutan bridge structure.

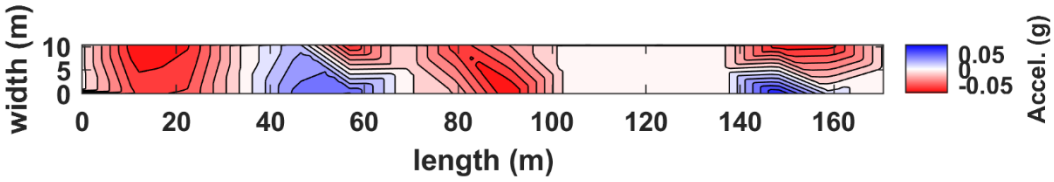

Figure B.277. Interpolated acceleration in plan view for truck pass 22 at the NOBL West Yutan bridge structure.

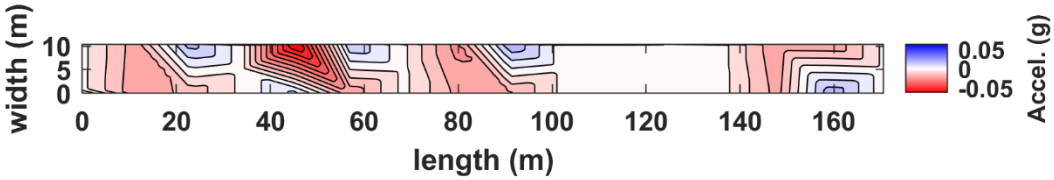

Figure B.278. Interpolated acceleration in plan view for truck pass 23 at the NOBL West Yutan bridge structure.

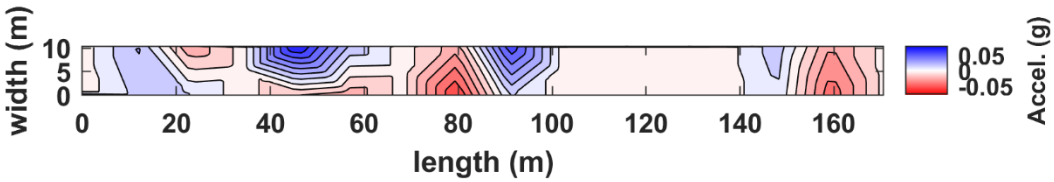

Figure B.279. Interpolated acceleration in plan view for truck pass 24 at the NOBL West Yutan bridge structure.

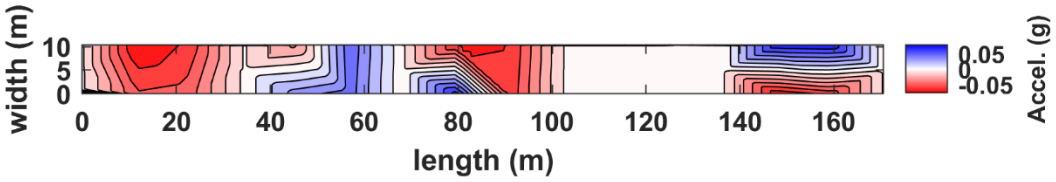

Figure B.280. Interpolated acceleration in plan view for truck pass 25 at the NOBL West Yutan bridge structure.

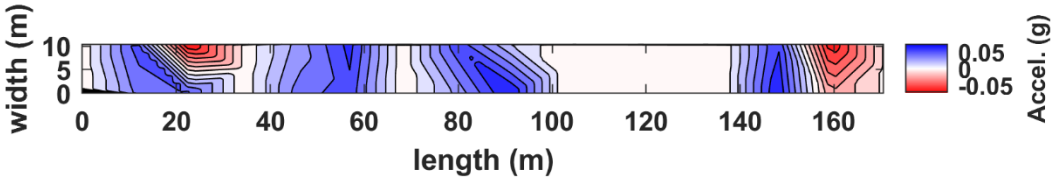

Figure B.281. Interpolated acceleration in plan view for truck pass 26 at the NOBL West Yutan bridge structure.

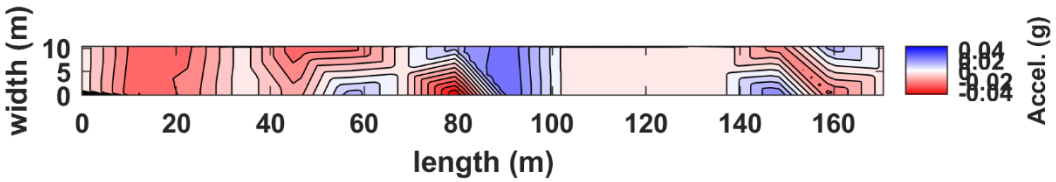

Figure B.282. Interpolated acceleration in plan view for truck pass 27 at the NOBL West Yutan bridge structure.

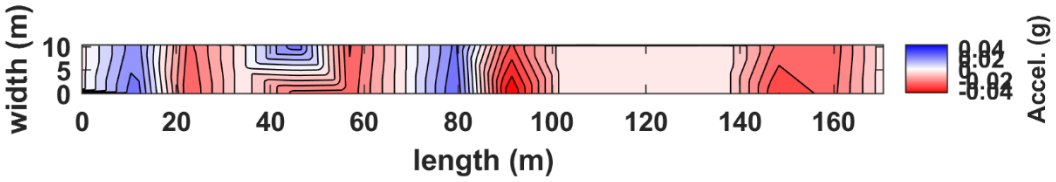

Figure B.283. Interpolated acceleration in plan view for truck pass 28 at the NOBL West Yutan bridge structure.

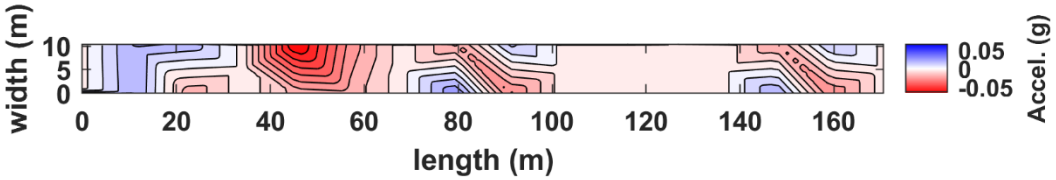

Figure B.284. Interpolated acceleration in plan view for truck pass 29 at the NOBL West Yutan bridge structure.

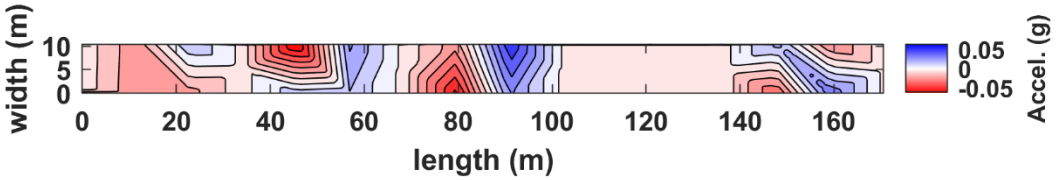

Figure B.285. Interpolated acceleration in plan view for truck pass 30 at the NOBL West Yutan bridge structure.

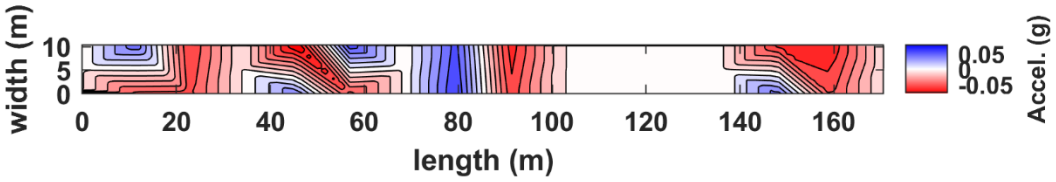

Figure B.286. Interpolated acceleration in plan view for truck pass 31 at the NOBL West Yutan bridge structure.

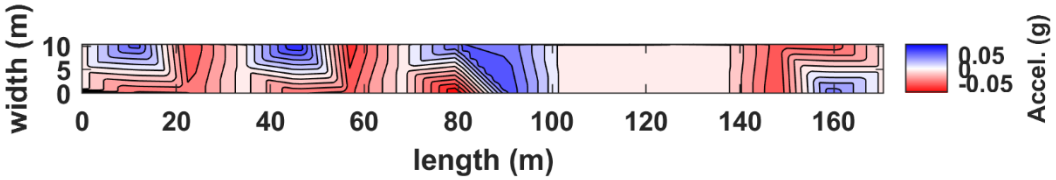

Figure B.287. Interpolated acceleration in plan view for truck pass 32 at the NOBL West Yutan bridge structure.

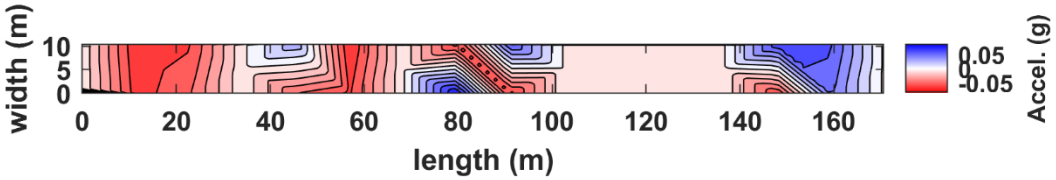

Figure B.288. Interpolated acceleration in plan view for truck pass 33 at the NOBL West Yutan bridge structure.

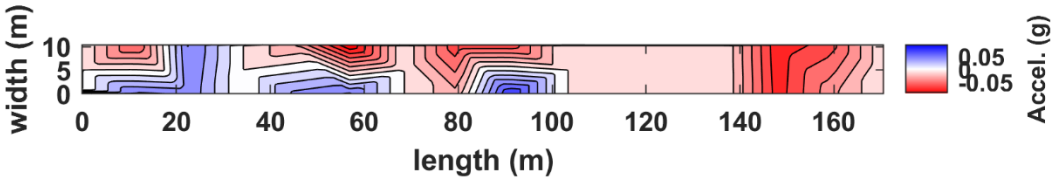

Figure B.289. Interpolated acceleration in plan view for truck pass 34 at the NOBL West Yutan bridge structure.

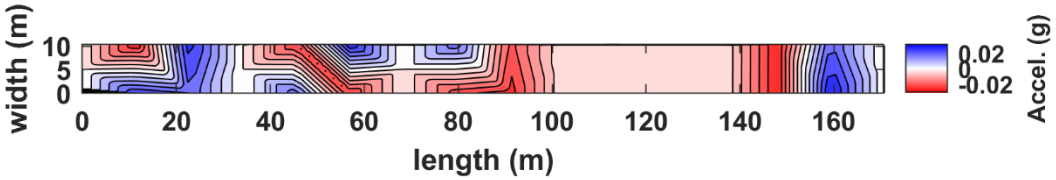

Figure B.290. Interpolated acceleration in plan view for truck pass 35 at the NOBL West Yutan bridge structure.

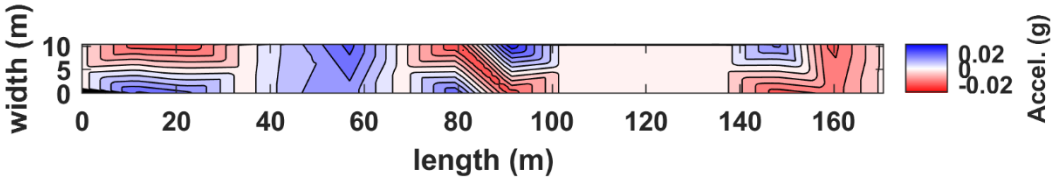

Figure B.291. Interpolated acceleration in plan view for truck pass 36 at the NOBL West Yutan bridge structure.

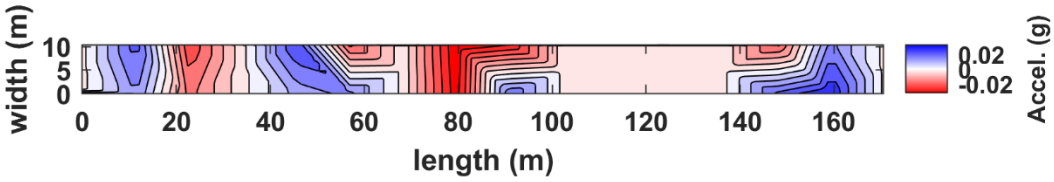

Figure B.292. Interpolated acceleration in plan view for truck pass 37 at the NOBL West Yutan bridge structure.

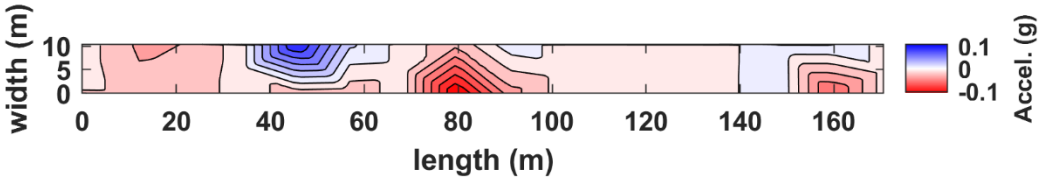

Figure B.293. Interpolated acceleration in plan view for truck pass 38 at the NOBL West Yutan bridge structure.

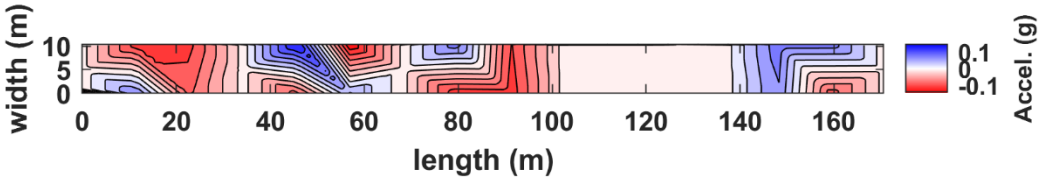

Figure B.294. Interpolated acceleration in plan view for truck pass 39 at the NOBL West Yutan bridge structure.

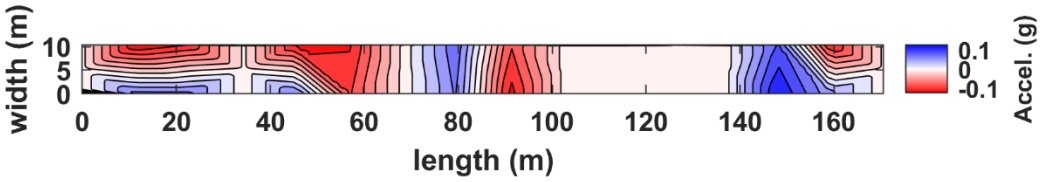

Figure B.295. Interpolated acceleration in plan view for truck pass 40 at the NOBL West Yutan bridge structure.

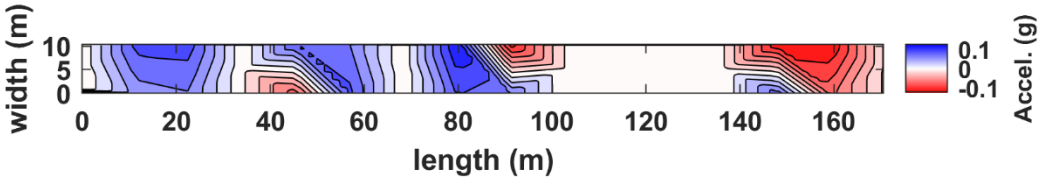

Figure B.296. Interpolated acceleration in plan view for truck pass 41 at the NOBL West Yutan bridge structure.

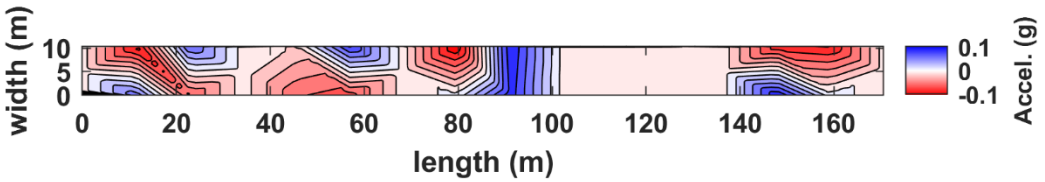

Figure B.297. Interpolated acceleration in plan view for truck pass 42 at the NOBL West Yutan bridge structure.

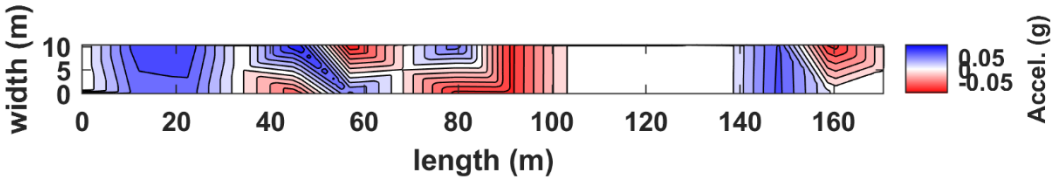

Figure B.298. Interpolated acceleration in plan view for truck pass 43 at the NOBL West Yutan bridge structure.

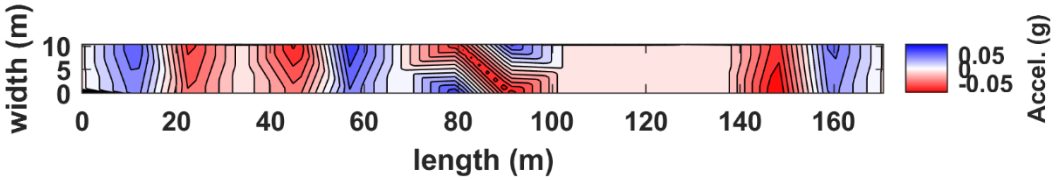

Figure B.299. Interpolated acceleration in plan view for truck pass 44 at the NOBL West Yutan bridge structure.

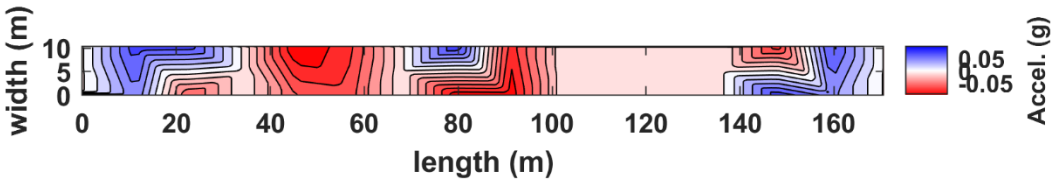

Figure B.300. Interpolated acceleration in plan view for truck pass 45 at the NOBL West Yutan bridge structure.

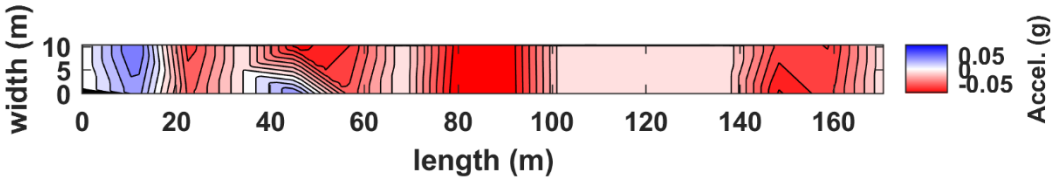

Figure B.301. Interpolated acceleration in plan view for truck pass 46 at the NOBL West Yutan bridge structure.

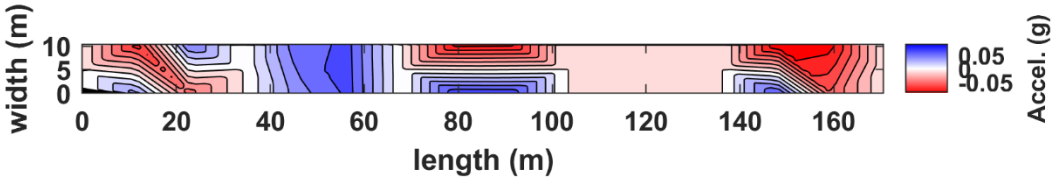

Figure B.302. Interpolated acceleration in plan view for truck pass 47 at the NOBL West Yutan bridge structure.

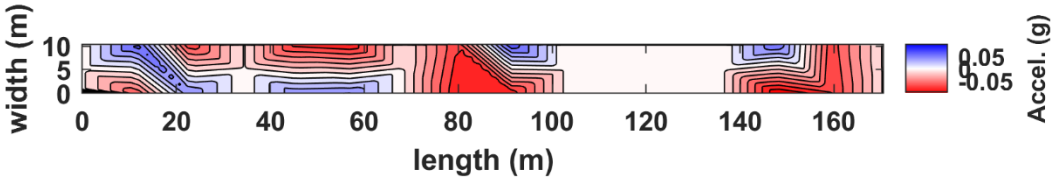

Figure B.303. Interpolated acceleration in plan view for truck pass 48 at the NOBL West Yutan bridge structure.

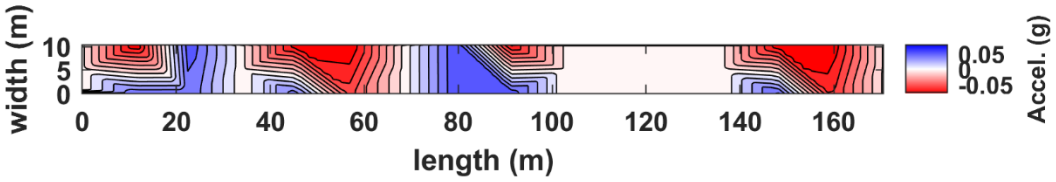

Figure B.304. Interpolated acceleration in plan view for truck pass 49 at the NOBL West Yutan bridge structure.

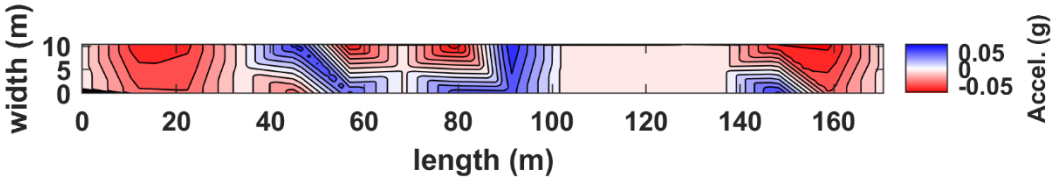

Figure B.305. Interpolated acceleration in plan view for truck pass 50 at the NOBL West Yutan bridge structure.

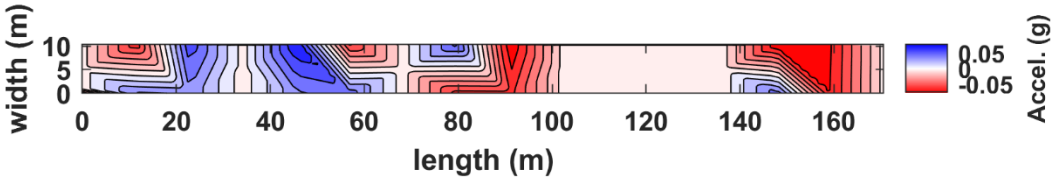

Figure B.306. Interpolated acceleration in plan view for truck pass 51 at the NOBL West Yutan bridge structure.

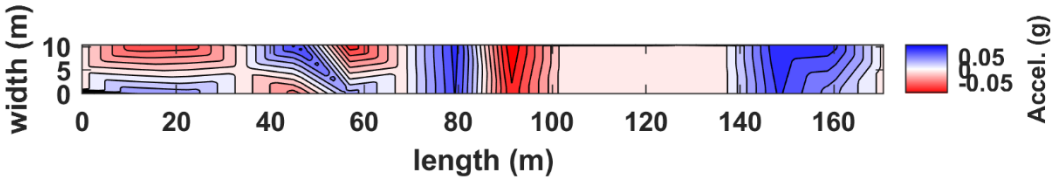

Figure B.307. Interpolated acceleration in plan view for truck pass 52 at the NOBL West Yutan bridge structure.

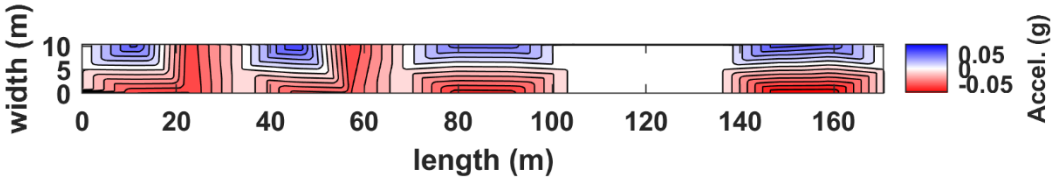

Figure B.308. Interpolated acceleration in plan view for truck pass 53 at the NOBL West Yutan bridge structure.

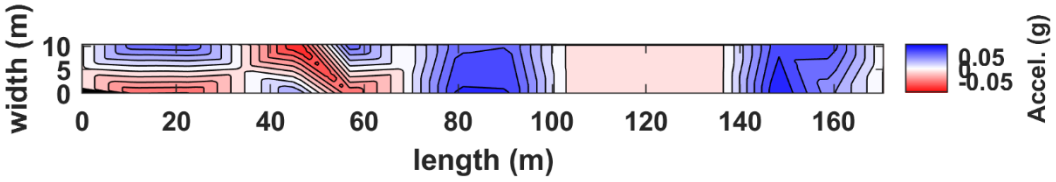

Figure B.309. Interpolated acceleration in plan view for truck pass 54 at the NOBL West Yutan bridge structure.

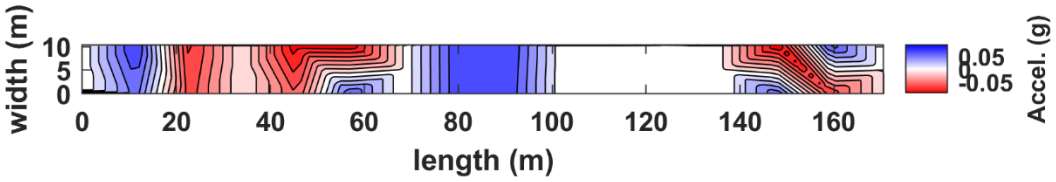

Figure B.310. Interpolated acceleration in plan view for truck pass 55 at the NOBL West Yutan bridge structure.

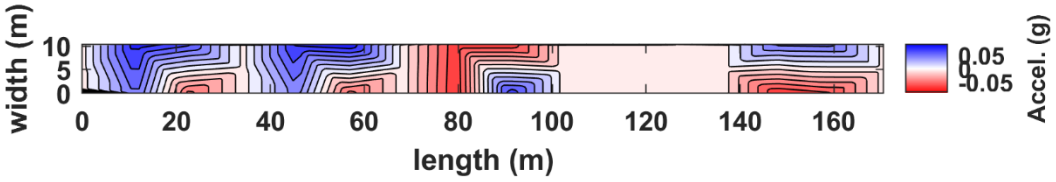

Figure B.311. Interpolated acceleration in plan view for truck pass 56 at the NOBL West Yutan bridge structure.

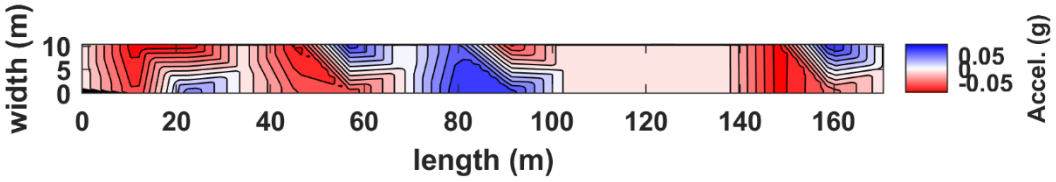

Figure B.312. Interpolated acceleration in plan view for truck pass 57 at the NOBL West Yutan bridge structure.

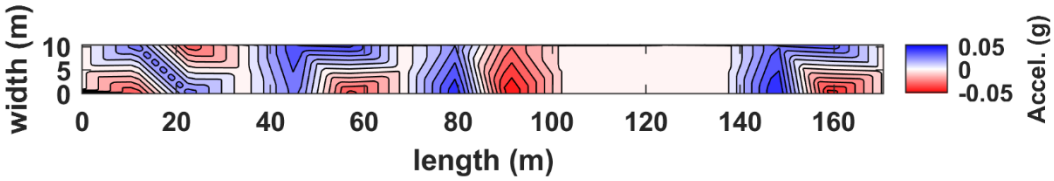

Figure B.313. Interpolated acceleration in plan view for truck pass 58 at the NOBL West Yutan bridge structure.

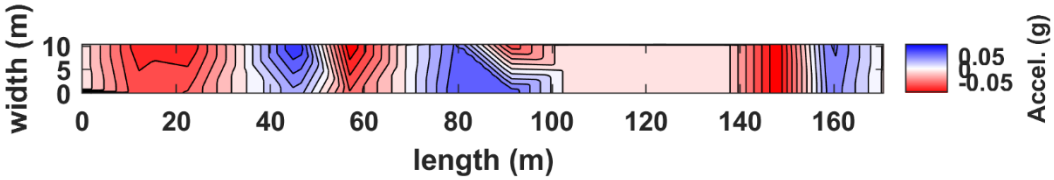

Figure B.314. Interpolated acceleration in plan view for truck pass 59 at the NOBL West Yutan bridge structure.

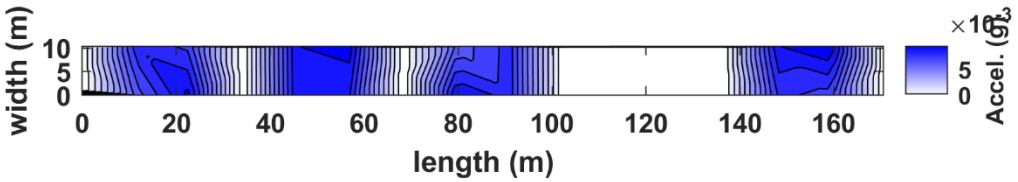

Figure B.315. Interpolated absolute-valued acceleration in plan view for truck pass 01 at the NOBL West Yutan bridge structure.

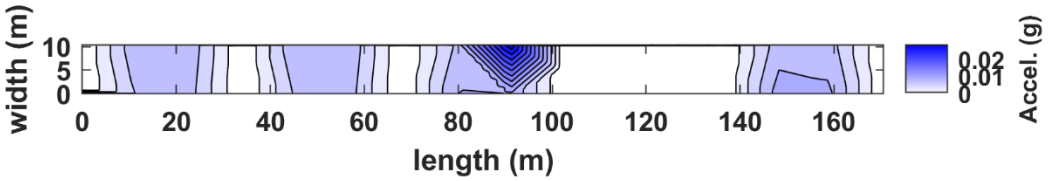

Figure B.316. Interpolated absolute-valued acceleration in plan view for truck pass 02 at the NOBL West Yutan bridge structure.

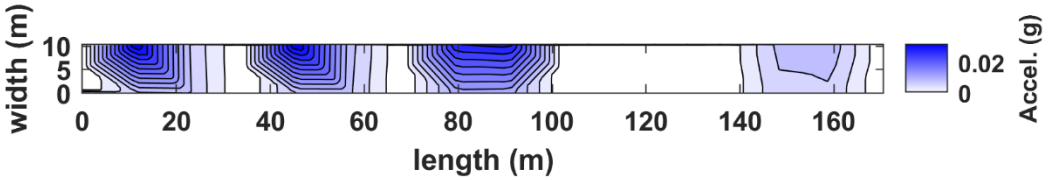

Figure B.317. Interpolated absolute-valued acceleration in plan view for truck pass 03 at the NOBL West Yutan bridge structure.

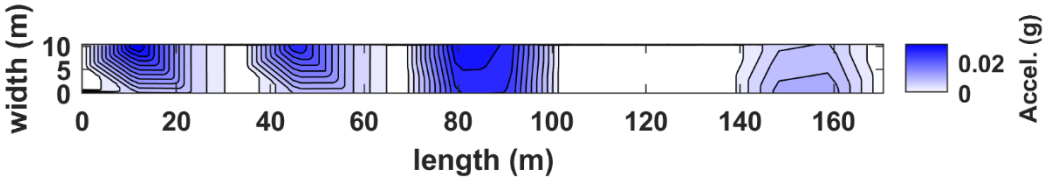

Figure B.318. Interpolated absolute-valued acceleration in plan view for truck pass 04 at the NOBL West Yutan bridge structure.

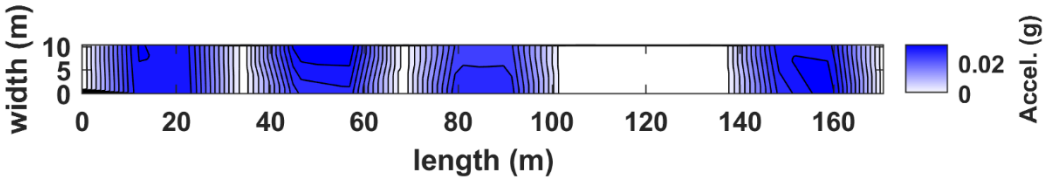

Figure B.319. Interpolated absolute-valued acceleration in plan view for truck pass 05 at the NOBL West Yutan bridge structure.

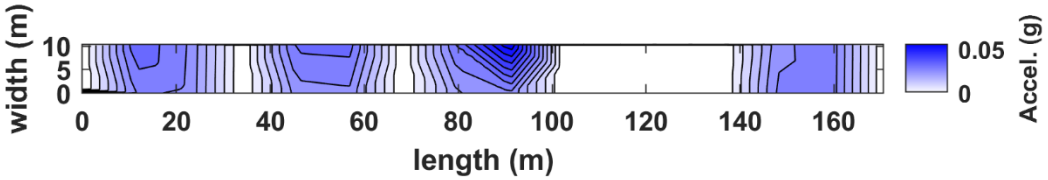

Figure B.320. Interpolated absolute-valued acceleration in plan view for truck pass 06 at the NOBL West Yutan bridge structure.

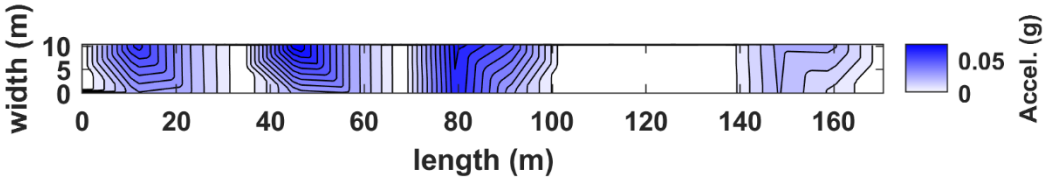

Figure B.321. Interpolated absolute-valued acceleration in plan view for truck pass 07 at the NOBL West Yutan bridge structure.

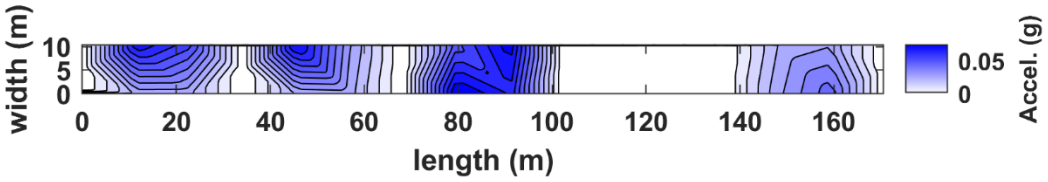

Figure B.322. Interpolated absolute-valued acceleration in plan view for truck pass 08 at the NOBL West Yutan bridge structure.

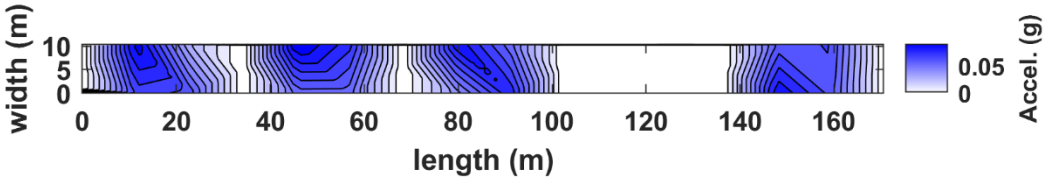

Figure B.323. Interpolated absolute-valued acceleration in plan view for truck pass 09 at the NOBL West Yutan bridge structure.

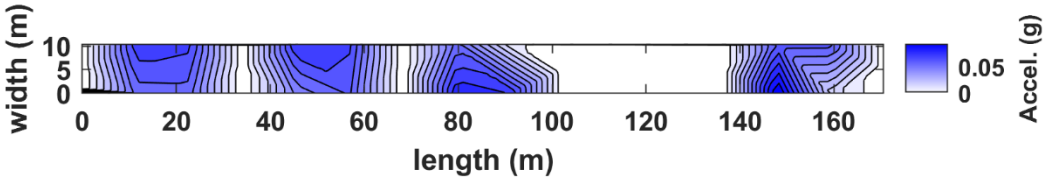

Figure B.324. Interpolated absolute-valued acceleration in plan view for truck pass 10 at the NOBL West Yutan bridge structure.

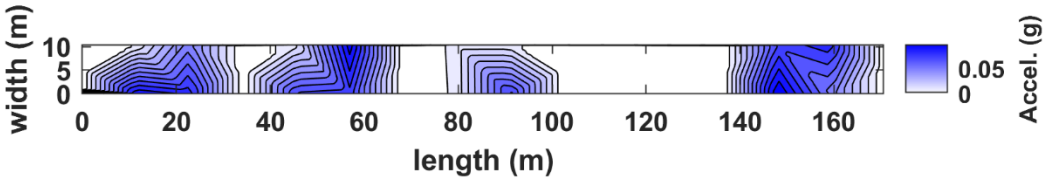

Figure B.325. Interpolated absolute-valued acceleration in plan view for truck pass 11 at the NOBL West Yutan bridge structure.

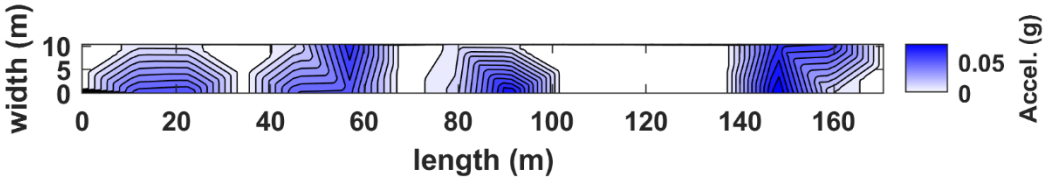

Figure B.326. Interpolated absolute-valued acceleration in plan view for truck pass 12 at the NOBL West Yutan bridge structure.

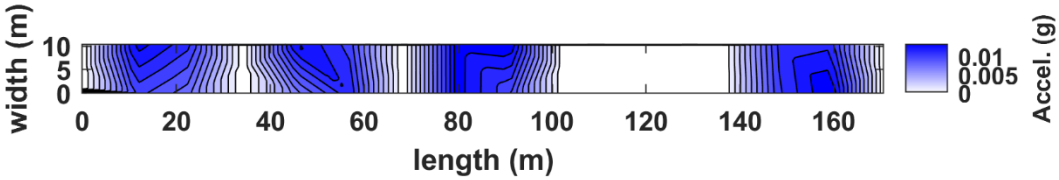

Figure B.327. Interpolated absolute-valued acceleration in plan view for truck pass 13 at the NOBL West Yutan bridge structure.

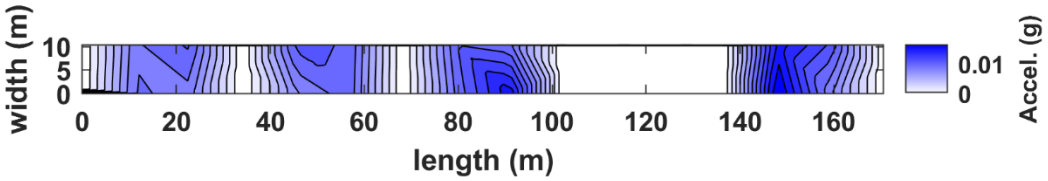

Figure B.328. Interpolated absolute-valued acceleration in plan view for truck pass 14 at the NOBL West Yutan bridge structure.

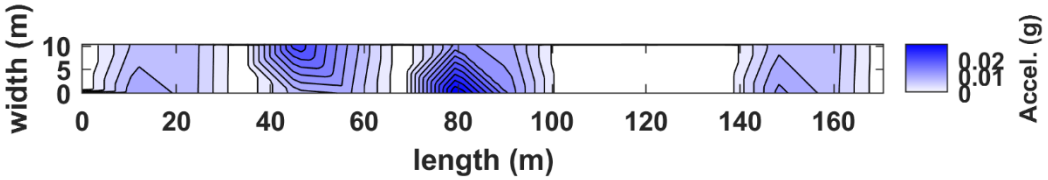

Figure B.329. Interpolated absolute-valued acceleration in plan view for truck pass 15 at the NOBL West Yutan bridge structure.

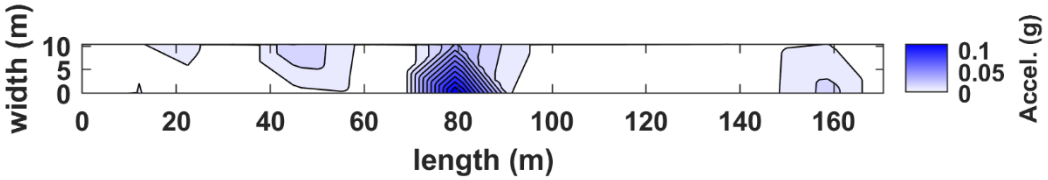

Figure B.330. Interpolated absolute-valued acceleration in plan view for truck pass 16 at the NOBL West Yutan bridge structure.

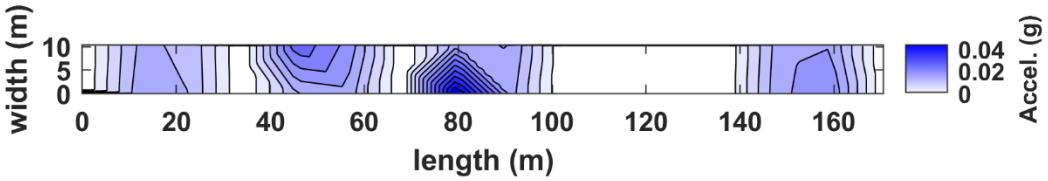

Figure B.331. Interpolated absolute-valued acceleration in plan view for truck pass 17 at the NOBL West Yutan bridge structure.

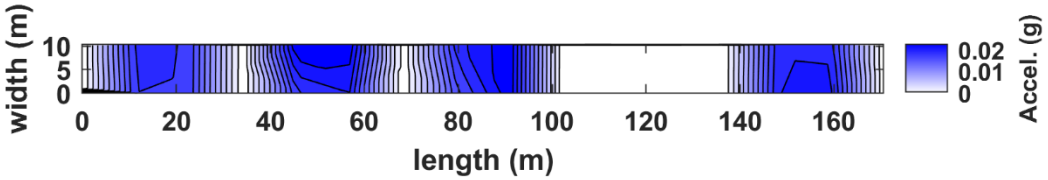

Figure B.332. Interpolated absolute-valued acceleration in plan view for truck pass 18 at the NOBL West Yutan bridge structure.

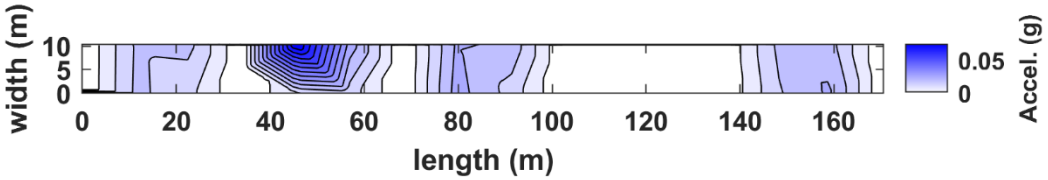

Figure B.333. Interpolated absolute-valued acceleration in plan view for truck pass 19 at the NOBL West Yutan bridge structure.

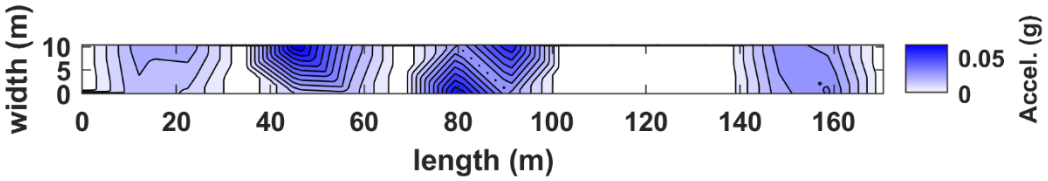

Figure B.334. Interpolated absolute-valued acceleration in plan view for truck pass 20 at the NOBL West Yutan bridge structure.

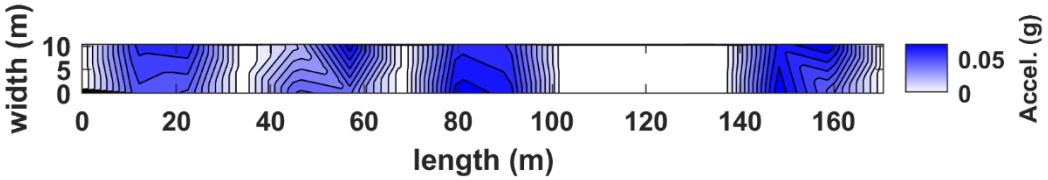

Figure B.335. Interpolated absolute-valued acceleration in plan view for truck pass 21 at the NOBL West Yutan bridge structure.

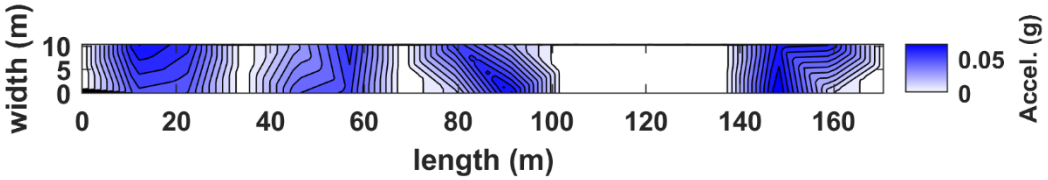

Figure B.336. Interpolated absolute-valued acceleration in plan view for truck pass 22 at the NOBL West Yutan bridge structure.

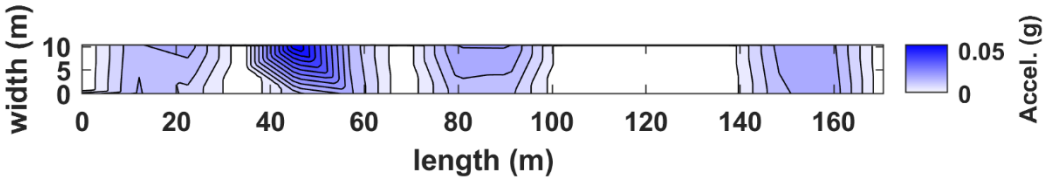

Figure B.337. Interpolated absolute-valued acceleration in plan view for truck pass 23 at the NOBL West Yutan bridge structure.

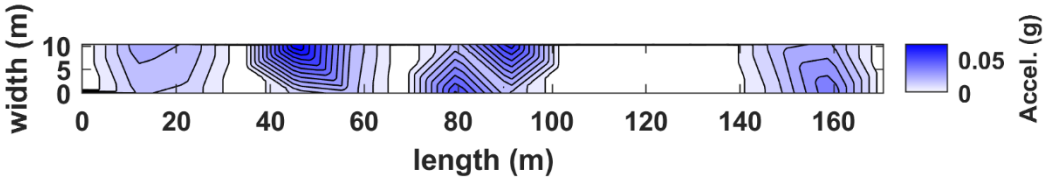

Figure B.338. Interpolated absolute-valued acceleration in plan view for truck pass 24 at the NOBL West Yutan bridge structure.

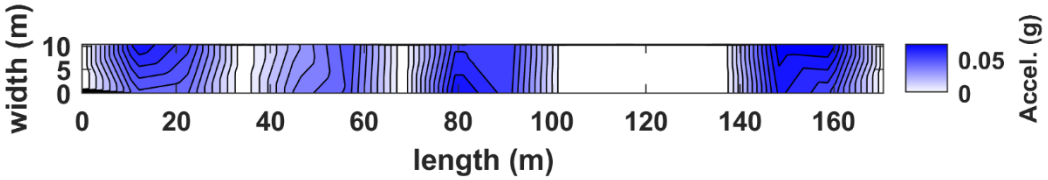

Figure B.339. Interpolated absolute-valued acceleration in plan view for truck pass 25 at the NOBL West Yutan bridge structure.

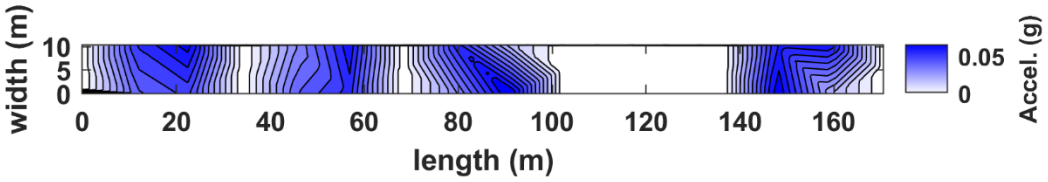

Figure B.340. Interpolated absolute-valued acceleration in plan view for truck pass 26 at the NOBL West Yutan bridge structure.

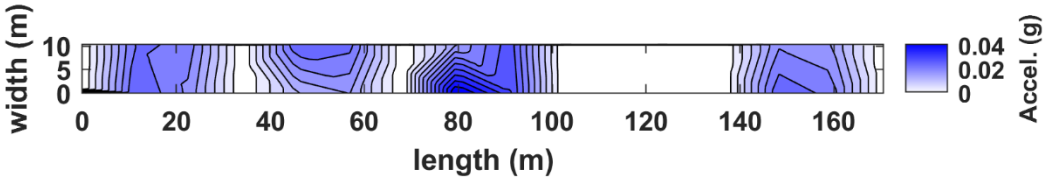

Figure B.341. Interpolated absolute-valued acceleration in plan view for truck pass 27 at the NOBL West Yutan bridge structure.

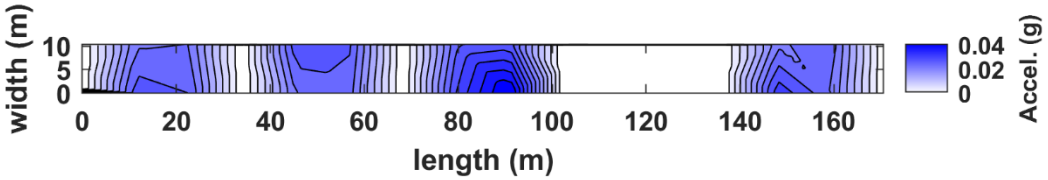

Figure B.342. Interpolated absolute-valued acceleration in plan view for truck pass 28 at the NOBL West Yutan bridge structure.

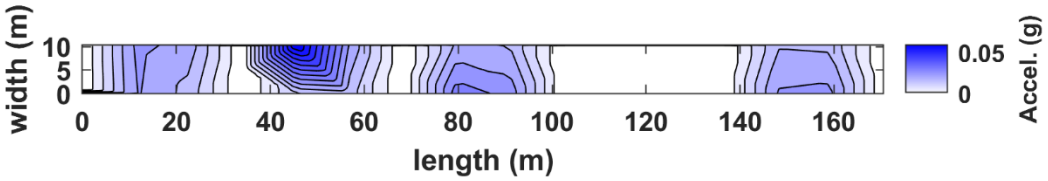

Figure B.343. Interpolated absolute-valued acceleration in plan view for truck pass 29 at the NOBL West Yutan bridge structure.

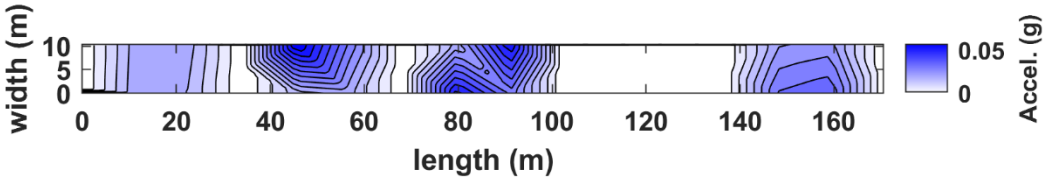

Figure B.344. Interpolated absolute-valued acceleration in plan view for truck pass 30 at the NOBL West Yutan bridge structure.

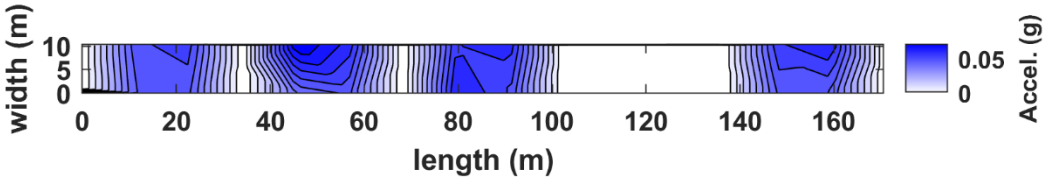

Figure B.345. Interpolated absolute-valued acceleration in plan view for truck pass 31 at the NOBL West Yutan bridge structure.

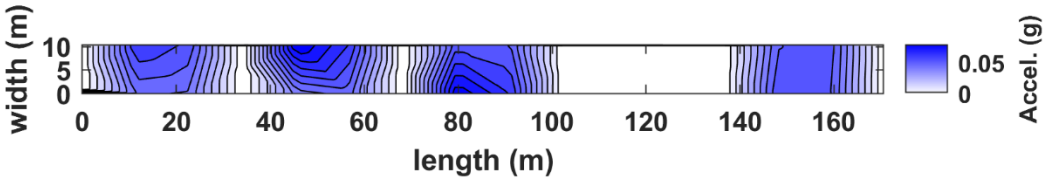

Figure B.346. Interpolated absolute-valued acceleration in plan view for truck pass 32 at the NOBL West Yutan bridge structure.

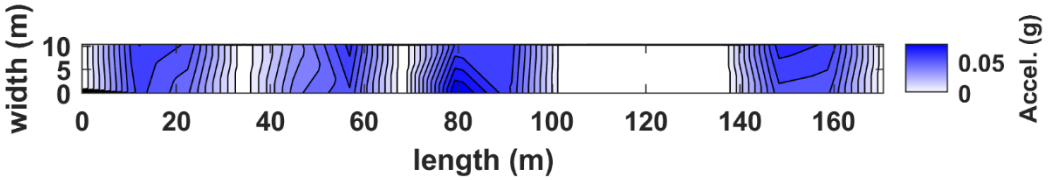

Figure B.347. Interpolated absolute-valued acceleration in plan view for truck pass 33 at the NOBL West Yutan bridge structure.

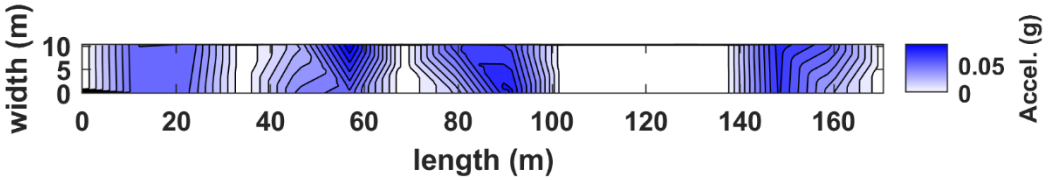

Figure B.348. Interpolated absolute-valued acceleration in plan view for truck pass 34 at the NOBL West Yutan bridge structure.

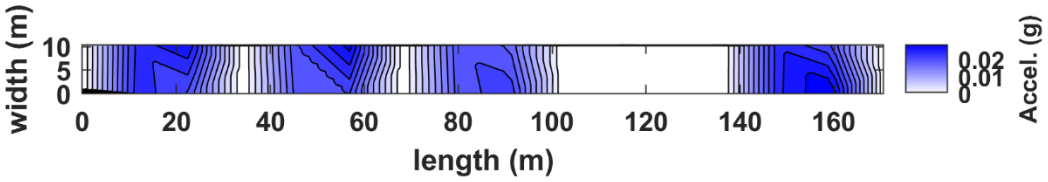

Figure B.349. Interpolated absolute-valued acceleration in plan view for truck pass 35 at the NOBL West Yutan bridge structure.

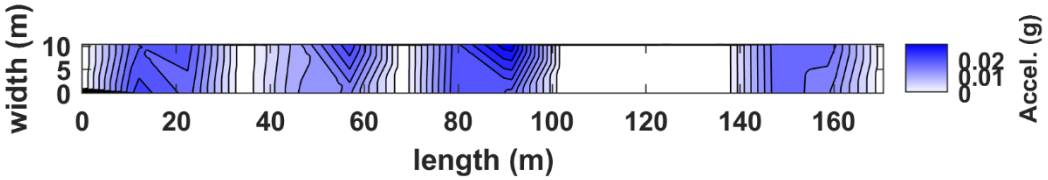

Figure B.350. Interpolated absolute-valued acceleration in plan view for truck pass 36 at the NOBL West Yutan bridge structure.

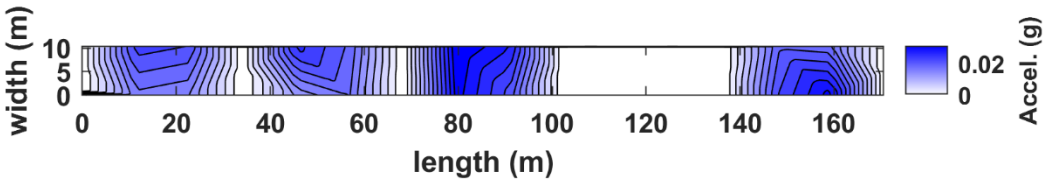

Figure B.351. Interpolated absolute-valued acceleration in plan view for truck pass 37 at the NOBL West Yutan bridge structure.

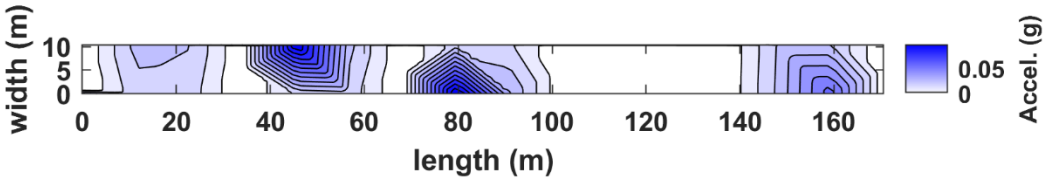

Figure B.352. Interpolated absolute-valued acceleration in plan view for truck pass 38 at the NOBL West Yutan bridge structure.

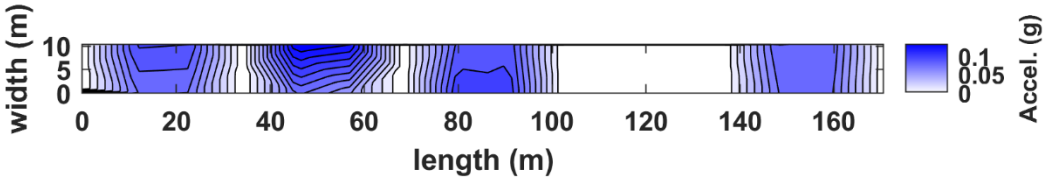

Figure B.353. Interpolated absolute-valued acceleration in plan view for truck pass 39 at the NOBL West Yutan bridge structure.

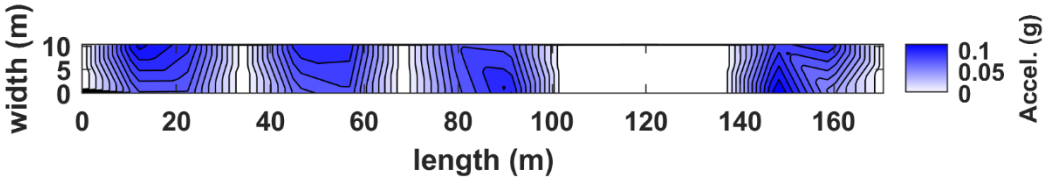

Figure B.354. Interpolated absolute-valued acceleration in plan view for truck pass 40 at the NOBL West Yutan bridge structure.

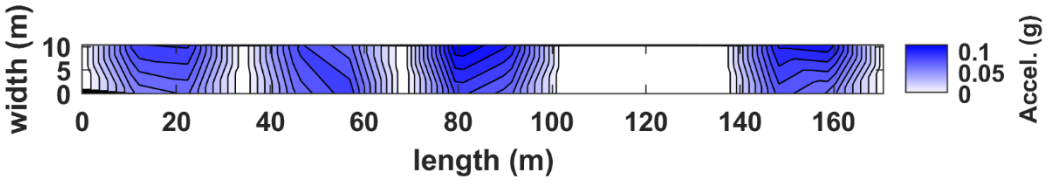

Figure B.355. Interpolated absolute-valued acceleration in plan view for truck pass 41 at the NOBL West Yutan bridge structure.

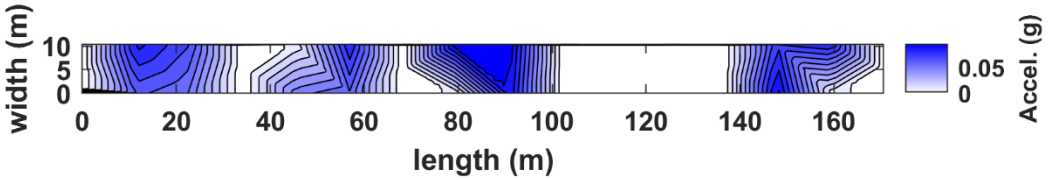

Figure B.356. Interpolated absolute-valued acceleration in plan view for truck pass 42 at the NOBL West Yutan bridge structure.

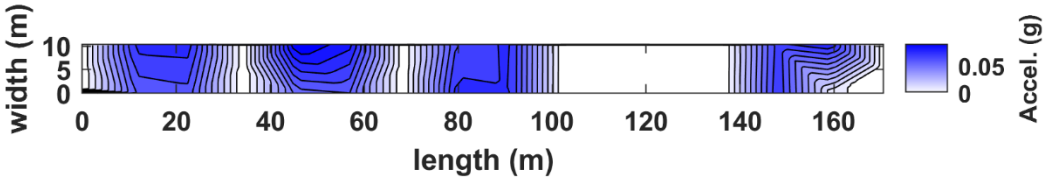

Figure B.357. Interpolated absolute-valued acceleration in plan view for truck pass 43 at the NOBL West Yutan bridge structure.

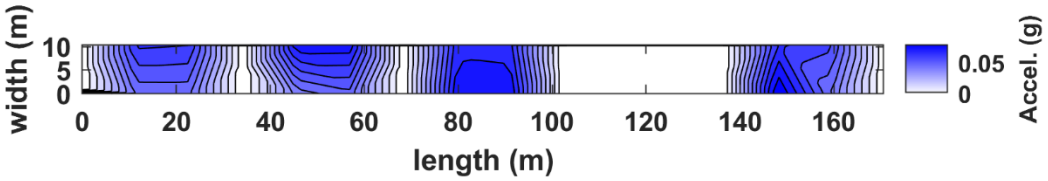

Figure B.358. Interpolated absolute-valued acceleration in plan view for truck pass 44 at the NOBL West Yutan bridge structure.

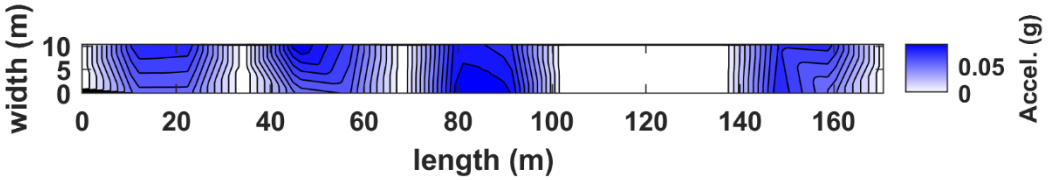

Figure B.359. Interpolated absolute-valued acceleration in plan view for truck pass 45 at the NOBL West Yutan bridge structure.

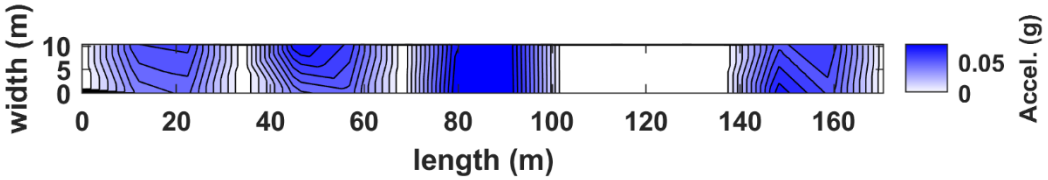

Figure B.360. Interpolated absolute-valued acceleration in plan view for truck pass 46 at the NOBL West Yutan bridge structure.

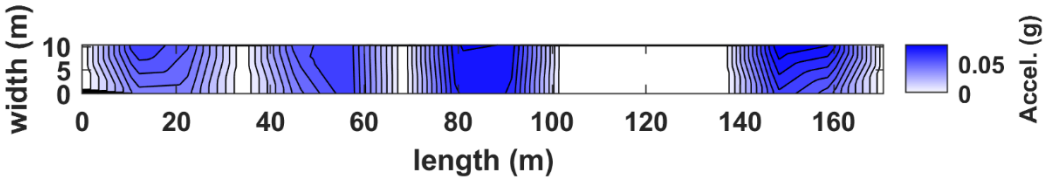

Figure B.361. Interpolated absolute-valued acceleration in plan view for truck pass 47 at the NOBL West Yutan bridge structure.

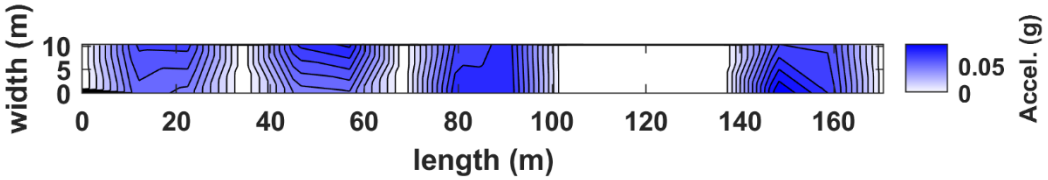

Figure B.362. Interpolated absolute-valued acceleration in plan view for truck pass 48 at the NOBL West Yutan bridge structure.

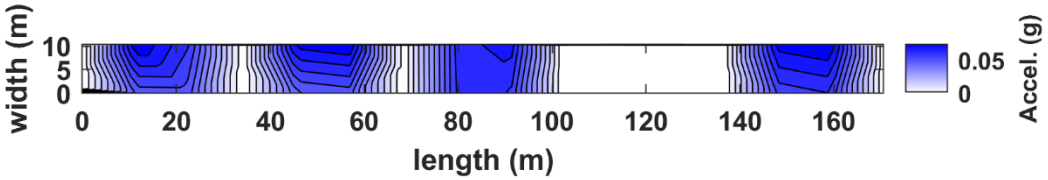

Figure B.363. Interpolated absolute-valued acceleration in plan view for truck pass 49 at the NOBL West Yutan bridge structure.

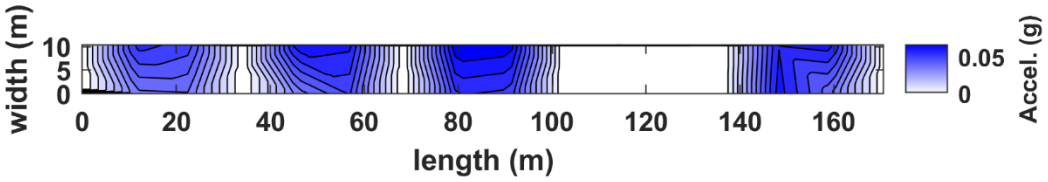

Figure B.364. Interpolated absolute-valued acceleration in plan view for truck pass 50 at the NOBL West Yutan bridge structure.

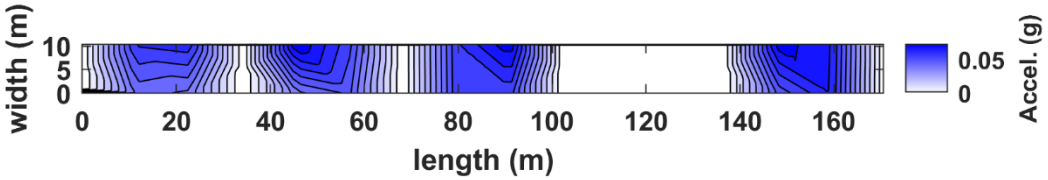

Figure B.365. Interpolated absolute-valued acceleration in plan view for truck pass 51 at the NOBL West Yutan bridge structure.

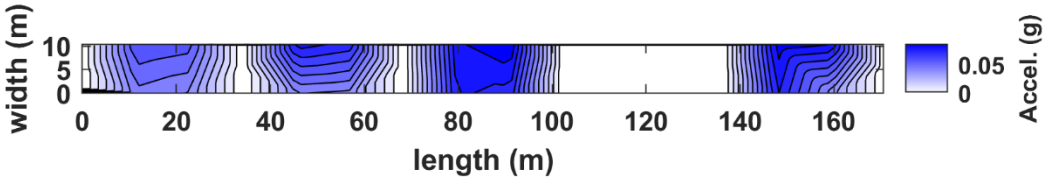

Figure B.366. Interpolated absolute-valued acceleration in plan view for truck pass 52 at the NOBL West Yutan bridge structure.

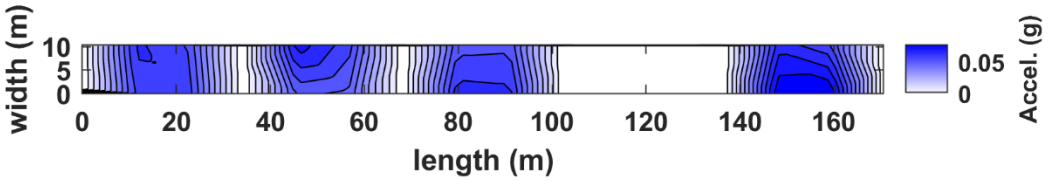

Figure B.367. Interpolated absolute-valued acceleration in plan view for truck pass 53 at the NOBL West Yutan bridge structure.

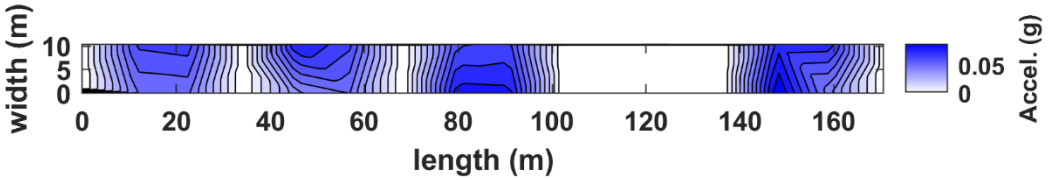

Figure B.368. Interpolated absolute-valued acceleration in plan view for truck pass 54 at the NOBL West Yutan bridge structure.

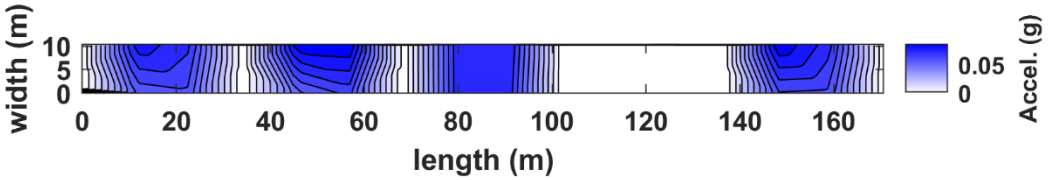

Figure B.369. Interpolated absolute-valued acceleration in plan view for truck pass 55 at the NOBL West Yutan bridge structure.

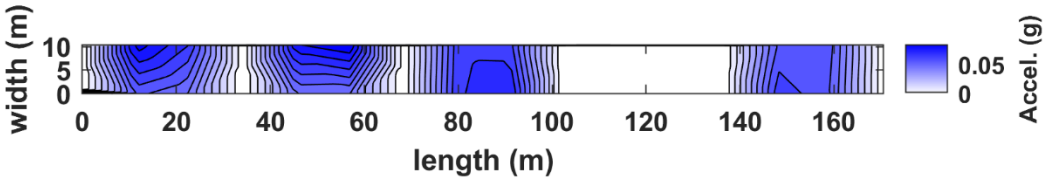

Figure B.370. Interpolated absolute-valued acceleration in plan view for truck pass 56 at the NOBL West Yutan bridge structure.

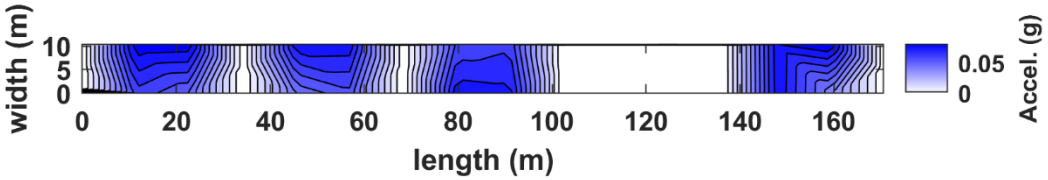

Figure B.371. Interpolated absolute-valued acceleration in plan view for truck pass 57 at the NOBL West Yutan bridge structure.

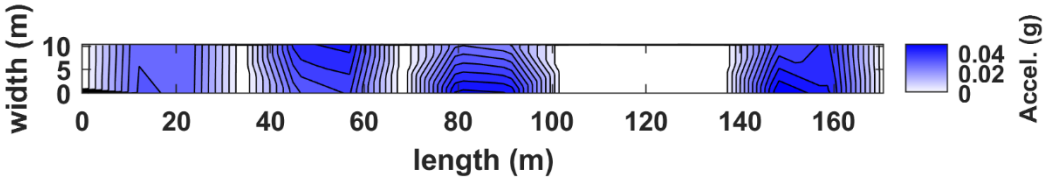

Figure B.372. Interpolated absolute-valued acceleration in plan view for truck pass 58 at the NOBL West Yutan bridge structure.

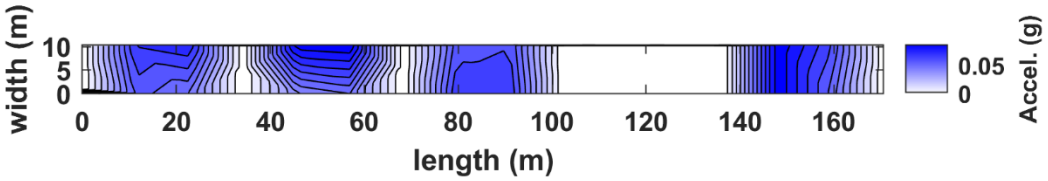

Figure B.373. Interpolated absolute-valued acceleration in plan view for truck pass 59 at the NOBL West Yutan bridge structure.

Appendix C.

Live Load Test and Computational Model Details

Table of contents

List of Figures

List of Tables

1 Overview

NOBL North bridge at Omaha, a 42-year-old prestressed I-girder bridge located on state route 36 over the Glenn Cunningham Reservoir north of Omaha, Nebraska, was subjected to diagnostic load testing. This three-span bridge was typical of a 1970s prestressed concrete bridge. Precast girders were placed as simply spanning elements between abutments and piers. Next, the concrete deck and diaphragms were cast-in-place, making the structure continuous for subsequent dead and live loads, including barriers and asphalt overlay. Due to operational programming, the structure was removed from service although its structural condition was and remains very good. The diagnostic load testing included investigations and comparisons of experimentally and analytically obtained live load structural response.

During this test, strains were measured at four different bridge locations to assess girder load distribution and determine dynamic effects, and to validate FEMs for potential future applications. Experimental data was collected from ST350 strain transducers from Bridge Diagnostics Inc (BDI). ST350 data was sampled at sufficiently high strain rates to capture dynamic strain amplifications. Tests described herein were short term and strain readings were zeroed at the start of each test run so that any thermally-induced strains were neglected.

Field test results were compared with analytical calculations. Finite element models (FEMs) in 2D and 3D were developed for this bridge using SAP2000™, CSiBridge™, AASHTOWare BrR™, and COMSOL™. Construction plans and supplementary correspondence provided by the Nebraska Department of Transportation (NDOT) primarily guided the geometry and material properties implemented in the bridge models. The analytical studies included explorations of various modeling assumptions, such as rotational restraint applied to the girder superstructure by abutments and piers.

Girder distribution factors (GDFs) quantify the proportion of live load carried by individual girders and are a common focus of field testing evaluations. The load test results were compared to AASHTO LRFD (2020) and AASHTO Standard Specifications (2002) approximate GDFs, and to GDFs determined from 3D FEMs. According to AASHTO Standard Specifications and AASHTO LRFD, dynamic load factors (DLF) are conservative compared to actual values. For example, the typical DLF used for design according to

AASHTO LRFD is 0.33, but literature available from multiple NCHRP studies note that the mean is approximately 0.1. While the discrepancy between the nominal design value and the mean value is ostensibly addressed through the selection of the live load factor using reliability analyses, the AASHTO Manual for Bridge Evaluation (MBE) allows the measured dynamic amplification to be used as a direct substitution for the code-specified value of 0.33 without additional reliability-based recalibration. This study included an investigation of actual DLF values by comparing bridge responses when subjected to trucks traveling at varying speeds.

2 Prestressed Concrete Bridge Details

NOBL North bridge at Omaha was built in 1979, and is located on State Route 36, north of Omaha, , Nebraska (41°21'54.7"N, 96°03'20.7"W). Sample images of the bridge are shown in **Error! Reference s ource not found.**. The bridge is a three-span, simple-made-continuous prestressed concrete girder bridge designed as a composite section. This concrete bridge was originally designed for a potential four-lane divided highway expansion in 1979 but has seen only minimal traffic loads. as its adjacent twin to the south has supported all traffic on SR 36 since construction. As illustrated in **Error! Reference source not found.**, v arious forms of deterioration can be observed in this structure despite its minimal use, including localized scour at the abutment, abutment cracking, suspected delamination near the bridge deck weep holes, and cracks in the asphalt deck overlay. S036 02040L has nominal span lengths of 48, 60, and 48 ft, as shown in Figure C.374. The bridge is comprised of five Nebraska Type 3A girders spaced at 8 ft 8 in, as shown in Figure C.375 with 0-degree skew. The average deck thickness is 7.5 in., and the overhang is 3 ft-10 in..

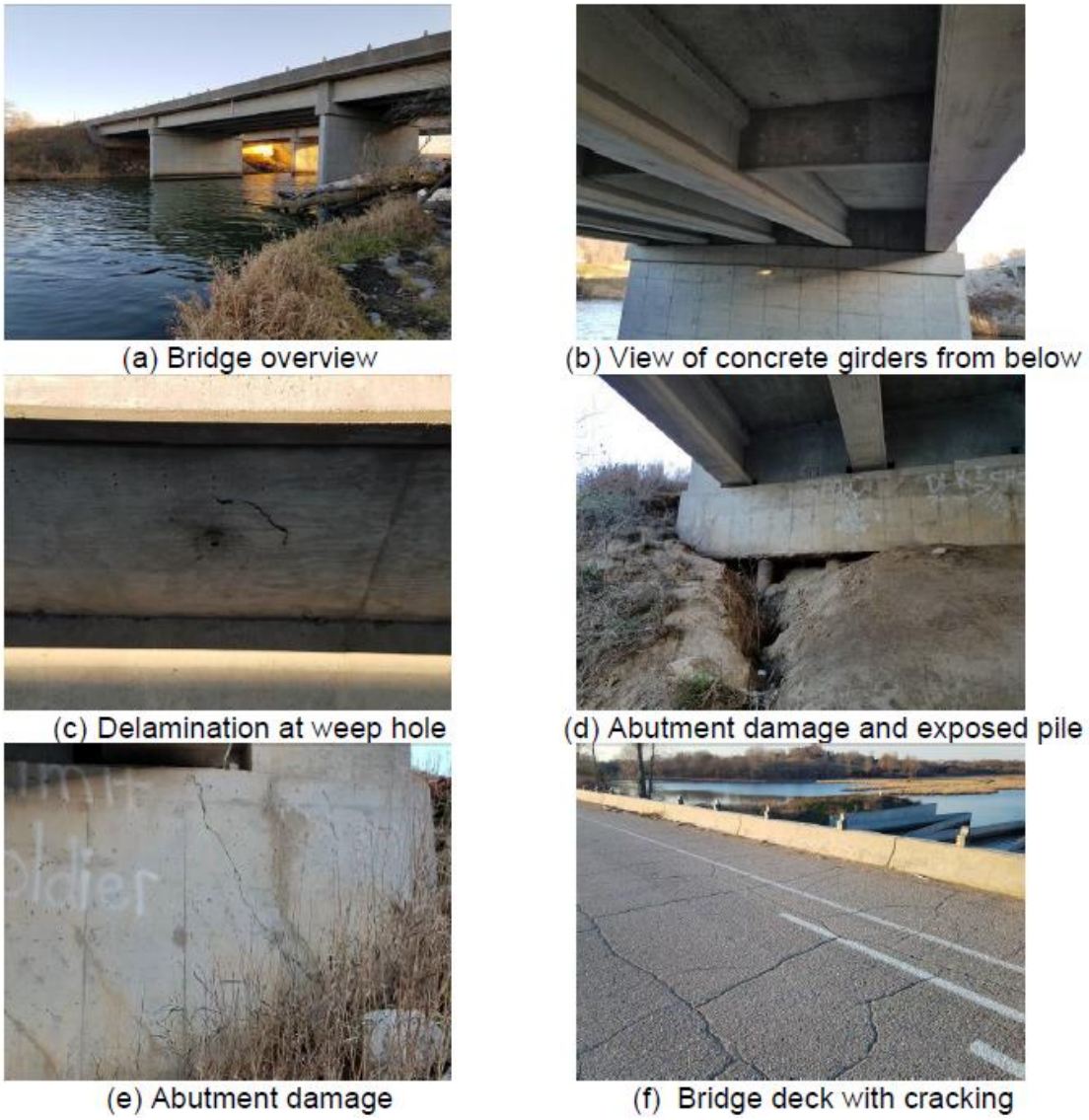

Figure C.1. Sample images of the concrete girder bridge.

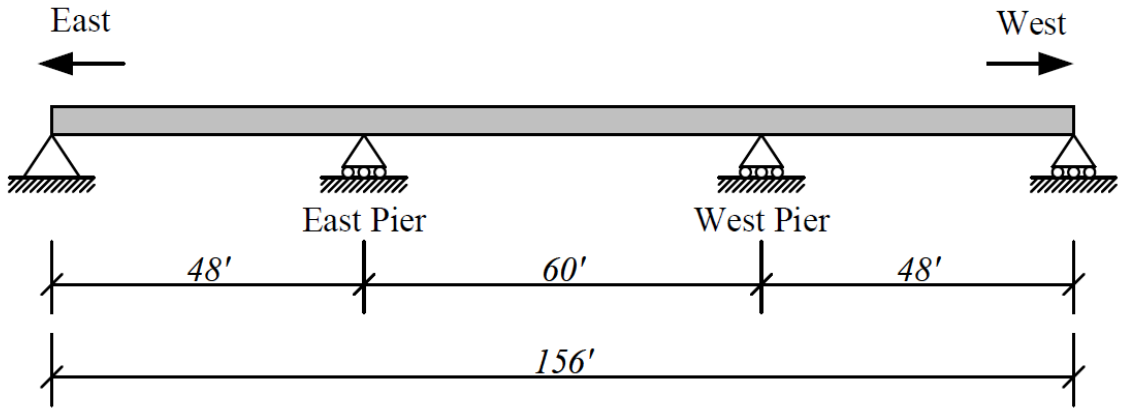

Figure C.374. Schematic elevation of bridge.

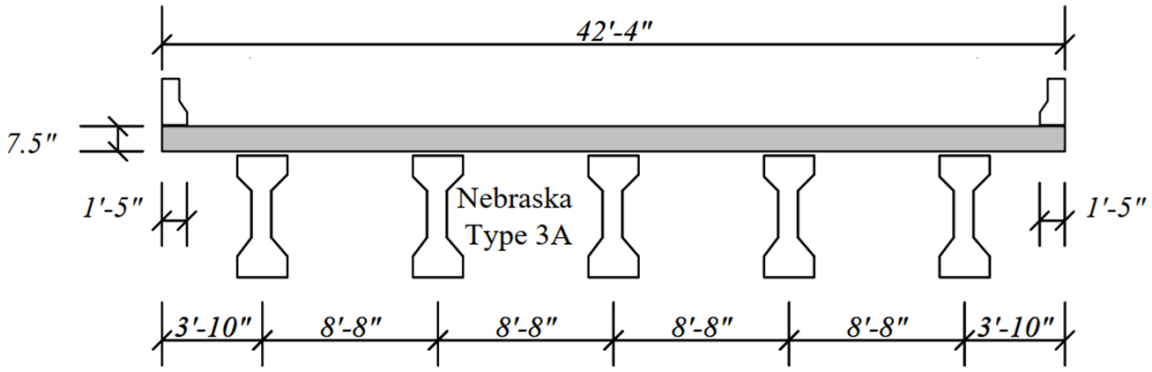

Figure C.375. Schematic cross section of the bridge.

3 Instrumentation

During the field tests, strain transducers were installed on four cross-sections of the bridge, as shown in Figure C.376. To evaluate the degree of rotational fixity at abutments while avoiding the influence of disturbed condition stress and strain fields near bearings, the strain transducers were positioned 3 ft from the east abutment bearings' centerline. Similarly, maximum negative bending moments of the simple-made-continuous bridge were anticipated and investigated near the piers by installing strain transducers 3 ft away from the bearing centerlines on the east and west sides of the east pier. Each bearing centerline was offset 10 inches from the pier centerline, so that strain gages were located 3 ft-10 in. from the pier centerline. The positive moment was monitored at 0.4L of the east end span (19.2 ft to the east abutment centerline).

A total of forty-four (44) strain transducers were attached at the four selected cross-sections. Figure C.377 shows the strain locations on the girder and the bottom of the concrete deck. On each girder, strain transducers were attached to the center of the bottom flange. Additionally, girder web strain transducers were installed to determine the neutral axis and evaluate the bridge behavior of non-composite and composite sections. A strain transducer was attached to the bottom of the concrete deck 2 in. from the side of the top flange of the center girder (G3) for each cross section. Transducers were attached to the concrete with adhesively bonded metal tabs, as shown in Figure C.378. Transducers were connected to nodes by cables. Each node collected up to four channels of strain gage data and broadcasted the data wirelessly to a base station placed near the east bridge abutment. The base station projected a local wireless network to

transmit strain gage data to a computer running STS-LIVE software from BDI. Instrumentation of the bridge was completed on Aug 2, 2021, and bridge testing was completed on Aug 3, 2021. The sample rate was 1 kHz (0.001 seconds between samples), and the strain was zeroed at the beginning of each live load run.

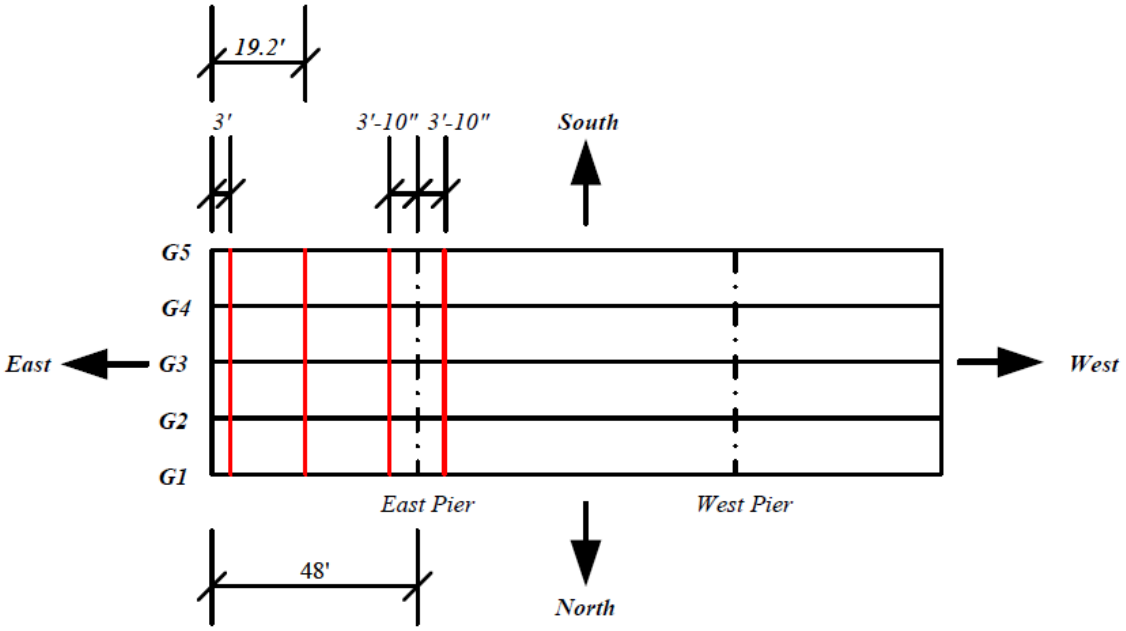

Figure C.376. Strain transducers installation locations in the bridge.

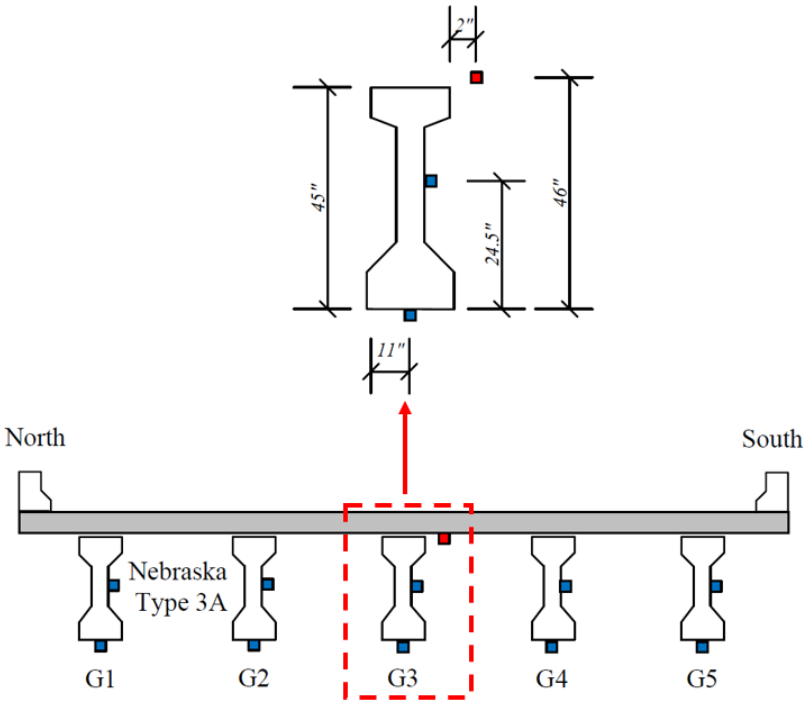

Figure C.377. Strain transducers installation locations in the bridge cross-section

Figure C.378. Strain transducer attached to the bottom flange of girder.

4 Load Cases

Two 3-axle trucks (Legal Type 3 vehicles) were provided by NDOT for bridge loading. The gross weights of truck A and truck B are 51.16 kips and 50.4 kips, respectively. Figure C.379 shows the truck A used in the load test. Figure C.380 shows the configuration for a Nebraska Legal Type 3 truck. Only total truck weight was supplied, not weight by axle or wheel, so each test truck axle load was assumed to be proportional to the Type 3 configuration. As shown in Figure C.380, the width of test trucks was assumed to be 6 ft.

Girder distribution factors were evaluated by driving trucks across the bridge at various transverse locations, as illustrated in Figure C.381. Single- and two-lane loaded cases were considered. The transverse location cases (single-lane and two-lanes loaded) are assumed to capture critical GDFs for the interior girders; however, two trucks side-by-side with the outermost truck positioned two ft away from the rail was not evaluated, which might result in critical GDFs for the exterior girders.

The following total six cases were considered:

- Case 1: North, 2 ft away from rail

- Case 2: Center
- Case 3: South, 2 ft away from rail
- Case 4: North lane (truck path 5 ft offset from bridge centerline)
- Case 5: South lane (truck path 5 ft offset from bridge centerline)
- Case 6: Side-by-side in painted lanes

As shown in Table C.1, a total of 32 load tests were performed. First, truck A was driven singly at the center of each lane from both east and west directions, at a crawling speed (5 mph). Then, truck B was driven from both directions at 10 mph at the center. The runs in the center of the lane were repeated at increasing speeds of 20, 40, and 60 mph. Truck A was driven in both the north and south lanes at different speeds. Truck A was also driven in both directions at crawling speeds two ft from the north and south rails. In side-by-side cases, truck A was in the north lane and truck B in the south lane. Figure C.382 shows the two trucks as they approach the bridge.

Figure C.379. Load test truck A.

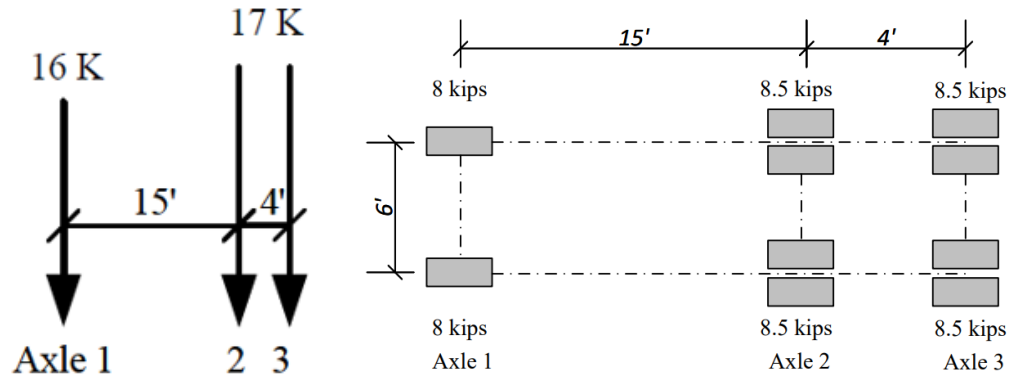

Figure C.380. NE Type 3 truck configuration.

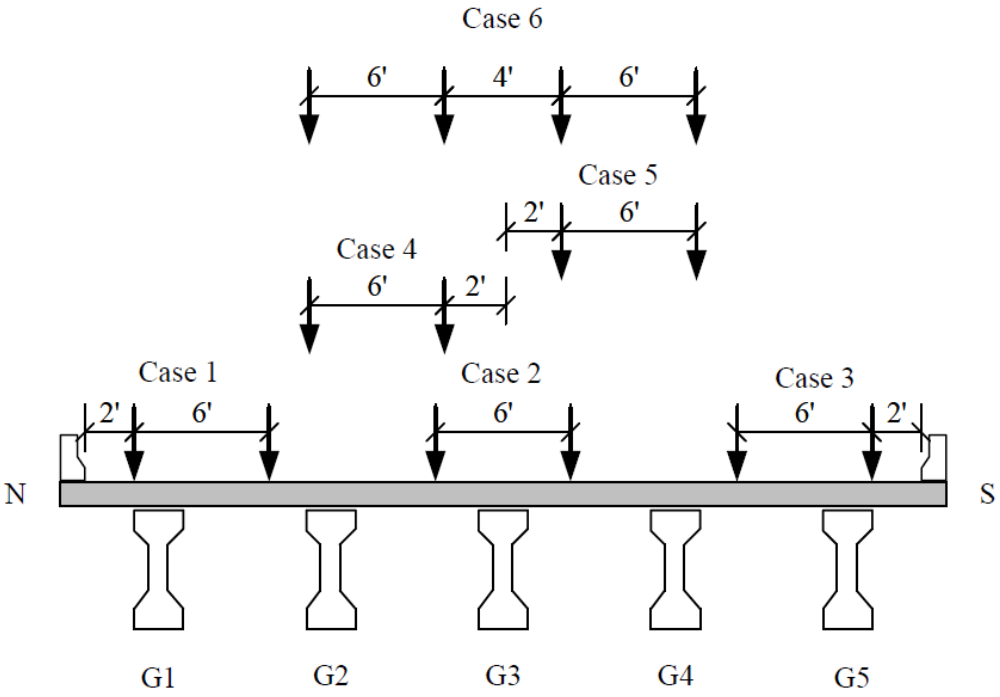

Figure C.381. Transverse locations of trucks on the bridge.

Figure C.382. Side-by-side truck load test.

Table C.1. Load test runs.

Run #	Truck	Direction	Lane	Speed (mph)
1	A	W	Center	5
2	A	E	Center	5
3	B	W	Center	10
4	B	E	Center	10
5	A	W	Center	20
6	A	E	Center	20
7	B	W	Center	40
8	B	E	Center	40
9	A	W	Center	61
10	A	E	Center	60
11	A	W	North	10
12	A	E	North	10
13	A	W	South	10
14	A	E	South	10
15	A	W	North	40
16	A	E	North	40
17	A	W	South	40
18	A	E	South	40
19	A	W	North	60
20	A	E	North	60
21	A	W	South	60
22	A	E	South	60
23	Dual side by side	W	A at North/ B at South	10
24	Dual side by side	E	A at North/ B at South	10
25	Dual side by side	W	A at North/ B at South	40
26	Dual side by side	E	A at North/ B at South	40
27	Dual side by side	W	A at North/ B at South	60
28	Dual side by side	E	A at North/ B at South	59
29	A	W	North 2 ft from Rail Edge	5
30	A	E	North 2 ft from Rail Edge	5
31	A	W	South 2 ft from Rail Edge	5
32	A	E	South 2 ft from Rail Edge	5

5 Finite Element Analysis

For this study, both two-dimensional (2D) and two-dimensional (3D) finite element methods (FEM) were applied to investigate structural behavior. Analyses were performed using SAP2000™, CSiBridge™,

AASHTOWare Bridge Rating™ (BrR), and COMSOL™ finite element programs. The following types of models were used:

Line-girder analysis:

- SAP2000 model with beam elements,

3D FEM analysis:

- 3D CSiBridge model with shell elements for slab and beam elements for girders,
- 3D AASHTOWare BrR model with shell elements for slab and beam elements for girders,
- 3D COMSOL model with solid elements for slab and girders.

Per information from bridge plans and correspondence with NDOT personnel, specified compressive strength of the concrete deck was taken as 4 ksi, and the NE Type 3A girders' specified compressive strength was taken as 6 ksi. AASHTO LRFD Equation (5.4.2.4-1) was used to estimate concrete moduli of elasticity. Detailed information about bridge dimensions is provided in Figure C.374 and Figure C.375.

In the following FEMs, the Type 3 truck (50 kips) was used, which is similar to the test trucks used in field tests. The input data included axle loads and axle spacings, as shown in Figure C.380. All analysis results correspond to static loading. The trucks' transverse positions were modeled in CSiBridge and COMSOL to match the actual tests, as shown in Figure C.381. AASHTOWare BrR automatically generated stepped truck paths across the bridge width, and therefore enveloped the load test paths. Critical longitudinal truck positions were determined to produce the maximum positive bending moment at 0.4L of end span and the maximum negative bending moment near the east pier. For this geometry, the maximum bending moment of end spans does not occur at 0.4L. However, the critical location is typically within 2 percent of the span length near 0.4L.

5.1 Line Girder Analysis, SAP2000

Based on a 2D numerical analysis in SAP2000, Figure C.383 shows the moment envelope for one Type 3 truck passing over the bridge from east to west. The bridge was modeled using beam elements. Boundary

conditions were assumed to be the same as shown in Figure C.374. The maximum positive moment critical location is approximately 0.42L of the end span. At 0.4L, the maximum positive moment is 364 kip-ft. The maximum positive moment at the middle span is approximately 373 kip-ft, about 2% larger than at 0.4L of the end spans. At 3 ft - 10 in. east of the east pier centerline, the negative moment is -220 kip-ft, larger than the negative moment west of the east pier centerline, -180 kip-ft.

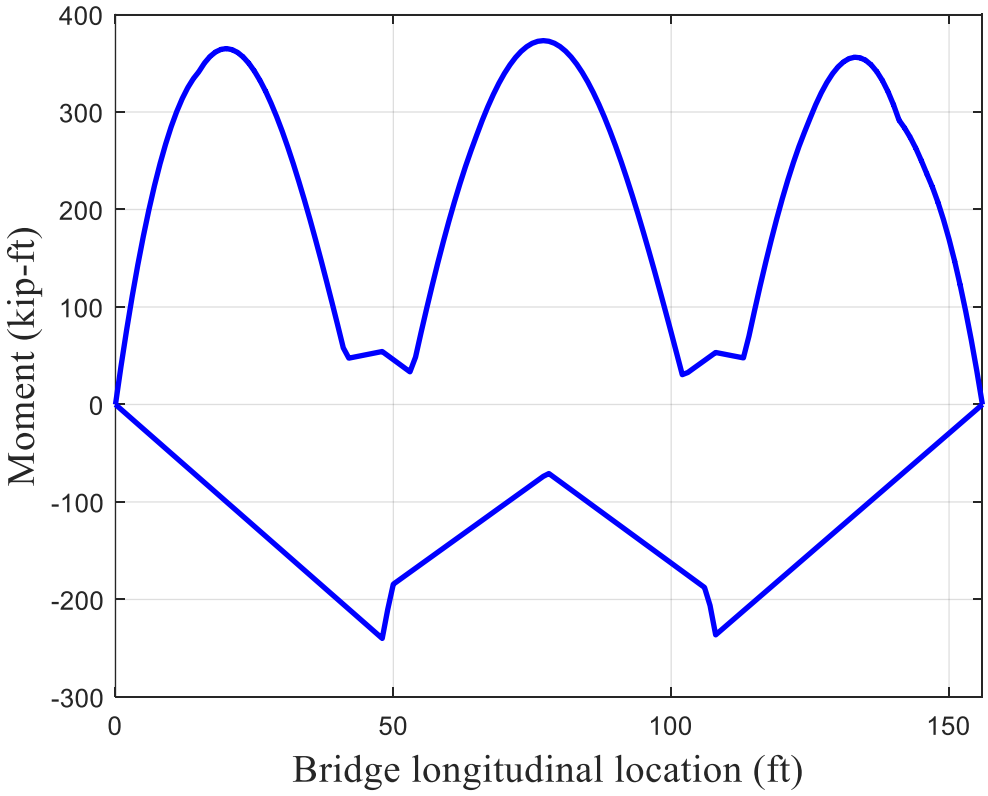

Figure C.383. Moment envelope of a type 3 truck on the bridge.

5.2 3D FEM Analysis, CSiBridge

Both the superstructure and substructure, including girders, pier caps, and piers were modeled in CSiBridge. Prestressed girders were modeled as beam elements. Four-node shell elements with three dimensions and six degrees of freedom were used to model the concrete slab. Link elements connected the girders and deck to simulate composite action. Girder connections to bearings were also modeled using link elements.

All translations were restrained at the east abutment and all rotational boundary conditions were modeled as free. All translations were fixed except the bridge longitudinal direction for the west abutment and piers, and all rotations were free. Strain gage data collected near abutments indicated that negative strains were absent or negligible, thus assuming free rotations of abutments is consistent with measured structural response.

Figure C.384 presents the coordinate system and the model mesh, which was discretized at a 1 ft increment in both the super- and substructure. The substructure was modeled as a series of rectangular columns to represent the concrete wall at the piers. Material properties were assigned as described previously. The CSiBridge model was used to explore the influence of intermediate diaphragms on GDFs by configuring separate models including and excluding diaphragms at midspan locations. The connections between the girders and the piers were Configured so that the superstructure maintained continuity but rotated independently of the substructure. The piers therefore provided only vertical restraint to the superstructure.

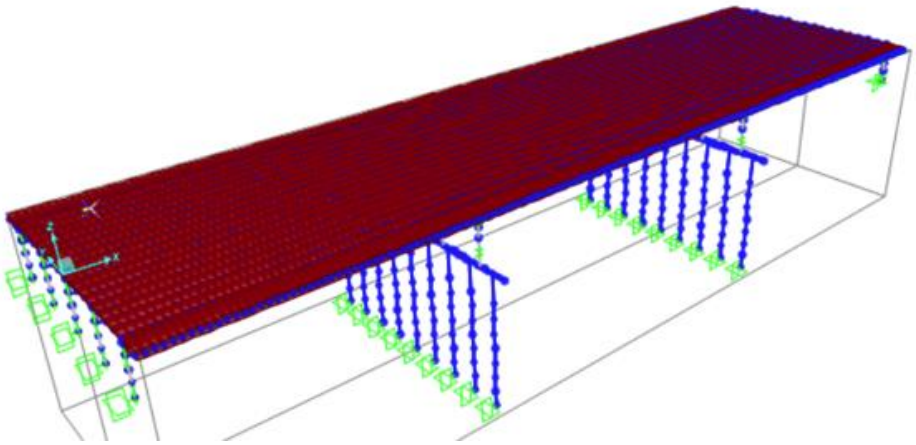

Figure C.384. CSiBridge 3D numerical model.

Legal Type 3 wheel loads were modeled as point loads (two points loaded per axle). Based on preliminary analysis, CSiBridge used a live load path analysis to determine the maximum moments, which produced similar results to statically placing trucks at the critical location. The bridge moment envelope is shown in Figure C.385, plotted together with the envelope shown previously from SAP2000 in Figure C.383. The envelope shown is for the model without diaphragms, which is believed to more closely represent the actual

behavior of the bridge, with diaphragms interacting with girders only through compression bearing in the bridge drawings.

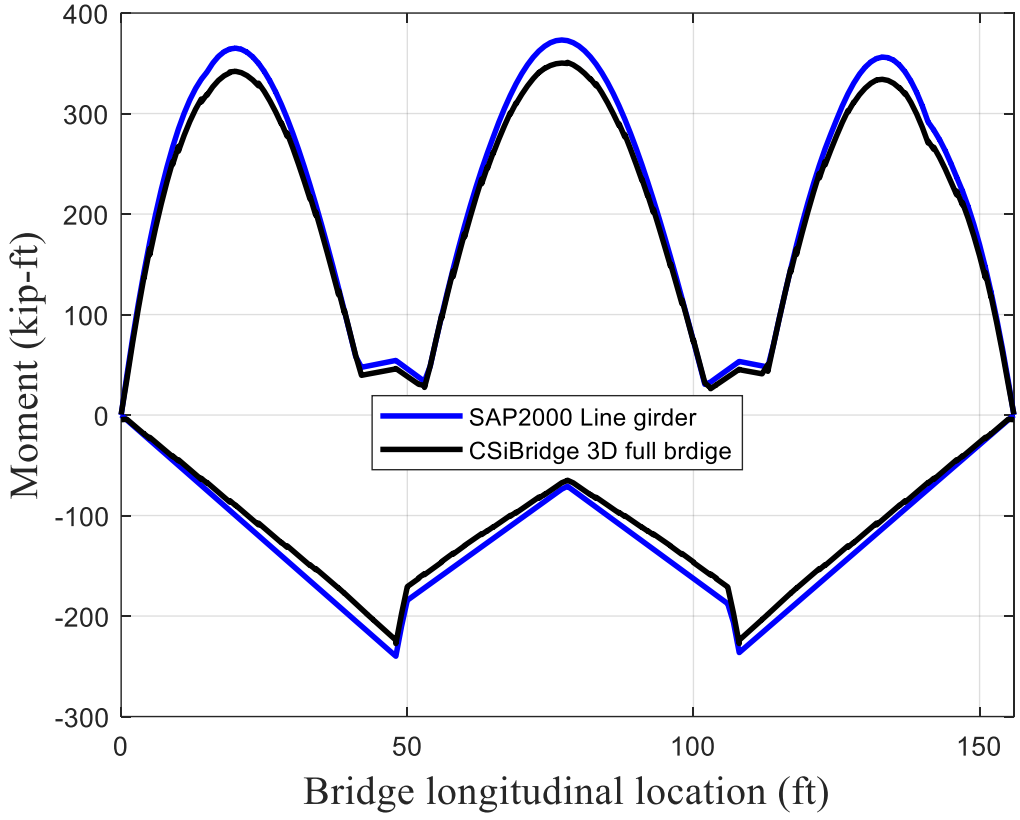

Figure C.385. CSiBridge and SAP2000 full-bridge moment envelopes for a legal type 3 truck from east to west.

5.3 3D FEM Analysis, AASHTOWare BrR

AASHTOWare BrR was also used to perform 3D FEM analysis. Figure C.374 and Figure C.375 show the dimensions of the bridge used in the model. Note – the barriers were not included in the structural model. The concrete deck and prestressed girder compressive strengths and moduli of elasticity were the same as in CSiBridge model. Also similar to CSiBridge, girders were modeled using beam elements, and the concrete deck as modeled using shell elements. As shown in Figure C.386, the intermediate diaphragms were not included. Figure C.387 shows an isometric view of the finite element model. AASHTOWare BrR automatically generated stepped truck paths to provide critical load effects for girders instead of providing full-bridge load effects. In order to compare the results between the different software packages, an exterior

girder was used. For SAP2000 (1D line girder), the lever rule GDF was used. The truck position is 2 ft from the rail in CSiBridge and AASHTO BrR 3D. Figure C.388 shows the exterior girder result of the SAP2000 model is more conservative than the two other 3D models. The differences between CSiBridge and AASHTO BrR 3D models are not significant.

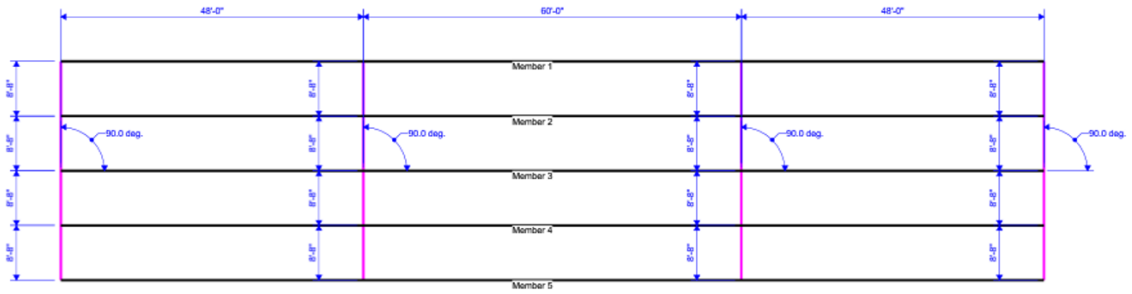

Figure C.386. NOBL North bridge BrR model plan view.

Figure C.387. NOBL North stage 2 (and 3) FEM.

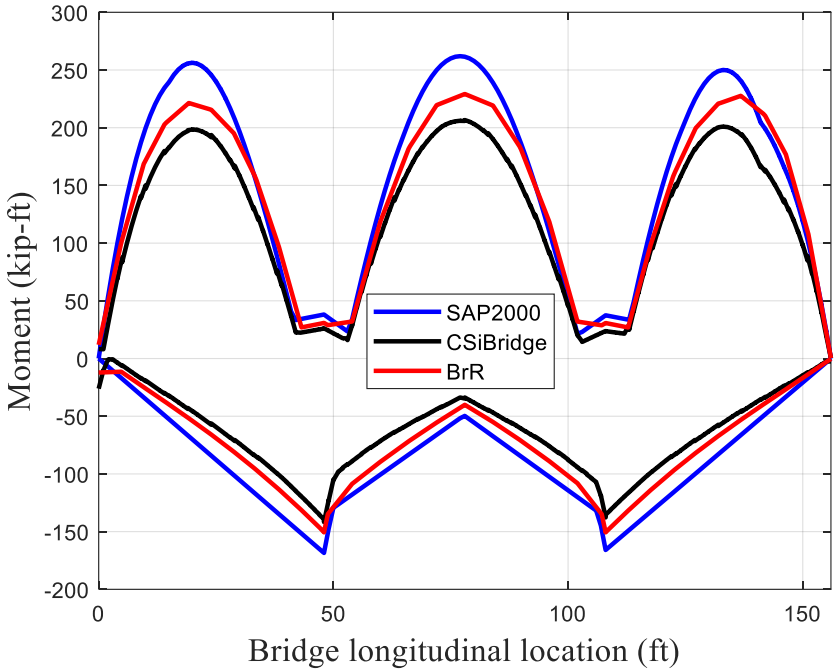

Figure C.388. BrR exterior girder moment diagram for one type 3 truck from east to west.

5.4 3D FEM Analysis, COMSOL

COMSOL was used to model the bridge deck, diaphragm, barrier, and girders with solid elements meshed with several approaches including tetrahedrals and quadrilaterals with various densities ranging from 500,000 to 1,000,000 total degrees of freedom for the entire model. Truck tire load patches were statically positioned to produce critical positive moment in the end span at 0.4L. For the interior load placements, the results from COMSOL with and without barriers are similar to corresponding cases in CSiBridge . Figure C.389 displays a 3D view of the barrier, deck, and girder elements for the FEM in COMSOL.

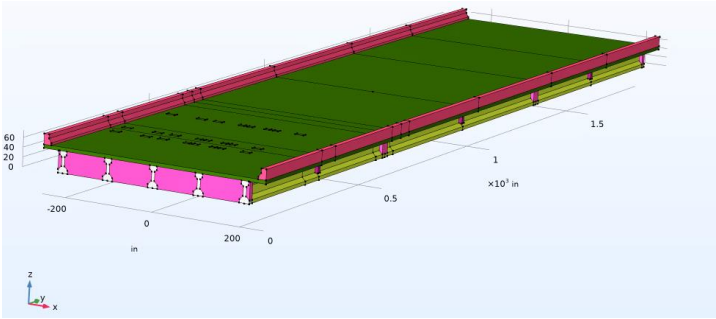

Figure C.389. COMSOL bridge solid model.

6 Load Test and FEM Results

CSiBridge results were used for comparisons to the test results. To compare the test results with FEM analysis, the FEM values were taken at the locations where strain transducers were installed. The live load strains plotted against time were also evaluated for reasonableness. Additionally, the influence line of 3 ft-10 inches east and west of the pier and 0.4L of the end span were plotted to aid in evaluating the load test results. Note, the maximum positive moment ordinates at 0.4L are approximately double those for negative moments near the east pier, based on the influence line values shown in Figure C.390. The analysis and test data are expected to follow this trend.

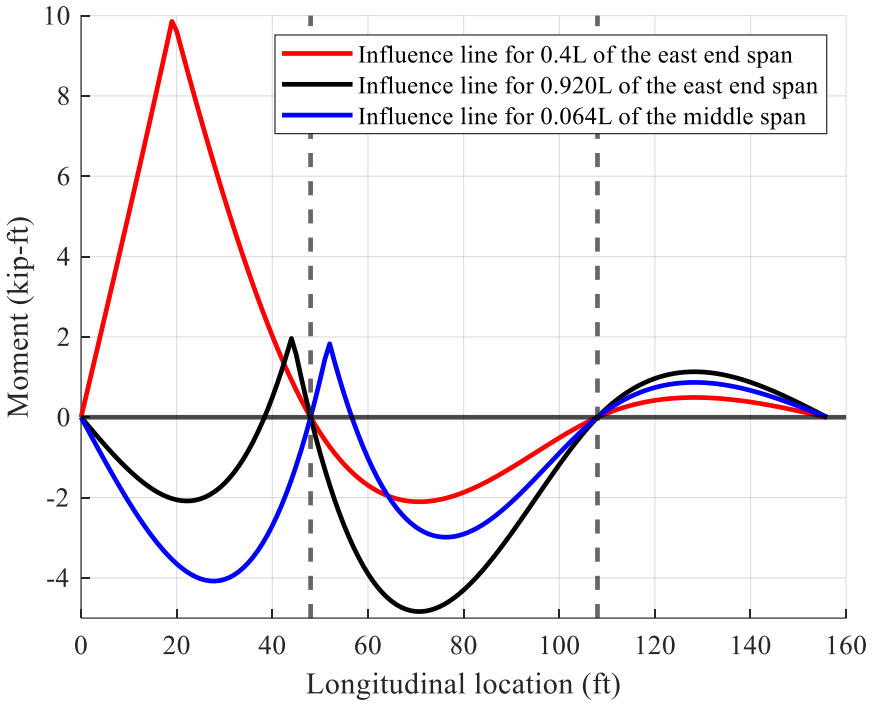

Figure C.390. Influence lines near the pier and the 0.4L of end span.

6.1 Load Test Strain Plotted with Time

Transducers located at 0.4L of the east end span measured the positive moment response and were used to quantify GDFs. Figure C.391 shows the truck position to produce maximum longitudinal live load strain when the truck's forward rear axle is about 0.4L of the end span.

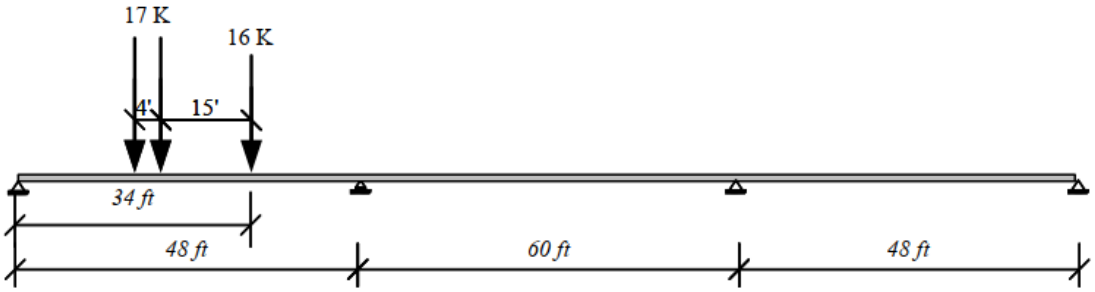

Figure C.391. Critical truck position for 0.4L of the end span.

As truck A crawls at 5 mph from east to west at the center, Figure C.392 shows the measured values for the transducers at 0.4L of the end span. Time (seconds) is shown on the x-axis, and microstrain ($\mu\varepsilon$) is shown on the y-axis. Strains were zeroed at the beginning of each run; the following figures only include windows of time with significant strain values (when live load was on the bridge). As expected for Run 1, peak strains occurred on the bridge's middle girder (G3). At the bottom of G3, the maximum strain value is about +32 $\mu\varepsilon$. Because of the intended transverse symmetrical load position, the strains for G2 and G4 should be similar. However, G4 has greater strains than G2 presumably due to a slightly off-center transverse truck positioning.

Unexpectedly, the test strains at G2 are similar at the bottom flange and the web, implying axial rather than flexural deformation. This results does not seem reasonable, yet the recorded strains are nonzero and outside the noise band, suggesting that the data is real and not spurious noise. This abnormality may reflect torsional influences on the girder cross-section strains that could have obfuscated the primary flexural response. In situations where loads travel along the center of the bridge width, exterior girders G1 and G5, as expected, carried a lesser load. The critical truck location in Figure C.391 was assumed to occur at 15 seconds as shown in Figure C.392, due to the lack of axle load longitudinal position information.

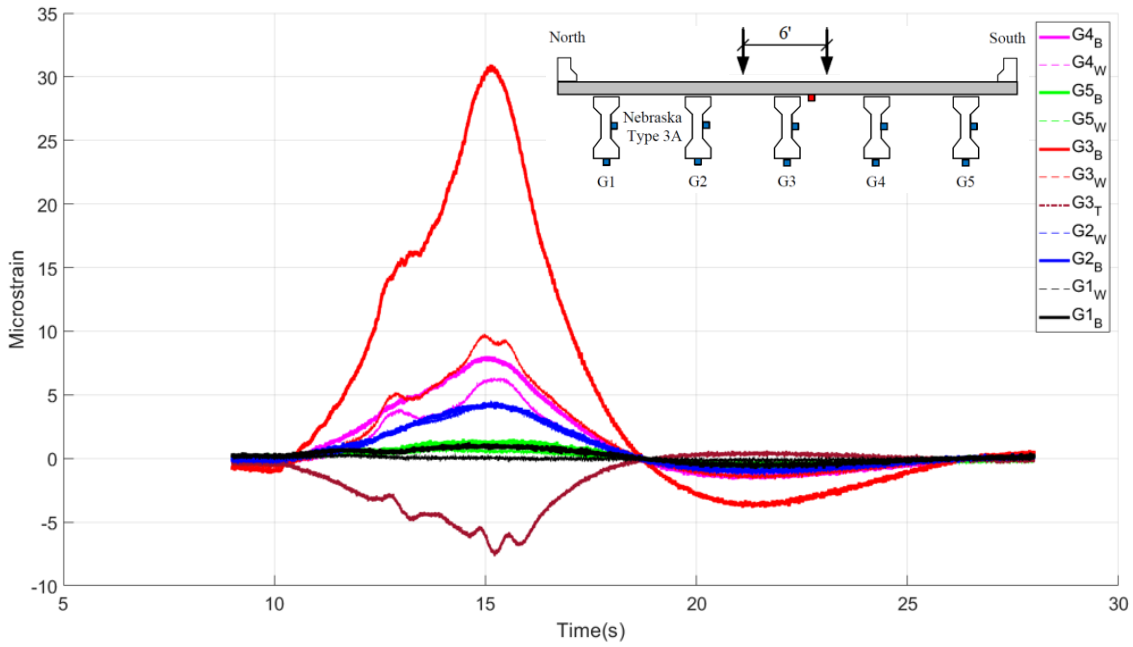

Figure C.392. Strain transducer results at 0.4L end span for one truck A at the center from east to west.

The transducers located at 3 ft–10 in. east of the pier were used to measure the negative moment response and calculate GDFs. The maximum longitudinal live load strain occurs with the truck located in the middle span, where the front axle load is 84 ft from the east abutment, as shown in Figure C.393.

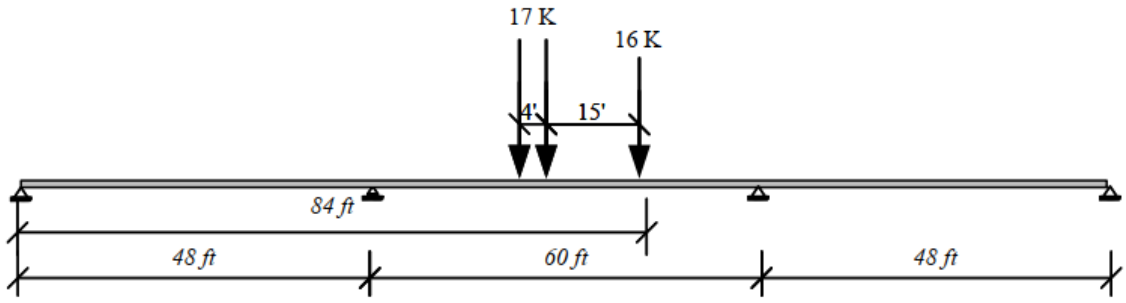

Figure C.393. Critical truck position at 3 ft-10 in. east side of the pier.

In Figure C.394, the strains are displayed for the transducers at 3 ft-10 in. east of the pier when truck A crawls (5 mph) along the bridge centerline from east to west. As expected, peak strains occurred in the middle girder (G3). The largest compressive strain at the bottom of G3 is about -16 $\mu\varepsilon$. Girder G3's bottom strains can be explained by the influence line in Figure C.390. The strain peaks at the end span, just when

the rear axles are near the peak of the influence line, and then decreases when the truck enters the middle span. As expected, the bottom of the G3 strain peaks around 21 secs when the truck is positioned in the middle span. There are three spikes recorded at the deck near G3, which may result from localized effects due to wheel passage. To capture this effect, COMSOL was used to analyze one truck at the center lane close to supports. The wheel patch loads were assumed to be 10 in x 20 in. As illustrated in Figure C.395, the typical bottom surface longitudinal deck stress at bridge cross-sections near midspan was on the order of -20 psi (negative indicating compression), and 130 psi (positive indicating tension) directly below the wheels. Taking a deck as a transverse beam, this local behavior in the middle of the span is much smaller because the girders are significantly more flexible than near the supports, as illustrated in Figure C.392.

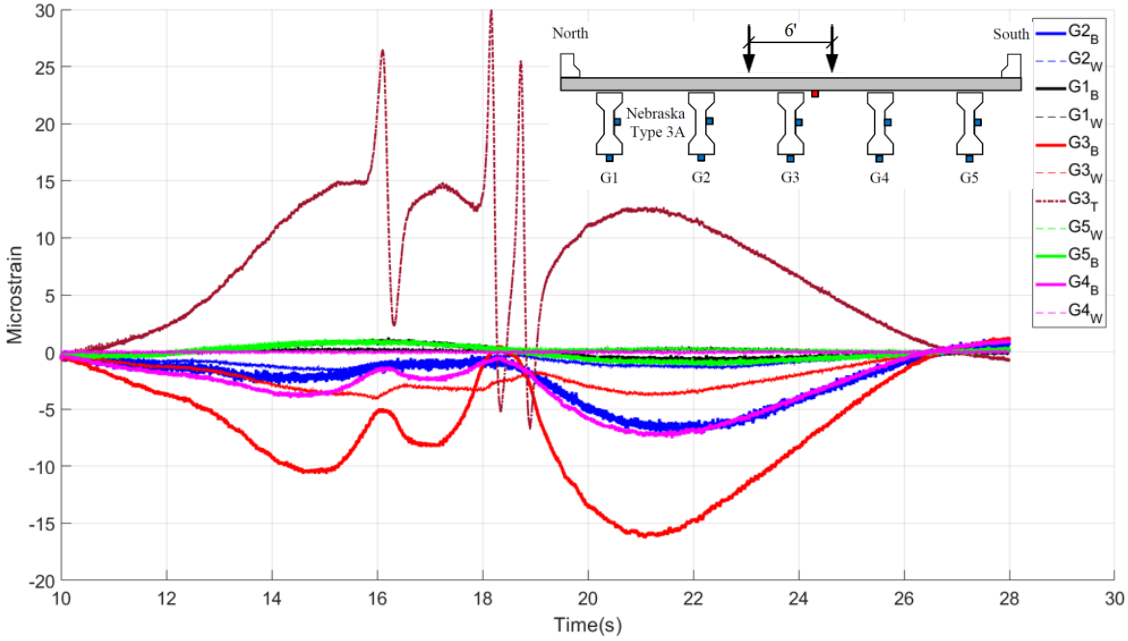

Figure C.394. Strain transducers results at east side of the pier for one truck A at the center from east to west.

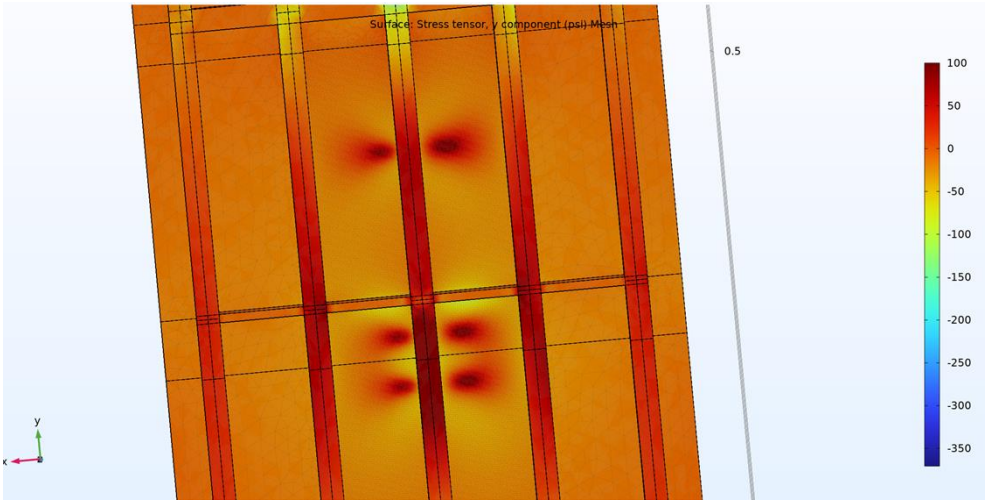

Figure C.395. COMSOL stress diagram for one truck at the center near the pier.

Longitudinal strain transducers located at 3 ft–10 in. on the west side of the pier measured the negative moment response and were used to compute GDFs. The maximum longitudinal live load strain occurs with the truck located on the end span when the leading axle load is 38 ft from the east abutment, as shown in Figure C.396.

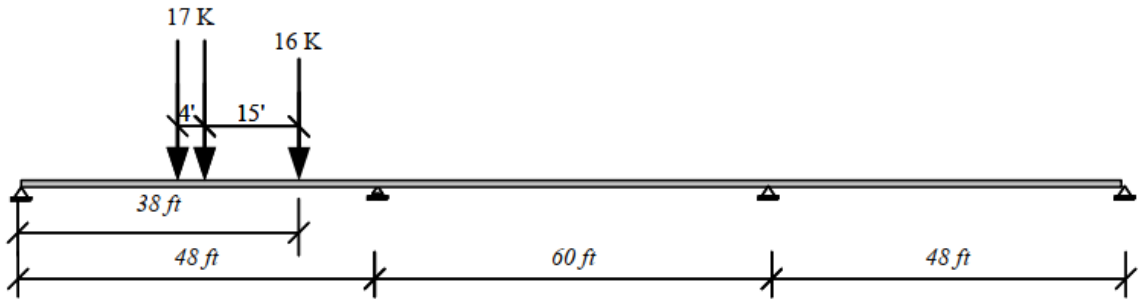

Figure C.396. Critical truck position at 3 ft-10 in. west side of the pier.

Strains are shown in Figure C.397 for the west side of the pier when truck A moves at 20 mph from east to west. Figure C.397 shows some dynamic oscillations that were absent in tests conducted with lower truck speeds, but the magnitude of oscillations relative to the moving average was minor. As expected, the peak strain occurred in the bridge's middle girder (G3). The largest compressive strain at the bottom of G3 is -

13 $\mu\varepsilon$. Figure C.394 and Figure C.397 show that the maximum strain values at the east and west of the pier are close, providing a degree of confidence in the test results.

Influence line analysis and the resulting load position shown in Figure C.396 predicted peak response would occur when the load was positioned in the end span, but test results indicated peak response with load in center span. The disagreement may reflect incongruity between the assumed continuity condition – with the continuous superstructure rotationally decoupled from and bearing at only a single line on the substructure – versus the reality of separated girder bearing lines as-built. In the following strain and GDF plots, only the east side of the pier is considered because it has a slightly greater result than the west side.

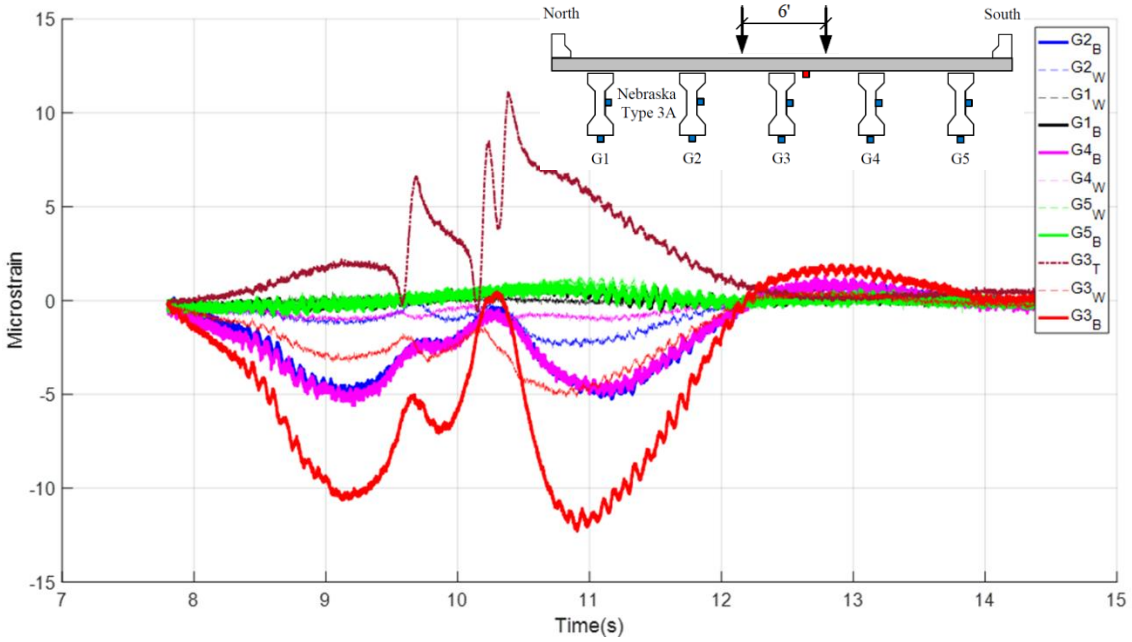

Figure C.397. Strain transducers results at west side of the pier for one truck A at the center from east to west.

6.2 Test and FEM Strain and GDF Results

GDFs were determined using strain data measured at the bottom of the girders. The section modulus of exterior girders is slightly higher than that of interior girders due to the stiffening effect of curbs and barrier walls. This project used the same GDF model as Stallings and Yoo (1993), which uses weighted strains to incorporate the different section moduli of the girders. Stallings and Yoo noted that the AASHTO LRFD GDFs characterize load on a per-lane basis, with different mathematical functions to represent single-

versus multi-lane loading. To make comparisons with AASHTO LRFD GDFs, the GDF model has been modified with the number of lanes loaded term, N_L as follows:

$$GDF_i = N_L \frac{M_i}{\sum_{j=1}^{k} M_j} = N_L \frac{ES_i\varepsilon_i}{\sum_{j=1}^{k} ES_j\varepsilon_j} = N_L \frac{E\frac{S_i}{S_l}\varepsilon_i}{\sum_{j=1}^{k} E\frac{S_i}{S_l}\varepsilon_j} = N_L \frac{\varepsilon_i W_i}{\sum_{j=1}^{k} \varepsilon_j W_j} \quad \text{(Eqn.1)}$$

where:

N_L = number of lanes loaded,

M_i = bending moment at the i th girder,

E = modulus of elasticity,

S_i = section modulus of the ith girder,

S_l = typical interior section the modulus,

ε_i = maximum bottom-flange static strain at the ith girder,

W_i = ratio of the section modulus of the ith girder to that of a typical interior girder, and

k = number of girders.

To evaluate barrier effects on GDFs, GDFs were evaluated with the additional stiffness contribution to the exterior girders from the barriers assuming no slip at the deck-to-barrier interface, but the results were not significantly different in comparison to GDFs ignoring barrier stiffness. As a result, the W_i was assumed to be one for both interior and exterior girders, which slightly overestimated interior girder GDFs and underestimated exterior girder GDFs.

The following load test GDFs are based on single or two trucks crawling at 5 mph or 10 mph for various transverse locations. FEM GDFs were derived from CSiBridge models both with and without diaphragms. Under crawling-speed tests, Figure C.398 and Figure C.399 show the bottom girder strains at 0.4L of the end span and corresponding GDFs for one truck A traveling from east to west . Results are presented for truck A passing over the bridge at the center, and 2 ft from the north and south barrier railings. Strains are measured for each loading condition, and GDFs are derived from the strain measurements. For comparison, specified GDFs according to AASHTO Standard Specifications (2002) “S-over” method and AASHTO

LRFD (2020) for single- and multi-lane loading on girder bridges were calculated. For the AASHTO GDFs, the K_g value was calculated using as-built drawings, the multiple presence factor (MPF) was removed for single-lane loaded interior GDFs, and the lever rule (not including the MPF) was used to calculate the GDFs for the single-lane exterior girders. Figure C.398 shows that, as expected, the maximum strain occurred at G3 for center lane cases and exterior girders (G1 or G5) for trucks passing adjacent to barriers. However, there are some noticeable differences between strains from load tests and FEMs. With single-lane loading at the center, the maximum positive strain at G3 is about +31 $\mu\varepsilon$, close to the FEM at G3 for the model without diaphragms . However, other girders exhibit lower load test strain results than FEM.

The bottom flange load test strain sum is about half that of FEM, as shown in Figure C.398. There are several possible reasons for the lower strains observed in load tests than in FEMs. According to Nowak (2003), one possible reason for lower strain from tests compared to FEM is the presence and appropriate stiffness influence of partial fixity conditions at supports. Concrete decks and girders may have a higher modulus of elasticity than the AASHTO equation indicates, which would result in lower measured strains and apparent underestimation of total load effects. Due to the barrier effect, the section modulus for exterior girders is slightly higher than the interior section modulus. As expected, a truck positioned close to the barrier tends to cause higher exterior girder strain values. GDF distributions across the bridge cross-section for trucks 2 ft near north and south barriers trend reasonably and symmetrically according to load positions. However, when one truck travels along the bridge centerline, the G3 GDF is unexpectedly higher than both the AASHTO single-lane interior GDF and the AASHTO Standard GDF. The sum of strains for a truck near the rails is also approximately half that from FEMs.

Figure C.399 shows that the load test GDFs at this location are more similar to the results of the FEM without diaphragms, which indicates that the diaphragms are not acting with transverse flexural continuity through the girders. On close inspection of the bridge drawings, the diaphgragms are found to only interact with the girders through compression bearing. Reinforcing at the top of the diaphragms ties the diaphgrams to the deck, but no reinforcing crosses the interfaces of diphragms and girder flanges or webs. Therefore, complex torsional effects and compression-only contact interactions may also be influencing both flange

and web strains that are currently unaccounted for in the 3D FEM models, which represent the girders only as beam elements with rigid links to deck shells and therefore little induced torsional response.

Figure C.400 and Figure C.401 show negative strain and GDFs at the east of the pier for one truck A passing from east to west at crawling speed. G3's maximum negative strain is -16 $\mu\varepsilon$, which is lower than the results of the FEMs, as shown in Figure C.400. Also, the sum of strains from the bottom flange load tests is about half that of strains from FEMs. As noted previously, a partial fixity condition at bridge supports as constructed, a higher modulus of elasticity than calculated, and barrier and complex torsional effects may all play a role in the lower test strains. Negative strains near the pier agree better with the FEM without diaphragms than positive strains at 0.4L end span. The slight asymmetry between G1 at north rail 2 ft loading and G5 at south rail 2 ft loading may be caused by the transverse location for the truck on the bridge not being precisely symmetrical. The AASHTO LRFD GDFs for the negative moment region here were determined by the average span length ((Span1+Span2)/2). For single-lane loading cases, the measured GDFs for exterior girders do not exceed code-specified values, while the GDFs for interior girder G3 is close to the GDF for AASHTO single lane loading.

Furthermore, the superposition of the strain data for single trucks was compared to the results of two trucks side-by-side in order to verify the linear-elastic behavior of the bridge. Under crawling-speed tests, Figure C.402 and Figure C.403 show the bottom girder strains and GDFs for one or two trucks traveling from east to west at the 0.4L end span of the bridge. Plots were drawn for the north and south lanes, and for lanes loaded side by side. The side-by-side load tests were performed with truck A loaded at north and truck B loaded at south. The strains due to a single truck occupying north and south lanes produce nearly the same results as strains due to two trucks side-by-side at the center as shown in Figure C.402 and Figure C.403.

For a two-lane loaded case, the sum of bottom girder strains is also about half of the sum of strains from FEMs. Three possible reasons for the lower test strains could be partial fixity in the actual bridge, a higher modulus of elasticity than calculated, and barrier effects. Figure C.403 shows that the trend of GDFs generally agrees with that of the FEM without diaphragms.

In theory, the strain of G2 at the north lane loading should be close to that of G4 at the south lane loading, but in the load tests, truck A may be closer to the center than truck B. The measured interior GDF in all of the considered single lane loading cases are less than or close to AASHTO LRFD single lane loaded GDF. Load test GDFs for exterior girders are smaller than AASHTO lever rule GDFs. The load test GDF at G3 for two trucks loaded at the center is unexpectedly higher than AASHTO interior GDF and AASHTO Standard interior GDF, indicating that diaphragms may not have the continuity assumed.

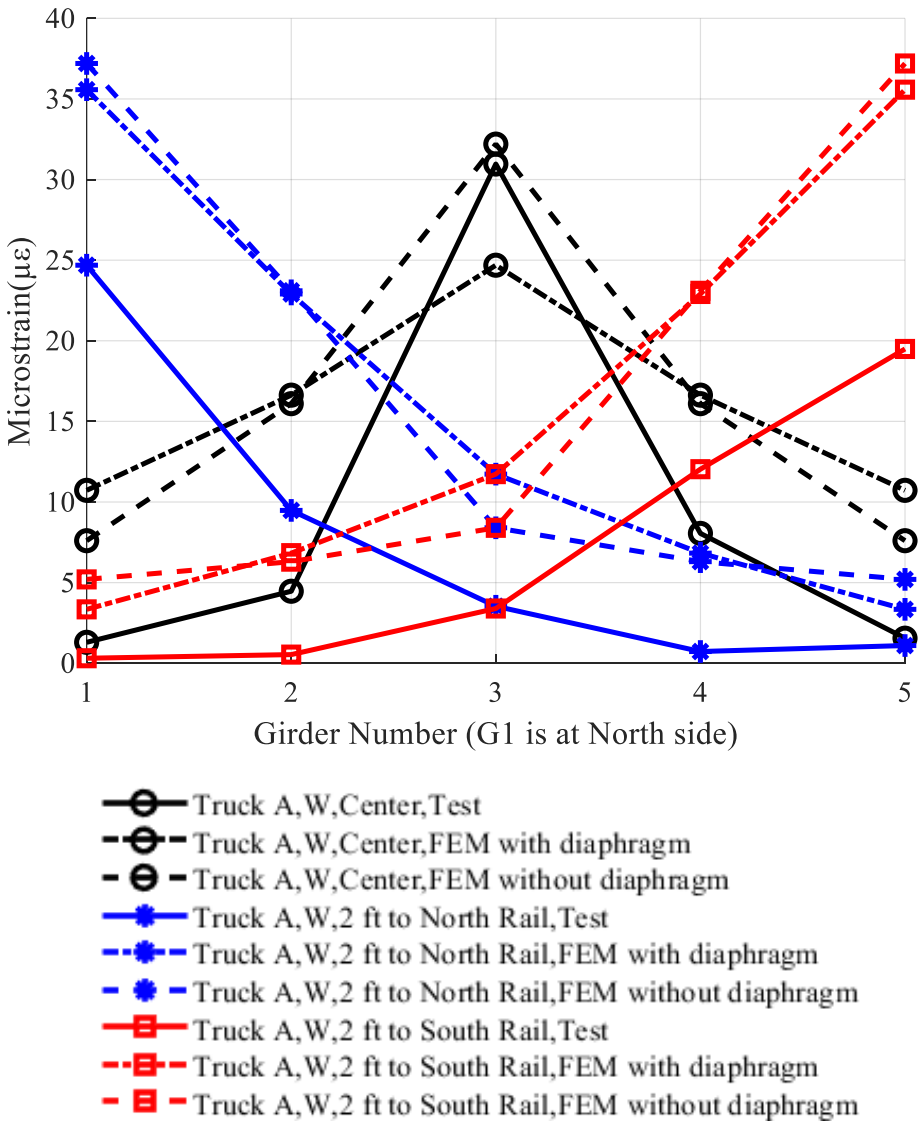

Figure C.398. Positive strain at 0.4 L of east end span, west direction loading

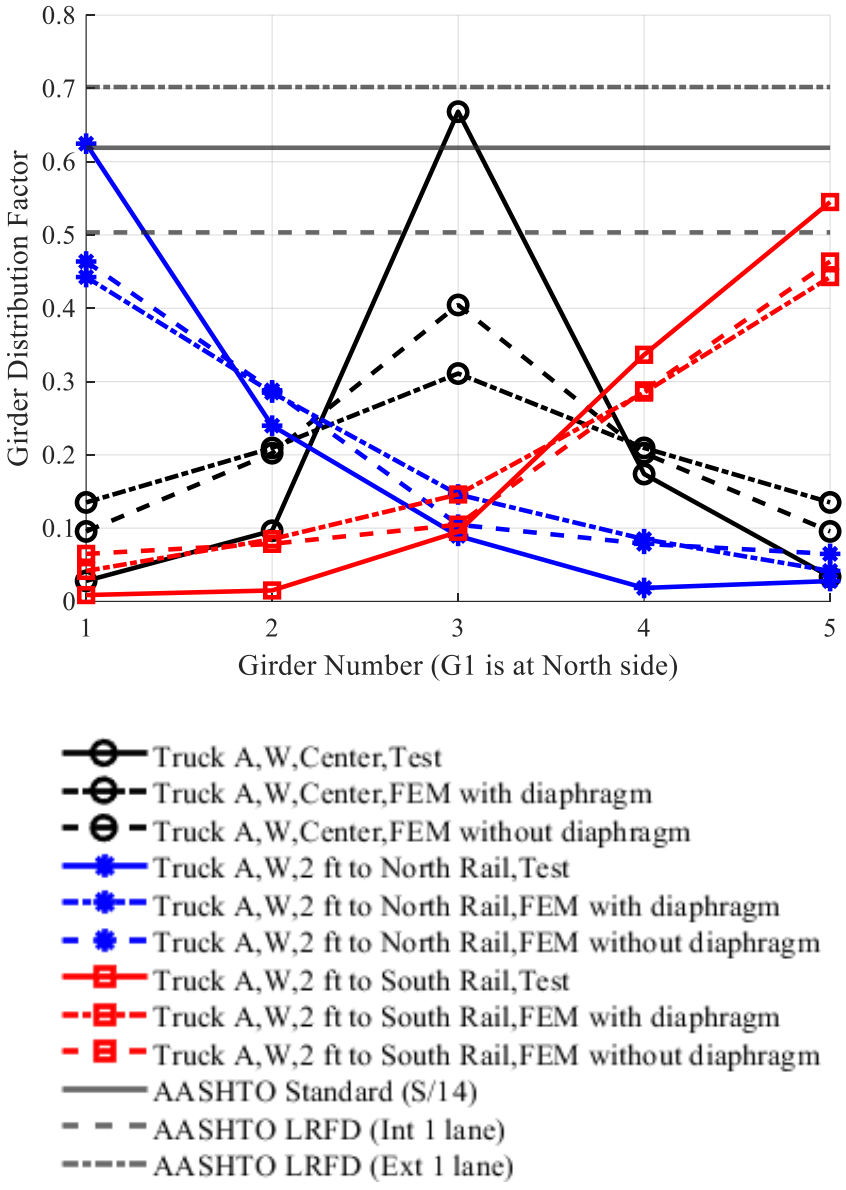

Figure C.399. GDF from positive strain at 0.4 L of east end span, west direction loading.

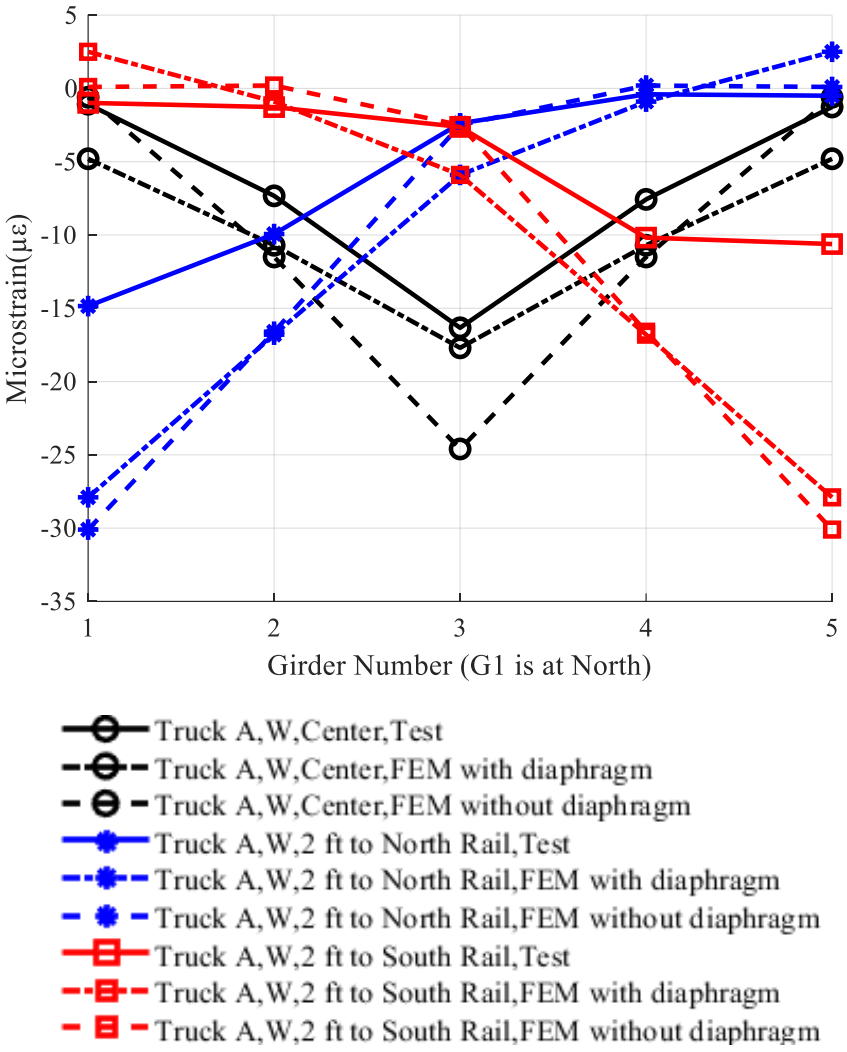

Figure C.400. Negative strain near east side of pier, west direction loading.

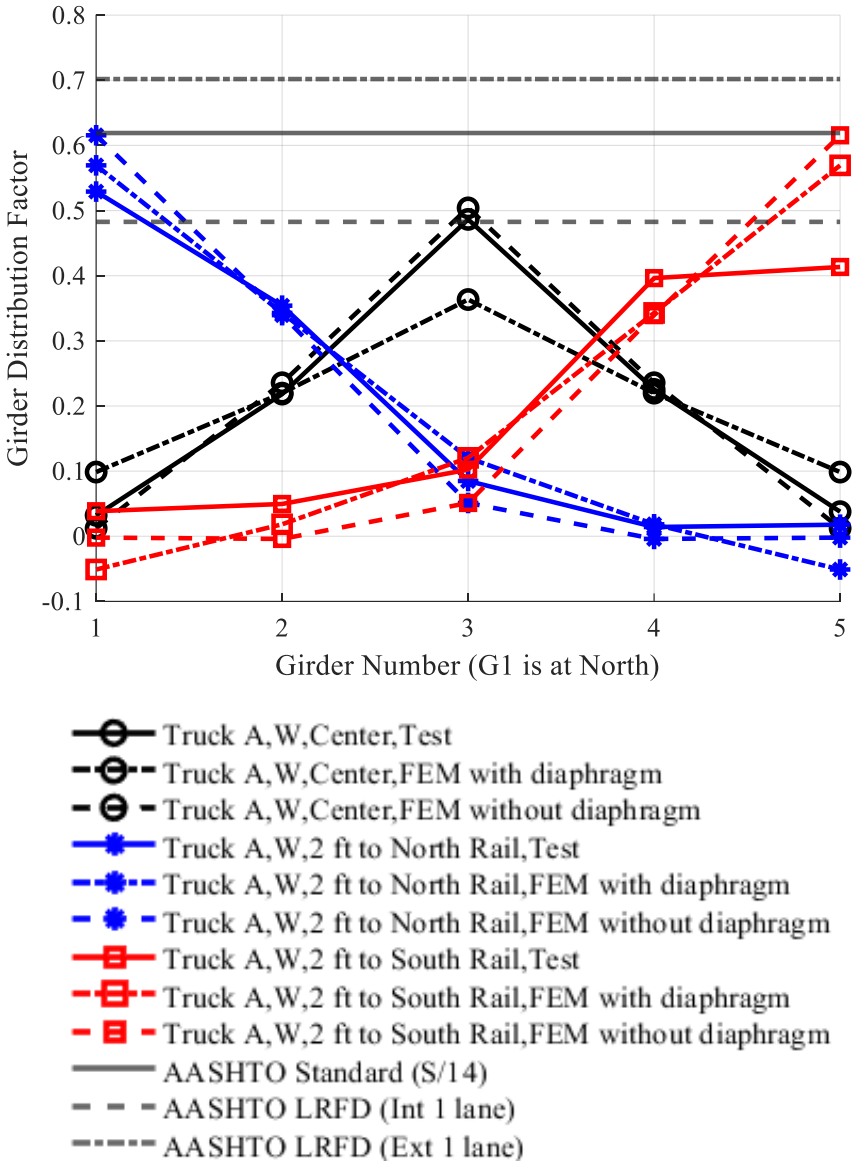

Figure C.401. GDF from negative strain near east side of pier, west direction loading.

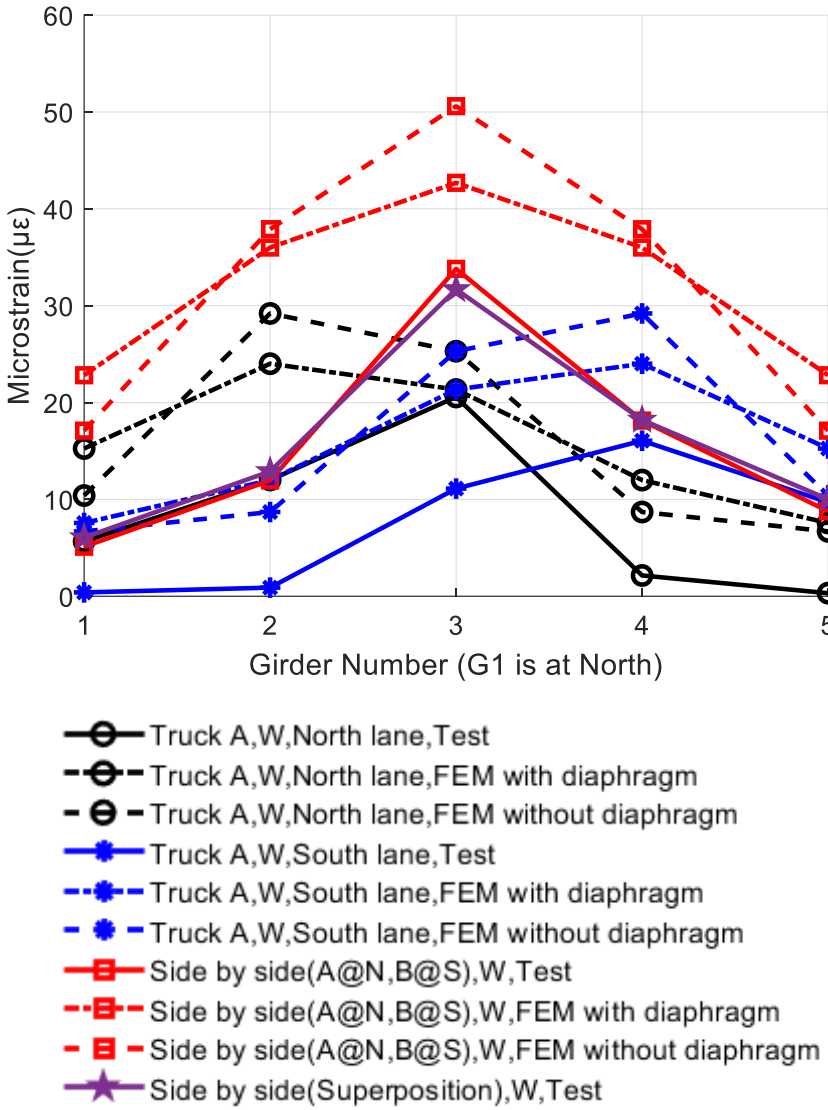

Figure C.402. Positive strain at 0.4 L of east end span, side-by-side loading, west direction loading.

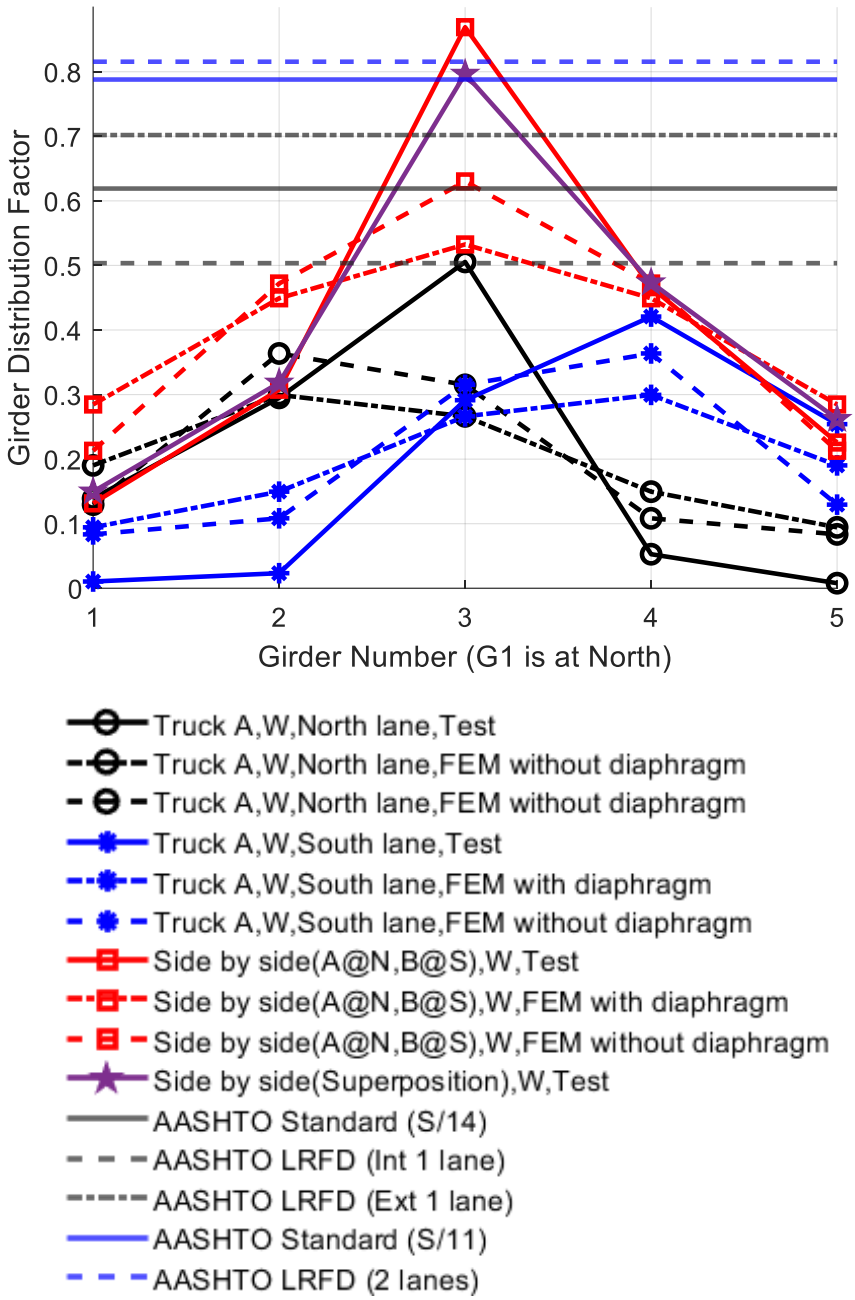

Figure C.403. GDF from positive strain at 0.4 L of east end span, side-by-side loading, west direction loading.

6.3 Dynamic Load Allowance Results

As a result of this study, the dynamic load factor (DLF) was calculated as the ratio between the maximum dynamic strain and the maximum crawling speed (static) strain at the bottom of girders as follows:

$$DLF = \frac{\varepsilon_{dyn}}{\varepsilon_{stat}} \qquad \text{(Eqn.2)}$$

where ε_{dyn} = maximum dynamic strain under the vehicle traveling at normal speed; and ε_{stat} = maximum static strain from crawling speed. DLFs were determined based on the most significant static strains at the 0.4L end span location of the G3 bottom girder. DLFs were calculated using strains from truck A and truck B from crawling speeds to up to 61 mph and by assuming truck A and truck B are practically identical. In Table 2, the DLFs are small for all cases and subject to possible errors. Also, DLFs decrease with increasing speed. The maximum IM obtained from all data sets is 0.3% (Girder 3, 10 mph), which is much smaller than the value (33%) recommended by AASHTO LRFD (2020). The tabulated DLF results should be considered preliminary, and not reliable in an absolute sense. The results are only provided to convey approximate supporting data indicating that dynamic amplifications were negligible.

Table C.2. Load Test Runs for Calculating DLFs.

Run #	Truck	Direction	Lane	Speed (mph)	Microstrain (με)	DLF (%)
1	A	W	Center	5	30.96	NA
3	B	W	Center	10	31.04	0.3%
5	A	W	Center	20	30.46	-1.6%
7	B	W	Center	40	30.50	-1.5%
9	A	W	Center	61	30.24	-2.3%

6.4 Neutral Axis Location

Under normal operating conditions, the bridge response should not exceed elastic response levels. G3 strains measured under loading from one truck A at a crawl speed from east to west were used to determine whether the bridge behaves as composite or non-composite. Transducers were placed on the bottom flange of G3 at 0.4L of the end span, as shown in Figure C.376 and Figure C.377. Using the distance between the web and bottom flange transducers (24.5 in.), the neutral axis of the beam can be calculated as follows:

$$Curvature = \frac{\varepsilon_{bot} - \varepsilon_{web}}{24.5"} \quad \text{(Eqn.3)}$$

$$NA = \frac{\varepsilon_{bot}}{Curvature} \quad \text{(Eqn.4)}$$

where ε_{bot} is the maximum strain at the bottom of the girder, ε_{web} is the maximum static strain at the web, and NA is the neutral axis location relative to the bottom of the girder. Based on the above equations, the neutral axis is 36.22 in. In a preliminary analysis, it was estimated that the location of the composite neutral

axis would be 37.39 in. A difference of about 3% between the theoretical and calculated neutral axis indicates that the G3 behaves as a composite girder with the deck, consistent with the assumptions routinely employed in this study.

7 Summary and Conclusions

This study aimed to develop computational models representing the Nebraska Outdoor Bridge Lab North Omaha bridge (S036 02040L) and collect physical data to validate the FEM models. The models and load test data can be used by other researchers using the NOBL North bridge. The load test was limited to an out-of-service 42-year-old simple-made-continuous three-span prestressed I-girder bridge located on state route 36 over the Glenn Cunningham Reservoir north of Omaha, Nebraska. During the field load tests, one-lane and two-lane loaded cases were taken into account to calculate the GDFs and DLFs and provide insight into the bridge behavior. NE Legal Type 3 trucks were used for the tests, and different locations, crawling speeds, and normal truck speeds were considered.

CSiBrdge, SAP2000, COMSOL, and AASHTOWare BrR were used to develop 2D line girder analysis and 3D FEMs. Shell, beam, and solid elements were used in the FEMs. CSiBridge models without barriers and with or without diaphragms were compared with load test results to determine if the model represents actual bridge behavior. Load tests and FEM analyses were also used to compare GDFs with AASHTO Standard (2002) and AASHTO LRFD (2020). Below are several takeaways from the study:

- The measured GDFs are generally close to those obtained from FEM analysis, but with some exceptions: For one truck or two trucks side-by-side in the center lane, GDF at G3 is higher than AASHTO interior GDFs (accounting for MPF).
- Load test GDFs for exterior girders are smaller than AASHTO lever rule GDFs.
- For 0.4L of the end span, load test GDFs are more similar to computational results without diaphragms assumed continuous through girders.
- The sum of bottom girder load test strains is about half of the sum from FEM (potentially influenced by barrier participation, underestimated modulus of elasticity, partial fixity of supports in the natural bridge, and perturbation of measured strains by torsional effects).

- Load tests observed localized behavior near piers at the bottom of the concrete deck inconsistent with beam theory, likely a result of concentrated wheel loads near instrument locations.

The results indicate that the trends of strains and GDFs between load tests and FEMs are reasonably close; however, the magnitudes have some noticeable differences. The load tests recorded lower strains than predicted by the FEMs, possibly because some structural parameters (barriers at the middle span, diaphragms, modulus of elasticity, etc.) were not measured, complex torsional stress and strain fields perturbed the measurements, or due to hardware, software, or user errors with the strain transducer system. Future research would be beneficial to instrument diaphragms and barriers in positive moment regions to improve understanding of diaphragm behavior, update load distributions, estimate composite barrier participation, and more closely examine potential torsional effects in girders. Strain transducers could also be installed on one or both piers to investigate vertical strains associated with continuity participation and braking loads. It is also recommended that the load test be performed with heavier loads and that the modulus of elasticity be verified with non-destructive testing.

8 REFERENCES

American Association of State Highway and Transportation Officials (AASHTO). (2002) Standard Specification for Highway Bridges, 17th Ed, Washington, D.C.

American Association of State Highway and Transportation Officials (AASHTO). (2020). AASHTO LRFD Bridge Design Specifications, 9th Ed., Washington, DC.

Bridge Diagnostics, Inc. (2018). BDI Strain Transducer ST350 Manual. https://bditest.com/wp-content/uploads/2019/01/Manual-Strain-Transducer-ST350-201511-Rev-A-.pdf.

COMSOL(6.0), COMSOL, Inc. 100 District Avenue Burlington, MA, United States.

CSiBridge (V23), Computers & Structures Inc. New York, NY, United States.

MATLAB (2022a), The MathWorks, Inc., Natick, Massachusetts, United States.

Nowak, A. S., Eom, J., & Ferrand, D. (2003). Verification of girder distribution factors for continuous steel girder bridges (Research Report RC-1429). https://www.michigan.gov/documents/mdot_c&t_rc-1429_71596_7.pdf.

Nowak, A. S., Eom, J., Sanli, A., & Till, R. (1999). Verification of girder-distribution factors for short-span steel girder bridges by field testing. Transportation Research Record, 1688(1), 62-67. https://doi.org/10.3141/1688-08.

SAP2000 (V23), Computers & Structures Inc. New York, NY, United States.

Stallings, J. M., & Yoo, C. H. (1993). Tests and ratings of short-span steel bridges. Journal of Structural Engineering, 119(7), 2150-2168. https://doi.org/10.1061/(ASCE)0733-9445(1993)119:7(2150).